1994-95 ANNUAL REPORT

Reactions of Toxic Pollutants in Soil Systems

KEARNEY FOUNDATION OF SOIL SCIENCE
DIVISION OF AGRICULTURE AND NATURAL RESOURCES
UNIVERSITY OF CALIFORNIA

1994-95 ANNUAL REPORT

Reactions of Toxic Pollutants in Soil Systems

EDITED BY DEBORAH SILVA

DR. ANDREW C. CHANG, DIRECTOR
KEARNEY FOUNDATION OF SOIL SCIENCE
DIVISION OF AGRICULTURE AND NATURAL RESOURCES
UNIVERSITY OF CALIFORNIA

Contents

Annual Progress Reports

Appendix

Kearney Foundation of Soil Science: A Brief Overview

The report that follows is the fourth in a series of five Annual Reports issued by the Kearney Foundation of Soil Science on the Foundation's current five-year research mission for 1991-96, **Reactions of Toxic Pollutants in Soil Systems**. Many of the Foundation's research projects are funded for two to three years; thus, several investigators are reporting intermediate and final research progress on projects that began in 1991-93. Other reports represent first-year progress on projects whose funding cycle began in 1994-95. Each progress report indicates when the study was undertaken. Please refer to the Foundation's previous Annual Reports for this mission, as needed.

For more than 50 years, the M. Theodore Kearney Foundation of Soil Science at the University of California has established an impressive record in addressing critical research needs in the state and providing an intellectual forum for international leadership in soil science research. The Foundation has an endowment fund of more than $2 million, which supports, through a competitive grants process, fundamental and applied research by University faculty and Cooperative Extension personnel in the fields of soils, plant nutrition, and water science.

Mitigating the impacts of soil pollution is one of the major challenges facing California in the 1990s. Events that occur in soil have profound effects on surface water qualith and groundwater quality, but the dynamics of the relationship between soil quality and water quality need additional study. At present, scientists lack sufficient data from field situations on the movement, transformation, and fate of soil contaminants that influence water quality. Whether soil contamination arises from seepage of solvents used to clean aircraft at military bases, from leaking petroleum storage tanks at industrial sites, from normal application of fertilizers and pesticides in farming operations, from waste disposal, or from buildup of toxic levels of metals due to trace element-laden agricultural drainage water, University of California soil scientists are the experts who must develop the knowledge base to predict the fate of toxics, provide leadership in remediation strategies, and recommend scientifically sound techniques to prevent future degradation of soil and water quality in the state.

Pesticides provide a good example of soil contaminants requiring further study. Half of the pesticides used in the United States are applied in California, which ranks fifth worldwide in terms of agricultural revenue. The state accounts for 25% of the world's annual pesticide usage. The pressing need for additional scientific research about the transport and fate of toxic chemicals as they travel down the soil profile becomes unequivocal when such consumption of xenobiotic compounds is coupled with the state's dependence on irrigation agriculture and its public health mandate to sustain groundwater quality for domestic use.

Current Mission: Reactions of Toxic Pollutants in Soil Systems

The Foundation's 1991-96 mission, **Reactions of Toxic Pollutants in Soil Systems**, represents the first time the Foundation has focused on examination of soil pollution problems rather than production of agricultural products. Environmental problems, such as soil pollution, are characterized by an intimate intertwining of physical, chemical, and biological processes that require multidisciplinary research approaches. Many chemical sources of contamination are not miscible in water, but they can be transported, degraded, and transformed in soil. These soil processes need to be studied and managed for the protection of the state's natural resources and the public health of its

citizens. The reactions, mechanisms, and interactions that occur in the soil's vadose region above the water table and in ground water under saturation conditions are not understood fully. The current five-year Kearney mission focuses only on soil pollution problems in the vadose zone as stated in the outline below:

I. Investigate soil mechanisms, processes, and interactions that control transport, degradation, transformation, and crop uptake of toxic pollutants

   Quantify and model soil processes that determine mobility and reactivity of pollutants in soil and the vadose zone, resulting in groundwater pollution.

   Investigate interactions of soil, water, rhizosphere, and pollutants

   For multi-phase and/or multi-pollutant systems, investigate physical, chemical, and biological reactions and porous media transport involved

II. Develop methodology for scaling up microscopic soil mechanisms and reactions to field-scale processes that apply to agricultural and urban soils

   Investigate spatial variation of physical, chemical, and biological reactions in soil and the vadose zone

   Improve predictive accuracy, including mathematical models' description of soil reactions

   Develop management strategies, including application of the Geographical Information System, to prevent soil and water pollution by toxic environmental pollutants.

The fundamental knowledge base, including remediation and management strategies, developed by this mission on toxics during this period will be applicable throughout the state and will serve as a basis for developing application-related programs in agricultural and urban environments. Many soil science issues, such as the fate of toxics, know few boundaries between agricultural and urban soil.

History

The Kearney Foundation of Soil Science was established by the Regents of the University of California in 1954 to conduct research in soil science, plant nutrition and water science. Mr. M. Theodore Kearney, a prominent Fresno area farmer and founding member of the California Raisin Growers Association, died in 1906 and bequeathed his entire Fruit Vale Estate, worth close to $1.1 million, to the Regents of the University of California for agricultural research purposes. Over the years, Mr. Kearney had developed a fruitful working relationship with UC soil scientists whose advice regarding problems with drainage, salinity, and sodium had been essential to his ranch's success. Approximately 1,500 acres of Mr. Kearney's 5,000 acre Fruit Vale Estate had been planted to grapes for raisin production and the remainder was planted to alfalfa.

It was on Mr. Kearney's farm that University of California Professor W. P. Kelley conducted his classical experiments on alkali soil reclamation. UC Professor E. J. Wickson conducted field research on viticulture there. W. W. Mackie of the United States Department of Agriculture was the first to investigate land reclamation using a tile drainage system at the Kearney property in 1905. Mr. Kearney admired UC Professor E. Hilgard,

widely regarded as the "father" of the California Agricultural Experiment Station. Dr. Hilgard began alkali soil studies in the San Joaquin Valley on horseback in 1877.

In 1908, the University took over management of the Kearney estate, located 10 miles west of Fresno, and operated it as a commercial farm until 1948, when the Regents authorized its sale. Income and proceeds from the sale of the farm resulted in the establishment of the Kearney Foundation of Soil Science in 1954 and the University's Kearney Agricultural Center in Parlier.

The early record shows that the in-house research staff of the Kearney Foundation was at the cutting edge of soils research. Their work had major spinoffs not only in agricultural production but also in human and animal health. For example, UC scientists funded by the Foundation studied the generation of radon gas in soils, discovered the importance of cobalt and molybdenum in nitrogen fixation, used ^{15}N isotopes for research, and determined selenium concentrations by X-ray fluorescence.

By the late 1960s, income from the endowment fund was insufficient to support the salaries and research programs of resident scientists, so the Foundation was reorganized to tackle new research missions every five years and to allocate research funds through a competitive grants process to existing faculty and Extension specialists, and farm advisors in the statewide Agricultural Experiment Station. The Foundation's research missions, established in five year cycles since 1970, have focused previously on nitrogen in the environment (1970-75), trace elements (1975-80), salinity (1980-85), and water penetration problems in irrigated soils (1986-91).

Administration

The Associate Vice President for Agriculture, Division of Agriculture and Natural Resources, appoints a Director of the Kearney Foundation from one of the three Agricultural Experiment Station campuses (Berkeley, Davis, or Riverside) to oversee carrying out the designated mission. Dr. Andrew C. Chang, Professor of Agricultural Engineering and Agricultural Engineer in the Citrus Research Center - Agricultural Experiment Station at Riverside, is Director of the current mission. A Technical Committee and an Advisory Committee are appointed by the Director to help establish research priorities, administer the competitive grants process, and ensure that sufficient research progress and information dissemination occur. Current members of the Technical and Advisory Committees are listed in the Appendix.

Information Dissemination

Since the 1980s, the Foundation has published an Annual Report of research progress. The Foundation also conducts workshops, holds seminars and technical conferences, and issues special reports to fulfill each mission's research objectives and to communicate research accomplishments.

In March 1996, the Foundation published **Background Concentrations of Trace and Major Elements in California Soils**, a special report that includes the first comprehensive, scientific database on total background concentrations of 46 trace and major elements in 50 benchmark soils selected from throughout the state. The database is essential to systematic, accurate assessments of anthropogenic and natural causes of elevated trace element concentrations and should be useful to industries attempting to monitor their own effects on trace element levels in soils and to public agencies charged with assessing the severity of trace element pollution problems. The information will

facilitate accurate interpretations of experimental and field data and will facilitate scientifically defensible decisions by industries and policy makers.

In September 1995, the Foundation sponsored an international conference, **Vadose Zone Hydrology: Cutting Across Disciplines**, and published the conference's Proceedings. The conference honored the research partnership of James W. Biggar and Donald R. Nielsen.

In September 1994, the Foundation hosted a Soil Science Conference that highlighted research progress on Foundation-funded projects; reviewed the roles of soil science at the University of California (UC); and made recommendations for the 1996-2001 Kearney research mission. Speakers included prinicpal investigators on Kearney projects, UC administrators, an industry colleague, and Kearney Foundation directors..

In June 1994, the Foundation jointly sponsored a Biosolids and Compost Workshop in conjunction with the Southern California Compost Coalition and the UC Cooperative Extension Waste Management Workgroup. The three agencies developed and published the first **Southern California Biosolids Resource Book** in 1995. It is available by request from the Cooperative Extension Office in the Department of Soil and Environmental Sciences at UC Riverside.

In June 1993, the Foundation convened a Soil Pollution Workshop, which focused on identifying research and development needs in California, ranking the state's most important soil pollution problems, and recommending applied research approaches. The Foundation issued a report summarizing the workshop results.

Additional copies of Annual Reports, the special report on Background Concentrations of Trace and Major Elements in California Soils, the Vadose Zone Hydrology Conference Proceedings, and the Soil Pollution Workshop Report are available upon request from the Office of the Kearney Foundation Director, Dr. Andrew C. Chang.

Effect of Microscale Heterogeneity on Biodegradation of Pollutants in Soil

KATE M. SCOW
Department of Land, Air and Water Resources, Davis Campus

Summary

The biodegradation kinetics of pollutants in soil are strongly impacted by the rates of mass transfer of pollutants from locations where they are sorbed or sequestered to locations where there are microbial populations able to biodegrade them. The considerable spatial heterogeneity of soil makes it a challenge to understand the mechanisms involved in the metabolism of sorbed chemicals. The effect of spatial heterogeneity on biodegradation of phenanthrene was studied in mixtures of soils differing in their biodegradation and sorption properties. The biodegradation kinetics of phenanthrene in 8 soils could be described by a compartment model which included soluble, labile-sorbed, and resistant-sorbed phases of phenanthrene and first order biodegradation occurring in the labile phase. There was spatial heterogeneity in the distribution of microbial populations able to use toluene in a soil column through which toluene and trichloroethylene diffused. The differences in population density resulted in different rates of biodegradation of toluene at different locations within the column. A coupled mass transfer-biodegradation model could describe biodegradation of toluene in the soil column. With the exception of initial population density, which decreased from the inlet to outlet side of the column, all other parameters describing biodegradation were uniform at all locations.

Key Words: biodegradation, sorption, desorption, pollutants, soil microbiology, coupled processes.

Project Objectives Addressed in 1994-95

To determine the impact of soil spatial heterogeneity on rates of biodegradation of chemicals in soil and improve kinetic models describing biodegradation in heterogeneous systems under batch and column conditions.

Research Plan and Procedures

Biodegradation of phenanthrene was measured in modified biometer flasks using ^{14}C-radiolabeled chemical to determine the amount of $^{14}CO_2$ mineralized over time. Disappearance of toluene and trichloroethylene (TCE) was measured by headspace analysis combined with gas chromatography in batch systems. To distinguish between abiotic and biotic processes and for use in sorption and desorption experiments, soil samples were sterilized with cobalt-60 irradiation at Crocker Nuclear Laboratory on the UC Davis campus.

To further clarify the roles in biodegradation kinetics of sorption and inter- and intra-aggregate transfer, a series of experiments were performed in which phenanthrene was added to a small amount (3 g dry weight) of a first soil and then this phenanthrene-spiked soil was mixed into a larger amount (17 g dry weight) of a second soil. For example, for two soils, A and B, biodegradation would be measured in four systems where: (1) Three grams of A spiked and then mixed into 17 g of B; (2) Three grams of B spiked and then mixed into 17 g of A; (3) Three grams of A spiked and mixed into 17 g of A; and, (4) Three grams of B spiked and mixed into 17 g of B.

The experimental apparatus used in the column studies on the biodegradation of toluene and TCE was a two-chamber diffusion cell consisting of a soil column with air chambers attached at either end (Fig. 1). One of the chambers (the inlet chamber) is equipped with a piston mechanism used to separate the soil column from the inlet chamber in order to establish initial conditions. Magnetic stirrers are placed inside both chambers to maintain them at well-mixed conditions throughout the experiment. Initially, the piston is pushed against the soil column and chemical vapor is injected into the inlet chamber. The vapors are allowed to mix and equilibrate. The experiment is started by pulling the piston back and allowing the gas to diffuse through the soil column and into the exit chamber. Gas samples are taken from the inlet and exit chambers and from column sampling ports placed at 2.5, 5, 10, and 15cm from the inlet chamber. Gas samples from the end-chambers were taken using a 1 mL gas-tight syringe and analyzed using a Hewlett Packard 5890A gas chromatograph equipped with a Flame Ionization Detector (FID).

The soil column was 20 cm in length, and 7.6 cm in diameter. Preparation of the soil column was done as follows: 7 cm columns were attached to either end of the soil column and the entire column was packed with air-dry Yolo silt loam. Enough water was added uniformly to either end of the packed soil to bring it to a volumetric water content of approximately 25%. The column was allowed to equilibrate in a cold room for 12-16 weeks, at which time

the two extra end-columns were cut off and discarded, while the middle column was used in the experiment. Uniformity of packing was checked using gamma attenuation, and similarity of water content in the discarded columns was checked at the end of the equilibration period, as was the soil column itself at the end of the experiments.

Results and Discussion

A. Effect of spatial heterogeneity on biodegradation of phenanthrene

Experiments were conducted in which several soils that varied in their phenanthrene biodegradation rates and sorption characteristics were mixed together in different proportions and under different starting conditions with respect to phenanthrene location. In the first experiment, a soil with very slow phenanthrene degradation kinetics (Forbes) was mixed with one exhibiting much faster degradation kinetics (Tinker). The biodegradation of 50 ng phenanthrene per g of soil was governed by the soil into which the spiked soil was mixed and which was present in a larger amount. Therefore, phenanthrene spiked onto 3 g of Forbes and mixed into 17 g of Tinker degraded at about the same rate as did phenanthrene spiked onto Tinker and mixed into Tinker (Flg. 2). A similar phenomenon was observed when Forbes soil was the soil into which the spiked soils were mixed.

In a second set of experiments, two soils which degraded phenanthrene relatively quickly, Tinker and Yolo, were used. Yolo, however, degrades phenanthrene faster than does Tinker. The soils also differed in having very different organic carbon contents and, thus, sorption partition coefficients. Tinker has a K_{oc} approximately 10 times higher than that of Yolo. The biodegradation of phenanthrene spiked onto 3 g of Yolo soil and mixed into 17 g of Tinker was similar to that measured when phenanthrene spiked onto Tinker was mixed into Tinker soil. When phenanthrene was spiked onto Tinker soil and mixed into Yolo soil, however, the initial biodegradation was considerably slower than phenanthrene spiked onto Yolo soil and mixed into Yolo soil. This result suggested that mass transfer of phenanthrene out of the stronger sorbing Tinker soil may be limiting the biodegradation of the chemical in the Yolo soil. Additional experiments will be conducted to evaluate this hypothesis.

To test the hypothesis that the slow rate of biodegradation of phenanthrene in Forbes soil is due to mass transfer limitations, the soil was inoculated with a pure culture of *Arthrobacter* sp. RP 17 that can use phenanthrene as a sole carbon and energy source. A concentration of 50 ng phenanthrene per g of soil was degraded far more rapidly in the inoculated than uninoculated soil, even when inoculation was done 7 days after the phenanthrene had been added to the soil (Fig. 3). This result indicated that the very slow rate of biodegradation in Forbes soil was more likely due to low numbers of indigenous biodegrading organisms rather than to mass transfer limitations of the substrate.

B. Description of coupled mass transfer and biodegradation of volatile organic chemicals in soil diffusion chambers

Toluene and TCE are volatile organic chemicals (VOCs) with low sorption partition coefficients relative to that of phenanthrene. The biodegradation of these chemicals by indigenous soil microbial populations was measured in soil columns through which the chemicals moved via diffusion under transient conditions (following a single pulse). TCE degradation requires the presence of toluene for enzyme induction (Fan and Scow, 1993) and the ratio of toluene to TCE concentration controls the rate of TCE degradation. Because TCE diffuses more rapidly than does toluene, there was potential for considerable spatial variability within the column in the concentration ratios of the two chemicals.

To obtain the parameters describing the biological components of VOC biodegradation, the kinetics of biodegradation of toluene and TCE measured under batch conditions were characterized using nonlinear regression techniques. The kinetics of toluene biodegradation could be described by two Monod equations, one linking degradation rate to population growth and the other describing growth:

$$dC/dt = [(\mu_{max} \bullet C)/ (K_s + C) \bullet 1/Y \bullet B]$$

$$dB/dt = [(\mu_{max} \bullet C)/ (K_s + C) - b] \bullet B$$

where C is pollutant concentration (μg per ml of soil solution); μ_{max} is the maximum specific growth rate (per hr); K_s is the half saturation constant (μg per ml); Y is the yield coefficient (μg cells per ml/ μg pollutant per ml); B is the population density (μg cells per ml); and b is the population decay rate (per hr).

Input parameters for yield and half saturation constant were determined independently by direct measurement. The other parameters were obtained by curve-fitting. Toluene degradation in the presence of high TCE concentrations could be described by incorporating competitive inhibition (Haldane kinetics) and inactivation effects due to toxicity into the Monod expression. TCE degradation could be described by a Michaelis-Menten expression in which the specific rate of TCE degradation was a function of the rate of toluene degradation. The same set of parameters could be used to reasonably describe data from twenty independent experiments conducted at different initial concentrations of toluene and TCE.

Column experiments were conducted in which toluene was initially present at 40 μg per ml and TCE at 1 μg per ml. In order to eliminate the effect of growth of microbial populations on the kinetics and to make the population uniform throughout the column, experiments were conducted using Yolo soil that had been pre-acclimated by flushing with a toluene concentration of 40 μg per ml. Fig. 4 shows the change in toluene concentration over time in the inlet chamber and within the soil column at 2.5, 5, 10, and 15 cm. Toluene concentrations initially increased, then decreased, at the column ports, most

likely reflecting shifts in the processes controlling the toluene breakthrough. Initially, diffusive transport supplied the chemical in excess of the rate at which it could be metabolized, thus causing concentrations to increase. Then a decrease in concentration was observed, demonstrating that it was metabolized at a rate faster than mass transfer could replace it. The change in concentration was modeled by a coupled diffusion-sorption-biodegradation model:

$$R \bullet \varepsilon \bullet \partial C/\partial t = D_p (\partial^2 C/\partial x^2) - [(\mu_{max} \bullet C)/ (K_s + C) \bullet 1/Y \bullet B]$$

$$R = 1 + \theta/(\varepsilon \bullet K_H) + (\rho_b \bullet K_d) / (\varepsilon \bullet K_H)$$

where θ is the soil water content; K_H is the Henry's coefficient (dimensionless); ρ_b is the bulk density (g soil per cm^3); K_d is the sorption partition coefficient (cm^3 per g); and ε is the air filled porosity (cm^3 air per cm^3 soil).

Input parameters were measured either under sterile conditions (to obtain the diffusion coefficient, retardation factor parameters, water content, and porosity) or nonsterile batch conditions (to obtain the biological parameters as discussed above). It was possible to fit disappearance curves for toluene from the inlet chamber and within the columns using an identical set of parameters describing mass transfer and biodegradation (Fig. 5), with the exception of the initial population density term. This value varied by a factor of approximately 8 between the 2.5 to the 15 cm port and indicated that there was spatial variation in initial biomass even though attempts had been made to homogenize the population by pre-acclimation with toluene.

In conclusion, heterogeneity in the population distribution within the column resulted in spatially varying rates of toluene biodegradation. This variation could not be discerned by analysis of the decrease in toluene concentration in the inlet chamber. A similar phenomenon could occur with soil column studies in which breakthrough curves of the solution concentration are measured. Usually the same set of parameters, including population density, is used to describe biodegradation throughout the entire column. Under some conditions, omitting consideration of spatial variability could lead to erroneous conclusions about coupled mass transfer-biodegradation processes or could lead to poor fits of experimental data to the models used.

C. Improvement of coupled sorption-biodegradation models for analyzing pollutant mineralization in heterogeneous systems

Improvements were made to nonlinear regression techniques used to estimate the kinetic parameters describing biodegradation of chemicals by microbial populations in soil. Traditionally, kinetic models describe the mineralization of a chemical as cumulative carbon dioxide evolved over time. A problem with this approach is the generation of correlated errors such that the ith data point is not independent of the ith-1 data point. This results in nonrandom distribution of the residuals associated with the regression. Therefore, to avoid such error, the models were fit to rate data (first derivatives).

Comparisons of fits using rate versus cumulative data showed that use of rates could better discriminate among different models and resulted in improved random distribution of residuals.

Interpretation of biodegradation kinetics in soil is confounded by the physical interactions, such as sorption, of chemicals with the soil matrix. Complex models that couple mass transfer and biodegradation processes have been developed and adequately describe biodegradation in defined experimental systems (Scow and Hutson, 1992; Chung et al., 1993). It is difficult in soil, however, to independently measure all input parameters required for these models and thus simpler approaches are needed. We approached this problem by measuring and analyzing data describing the biodegradation of radiolabeled phenanthrene (which is strongly sorbed) at a low concentration (to minimize growth of microbial populations) in 8 soils differing in their organic matter content.

None of the data were fit well by commonly used biodegradation models based on the Monod equation (e.g., Monod with growth, first order, zero order, Michaelis-Menten, logarithmic), all of which assume the pollutant substrate is completely available to soil microorganisms. First order kinetics described only the middle portion of the curves, after removal of portions of the curve where there was an initial acceleration and later deceleration greater than predicted by first order. Most of the data could be reasonably fit by a compartment model in which the pollutant was assumed to be distributed among an aqueous phase, a labile-sorbed phase, and a resistant-sorbed phase. Biodegradation was assumed to occur, by first order kinetics, only in the aqueous phase. The aqueous phase was assumed to be in equilibrium with the labile sorbed phase, and there were first order mass transfer rates between the labile and resistant sorbed phases.

References

Chung, G.-Y., B.J. McCoy, and K.M. Scow. 1993. Criteria to assess when biodegradation is kinetically limited by intraparticle diffusion and sorption. Biotechnol. and Bioeng. 41:625-632.

Fan, S., and K.M. Scow. 1993. Biodegradation of trichloroethylene and toluene by indigenous microbial populations in soil. Appl. Environ. Microbiol. 59:1911-1918.

Scow, K. M., and J. Hutson. 1992. Effect of diffusion and sorption on the kinetics of biodegradation: theoretical considerations. Soil Sci. Soc. Amer. J. 56:119-127.

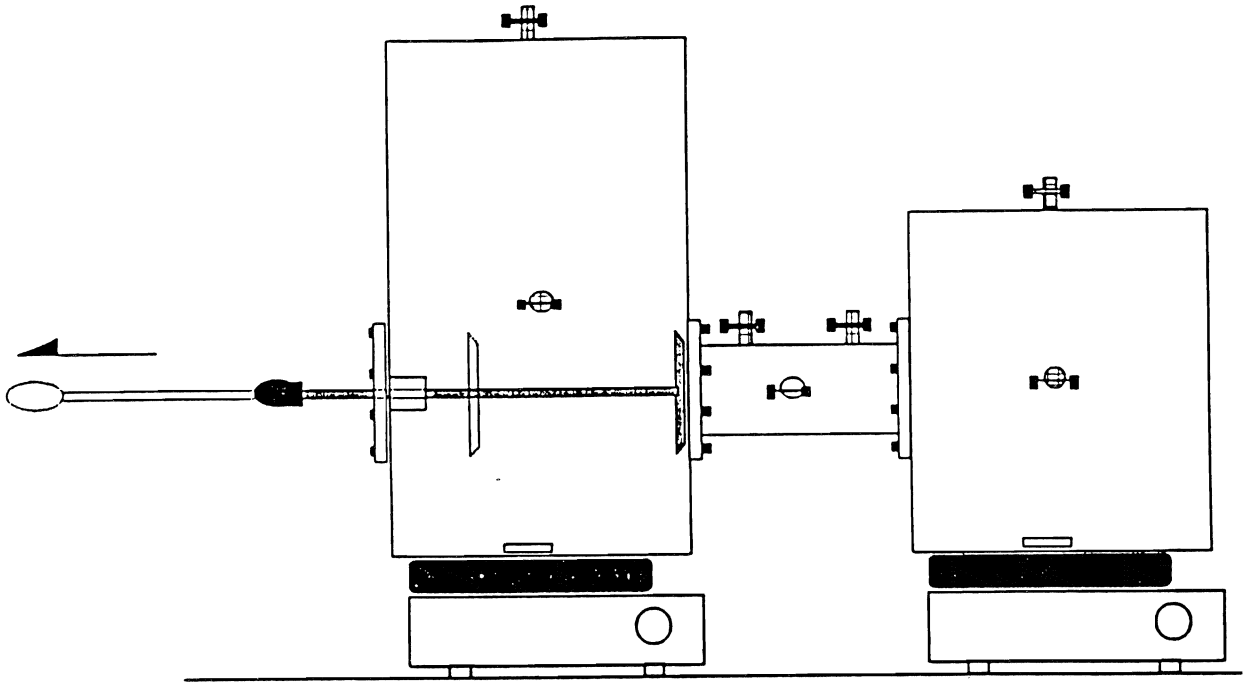

Figure 1. Diffusion chamber apparatus for measuring coupled mass transfer and biodegradation of volatile organic chemicals.

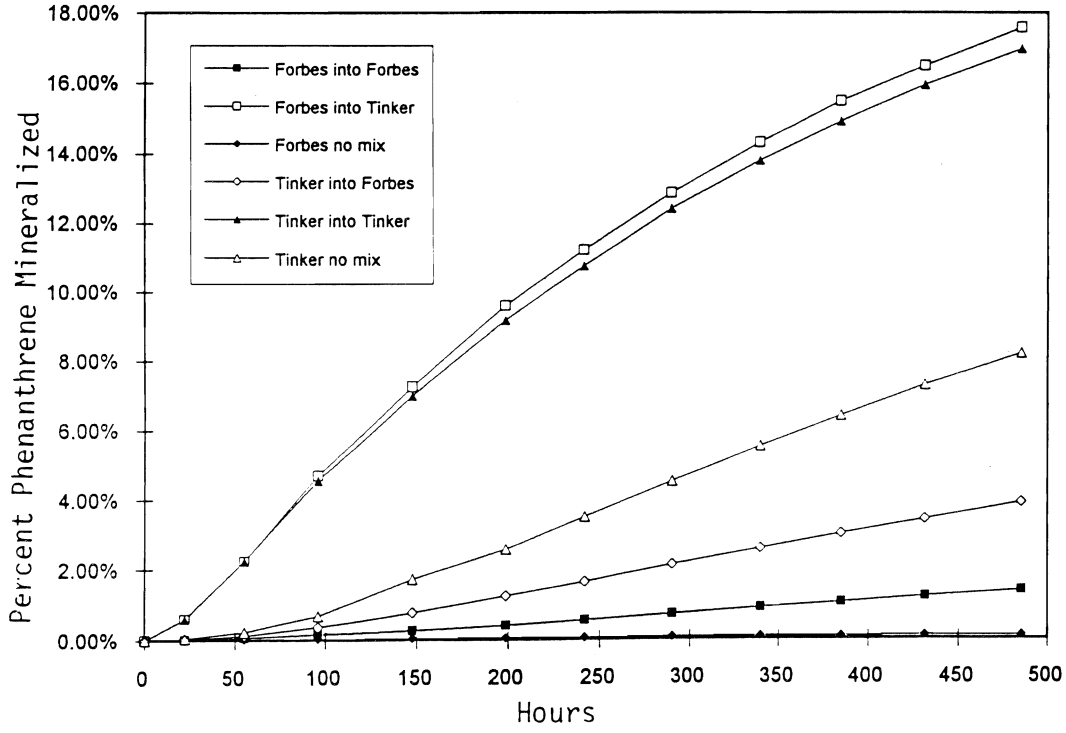

Figure 2. Biodegradation of 50 ng phenanthrene per g spiked onto 3 g of one soil and mixed into 17 g of another soil. For each symbol designation, the first soil name indicates soil onto which the chemical was initially spiked and the second soil name indicates the soil into which the spiked soil was mixed.

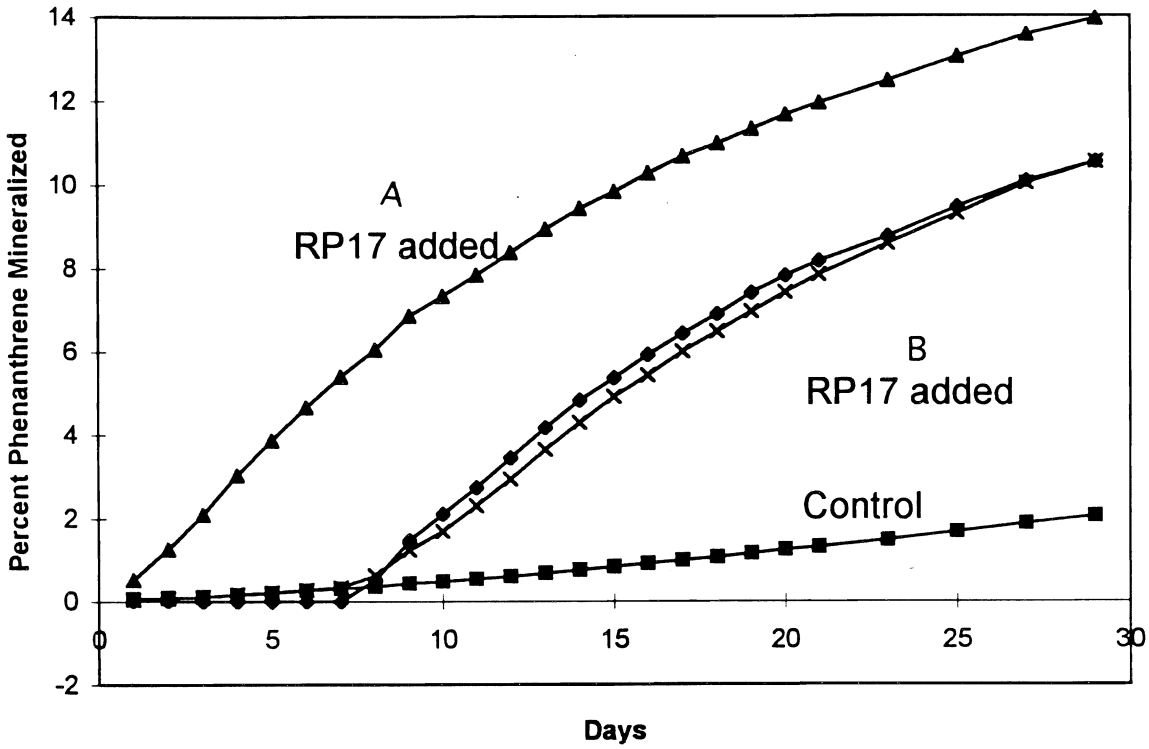

Figure 3. Biodegradation of 50 ng phenanthrene per g in Forbes soil that has not been inoculated (Control), or that has been inoculated with an *Arthrobacter* sp. strain RP 17. (A) designates soil that was inoculated at the same time that phenanthrene was added and (B) designates soil that was inoculated 7 days after the phenanthrene was added.

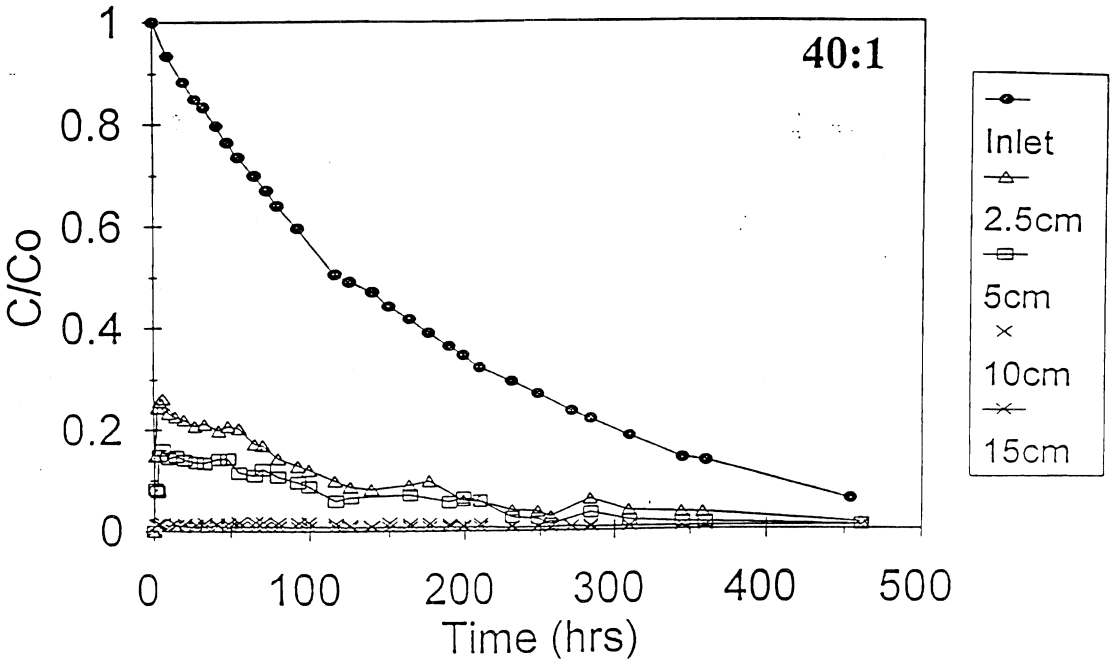

Figure 4. Changes in toluene concentration in soil diffusion chambers in the inlet chamber and at different locations within the soil column.

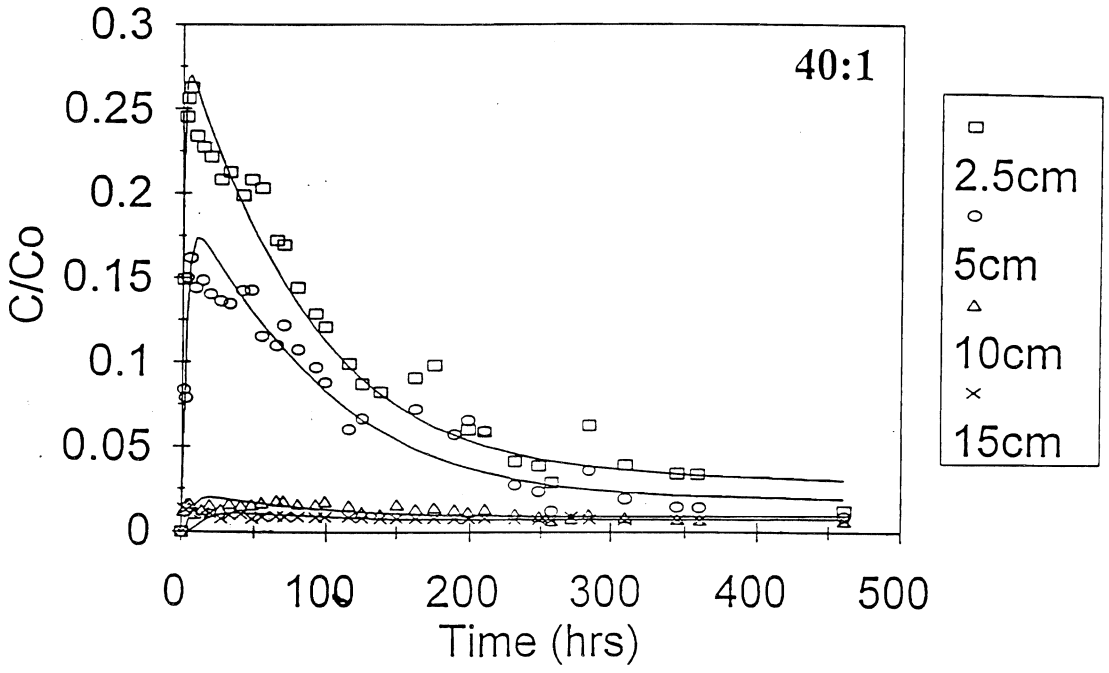

Figure 5. Comparison of model simulations to experimental data describing changes in toluene concentration in soil diffusion chambers at different locations within the soil column.

Rhizosphere Effects on Degradation of Pesticides in Soil

DAVID E. CROWLEY and SAM ALVEY
Department of Soil and Environmental Sciences, Riverside Campus

Summary

Rhizosphere effects on atrazine degradation were examined in soil that had not been exposed previously to atrazine, before and after inoculation with an atrazine-degrading consortium. In soil without the consortium, mineralization was slow, such that after 5 weeks, 11% of chain-labeled atrazine was N-dealkylated and only 2.4% of the ring-labeled atrazine was mineralized. Plants had no effect on atrazine mineralization, but formation of hydroxyatrazine was significantly enhanced in rhizosphere soil. Inoculation of this soil with the degrader consortium increased the rate of atrazine mineralization to 71% in nonplanted soils and 84% in rhizosphere soil after 4 weeks. Final size of the consortium was higher in the planted soil, which had a most probable number of 8.1×10^4 g^{-1} soil versus 2.7×10^3 in soil without plants. The results demonstrated that this consortium could be used to enhance degradation of atrazine in a nonhistory soil. Although survival of the consortium was increased in the rhizosphere, the rate of atrazine mineralization was not affected by plants in soil inoculated with a high population density of the degraders.

Key Words: biodegradation, microbial ecology, herbicide, phytoremediation, bioremediation.

Project Objectives Addressed in 1994-95

1. Determine the effects of a plant rhizosphere on rates of atrazine disappearance from soil inoculated with an atrazine degrader consortium isolated from a soil having a prior history of exposure to the contaminant.

2. Characterize the differential formation of recalcitrant atrazine metabolites that are produced in soil microcosms with and without plants.

Research Plan and Procedures

Triazine-based compounds are among the most commonly used herbicides in the United States (Smith, 1988), but they have been identified as a threat to groundwater quality in many areas where they have been applied for agriculture (U.S.EPA, 1990a,b). The half-life for transformation of the most commonly-applied triazine herbicide, atrazine (2-chloro-4-ethylamino-6-isopropylamino-s-triazine), to nonphytotoxic or less toxic metabolites is generally reported to take from 60 days to more than one year; whereas complete mineralization has been estimated at less than 40% of that applied (Assaf and Turco, 1994). Consequently, much of the parent compound and its metabolites slowly leach into the water table or are transported by runoff or erosion to surface water. In the United States, atrazine is now the second most common pesticide contaminant in community water systems and rural domestic wells (U.S. EPA, 1990b).

Prior to 1993, the isolation of microbes capable of partially degrading atrazine through hydroxylation or N-dealkylation were reported. More recently, there have been a number of reports of bacterial isolates and consortia that are capable of complete mineralization of atrazine through ring fission (Alvey and Crowley, 1995; Mandelbaum et al., 1993a; Radosevich et al., 1995; Yanze-Kontchou and Gschwind, 1994). Although there is very little understanding of the ecology of these degrader organisms and the environmental factors that control their activity, there has been considerable interest in their possible use for decontamination of groundwater or for reducing nonpoint water pollution by atrazine after it has served its function for weed control.

Degradation of atrazine in soils can involve both biological and chemical processes. The complete mineralization of atrazine is dependent on degrader populations, which appear to be rare or at insignificant levels in soils, resulting in atrazine's persistence and subsequent pollution of ground and surface waters. Nonbiological degradation of atrazine involves removal of the chlorine group by clay or organic matter-catalyzed hydrolysis, which generates hydroxyatrazine (Johnson and Fuhrmann, 1993; Li and Felbeck, 1972). Microbial degradation products include hydroxyatrazine, N-dealkyl metabolites, hydroxy-N-dealkyl metabolites (Anderson et al., 1980; Behki and Khan, 1986; Behki et al., 1993; Capriel et al., 1985; Donnelly et al., 1993; Giardina et al., 1982; Johnson and Fuhrmann, 1993; Qiao and Hummell, 1990; Winkelmann and Klaine, 1991) and ring-cleavage products that lead to complete mineralization (Alvey and Crowley,

1995; Grigg, et al., 1993; Mandelbaum et al., 1993a; Radosevich et al., 1995; Yanze-Kontchou and Gschwind, 1994). Some studies have suggested that the plant rhizosphere may be particularly important in promoting biological degradation of xenobiotics (Aprill and Sims, 1990; Ferro et al., 1994; Haby and Crowley, 1995; Haby, 1995; Hsu and Bartha, 1979; Sandman and Loos, 1984; Walton and Anderson, 1990), but this has not yet been investigated for atrazine.

The objectives of this study were to determine the effect corn plants would have on atrazine degradation in a soil with no previous exposure to atrazine, and the effect of plants on the survival and activity of a bacterial consortium that was introduced into this soil to achieve complete mineralization of atrazine and its metabolites. Rates of degradation and mineralization were determined by monitoring $^{14}CO_2$ evolution in soil microcosms amended with [^{14}C]-ethyl-chain or [^{14}C]-ring-labeled atrazine. The soils were also extracted and analyzed to determine differences in atrazine and atrazine-metabolite accumulation that occur in planted and nonplanted soils, with and without the degrader consortium. We were also interested in determining whether the rhizosphere provided a niche that might enhance survival of the degrader consortium after the atrazine had been mineralized.

Soil microcosm studies were performed using 175-ml jars containing 100 g air-dry, sieved, Handford sandy-loam soil (Coarse-loamy, mixed, nonacid, thermic Typic Xerorthent), pH of 6.8, with no known previous exposure to atrazine. Water content was checked daily and maintained at 15% water by weight or approximately -0.03 MPa in all microcosms. Individual microcosms were sealed using a rubber stopper with two ports (inlet and outlet) and a hole in the middle for the plant. Plants were sealed in the container using a low-melt, soft wax, and the microcosms then attached to a manifold via tubes from the ports in the stoppers for scrubbing of CO_2 before and after leaving the microcosms. Sterile CO_2-free air was introduced into the microcosms using a vacuum to pull ambient air through a sterile 0.2 mm filter and a single 2N NaOH trap that removed CO_2 prior to introduction of air into the microcosms. On the outflow side of each microcosm, a series of 2 in-line 2N NaOH-CO_2 traps were used for collection of $^{14}CO_2$, followed by a vial containing a polyurethane-foam puff through which the air was drawn to trap any volatile organics.

An experiment was conducted to examine the influence of plants on atrazine mineralization and metabolite formation in soil that had no prior exposure to atrazine. To separate the effects of plants from those of the root-associated microflora, treatments compared sterile-cultured plants with nonsterile plants. In sterile treatments, soil was autoclaved for 25 min, 3 times at 2-d intervals between each autoclaving. Corn seeds were surface sterilized and allowed to imbibe sterile water for 24 h prior to germination on sterile, tryptone-soy agar plates. Sterile seedlings were transferred to soil microcosms and maintained under sterile conditions until the shoots had emerged from the hole in the stopper and were large enough to be sealed with sterile wax. Ten repetitions were used for sterile treatments and 5 for nonsterile treatments. The plants were harvested and initial metabolite data determined after 5 weeks. After the 5-week incubation, wheat was planted and grown for an additional 3 weeks,

after which metabolite analysis was performed again. Both chain-labeled and ring-labeled atrazine were used in this experiment at a rate of 0.5 μCi/microcosm. The initial total concentration of atrazine in the microcosms was 3 mg kg^{-1} soil.

A second experiment examined growth and activity of an atrazine-degrader consortium isolated from a soil with a history of atrazine exposure (Alvey and Crowley, 1995) and inoculated into the nonhistory soil described above. Planted soil microcosms were either nonfertilized or amended with 100 mg kg^{-1} NH_4SO_4 and inoculated or noninoculated with the atrazine-degrader. Nonplanted soils received the same fertilizer treatment regime and included a poisoned control containing 10,000 mg kg^{-1} $HgCl_2$. No sterile treatments were included in the experimental design. Microcosms were incubated in a plant-growth chamber. All microcosms received 0.5 μCi of ring-labeled atrazine. The initial total concentrations of atrazine in the microcosms were 6 mg atrazine kg^{-1} soil.

Inoculum of the atrazine-degrading consortium, previously isolated by Alvey and Crowley (1995), was produced in mineral salts (MS) medium with atrazine as the sole source of nitrogen and glucose as a carbon source. The cells were harvested in late-log phase by centrifugation, washed 3 times in sterile P-saline buffer, and suspended in double-deionized water. Inoculated treatments received 7 ml of the suspension per microcosm to provide a cell density of 4.5×10^6 g^{-1} soil as determined by plating on tryptone-soy agar.

After the soil had been incubated for 28 d in the soil-plant microcosms in Experiment 2, the experiment was terminated and the entire soil in each microcosm removed and thoroughly mixed for enumeration of the atrazine-degrading consortium in each replicate microcosm by a most probable number (MPN) assay. The MPN vials were incubated at room temperature on a rotary shaker at 150 rpm for 21 d. After incubation, 1-ml aliquots were centrifuged at 12,000 rpm for 10 min. The supernatant was then analyzed by reverse-phase HPLC. Vials were scored positive if less than 25% of the atrazine remained in the solution.

Atrazine mineralization and ethyl-chain dealkylation were determined once a week by liquid-scintillation counting of the NaOH-CO_2-trapping solutions in a Beckman LS 5000TD liquid-scintillation counter (Beckman, Fullerton, CA). Samples were prepared by adding 7-ml Liquiscint' scintillation cocktail (National Diagnostics, Atlanta, GA) along with 1-ml double-deionized water and 200 ml aliquots of NaOH taken from the combination of both CO_2 traps.

Atrazine and metabolites were extracted from soil in a solution of 90% acetonitrile:10% 0.1M HCl (Montgomery and Freed, 1964). Soil extraction involved 3 successive extractions with an extractant to soil ratio of 4:1 and 30 min shaking on an orbital shaker at 300 rpm between extractions. Extracts were centrifuged at 12,000 rpm for 10 min and concentrated 8-fold under a dry stream of nitrogen. Extraction efficiency determined after 72 h incubation of atrazine and soil ranged from 85-90%. The HPLC method for simultaneous analysis of

atrazine and its metabolites was adapted from Rustum et al. (1990), and employed UV detection at 215 nm and 230 nm after separation by reverse-phase chromatography on a C-8 column. Standard retention times were determined for purified standards of atrazine, hydroxyatrazine, deethylatrazine, deisopropyl-atrazine, and diaminoatrazine. Fractions were collected on a Bio-Rad Model 2110 fraction collector (Biorad Laboratories, Hercules, CA). The total amount of atrazine or metabolite was calculated based on the specific activity (ratio of ^{14}C-atrazine to ^{12}C-atrazine) of atrazine used in each experiment. HPLC analyses of atrazine for the MPN assays utilized a more rapid procedure that does not separate atrazine from its metabolites. This simpler method employed a mobile phase of 50% acetonitrile, 50% double-deionized water on a column whose packing material has 18 carbon aliphatic chains, using UV detection at 215 nm.

Atrazine concentrations in the plant or that remained bound to the soil after extraction were determined to complete a mass balance. Plant tissue was digested in Scintigest and H_2O_2 and scintillation counted to determine plant uptake of atrazine. Soil-bound residues of atrazine were determined by placing 0.1 g previously extracted, dry soil into scintillation cocktail and liquid-scintillation counting.

Results

In soil that had not previously been exposed to the herbicide, mineralization of atrazine by the indigenous microflora was typical of rates reported in field studies. After 5 weeks, 11% of the ethyl-chain labeled atrazine was N-dealkylated while only 2.4% of the ring-labeled atrazine was mineralized to $^{14}CO_2$ (Fig. 1). There was no significant difference in N-dealkylation or mineralization of atrazine in planted versus nonplanted soils. In contrast, introduction of the atrazine-degrader consortium into this soil (Experiment 2) significantly increased the rate of mineralization of ring-labeled atrazine to 71% in inoculated, nonplanted soils and 84% in inoculated soil planted with corn (Fig. 2). As in Experiment 1, plants had no significant effect on the rate of degradation in either the inoculated or noninoculated soils. In the absence of the degrader consortium, only 1-3% of the atrazine was mineralized by the indigenous microflora, with the exception of the treatment planted with corn and amended with nitrogen, in which the indigenous microflora mineralized 18% of the atrazine. This difference was not significantly different from the other noninoculated treatments at the 0.05 level of significance. Addition of nitrogen to the inoculated treatments had no statistically significant effect on atrazine mineralization, irrespective of the presence of plants (Fig. 2).

At the end of Experiment 2, an MPN of atrazine degraders was performed for both the planted and nonplanted soils that were noninoculated or inoculated with the atrazine-degrader consortium. There was no atrazine-degrading population found in the noninoculated-soil treatments despite the occurrence of at least some low mineralization activity as indicated by the evolution of $^{14}CO_2$. The data did show, however, that survival of the degrader population in the

inoculated soils was 30-fold greater in planted soils compared to the nonplanted soils. Actual consortium unit numbers were 8.1×10^4 g^{-1} in planted soil with a 95% confidence interval from 2.45×10^4 to 2.67×10^5 versus 2.7×10^3 g^{-1} in nonplanted soil with a 95% confidence interval of 0.8×10^3 to 8.9×10^3.

The parent compound atrazine comprised greater than 50% of the extractable residue in all treatments in both experiments, except in the nonsterile, planted treatment in Experiment 1, where atrazine comprised only 29% of the extractable fraction (Fig. 3). The second most predominant residue in both experiments was hydroxyatrazine. In soil without the degrader consortium (Experiment 1), formation of hydroxyatrazine in the planted treatments was significantly higher than in nonplanted treatments, comprising 57% vs. 18% of the extractable residues under nonsterile conditions and 41% vs. 10% under initially-sterile conditions (Fig. 3). All metabolites other than hydroxyatrazine in Experiment 1 made up 10% or less of the extractable radioactivity (Fig. 3). A similar trend was observed in Experiment 2, where hydroxyatrazine formation in planted soils was more than twice that found in nonplanted soils. However, in this latter experiment, hydroxyatrazine comprised less than 20% of the total remaining atrazine in planted soil and less than 10% in the nonplanted soil (data not shown).

After the initial 5-week period in Experiment 1, the corn plants were harvested and the microcosms incubated for an additional 3 weeks. During this additional 3-week incubation, atrazine levels continued to drop in the previously planted nonsterile soil, while metabolites in the category "other" (hydroxydeethylatrazine, hydroxydeisopropylatrazine, and hydroxydiamino-atrazine) increased from 5% to 31% with a corresponding drop in hydroxyatrazine levels from 57% to 30% (Fig. 4). A similar trend occurred in the initially sterile, previously planted soil where the atrazine level dropped from 53% to 26%, and the other metabolite category increased from less than 2% to 29%. In contrast, soils not previously planted had only minor changes in the atrazine residue percentages. The level of atrazine in nonplanted soils was 52% in the nonsterile soil and 57% in the initially sterile soil. The "other" metabolites remained below 12% of the extractable fraction for both the nonplanted treatments. Hydroxyatrazine comprised 21% of the extractable residues in the nonsterile soil and 15% in the initially sterile soil, corresponding to increases of only 3% and 5% respectively (Fig. 4). Conversion of atrazine to less phytotoxic metabolites in Experiment 1 was greatest in the nonsterile, planted soil as evidenced by 70% germination and 50% survival of wheat seedlings versus 30-40% germination and no survival of wheat seedlings in microcosms that had been incubated without plants (data not shown).

In Experiment 1, a mass balance for atrazine was performed after 5 weeks in microcosms with corn and again after a 3-week post-harvest incubation. The mass balance after the 5-week period with corn plants demonstrated that plant uptake of atrazine and (presumably metabolites) was a significant loss pathway from the soil. In the planted, nonsterile treatment, 28% of the radioactivity added to the soil was accounted for in the plant, and 23% in the planted, initially-sterile treatment. The extractable percentage of radioactivity

in the planted treatments was 39% in nonsterile, planted soil and 54% in sterile, planted soil. Under nonplanted conditions, the total extractable radioactivity was 72% in the initially-sterile treatment and 78% under nonsterile conditions. Total recovery for this first mass balance ranged from 84% to 94% (Table 1). No volatile losses were measured in the organic solvent traps. In the mass balance after the 3-week additional incubation, the percentages of total extractable residues went down slightly, such that recovery of radioactivity ranged from 83% to 90% (data not shown). In the second experiment, total recovery of atrazine ranged from 93% to 104% (Table 2). Significantly less atrazine was found in the plant in both the inoculated and noninoculated treatments. This was likely due to lower transpiration of water through the plant, as evident by the smaller and less frequent irrigations required to maintain a 15% soil moisture.

Discussion

Among the various xenobiotics that may have enhanced degradation in the rhizosphere, atrazine is a particularly good candidate, since it accumulates in surface soils that are normally occupied by plant roots. At field application rates, it is present at relatively low concentrations that may preclude the growth and maintenance of an effective degrader population size (Qiao and Hummel, 1990). This latter problem is particularly critical for atrazine, which has a highly oxidized triazine ring that provides little or no energy for microbial growth (Radosevich et al., 1995). Thus, atrazine-degrader organisms can only acquire energy by utilizing carbon in the side chains attached to the ring or by growth on other carbon compounds contained in soil organic matter or root exudates. Atrazine has also been shown to serve as a nitrogen source for microbial growth (Alvey and Crowley, 1995; Mandelbaum et al., 1993a; Radosevich et al., 1995), which may be enhanced by plant uptake of nitrogen and simultaneous deposition of carbon, thereby providing a selective advantage for microorganisms that are able to derive nitrogen from the triazine ring.

Previously, it has been shown that many xenobiotics degrade faster in the rhizosphere than in bulk soils (Aprill and Sims, 1990; Ferro et al., 1994; Haby and Crowley, 1995; Hus and Bartha, 1979; Walton and Anderson, 1990). This has been generally attributed to increased microbial population numbers in the rhizosphere (Curl and Truelove, 1986), or specific selection pressures that enhance the size of the degrader population. In this research, the importance of kinetics of atrazine degradation in relation to population size of the consortium was not determined, since the consortium was introduced into the soil at a relatively high inoculation density. Nonetheless, the fact that there was enhanced survival of the consortium in rhizosphere soil after 4 weeks suggests that plants might have an important role in sustaining atrazine degraders in the absence of atrazine or when the compound is present at very low concentrations. This possibility needs to be examined further in long-term survival studies, and may have practical application in the field where, atrazine-contaminated machinery is periodically cleaned, or in riparian strips adjacent to fields that are used to reduce water contamination from soil runoff. On the other hand, in situations where degrader organisms are added directly for

bioremediation of highly contaminated soils, our data suggest that the presence of plants may not augment rapid mineralization of atrazine if the consortium is added at a high population density.

Among the various metabolites of atrazine that formed during the 4-week incubation period, hydroxyatrazine was predominant in all treatments under both sterile and nonsterile conditions (Fig. 3). However, there were large differences in the amounts of hydroxyatrazine that accumulated under the different experimental regimes. The lowest accumulation of hydroxyatrazine occurred in the sterile, nonplanted treatment, which reflects chemical degradation processes. This is known to be affected more by soil organic matter than by soil clay content (Li and Felbeck, 1972), and has been shown to be catalyzed by humic acids in liquid culture (Li and Felbeck, 1972). In relation to the sterile, nonplanted treatment, approximately 25% more hydroxyatrazine accumulated under nonsterile conditions. Skipper et al. (1967) found virtually no hydrolysis due to microbial populations, however bacteria have since been isolated that are capable of this process (Behki et al., 1993; Mandelbaum et al., 1993a,b; Radosevich et al., 1995). In comparison to the nonplanted treatments, almost twice as much hydroxyatrazine accumulated in the planted treatments, suggesting either plant-mediated production of this metabolite or enhanced microbial hydrolysis of atrazine in the corn rhizosphere.

Comparison of data from the sterile and nonsterile planted microcosms strongly suggests that the corn by itself could have directly caused the large increase in hydroxyatrazine accumulation. Although the sterile soils in Experiment 1 eventually became contaminated with bacteria introduced by watering, or that survived the seed sterilization treatment, the microbial community that developed in these contaminated microcosms is almost certainly less diverse and would not necessarily be expected to contain bacteria that hydrolyze atrazine. The mechanism by which corn resists the phytotoxic effects of atrazine is by the conversion to hydroxyatrazine within the plant tissue (Humburg et al., 1989; Montgomery and Freed, 1964). Moreover, comparison of results for the two separate experiments showed that increased transpiration and accumulation of atrazine in the plants under greenhouse conditions was associated with greater hydroxyatrazine accumulation in the planted soils (data not shown). This strongly suggests that atrazine taken up by the plant may have been re-excreted as hydroxyatrazine after hydrolysis in the plant. However, whether accumulation of hydroxyatrazine in the planted soils might be due to plant release of extracellular enzymes or by plant uptake, detoxification, and resecretion of hydroxyatrazine into the rhizosphere is still a matter of speculation.

Further incubation of the planted soils demonstrated that hydroxyatrazine was a relatively transient molecule with subsequent formation of hydroxylated N-dealkyl metabolites (Fig. 4). This may have occurred because the molecule is less toxic after removal of the chlorine, or perhaps removal of the chlorine group makes the molecule more susceptible to N-dealkylation reactions.

Conclusion

Soil that had not previously been exposed to atrazine did not have a culturable atrazine-degrader population and mineralized only 2% of the [^{14}C]-ring-labeled atrazine after 5 weeks. Plants had no effect on the rate of mineralization by the indigenous community, indicating that there was no selective enrichment of atrazine degraders in this particular soil by the plant rhizosphere. However, corn plants resulted in a higher rate of hydroxyatrazine formation than in nonplanted soils, and reduced subsequent phytotoxicity to other susceptible plant species. After introduction of a bacterial consortium into this soil, atrazine mineralization greatly increased, such that from 71 to 84% of the added atrazine was degraded in 4 weeks. Although there was no significant effect of plants on the rate of atrazine mineralization by the consortium, survival of the degrader consortium was enhanced 30-fold in the planted soils. This enhanced survival suggests that riparian buffer zones between fields and adjacent surface waters might be advantageous to the detoxification of atrazine and maintenance of higher population numbers of atrazine-degrader consortia in soils that contain such microorganisms or that are inoculated with these degraders to decrease nonpoint pollution from this widely-used herbicide.

References

Alvey, S. and D.E. Crowley. 1995. Influence of organic amendments on biodegradation of atrazine as a nitrogen source. In press.

Anderson, J.F., G.R. Stephens, and C.T. Corke. 1980. Atrazine and cyanazine activity in Ontario and Manitoba soils. Can. J. Plant Sci. 60:773-781.

Aprill, W. and R.C. Sims. 1990. Evaluation of the use of prairie grasses for stimulating polycyclic aromatic hydrocarbon treatment in soil. Chemosphere. 20: 253-265.

Assaf, Nasser, A. and R.F. Turco. 1994. Influence of carbon and nitrogen application on the mineralization of atrazine and its metabolites in soil. Pesticide Sci. 41:41- 47.

Behki, R.M. and S.U. Khan. 1986. Degradation of atrazine by *Pseudomonas*: N-dealkylation and dehalogenation of atrazine and its metabolites. J. Agric. Food Chem. 34:746-749.

Behki, R., E. Topp, W. Dick, and P. Germon. 1993. Metabolism of the herbicide atrazine by *Rhodococcus* strains. Appl. Environ. Microbiol. 59:1955-1959.

Capriel, P., A. Haisch and S.U. Khan. 1985. Distribution and nature of bound (nonextractable) residues of atrazine in a mineral soil nine years after herbicide application. J. Agric. Food Chem. 33:567-569.

Curl E.A. and Truelove B. 1986. The Rhizosphere. Springer-Verlag, NY

Donnelly, P.K., J. Entry and D. L. Crawford. 1993. Degradation of atrazine and 2,4-dichlorophenocyacetic acid by mycorrhizal fungi at three nitrogen concentrations in vitro. Appl. Environ. Microbiol. 59:2642-2647.

Ferro, A.M. R.C. Sims and B. Bugbee. 1994. Hycrest crested wheatgrass accelerates the degradation of pentachlorophenol in soil. J. Environ. Qual. 23:272-279.

Giardina, M.C., M.T. Giardi and G. Filacchioni. 1982. Atrazine metabolism by *Nocardia*: Elucidation of initial pathway and synthesis of potential metabolites. Agric. Biol. Chem. 46:1439-1445.

Grigg, B. C., R.F. Turco, and N.A. Assaf. 1993. Bioremediation of atrazine at elevated soil concentrations. Abstracts ASA-CSSA-SSSA Meetings Cincinnati OH Nov. 1993.

Haby P.A. and D.E. Crowley. 1995. Biodegradation of 3-chlorobenzoate as affected by rhizodeposition and selected organic substrates. Submitted to J. Environ. Qual.

Haby, P.A. 1995. Degradation of 3-chlorobenzoate in rhizosphere soils. M.S. thesis. University of California, Riverside.

Hsu, S. and R. Bartha. 1979. Accelerated mineralization of two organophosphate insecticides in the rhizosphere. Appl. and Environmental Microbiol. 37: 36-41.

Humburg, N.E., S.R. Colby, R.G. Lym, E.R. Hill, W.J. McAvoy, L.M. Kitchen, and R.Prasad, Eds. *Herbicide Handbook of the Weed Science Society of America*, 6th ed. Champaign, IL: Weed Science society of America, 1989), p. 301

Johnson, R.M. and J.J. Fuhrmann. 1993. Degradation of atrazine and metolachlor in subsoils from an Atlantic Coastal Plain watershed. In: Sorption and Degradation of Pesticides and Organic Chemicals in Soil. SSSA special pub. no. 32. p. 27-31.

Li. G. and G. T. Felbeck, Jr. 1972. Atrazine hydrolysis as catalyzed by humic acids. Soil Science. 114:201-209.

Mandelbaum, R. T., L. P. Wackett, and D. L. Allan. 1993a. Mineralization of the s-triazine ring of atrazine by stable bacterial mixed cultures. Appl. Environ. Microbiol. 59:1695-1701.

Mandelbaum, R. T., L. P. Wackett, and D. L. Allan. 1993b. Rapid hydrolysis of atrazine to hydroxyatrazine by soil bacteria. Eviron. Sci. Technol. 27:1943-1947.

Montgomery, M.L. and V.H. Freed. 1964. Metabolism of triazine herbicides by plants. J. Agric. Food Chem., 12:11-14.

Qiao, X. and H.E. Hummel, 1990. Atrazine depletion after one growth period under conditions of various cropping regimes in the southern Wetterau of Germany.

Radosevich, M., S.J. Taina, Y.L. Hao, and O.H. Touvinen. !995. Degradation and mineralization of atrazine by a soil bacterial isolate. Appl. Environ. Microbiol. 61::297-301.

Rustum, A., M., S. Ash and A. Saxena. 1990. Reversed-phase high-performance liquid chromatographic method for the determination of soil-bound [^{14}C]-atrazine and its radiolabeled metabolites in a soil metabolism study. J. Chromatography. 22:209-218.

Sandman, E.R. and M.A. Loos. 1984. Enumeration of 2,4-D-degrading microorganisms in soils and crop plant rhizospheres using indicator media; high populations associated with sugarcane (*Saccharum officinarum*) Chemosphere 13:1073-1084.

Smith, J.A. 1988. Manmade organic compounds in the surface waters of the United States - a review of current understanding. U.S. Geological Survery, Circular 1007. United States Government Printing Office, Denver, CO. 92p.

Skipper, H.D., C.M. Gimour and W. R. Furtick. 1967. Microbial versus chemical degradation of atrazine in soils. Soil Sci. Soc. Amer. Proc. 31:653-656.

U.S. Environmental Protection Agency. 1990a. National Pesticide Survey: Project Summary. Office of Pesticides and Toxic Substances. 10 pages.

U. S. Environmental Protection Agency. 1990b. Summary results of EPA's national survey of pesticides in drinking water wells. Office of Pesticides and Toxic Substances. 16 pages.

Walton, B.T., and T.A. Anderson. 1990. Microbial degradation of trichloroethylene in the rhizosphere: potential application to biological remediation of waste sites. Appl. Environ. Microbiol. 56:1012-1016.

Winkelmann, D.A. and S.J. Klaine. 1991. Degradation and bound-residue formation of atrazine in a western Tennessee soil. Environ. Toxicol. Chem. 10:335-345.

Yanze-Kontchou, C., and N. Gschwind. 1994. Mineralization of the herbicide atrazine as a carbon source by a *Pseudomonas* strain. Appl. Environ. Microbiol. 60:4297-4303.

Table 1. Ring-labeled ^{14}C-atrazine mass balance after 5 weeks in soil and plant microcosms.

Treatment	Total Recovery	Soil Extractable	Soil Bound	CO_2	Plant Uptake
	----------Percentage of Total Radioactivity Added----------				
Nonsterile no plants	94 ± 13*	78 ± 9	14 ± 5	2.4 ± 0.4	na
Sterile no plants	88 ± 14	72 ± 14	16 ± 1	0.2 ± 0.1	na
Nonsterile with plants	84 ± 7	39 ± 6	15 ± 3	2.2 ± 0.1	28 ± 1
Sterile with plants	84 ± 12	54 ± 5	16 ± 5	1.0 ± 0.2	23 ± 3

* All error values represent one standard deviation of the mean of either 5 or 10 replicates.

Table 2. Atrazine mass balance soil-plant microcosm Experiment 2.

Treatment	Total Recovery	Soil Extractable	Soil Bound	CO_2	Plant Uptake
	----------Percentage of Total Radioactivity Added----------				
No plants	95 ± 6*	83 ± 6	10 ± 1	2 ± 0	na
No plants Inoculated	98 ± 3	23 ± 2	4 ± 1	71 ± 3	na
Plants	93 ± 8	75 ± 8	8 ± 1	2 ± 0	8 ± 0.5
Plants Inoculated	104 ± 7	13 ± 1	3 ± 1	84 ± 6	4 ± 0.5

* All error values represent one standard deviation of the mean of 4 replicates.

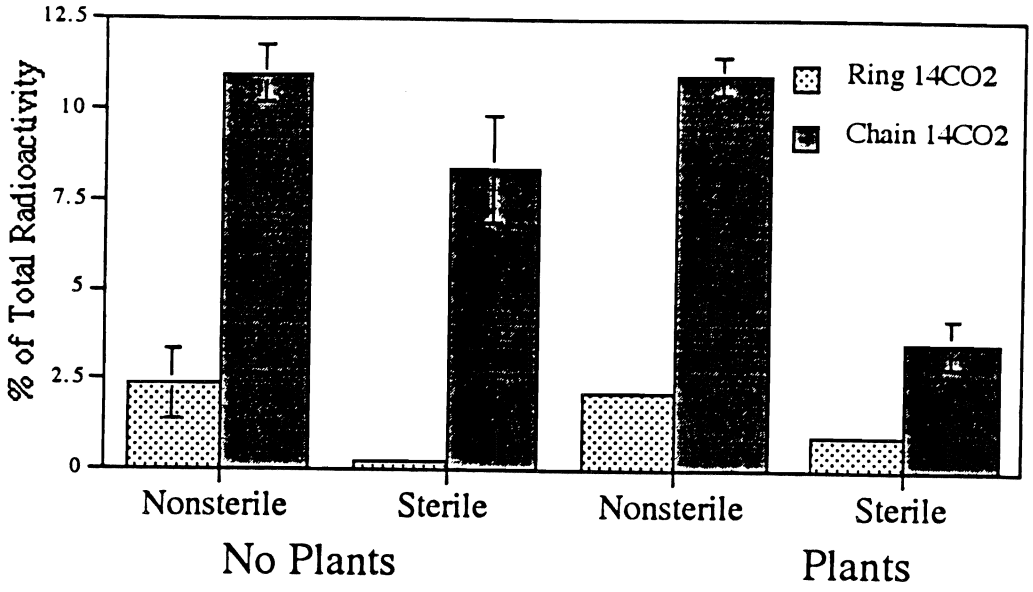

Figure 1. Mineralization of ring-labeled ^{14}C-atrazine and N-dealkylation of [^{14}C]-ethyl chain-labeled atrazine in planted and nonplanted soils after 5 weeks. Each column represents the mean of 5 replicates. Error bars represent the standard error of the mean.

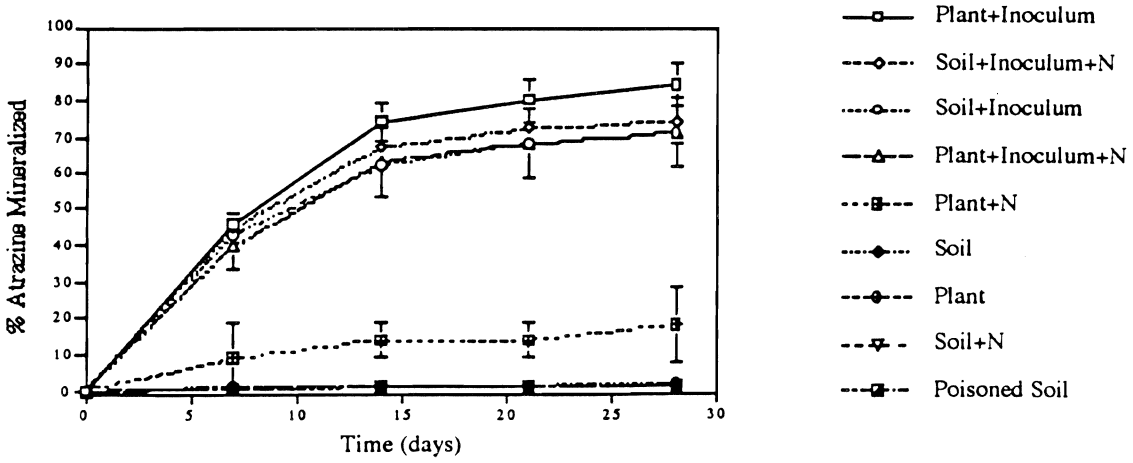

Figure 2. Mineralization of ring-labeled ^{14}C-atrazine in inoculated soil with and without plants. Each point represents the mean of 4 replicates. Error bars represent the standard error of the mean. All soils inoculated with the consortium had significantly greater degradation of atrazine than the noninoculated soils as determined by Student-Newman-Keuls Mean Separation Test.

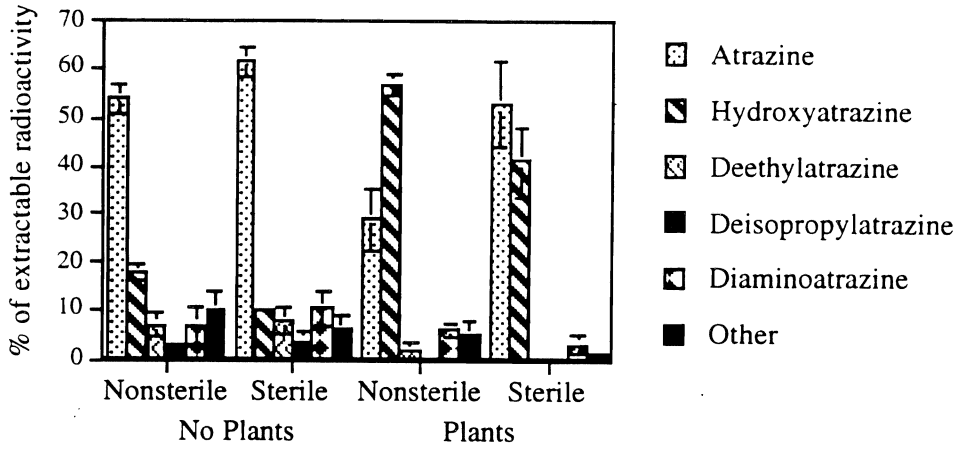

Figure 3. Atrazine metabolite formation in planted and nonplanted soil after 5 weeks. Each column represents the mean of 5 replicates. Error bars represent the standard error of the mean.

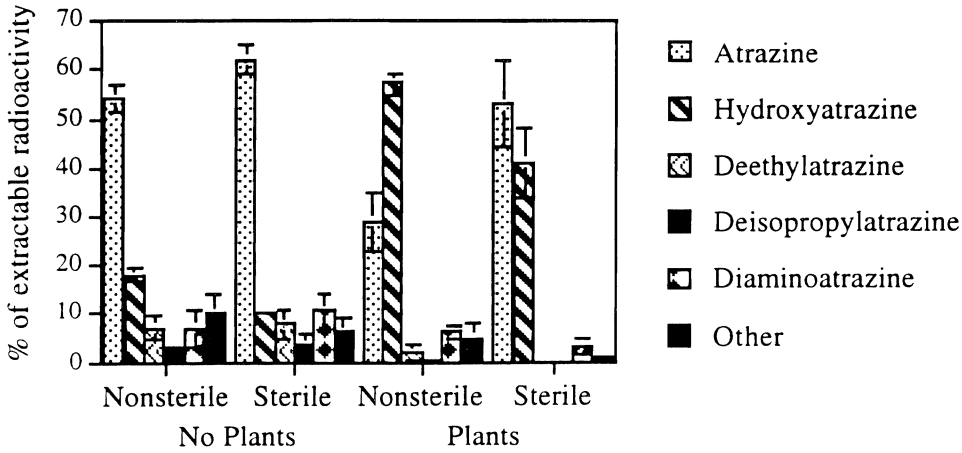

Figure 4. Effect of an additional 3-week post-harvest incubation on atrazine metabolite formation in soil. Each column represents the mean of 5 replicates. Error bars represent the standard error of the mean.

Microbial Community Activity in Vadose Material Exposed to Chlorinated Hydrocarbon Vapors in a Hazardous Waste Disposal Site at Los Alamos National Laboratory

K. A. DUNKIN AND M. K. FIRESTONE
Department of Environmental Science, Policy and Management, Berkeley Campus

Summary

Subsurface material from two boreholes (54-1009 and 54-1018) were sampled aseptically from 26 m below the surface in a hazardous waste disposal site at Los Alamos National Laboratory. Numbers of bacteria as total numbers of cells determined with acridine orange were below detection for material from 54-1009 and measurable for material from borehole 54-1018. Viable heterotrophic bacteria were below detection levels for 54-1009 and were between below detection to 7000 CFU g^{-1} dry subsurface material for 54-1018. A range of community activities were tested: nitrification potentials, denitrification potentials, respiration, dehydrogenase activity, utilization of ^{14}C-acetate and utilization of ^{14}C-glutamate. No activity was detected in samples from 54-1009 but 54-1018 had measurable rates of most activities in one of the subsampled cores. Biodegradation of 1,1,1-trichloroethane was not detectable in the subsurface material.

Key Words: soil microbiology, 1,1,1-trichloroethane, microbial ecology, subsurface, Los Alamos National Laboratory

Project Objectives Addressed in 1994-1995

1 To measure microbial community numbers and activities in subsurface material from two boreholes taken from a hazardous waste disposal site at Los Alamos National Laboratory.

2. To evaluate the impact of contamination on the microbial community.

Research Plan and Procedures

The objective of this study was to examine the activity of the microbial community in samples taken from the subsurface of the contaminated Materials Waste Disposal Area L at Los Alamos National Laboratory, New Mexico. A preliminary study of subsurface material taken from a nearby uncontaminated site demonstrated 10 to 100 bacterial colony forming units (CFU) per gram material at depths of 50, 150 and 175 ft, and determined that microscopic counts were 3-4 orders of magnitude greater than plate counts, but activity assessments were not made (Hersman et al., 1988). For this study, bacterial numbers were determined using plate counts and direct counts. Activities of the microbial community were determined using several different activity assays. The potential for the microbial community to degrade 1,1,1-trichloroethane (1,1,1-TCA), which was a contaminant at the site, was evaluated. Concentrations of vapor phase contaminants were determined by researchers at Los Alamos National Laboratory. Selected physical parameters of the subsurface were determined.

Site Description and Sampling

The study site was located at the Los Alamos National Laboratory, Los Alamos, New Mexico, USA. The site was the historical location for disposal of non-radioactive chemical waste into the subsurface through shafts and pits. Two vertical boreholes were drilled; well number 54-1009 was drilled in November of 1993 in Material Disposal Area L and well number 54-1018 drilled in April 1995. Borehole 54-1018 was 0.4 km southeast of borehole 54-1009 in an area outside of Material Disposal Area L. Subsurface materials were sampled aseptically from approximately 25-26 m below the surface grade using wire-line drilling with a sterile split-spoon sampler lined with 152 X 63 mm d. sterile brass sleeves. Upon reaching the surface, samples remained in the split-spoon sampler while it was brought to a nearby laboratory and placed in a biological cabinet where the brass sleeves were removed. Sleeves from 54-1009 were immediately capped with sterile polypropylene caps then wrapped in teflon tape followed by plastic tape, creating a tight seal. Sleeves from 54-1018 were wrapped in sterile aluminum foil and plastic tape. Contamination from surface material was not considered a problem, and no tracers were employed. All samples were shipped overnight express to Berkeley, CA for analysis.

Once at Berkeley, subsurface material was aseptically transferred to 1 Qt. sterile mason jars and other sterile containers for analysis. Microbial community size and metabolic activities were determined using assays described below. The unconsolidated subsurface material was used without sieving or grinding but was well mixed prior to analysis. Material was stored at 17 C.

Colony Forming Units

Numbers of viable cells were determined on agar plates as CFUs. Two g (dry wt. eq.) were dispersed in 18 ml of 0.001 M sodium phosphate buffer, pH 7.2. with 0.01% Tween 20 in sterile screw capped tubes. Fifteen, 4 mm d. sterile glass beads were added to disperse the material, except for samples from 54-1018 in which beads were omitted. Tubes were placed horizontally on a reciprocating shaker (150 strokes min^{-1}) at 26 C for 30 min. Samples were then sonicated for 3 min at 50 W in a bath sonicator (Branson, Shelton, CT) and immediately serially diluted. One-tenth ml of each dilution was plated onto agar media containing 60 $\mu g\ ml^{-1}$ cycloheximide and incubated at 26 C. Several different media were used. PTYG media was used at 1% of the original recipe (Balkwill et al., 1989) and trypticase soy agar (TSA) was used at 1/10 the recommended strength. One-tenth TSA has been shown to support a wide range of heterotrophic bacteria (Martin, 1975). A medium consisting of 0.5 g/l ammonium chloride, 3.0 g/l sodium phosphate, and 10 ml of Hutner's mineral solution (Smibert and Krieg, 1994), at pH 6.8 was used without an additional carbon source to select for extreme oligotrophic bacteria (1/2 strength 21C). King's B medium was also used; this media has traditionally been used for cultivation of fluorescent psuedomonads and other fluorescent bacteria (Smibert and Krieg, 1994). Additionally, serial dilutions were heated to 80 C for 20 min and plated on 1/10 strength TSA to select for heat-resistant bacterial forms (Holt and Krieg, 1994).

Direct Counts

Serial dilutions from the direct plating procedure were preserved with formaldehyde solution (final concentration, 2%) and refrigerated for 2 to 5 days until analysis. One-tenth ml or 0.2 ml of either a 10^{-2} or 10^{-3} dilution were stained for 20 min with an acridine orange (200 mg l^{-1}) solution containing 2.5 % glutaraldehyde. Dilutions were used which allowed for the greatest number of cells to be visible. Samples were filtered through a 25 mm, 0.2 μm black-stained polycarbonate membrane (Poretics, Livermore, CA). Four replicate samples were made and all cells of green, red or orange color were counted in 20 fields within a 1600 μm^2 grid. Counting was performed at 1200X magnification on a Leitz-Wetzlar Ortholux II microscope (Germany) with 100 W Hg epiflourescent illumination and with a wide band-blue, high-intensity excitation filter (Band Pass 390-490 nm) and 515 nm barrier filter (LP515). Background counts were determined by staining 25 ml of dilution buffer with 1 ml of acridine orange for 20 min and filtering through the standard membrane.

1,1,1-TCA Degradation Potential Assay

Twelve g or six g (S2) subsamples of subsurface material were aseptically transferred to 250 ml sterile amber glass bottles. One set received enough minimal media (1/2 strength 21C recipe without agar) to bring the moisure content to 150% (150%MC) and a second set received sterile water to 30% moisture content (30%MC). Samples were prepared in triplicate. Sterile controls were made by autoclaving three sucessive times on alternate days for 20 min. Bottles were capped with Mininert caps (Precision Scientific) and 5 µl of 1,1,1-TCA (99% Purity, Sigma Chemical) was added by microsyringe. Bottles were placed on a rotating incubator (150 rpm) at 21-23 C.

Headspace gas samples of 50 µl were withdrawn with a gas tight syringe at 3 to 4 day intervals and injected directly into a gas chromatograph with a flame ionization detector (Varian S-5400, Walnut Creek, CA), at 180 C with a 6' x 1/8" SS 60/80 Carbopack B/1% SP-1000 separation column, (Alltech Associates, Deerfield, Il) at 160 C. Ultrapure N_2 was the carrier gas at 40 ml min^{-1}. Standards were made in glass dilution bottles following the EPA standard method for volatile compounds. Sample syringes were kept heated to 40 C and 3 matched syringes were rotated to minimize sample carry-over. High and low standards were run every 8th sample to insure calibration of the GC. Two injections were made of each sample for each time point unless they differed by more than 5% coefficient of variation; then 3 were made. Data were transformed into water phase concentrations through the use of a Henry's coeffcient of 1.13. Adsorption was not accounted for but was assumed to be uniform within sample types.

Nitrification Potential Assay

Potential rates of ammonium oxidation to nitrite by nitrifying microorganisms were determined in the subsurface material in the presence of chlorate, which blocks the autotrophic oxidation of nitrite to nitrate (Belser and Mays, 1980). The procedure followed the method of Schimel, et al. with 0.5 mM $(NH_4)_2SO_4$ as the nitrogen source (Schimel et al., 1984). The assay was made over 24 hr. Solutions were analyzed for nitrite colorimetrically with a QuikChem AE ®automated ion analyzer (Latchat Instruments, Milwaukee, WI). Regressions of nitrite concentrations over time were used to determine the rate of nitrite production.

Dehydrogenase Activity

Community dehydrogenase activity was measured using the reduction of iodonitrotetrazolium violet (INT) to INT-formazan (Trevors et al., 1982). Two g samples were placed in sterile scintillation vials and equilibrated at 30% moisture content for 48 hr. At the start of the assay, 500 µl of a 2 mg ml^{-1} solution of INT were added. The samples were incubated at 17 C for 24 hr. INT-formazan was extracted with 5 ml of N,N,-dimethylformamide. The absorbance of the INT-formazan was measured on a UV/VIS spectrophotometer at 485 nm. Concentrations were calculated from a standard curve of INT-formazan.

Community Respiration

For 54-1009 samples, community respiration was measured on 15 g (dry wt eq). of material with an automated respirometer attached to a gas chromatograph (Varian 90-P, Walnut Creek, CA) with a thermal conductivity detector (120 C), a 2 m X 1/8 in. Porpack Q 80-100 mesh separation column at 45 C and He as the carrier gas at 20 ml min^{-1} (Brooks and Paul, 1987). Sampling and flushing of sample headspace was repeated every 12 hours. Samples were equilibrated to 30% moisture content and incubated at 26 C.

Samples from 54-1018 were measured manually in order to use a more sensitive gas chromatograph and to conserve sample material. Five g (dry wt. eq) of subsurface material was placed in a 65 ml serum vial, and the material was adjusted to 30% moisture content with sterile distilled water. The vials were sealed with butyl septa. Once a week for 5 weeks, 100 µl samples of the head space were removed via syringe and analyzed on a gas chromatograph (Hach-Carle, Series 100, Loveland, CO) with a thermal conductivity detector at 50 C, using He as the carrier gas at 20 ml min^{-1} through a 2.0 m X 1/8 in. column packed with Porpack N, 80-100 mesh at 70 C. Rates of CO_2 evolution were determined by regression.

Utilization of Added Substrates

Five 5 g samples from 54-1009 equilibrated for 24 hr at 30% moisture content received 100 µl of 72 nmolar [2-^{14}C]-Acetic Acid (18 MBq/l) (Amersham, Arlington Heights, IL), and were incubated at 26 C. The ^{14}C-CO_2 evolved was trapped on Whatman no. 2 filter paper containing 100 µl of phenylethylamine. At 5 to 7 day intervals, the filter paper was removed and placed in a scintillation vial with 5 ml of scintillation fluid. Activity was estimated as disintegrations per minute on a liquid scintillation counter (Beckman Instruments, LS9000, Palo Alto, CA). Samples from 54-1018 received 100 µl of L-{U-^{14}C- glutamic acid}(Amersham Corp, Arlington Heights, IL) and were analyzed as for 54-1009. The percent of added substrate utilized was determined.

Denitrification Potential Assay

Denitrification of added nitrate in the presence of excess carbon, acetylene, and reduced oxygen tension was assayed by gas chromatography on 2 g subsamples of 54-1018. Samples were incubated with 2 g carbon as glucose and 0.2 g nitrogen as potassium nitrate in sterile 65 ml serum vials sealed with butyl septa. Acetylene was added to 6 kPa. N_2O in the headspace was measured on a SRI 8610 gas chromatograph (SRI Instruments, Torrance, CA) with an electron capture detector at 235 C and with 5% methane/ 95% argon mixture as the carrier gas. The separation column was 80 cm X 1/8 in. Porapack Q with a 200 cm X 1/8 in. back flush column at 70 C. Manual injections of 100 µl were made into sample headspace over 5 to 7 days. Regression of the change in concentration of N-N_2O was used to determine the potential rate of denitrification.

Physical Characteristics

Physical parameters of the subsurface material were determined using standard methods. Soil pH was determined in soil pastes made with H_2O. Water content was determined after drying at 105 C for 1-2 days. Water potential was determined on a thermal couple psychrometer (Decagon Devices, Pullman, WA). Total C and N were determined by combustion on an automated carbon and nitrogen analyzer (Carlo-Erba , NA1500, Milan).

Statistics

Linear regression analysis to determine rate constants was performed using Statview statistical software (Abacus Concepts, Berkeley, CA). Rates were considered to be significantly different from zero at $p \leq 0.05$. All analyses were performed with a minimum of 3 replicate subsamples.

Results

Subsurface Material

Samples from borehole 54-1009 consisted of three brass sleeves (152 mm length X 63 mm d.) from approximately 25.9, 26.2 and 26.5 m below the surface grade. The three sleeves were entirely filled and contained an average of 600.3 (2.6) [mean (standard deviation)] g of subsurface material. Samples from borehole 54-1018 consisted of 2 sleeves, one which was almost entirely filled with approximately 580 g of material (S1), and a second which was partially filled with approximately 300 g of material (S2). These samples were taken from approximately 26 m but the order of the sleeves in the sample core was not recorded.

The subsurface material from both cores were from the same lithological unit of Bandelier tuff. They were composed of slightly-welded, ash flow tuff from the Tshirege member which is thought to have flowed approximately 1.1 mil yr ago from the Valles Caldera (IT Corporation, 1987). The subsurface material was unconsolidated and was light grey to light pink in color. Material from both boreholes was dry, with water potentials of about $^{-}1$ J kg^{-1} for samples from 54-1009 and less than $^{-}5$ J Kg^{-1} in samples from 54-1018. Water contents reflected the low water activities (Table 1). The pH values of the two boreholes differed by more than 1 pH unit; pH 7.6 for samples from 54-1009 and pH 9.0 for samples from 54-1018. This difference might have been due to the location of 54-1009, which was directly adjacent to one of the hazardous waste disposal pits. This pit was used for many years as a disposal site for a wide variety of materials, mostly unrecorded, some of which may have been very acidic (V. Trujillo, personal communication). Bulk density could be determined in samples from borehole 54-1009, since the sample sleeves were filled with material, and was determined to be 1.23 g cm^{-3}. This low bulk density is due to the large number of vesicles common in tuffaceous materials. Samples from 54-1018 were disrupted during sampling and the sleeves only partially filled; bulk density could not be determined. Total C and N values were extremely low. Values for

total N were below the detection limit for 54-1009, and C was estimated to be approximately 0.05% by mass. In material from S1, C was approximately 0.03% by mass, with N below detection. S2 had 0.06%C, with N content also below detection.

Contaminant Concentrations

Thermal desorption gas chromatography-mass spectroscopy (TDGCMS) was used to analyze solid cored material from borehole 54-1009; all contaminants examined were below the detection limit of 5 $\mu g\ g^{-1}$ (J. Sollid, personal communication). Field sampling of volatile contaminants was not performed in borehole 54-1009; however, adsorption gas samples were taken at a separate but nearby sampling well, 54-1010, and analyzed by TDGCMS. These samples indicated that the subsurface area near to 54-1009 was contaminated with an organic vapor plume consisting primarily of 1,1,1-trichloroethane (1,1,1-TCA), trichloroethene (TCE), and tetrachloroethene (PCE), among other contaminants (J. Sollid, personal communication, Table 2). The chlorofluorocarbons, CFC 11 and CFC 113, were also present in this area (Table 2).

Core samples from borehole 54-1009 were analyzed at Berkeley for gas phase contaminants prior to opening the brass sleeves. A sterile needle and syringe were used to pierce the caps which covered the brass sleeves and to withdraw 1 ml of the gas phase. The gas phase was injected directly into a gas chromatograph with a flame ionization detector (Varian, Walnut Creek, CA), at 250 C, 6' x 1/8" SS 60/80 Carbopack B/1% SP-1000, (Alltech Associates, Deerfield, Il). The separation column temperature was ramped at 8 C $min.^{-1}$ from 45C to 220C and held for 15 min. Ultrapure N_2 was the carrier gas at 40 ml min^{-1}.

Chromatograms showed several peaks, and the chromatograms for each core were only slightly different. A peak at 12.5 min. retention time corresponded to the retention time for a standard injection of 1,1,1-TCA under the chromatographic conditions used. All other peaks remained unidentified but were assumed to be hydrocarbons and CFCs. Without the additional information provided by mass spectroscopy, the chromatograms alone cannot be used to confirm identification or quantity of unknown components. However, the chromatograms do confirm the presence of volatile hydrocarbons in these samples at the time of analysis. Gas chromatographic analysis of 54-1018 samples was not performed at Berkeley, since this borehole was subsequently used as a monitoring well in a pilot gas extraction project and actual gas concentrations from the well were made available (Table 2).

Vapor phase contamination at borehole 54-1018 was measured using down well photoacoustic radiometry (PAR) for the major contaminants: 1,1,1-TCA, TCE, CFC 113 and CFC 11 (J. Sollid, personal communication, Table 2). Concentrations determined by PAR vary by 1 or 2 from standard values determined using TDGCMS analysis (J. Sollid, personal communication). The data demonstrate the presence of contaminants in borehole 54-1018 at

approximately a magnitude similar to the concentrations in the area near to borehole 54-1009. Many of the contaminants found in 54-1010 by TDGCMS were not analyzed in borehole 54-1018, so their presence or absence cannot be confirmed.

Numbers of Active and Total Cells

The material from all three sleeves from borehole 54-1009 contained CFUs in very low numbers (Table 3). Between 2 to 14 CFUs were found on 40% of the plates, and the counts were always below 20 CFUs per plate for the lowest dilutions. Furthermore, CFUs did not decrease with dilution as expected. Three months after the initial plating, 60% of the plates had no detectable growth, indicating that microorganisms were not simply growing slowly.

Numbers of CFUs from samples of the two sleeves in 54-1018, S1 and S2, were highly variable (Table 3). Subsamples from S1 had CFUs below detection; only 2 of the dilution plates, made from this sample had 2 and 5 colonies. In contrast, the numbers of CFUs from S2 ranged from below detection for heat-tolerant bacteria to numbers reaching 7×10^3 CFUs g^{-1} when plated on King's B medium. The colonies from S2 plated on 1/10 TSA, 1% PTYG and 1/2 strength 21C media were dominated by smooth and opaque-yellow, orange, red and pink colonies; while colonies on King's B media were uniformly greenish but not fluorescent under UV illumination. The isolation of colorful colonies was also noted by Hersman et al. (1988) in their preliminary study of this area.

These results are indicative of a highly variable spacial distribution of the cells in the subsurface. High spacial variability of viable cells has been noted by others in studies of the subsurface (Haldeman et al. ,1993; Russell et al., 1994) and the spacial distribution seems to be independent of the variability in subsurface physical characteristics (Colwell, 1989; Haldeman and Amy, 1993; Kieft et al., 1993; Kieft et al.,1995). For example, Kieft et al. (1993) studied 4 separate pristine vadose environments with depths ranging from 25 m to 450 m and formed in volcanic tuff, basalt, sediments and paleosols. The numbers of viable cells were frequently below detection (29 out of 45 samples), but viable cell numbers reached as high as 2.5×10^7 CFUs g^{-1} for a pleistocene paleosol at 37 m.

The standard method of plate counting has traditionally relied on homogenization in order to reduce variability, but recent work by Stevens and Holbert (1995) has demonstrated that homogenization of subsurface material, resulting in reductions of cell density, may inhibit outgrowth of cells possibly due to cell growth density-dependence phenomena. Cell density dependence is known to be related to long lag times and even failure of culture growth in laboratory studies of pure cultures. In most environmental samples (such as surface soil), cell densities are high, and the initial 1/10 or 1/100 dilution and homogenization of the sampled material apparently causes no significant effect on cell outgrowth. However, in samples from the subsurface, low numbers of cells and the apparent patchy distribution could reduce the efficacy of standard

dilution procedures. The nonuniform dilution pattern observed in samples from borehole 54-1009 could have arisen from density dependence, since plating of flocks of cells may have enabled some CFUs to form while single cells may not have grown. Further studies on both subsurface cell distribution and the nature of density dependence are needed to determine if the standard methods used in plate counts are inappropriate for subsurface or other low cell-density environments.

Estimates of total cell numbers were made by staining subsurface material with acridine orange. Cell numbers in samples from 54-1009 were below the detection limit of 10,000 cells g^{-1} (Table 3). Some cells were visible in many of the microscopic fields viewed, but these numbers were so low as to be negligible when calculations included values from blank control samples. Total cell numbers in 54-1018 were variable by sample sleeve; numbers of cells in S1 were below detection, but S2 had approximately 4.5×10^7 cells g^{-1} (n=8) (Table 3). These results further support the spatially variable nature of cell distribution in the subsurface environment at Los Alamos National Laboratory.

In sample S2, the proportion of total cells to CFUs was about 10^4, or put another way, approximately 0.1% of the total cells counted were culturable under the conditions used. This amount is low, especially when compared to the 10% culturable common in surface soil. Many of the cells visible in direct counts could have been dead. Any sort of density-dependence response may also reduce the numbers of CFUs thus influencing the proportion of cultural cells. Interestingly, several studies of subsurface microbial communities have shown that storage and disruption of samples can increase CFUs (Brockman et al., 1992; Haldeman et al., 1995; Haldeman et al., 1994). Haldeman et al. (1995) demonstrated through the use of extractable cell lipids that the increase is sometimes due to resuscitation and growth of new bacterial types formerly not seen on culture plates.

In addition to disturbance, the selectivity of media was important in determining the numbers of viable cells. Since the subsurface environment was oligotrophic, media relatively low in carbon were used. One-half strength 21 C media contains only agar as a carbon source. Interestingly, the majority of CFUs were recovered on the most oligotrophic media. One-tenth TSA has been used in determining surface soil CFUs and 1% PTYG media have been preferred in the Department of Energy's deep subsurface microbiology program. However, the numbers of CFUs on these two media were essentially the same. The question of which media to use for determining viable counts is still an open one. Recently, a study using combinations of media components to evaluate recovery of CFUs from subsurface material showed that the addition of vitamins and activated charcoal gave the greatest yield (Stevens, 1995). Activated charcoal had a greater effect than all other components. Currently, activated charcoal is rarely used for general aerobic, heterotrophic plating media, but it is often used in plating microaerophilic organisms since it is thought to provide protection from oxygen toxicity.

Heat-resistant bacterial forms did not seem to be a component of the bacterial communities as no CFUs were found on any of the heat treated plates. Thisresult is in contrast to surface soil communities where a large proportion of the microbial community is able to form heat resistant spores. Working with deep subsurface volcanic tuff, Haldeman et al. (1993) were also unable to recover spore-forming microorganisms by heat treatment.

Biodegradation Potential of 1,1,1-TCA

Degradation potential of 1,1,1-TCA was tested in batch reactors. Concentrations of added 1,1,1-TCA remained within 2% of the sterile controls in both the 30% MC and the 150% MC experiments for samples from both 54-1009 and 54-1018 (Fig. 1). Degradation of 1,1,1-TCA has been measured in a contaminated subsurface aquifer material under both methanogenic and sulfate reducing conditions (Klecka et al., 1990). In contrast, 1,1,1-TCA-contaminated vadose zone material (depth not given) tested in batch reactors with prior enrichment of methanotrophic bacteria showed no degradation of 1,1,1-TCA after 960 hr of incubation at 20C (Broholm et al., 1991). In a series of studies, Bouwer and McCarty found that 1,1,1-TCA was degraded by a mixed, methanogenic culture seeded from sewage sludge with acetate as the primary carbon substrate, but no degradation occurred in mixed-denitrifying or aerobic cultures also seeded from sewage sludge (Bouwer and McCarty, 1983a; Bouwer and McCarty, 1983b).

Individual bacterial isolates known to transform 1,1,1-TCA include the common soil bacteria *Nitrosomonas europea* (Vannelli et al., 1990), 21 different unidentified anaerobic isolates from sludge and a *Clostridium* sp. isolated from sludge (Galli and McCarty, 1989).

Activity Assays

Estimates of rates for nitrification and respiration in samples from 54-1009 were not significantly different from zero; denitrification rates were not measured (Table 4). In samples from 54-1018, S2 had measurable rates of nitrification, respiration, and denitrification activity. Samples from S1 had measurable but low rates of respiration only (Table 4).

Dehydrogenase activity measured in a single time point-24 hr assay were below detection for samples from borehole 54-1009 (Table 5). Samples from borehole 54-1018 were about 2 times the detection limit. Interestingly, respiration rates in S1 were half as great as S2, but dehydrogenase activity levels were higher in S1 than in S2. The dehydrogenase assay was repeated 3 times and the pattern and magnitudes were the same each time.

These whole community assays provide some information about the activity of the community *in situ.* Measurements of respiration rates are often thought to be an index of microbial community size and are often used in surface soil assays. Nitrification activity may be an index of the size of the nitrifying population and is particularly useful to evaluate here, since nitrifying

organisms have been shown to degrade halogenated hydrocarbons (Vannelli et al., 1990). The low levels of activity in samples from 54-1009 mirror the low numbers of cells and the low numbers of CFUs.

The presence of measurable denitrification rates in the 54-1018 samples may reflect the possibility that denitrification conditions periodically exist in the subsurface. The presence of anaerobic microsites even in well-aerated surface soil has been confirmed. The possibility exists that oxygen consumption in microsites at 25 m depth might exceed rates of recharge from the surface.

In order to test for very low levels of activity in 54-1009, ^{14}C-labeled acetic acid was added and the amount of mineralized $^{14}CO_2$ evolved was measured. After 1 month of incubation, for both samples and combusted-control samples, the amount of $^{14}C0_2$ formed was less than 0.1% of the added substrate (Table 5). A parallel experiment was done with samples from 54-1018 but using ^{14}C-glutamic acid this time. The amount of $^{14}CO_2$ evolved was still a small percentage of the added material, and for samples from S2, it approached 2%. The extent of utilization for S1 was 0.3 % (Table 5).

Conclusion

The microbial communities at Los Alamos National Laboratory hazardous waste site at 26 m below the surface in two locations contaminated with chlorinated solvents and CFCs were examined. The numbers and activities were generally low; however, a few measurable activities were detected and viable bacterial cells were present. The interactions of the microbial community with the contaminants can only be inferred, since an uncontaminated control sample was not obtained. However, the presence of viable microorganisms at this deep, dry location and in the presence of considerable contamination has provided one more snapshot of the microbial community in the deep, unsaturated subsurface.

References

Balkwill, D. L., J. K. Fredrickson, and J. M. Thomas. 1989. Vertical and horizontal variations in the physiological diversity of the aerobic chemoheterotrophic bacterial microflora in deep southeast coastal plain subsurface sediments. Applied and Environmental Microbiology 55 (5):1058-1065.

Belser, L.W., and E.L. Mays. 1980. Specific inhibition of nitrite oxidation by chlorate and its use in assessing nitrification in soils and sediments. Applied and Environmental Microbiology 39 (3):505-510.

Bouwer, E. J., and P. L. McCarty. 1983a. Transformations of 1- and 2- carbon halogenated aliphatic organic compounds under methanogenic conditions. Applied and Environmental Microbiology 45 (4):1286-1294.

Bouwer, E. J., and P. L. McCarty. 1983b. Transformations of halogenated organic compounds under denitrification conditions. Applied and Environmental Microbiology 45 (4):1295-1299.

Brockman, F., T. L. Kieft, J. K. Fredrickson, B. N. Bjornstad, S. Li, W. Spangenburg, and P. E. Long. 1992. Microbiology of vadose zone paleosols in south central Washington state. Microbial Ecology 23:279-301.

Broholm, K., T. H. Christensen, and B. K. Jensen. 1991. Laboratory feasibility studies on biological in-situ treatment of a sandy soil contaminated with chlorinated aliphatics. Environmental Technology 12:279-289.

Brooks, P. D., and E. A. Paul. 1987. A new automated technique for measuring respiration in soil samples. Plant and Soil 101:183-187.

Colwell, F. S., 1989. Microbiological comparison of surface soil and unsaturated subsurface soil from a semiarid high desert. Applied and Environmental Microbiology 55 (9):2420-2423.

Galli, R., and P. L. McCarty. 1989. Biotransformation of 1,1,1-Trichloroethane, Trichloromethane and Tetrachloromethane by a *Clostridium* sp. Applied and Environmental Microbiology 55 (4):837-844.

Haldeman, D., and P. S. Amy. 1993. Bacterial heterogeneity in deep subsurface tunnels at Rainier Mesa, Nevada Test site. Microbial Ecology 25:183-194.

Haldeman, D. L., P. S. Amy, D. Ringelberg, and D.C. White. 1993. Characterization of the microbiology within a 21 m3 section of rock from the deep subsurface. Microbial Ecology 26:145-159.

Haldeman, D. L., P.S. Amy, D. Ringelberg, D.C. White, R.E. Garen, and W. C. Ghiorse. 1995. Microbial growth and resuscitation alter community structure after perturbation. FEMS Microbial Ecology 17:27-38.

Haldeman, D. L., P. S. Amy, D.C. White, and D.B. Ringelberg. 1994. Changes in bacteria recoverable from subsurface volcanic rock samples during storage at 4 C. Applied and Environmental Microbiology 60:2697-2703.

Hersman, L., W. Purtyman, and J. Sinclair. 1988. Preliminary microbiological analysis of the vadose zone, Parjarito Plateau, New Mexico. Annual meeting of the American Society for Microbiology. ASM Washington D.C:252.

Holt, J., and N. R. Krieg. 1994. Enrichment and Isolation. In P. Gerhardt (ed.) *Methods for General and Molecular Bacteriology*, . Washington, D.C.: American Society for Microbiology.

IT Corporation. 1987. Geological assessment of technical area 54 -area G and L, Los Alamos National Laboratory. Project # 301017.02.

Kieft, T. L., P. S. Amy, F. J. Brockman, J. K. Fredrickson, B. N. Bjorndstad, and L. L. Rosacker. 1993. Microbial abundance and activities in relation to water potential in the vadose zones of arid and semiarid sites. Microbial Ecology 2 6:59-78.

Kieft, T. L., J. K. Fredrickson, J.P. McKinley, B. N. Bjornstad, S. A. Rawson, T.J. Phelps, F. J. Brockman, and S. M. Pfiffner. 1995. Microbiological comparisons within and across contiguous lacustrine, paleosol and fluvial subsurface sediments. Applied and Environmental Microbiology 61 (2):749-757.

Klecka, G. M., S. J. Gonsior, and D. A. Markham. 1990. Biological transformations of 1,1,1-Trichloroethane in subsurface soils and groundwater. Environmental toxicology and chemistry 9:1437-1451.

Martin, J.K. 1975. Comparison of agar media for counts of viable soil bacteria. Soil Biology and Biochemistry 7:401-402.

Russell, C. E., R. Jacobson, D. L. Haldeman, and P. S. Amy. 1994. Heterogeneity of deep subsurface microorganisms and correlations to hydrogeological and geochemical parameters. Geomicrobiology Journal 12:37-51.

Schimel, J.P., M.K. Firestone, and K.S. Killham. 1984. Identification of heterotrophic nitrification in a Sierran forest soil. Applied and Environmental Microbiology 48 (4):802-806.

Smibert, R. M., and N. R. Krieg. 1994. Systematics. In P. Gerhard.(ed) *Methods for General and Molecular Bacteriology*, Washington, D.C.: American Society for Microbiology.

Stevens, T.O. 1995. Optimization of media for enumeration and isolation of aerobic heterotrophic bacteria from the deep terrestrial subsurface. Journal of Microbiological Methods 21:293-303.

Stevens, T.O., and B.S. Holbert. 1995. Variability and density dependence of bacteria in terrestrial subsurface samples: implications for enumeration. Journal of microbiological methods 21:283-292.

Trevors, J. T., C. I. Mayfield, and W. E. Innis. 1982. Measurement of electron transport system (ETS) activity in soil. Microbial Ecology 8:163-168.

Vannelli, T., M. Logan, D. Arciero, and A. B. Hooper. 1990. Degradation of halogenated aliphatic compounds by the ammonia-oxidizing bacterium *Nitrosomonas europaea*. Applied and Environmental Microbiology 56 4:1169-1171.

Table 1. Physical characteristics of Los Alamos National Laboratory subsurface material.

Bore Hole	pH	Water Content	Water Potential	Bulk Density
		kg kg^{-1}	J kg^{-1}	g cm^{-3}
54-1009				
25.9m	7.6	0.025	-1.30	1.23
26.2m	7.7	0.034	-0.98	1.23
26.5m	7.6	0.035	-0.92	1.23
54-1018				
S1	9.0	0.010	<-5	n.d.†
S2	9.0	0.013	<-5	n.d.

† n.d.; Not determined.

Table 2. Subsurface Gas Contaminant Concentrations[1].

		Bore Hole 54-1010†				Bore Hole 54-1018‡		
Compound	**Abbreviation**	**6.1m**	**9.1m**	**12.2m**	**15.2m**	**21.3m**	**37.2m**	**42.7m**
					mg m^{-3}			
1,1,1 - Trichloroethane	1,1,1 - TCA	730	1500	430	1700	316	264	376
Trichloroethene	TCE	390	880	210	550	63	54	74
Trichlorotrifluoroethane	CFC 113	43	72	74	250	91	62	111
Dichloromethane		14	82	7.5	200	n.d.¶	n.d.	n.d.
1,1- Dichloroethene	DCE	34	36	22	180	n.d.	n.d.	n.d.
1,2- Dichloroethane		18	57	2.1	74	n.d.	n.d.	n.d.
1,2- Dichloropropane		25	42	1.2	73	n.d.	n.d.	n.d.
Tetrachloroethene	PCE	84	59	37	54	n.d.	n.d.	n.d.
Chloroform		19	34	2.1	41	n.d.	n.d.	n.d.
Trichlorofluoromethane	CFC 11	26	18	23	34	4.8	4.8	6.5
1,1 - Dichloroethane		23	38	2.8	32	n.d.	n.d.	n.d.
Carbon Tetrachloride		2.4	11	1.6	17	n.d.	n.d.	n.d.
Benzene		b.d.§	3	b.d.	15	n.d.	n.d.	n.d.
Dichlorodifluoromethane		2.9	3.3	3.7	10	n.d.	n.d.	n.d.
Toluene		6.8	4	3.7	2.6	n.d.	n.d.	n.d.
Acetone		3.5	b.d.	b.d.	b.d.	n.d.	n.d.	n.d.

[1]Data from J. Sollid, Los Alamos National Laboratory.
† Adsorption gas samples analyzed by Thermal Desorption Gas Chromatography - Mass Spectroscopy.
‡ Analysis by down-well Photo Acoustic Radiometry (J. Sollid, personal communication)
§ b.d.; Below detection.
¶ n.d.; Not determined.

Table 3. Average colony forming units (CFUs) and direct counts for Los Alamos National Laboratory subsurface materials.[1]

Bore Hole	1/10 TSA	1/2 strength 21 C	King's B	1% PTYG	1/10 TSA, Heat shocked	AODC
			CFU g^{-1}			Cells g^{-1}
54-1009†	<200	<200	n.d.‡	<200	<200	b.d.§
54-1018						
S1	<200	<200	<200	<200	<200	b.d.
S2	3700	6100	7300	3900	<200	$4.5x10^7$

[1] n=3. See methods section for descriptions of media and culture conditions.
† Values represent independent analysis of three depths; 25.9m, 26.2m, and 26.5m.
‡ n.d.; Not determined.
§ b.d.; Below detection.

Table 4. Activity assays measured in subsurface material.

Bore Hole	Nitrification Potential	Respiration	Denitrification Potential
	ug NO_2^- g^{-1} hr^{-1}	ug CO_2-C g^{-1} hr^{-1}	ng N_2O-N g^{-1} hr^{-1}
54-1009†	n.s.‡	n.s.	n.d.§
54-1018			
S1	n.s.	0.015 (0.004)¶ p = 0.004	n.s.
S2	1.9 (0.6) p = 0.05	0.031 (0.005) p < 0.001	13.3 (2.9) p = 0.005

† Values represent independent analysis of three depths; 25.9m, 26.2m, and 26.5m.
‡ n.s.; Not significantly different from zero at p=0.05.
§ n.d.; Not determined.
¶ Values are means (standard error) of three subsamples.

Table 5. Activity assays measured in subsurface material.

Bore Hole	Dehydrogenase Activity	Acetic Acid Utilization	Glutamic Acid Utilization
	ug formazan $g^{-1}hr^{-1}$	%	%
54-1009†	< 0.100	< 0.10	n.d.‡
54-1018			
S1	0.234 (0.008)§	n.d.	0.33
S2	0.229 (0.008)	n.d.	1.91

† Values represent independent analysis of three depths; 25.9 m, 26.2 m, and 26.5 m.
‡ n.d.; Not determined.
§ Values are means (standard error) of three subsamples

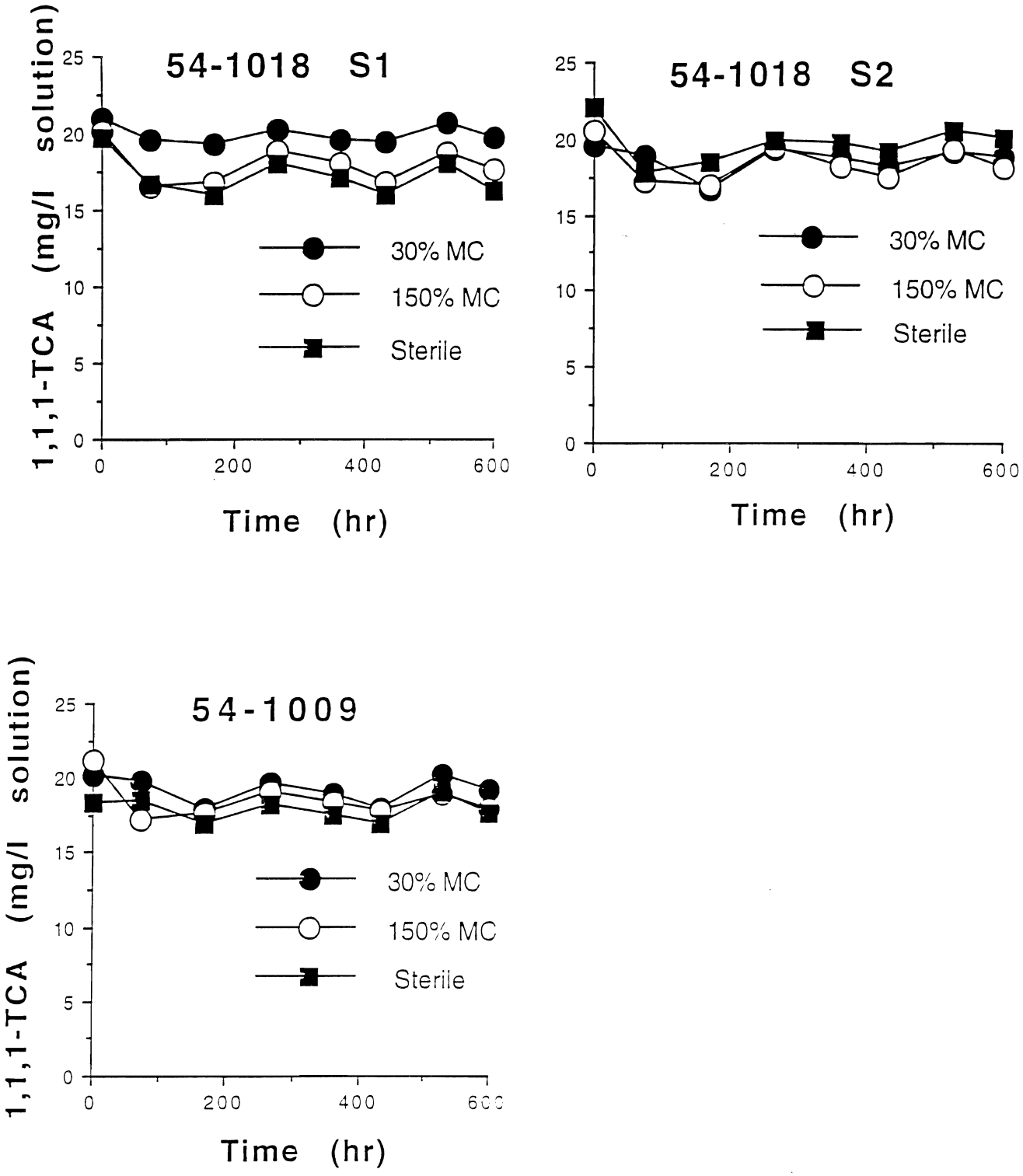

Figure 1. Degradation potential assay. Degradation assay of 1,1,1-TCA subsurface material in batch reactors. One set was performed at 150% moisture content (150% MC) and a second set was performed at 30% moisture content (30% MC). Sterile controls were autoclaved surface material with 150% MC.

Influence of Surfactants on Pyrene Desorption and Degradation in Soils

STEPHANIE L. THIBAULT, MICHAEL ANDERSON AND
WILLIAM T. FRANKENBERGER, JR.
Department of Soil and Environmental Sciences, Riverside Campus

Summary

Global contamination by polycyclic aromatic hydrocarbons (PAHs) is well documented and merits attention due to their toxicity, carcinogenicity, and potential to bioaccumulate (Boldrin et al., 1993; Heitkamp et al., 1988). PAHs in the environment originate from natural and anthropogenic sources. Although pyrene does not manifest carcinogenic characteristics, knowledge of its environmental behavior could increase understanding of the higher molecular weight, carcinogenic PAHs. Several studies have investigated pyrene degradation in pure culture experiments (Atlas, 1981; Boldrin et al., 1993; Grosser et al., 1991; Heitkamp et al., 1988; Walter et al., 1991), but information is lacking regarding its degradation by common soil pseudomonads

Pyrene degrading bacteria were enriched from contaminated soils collected at two sites in Southern California. The degraders were characterized and later identified as *Pseudomonas* spp. Both species were able to use pyrene, naphthalene, phenanthrene, benzoic acid, gentisic acid and protocatechuate as sole carbon sources. Growth curves showed dependence on the rate of pyrene dissolution. Approximately 10 to 25% of the pyrene was mineralized after 10 days when solates were pre-grown on pyrene.

Surfactants increase the concentration of a hydrophobic compound in the aqueous phase by solubilization. Colloidal aggregates (micelles) form at a critical surfactant concentration, providing increased solubilization or emulsification of the hydrophobic compound present. Increasing the compound concentration in the aqueous phase potentially increases its availability for microbial attack or removal by other remediation treatments.

Four surfactants (Simple Green™, Biosolve™, Witconol SN70 and sodium dodecyl sulfate [SDS]) were tested at five concentrations to determine their abilities to solubilize adsorbed pyrene. Their effectiveness, in descending order, was as follows: Witconol SN70 > Biosolve™ > SDS > Simple Green™. Witconol SN70 (0.2% v/v) solubilized 55% of the pyrene, whereas Simple Green™ was ineffective. Witconol SN70 demonstrated the greatest potential for use in remediating PAH-contaminated soils and was used to determine the effectiveness of the surfactant on increasing pyrene availability to microbial attack. Inoculation with pyrene degraders in the presence of Witconol SN70 was the most effective treatment for pyrene mineralization (46-80%) under unsaturated conditions, but the surfactant inhibited the effectiveness of these inoculants in soil slurries.

Key Words: polycyclic aromatic hydrocarbons, bioremediation, pseudomonads

Project Objectives Addressed in 1994-95

This study investigated the effect of surfactant addition on pseudomonad degradation of pyrene in soil.

Research Plan and Procedures

Soil samples were collected from Southern California. Soil (B) was obtained as a composite sample from a PAH-contaminated site in Riverside, California located adjacent to a railroad track. The second soil (K) was also a composite sample collected from a PAH-contaminated soil located near abandoned coke ovens in Fontana, California. Soil samples were kept at 4°C in Teflon containers during storage. After mixing, the soils were sieved to <2 mm. Total carbon was determined by dichromate oxidation (Nelson and Sommers, 1982), total nitrogen by the semimicro-Kjeldahl method (Bremner, 1965) and particle size analysis by the hydrometer method (Day, 1965). The pH and electrical conductivity were measured from a saturation paste extract. Table 1 provides the soil characteristics of the samples collected at each site.

Organisms capable of using pyrene as a sole source of carbon were isolated by enrichment culture from contaminated soils K or B and designated K-12 or B-24 depending on the soil from which they originated. Isolates were routinely maintained on a minimal salts medium (MSM) containing the following : 10 mM K_2HPO_4; 3 mM NaH_2PO_4; 10 mM $(NH_4)_2SO_4$; 1 mM $MgSO_4$; 0.1 mM $Ca(NO_3)_2$; 0.01 mM $Fe(NO_3)_3$; and a trace mineral solution containing; 0.001 mM $MnSO_4$; 0.001 mM $ZnSO_4$; 0.001 mM $CuSO_4$; 0.0001 mM $NiSO_4$; 0.0001 mM $CoSO_4$; 0.0001 mM Na_2MoO_4 with a final pH of 7.3. A 10 g soil sample was added to a 125 ml Erlenmeyer flask containing 100 ml of MSM spiked with 500 mg L^{-1} ^{14}C-labeled pyrene (specific activity: 32.3 mCi/mmol) (Aldrich, Milwaukee, WI) and placed on a rotary shaker (180 rpm) at 27°C. Following several transfers, those with continued turbidity were plated onto sterile mineral salts agar (MSA) containing MSM, agar (1.5%), and pyrene. Pyrene was aseptically sprayed onto the surface of the MSA plates in hexane:acetone (1:1) and colony formation was indicated by zones of clearing (Heitkamp et al., 1988).

Colonies from pyrene-containing MSA plates were streaked onto tryptic soy agar (TSA) plates and sent to the University of Auburn for identification.

Isolates' ability to use other compounds as growth substrates were determined. Phenanthrene, naphthalene, anthracene, fluoranthene, catechol, protocatechuate, gentisic acid, benzoate, *trans*-cinnamic acid and salicylic acid (50 mg) were added separately to 250 ml Erlenmeyer flasks and incubated in the dark on a rotary shaker (130 rpm) at 30°C. Growth was indicated by appearance of turbidity. Non-inoculated controls were employed to insure that turbidity was due to growth and not polymerization of media constituents.

Four surfactants, Simple Green™ (Sunshine Makers, Inc., Huntington Harbor, CA), Biosolve™ (Western States Biosolve, Huntington Beach, CA), Witconol SN70 (Witco Corporation, Houston, TX), and dodecyl sodium sulfate (SDS) (Fisher Scientific, Pittsburgh, PA), were tested for their effectiveness in desorbing pyrene. Critical micelle concentrations (CMC) were determined using a Nima TS9000 surface tensiometer (Coventry, England). Surfactant concentrations tested ranged from their CMC to 2X, 5X, 10X, and 20X the CMC. Sterile, deionized water was used as the control. An equilibrium slurry was prepared as previously described (Aronstein and Alexander, 1992). Preliminary experiments determined that equilibrium between solution and soil phases was reached after approximately 20 h. Samples were then counted on a Beckman LS 5000TD liquid scintillation counter (Beckman Instruments, Inc., Fullerton, CA). Experiments were also conducted in tandem to determine whether the concentration of surfactant was altered in the presence of the soil.

The effectiveness of Witconol SN70 and bacterial inoculation on pyrene degradation was investigated under both unsaturated (field-moist) and soil slurry conditions. Radiolabeled pyrene (0.45 mCi; 100,000 dpms) and 100 mg unlabeled pyrene were added to 500 ml Erlenmeyer flasks containing 25 g of air-dried (B) or (K) soil. Flasks then received the following treatments: K-12 or B-24 bacterial isolates, Witconol SN70 or the combination of a bacterial isolate plus the surfactant, Witconol SN70. The control consisted of untreated sample relying on the indigenous microbial population to degrade pyrene. Witconol SN70 was applied at a final concentration equal to 20X CMC (0.2% vol/vol). The bacterial isolate was added to a give a final density of 10^8 cells g^{-1} soil. The soil was maintained at field-moist conditions (12.5% vol/wt) or saturated (65 parts H_2O:35 parts soil) at 22±3°C for six weeks of incubation. Flasks were closed with Teflon lined stoppers and KOH was used to trap $^{14}CO_2$. Soil slurries were placed on a rotary shaker at 130 rpm. At appropriate time intervals, an aliquot of KOH was removed, added to 5 ml Liquiscint, and counted on a liquid scintillation counter.

On the basis of motility, Gram stain, oxidase, catalase, and pigment production, both isolates were determined to be pseudomonads. Biolog GN plates were inoculated with suspensions of both isolates in order to check the Biolog database for agreement with the identification by classical methods (Hensyl, 1994). Bacterial identification was confirmed by University of Auburn fatty acid analysis.

Turbidity increases were noted for both isolates in the presence of naphthalene, phenanthrene, benzoic acid, protocatechuate and gentisic acid. The K-12 isolate also displayed increased turbidity with anthracene, fluoranthene and *trans*-cinnamic acid as the sole carbon source; whereas, B-24 turbidity was enhanced on salicylic acid.

Linear growth was observed for both isolates when grown on pyrene, suggesting rate-limiting availability of the substrate into the aqueous phase. The solubility of pyrene has been determined to be 0.135 mg L^{-1} (Mackay and

Shiu, 1977). Doubling times for K-12 and B-24 isolates were 53.3 (r^2=0.94) and 49.5 h^{-1} (r^2=0.94), and growth rates were 0.014 and 0.013 h^{-1}, respectively (Fig. 1).

The CMCs for each surfactant were determined: Simple Green, 0.01%; SDS, 0.3%; Biosolve, 0.05%; and Witconol SN70, 0.01%. The overall efficacy of the surfactants on pyrene desorption increased with increasing concentration. The effectiveness of each surfactant in descending order (at 20X CMC) was as follows: Witconol SN70 > SDS > Biosolve > Simple Green (Table 2). No significant differences were observed for pyrene desorbed by Simple Green at the varying concentrations tested. Also of interest was that maximum desorption occurred after approximately 2 hours. As previously noted, equilibrium was attained after approximately 20 h in this study.

Partition coefficients were calculated using equations derived by Edwards et al. (1991) and were determined to be 3.25 for SDS and 4.17 for Witconol SN70. Partition coefficients were not calculated for Biosolve or Simple Green since their molecular weights were unavailable.

Results and Discussion

Unsaturated soil (B) exhibited enhanced mineralization upon treatment with the bacterial inoculant K-12 plus Witconol SN70 (60%) when compared to the isolate alone (48%) and no amendment (5%) (Fig. 3). The addition of bacterial isolate B-24 plus Witconol SN70 increased pyrene mineralization 43% over the untreated controls. Unsaturated soil (K) treatments containing K-12 and B-24 isolates with and without the surfactant, mineralized more pyrene than those treatments containing just the surfactant or the nontreated control (Fig. 4). The K-12 inoculant plus Witconol SN70 showed maximum pyrene mineralization of 80%.

Under saturated conditions, soil (B) treatments consisting of bacterial inoculations by K-12 or B-24 significantly increased pyrene mineralization relative to non-inoculated samples with maxima for both at 75% (Fig. 3). Soil (K) slurries showed 63% mineralization of pyrene upon inoculation with K-12 and B-24 (Fig. 4). The control mineralized 50% of the added pyrene. The presence of the surfactant under saturated conditions inhibited mineralization of pyrene in both soils.

Mineralization of lower molecular weight PAHs is well documented, however, only a few bacterial species have been reported as pyrene degraders (Boldrin et al., 1993; Cerniglia et al., 1986; Grosser et al., 1991; Heitkamp et al., 1988; Volkering et al., 1992). In one study, a *Mycobacterium* sp. was isolated from contaminated sediments and found to be subject to enzyme induction upon exposure to pyrene (Heitkamp et al., 1988). The *Mycobacterium* sp. grown in the presence of pyrene and dosed with chloramphenicol, to inhibit protein synthesis, mineralized significantly less pyrene. Isolate B-24 in this study showed significantly more pyrene mineralization when pre-grown in

pyrene (Fig. 2). Chloramphenicol was also added as a treatment to determine if enzymes were induced, but both K-12 and B-24 isolates were resistant to chloramphenicol at the concentration used (25mg ml^{-1}). The overall mineralization maxima of K-12 in pure culture was less than isolate B-24 even though the pyrene concentration was originally high in the K soil. The two *Pseudomonas* spp. isolated from soil (K) and soil (B) have yet to be studied regarding pathways and metabolic intermediates.

Growth rates measured for the *Pseudomonas* isolates were 0.014 and 0.013 h^{-1} for K-12 and B-24, respectively. Boldrin et al. (1993) reported a growth rate of 0.056 h^{-1} for a *Mycobacterium sp.* grown on pyrene and Walter et al. (1991) reported that *Rhodococcus* UW1 had a growth rate of 0.023 h^{-1}. Pyrene crystal size was shown to greatly influence pyrene degradation rates of the *Mycobacterium* sp. The smaller the crystal, the faster the growth rate. It has been suggested that crystal size can greatly effect the rate of dissolution between aqueous and solid phases (Stucki and Alexander, 1987; Thomas et al., 1986; Volkering et al., 1992).

Adsorption of pyrene onto soils is due to its hydrophobicity and is tempered in part by the fraction of organic carbon present in soil. The soil used in this experiment had an organic carbon content of 0.33%. Only 1.3% of the pyrene was detectable in the aqueous phase after equilibrium was obtained. Since pyrene is hydrophobic, it tends to be concentrated in the hydrophobic core of the surfactant micelle formed. It would therefore be desirable to choose a surfactant which, upon micellization, creates a large core and can solubilize more of the contaminant (Harwell, 1992). The log K_{OW} for pyrene is 5.18. The partition coefficients for SDS (3.25) and Witconol SN70 (4.17) indicate that these surfactants are effective in partitioning pyrene into the hydrophobic core of the micelle, with Witconol SN70 being more effective in its partitioning. Witconol SN70 is an alcohol ethoxylate (nonionic) which is biodegradable and does not cause soil dispersion (Abdul et al., 1990). These properties, along with its low CMC and its success in desorbing pyrene, make it an ideal candidate for remediation strategies of pyrene-contaminated unsaturated soils. Conversely, SDS has a higher CMC, causes some dispersion of soil colloids (probably due to the presence of the Na^+), and is therefore much less cost effective than the other surfactants tested. Several studies have suggested the effectiveness and use of surfactants at low concentrations or at concentrations below their CMCs to increase desorption and stimulate bioremediation (Aronstein and Alexander, 1992; Aronstein et al., 1991; Kile and Chiou, 1989); however, in preliminary studies we found that values at 1/2 CMC were not effective in desorbing pyrene. Both Biosolve™ and Simple Green™ are reported to be biodegradable and are not expensive.

Unsaturated soil conditions were investigated along with soil slurries since PAH contamination often occurs in the vadose zone and in groundwater. Treatments containing the inoculants and Witconol SN70 under field-moist conditions mineralized more pyrene than treatments of the inoculant without the surfactant. In a similar experiment, unsaturated hydrocarbon-containing

columns were washed with various surfactants and found to increase pyrene removal compared to unamended treatments (Scheibenbogen et al., 1994). Very few researchers have investigated the effects of surfactants on pyrene or on PAH mineralization under field-moist conditions. Our results show that more research is warranted.

The increase in mineralization observed for the inoculated bacterial treatments under soil slurry conditions could be attributed to an increase in compound availability due to agitation (Aronstein and Alexander, 1992). Since the percent of pyrene mineralized under soil slurry conditions was greater than that in pure culture, we surmise that the microbes may have enjoyed increased contact with the pyrene while preferring to anchor to soil particles. The application of the surfactant alone or in combination with the bacterial isolates did not promote mineralization of pyrene under soil slurry conditions for both soils. An adjunct experiment showed that isolate B was not adversely affected by the high concentrations of Witconol SN70 and did not use the surfactant as a carbon source under study conditions. From this result we conclude that the suppresion of pyrene mineralization under soil slurry conditions is not attributed to the preferential use of surfactant as a substrate. It may, however, be attributed to increased pyrene desorption and solubilization and therefore an increase in toxicity. In addition, it is possible that the native soil populations in the control treatments could have utilized the surfactant as a substrate and fortuitously utilized the pyrene, yielding higher mineralization rates than inoculated treatments containing surfactant. It has been reported that the degradation of phenanthrene was inhibited by the addition of a nonionic surfactant above the CMC (Laha and Luthy, 1991) and perhaps greater mineralization of pyrene could have been obtained under saturated conditions by using a lower surfactant concentration. However, naphthalene mineralization was shown to be unaffected by the addition of nonionic surfactants above their CMC (Liu et al., 1995).

Since available information regarding the biodegradation of pyrene in soils is limited, investigations of its environmental fate are needed. Because pseudomonads are competitive in soil environments, they may be able to survive upon inoculation into contaminated soils. The ability of these two isolates to utilize not only pyrene but other PAH compounds and some of their metabolic intermediates, suggests broad substrate specificity in the remediation of PAH-contaminated soils.

This study reveals that inoculation of pyrene degraders in the presence of a surfactant can increase mineralization of pyrene under unsaturated conditions. However, soil slurries were most effective with the inoculation of pyrene degraders without the added surfactant, indicating that the surfactant had some biostatic properties inhibiting mineralization.

References

Abdul, A. S., T. L. Gibson and D. N. Rai. 1990. Selection of surfactants for the removal of petroleum products from shallow sandy aquifers. Ground Water. 28:920-926.

Aronstein, B. N. and M. Alexander. 1992. Surfactants at low concentrations stimulate biodegradation of sorbed hydrocarbons in samples of aquifer sands and soil slurries. Environ. Toxicol. Chem. 11:1227-1233.

Aronstein, B. N., Y. M. Calvillo and M. Alexander. 1991. Effect of surfactants at low concentrations on the desorption and biodegradation of sorbed aromatic compounds in soil. Environ. Sci. Technol. 25:1728-1731.

Atlas, R. A. 1981. Microbial degradation of petroleum hydrocarbons: An environmental perspective. Microbiol. Reviews. 45:180-209.

Boldrin, B., A. Tiehm and C. Fritzsche. 1993. Degradation of phenanthrene, fluorene, fluoranthene, and pyrene by a *Mycobacterium* sp. Appl. Environ. Microbiol. 59:1927-1930.

Bremner, J. M. 1965. Total Nitrogen, p. 1171-1173. *In* C.A. Black (ed.), Methods of Soil Analysis, Part 2. Chemical and Microbiological Properties. Am. Soc. Agron., Inc., Madison, WI.

Cerniglia, C. E., D. W. Kelly, J. P. Freeman and D. W. Miller. 1986. Microbial metabolism of pyrene. Chem. Biol. Interactions. 57:203-216.

Day, P. R. 1965. Particle Fraction and Particle-Size Analysis., p. 548-567. *In* C.A. Black (ed.), Methods of Soil Analysis, Part 2. Chemical and Microbiological Properties. Am. Soc. Agron., Inc., Madison, WI.

Edwards, D. A., R. G. Luthy and Z. Liu. 1991. Solubilization of polycyclic aromatic hydrocarbons in micellar nonionic surfactant solutions. Environ. Sci. Technol. 25:127-133.

Grosser, R. J., D. Warshawsky and J. R. Vestal. 1991. Indigenous and enhanced mineralization of pyrene, benzo[a]pyrene, and carbazole in soils. Appl. Environ. Microbiol. 57:3462-3469.

Harwell, J. H. 1992. Factors affecting surfactant performance in groundwater remediation applications., p. 124-132. *In* D.A. Sabatini and R.C. Knox (ed.), Transport and Remediation of Subsurface Contaminants: Colloidal, Interfacial, and Surfactant Phenomena. American Chemical Society, Washington, DC.

Heitkamp, M. A., W. Franklin and C. E. Cerniglia. 1988. Microbial metabolism of polycyclic aromatic hydrocarbons: Isolation and characterization of a pyrene-degrading bacterium. Appl. Environ. Microbiol. 54:2549-2555.

Hensyl, W. R. 1994. Bergey's Manual of Determinative Bacteriology., p. *In* W.R. Hensyl (ed.), Williams and Wilkins, Baltimore, Maryland.

Kile, D. E. and C. T. Chiou. 1989. Water solubility enhancements of DDT and trichlorobenzene by some surfactants below and above the critical micelle concentration. Environ. Sci. Technol. 23:832-838.

Laha, S. and R. G. Luthy. 1991. Inhibition of phenanthrene mineralization by nonionic surfactants in soil-water systems. Environ. Sci. Technol. 25:1920-1930.

Liu, Z., A. M. Jacobson and R. G. Luthy. 1995. Biodegradation of naphthalene in aqueous nonionic surfactant systems. Appl. Environ. Microbiol. 61:145-151.

Mackay, D. and W. Y. Shiu. 1977. Aqueous solubility of polynuclear aromatic hydrocarbons. J. Chem. Eng. Data. 22:399-402.

Nelson, D. W. and L. E. Sommers. 1982. Total carbon, organic carbon and organic matter., p. 539-580. *In* A.L. Page (ed.), Methods of Soil Analysis, Part 2. Am. Soc. Agron., Inc., Madison, WI.

Scheibenbogen, K., R. G. Zytner, H. Lee and J. T. Trevors. 1994. Enhanced removal of selected hydrocarbons from soil by *Pseudomonas aeruginosa* UG2 biosurfactants and some chemical surfactants. J. Chem. Tech. Biotechnol. 59:53-59.

Stucki, G. and M. Alexander. 1987. Role of Dissolution Rate and Solubility in Biodegradation of Aromatic Compounds. Appl. Environ. Microbiol. 53:292-297.

Thomas, J. M., J. R. Yordy, J. A. Amador and M. Alexander. 1986. Rates of dissolution and biodegradation of water-insoluble organic compounds. Appl. Environ. Microbiol. 52:290-296.

Volkering, F., A. M. Breure, A. Sterkenburg and J. G. van Andel. 1992. Microbial degradation of polycyclic aromatic hydrocarbons: Effect of substrate availability on bacterial growth kinetics. Appl. Microbiol. Biotechnol. 36:548-552.

Walter, J., M. Beyer, J. Klein and H. J. Rehm. 1991. Degradation of pyrene by *Rhodococcus sp* UW1. Appl. Microbiol. Biotechnol. 34:671-676.

Table 1. Soil characteristics from which K-12 and B-24 bacterial isolates were enriched on pyrene.

Isolate	pH	Org. C (%)	Pyrene mg kg^{-1}	Total N (%)	EC_e (dSm^{-1})	Sand (%)	Silt (%)	Clay (%)	Textural Class
K-12	7.6	2.92	17000	0.01	6.2	80	7.5	12.5	sandy loam
B-24	7.8	0.33	-*	0.04	1.3	67.5	22.5	10	sandy loam

*below detection limits

Table 2. Percent of pyrene solubilized by each surfactant at the critical micelle concentration (CMC) and at 2X, 5X, 10X, and 20X CMC.

Conc.	SDS	Simple Green	SN-70	Biosolve
Water	1.75±0.15*	4.69±0.05	6.74±0.35	1.63±0.22
CMC	1.78±0.12	5.39±0.22	8.60±3.41	1.59±0.26
2X CMC	7.47±2.08	5.05±0.32	7.32±0.38	1.72±0.26
5X CMC	13.26±1.48	5.05±0.52	18.71±6.52	3.55±2.13
10X CMC	18.70±4.13	4.61±0.29	44.85±2.86	8.63±2.27
20X CMC	18.32±2.02	5.89±0.42	55.60±1.75	17.61±1.61

*Standard deviation

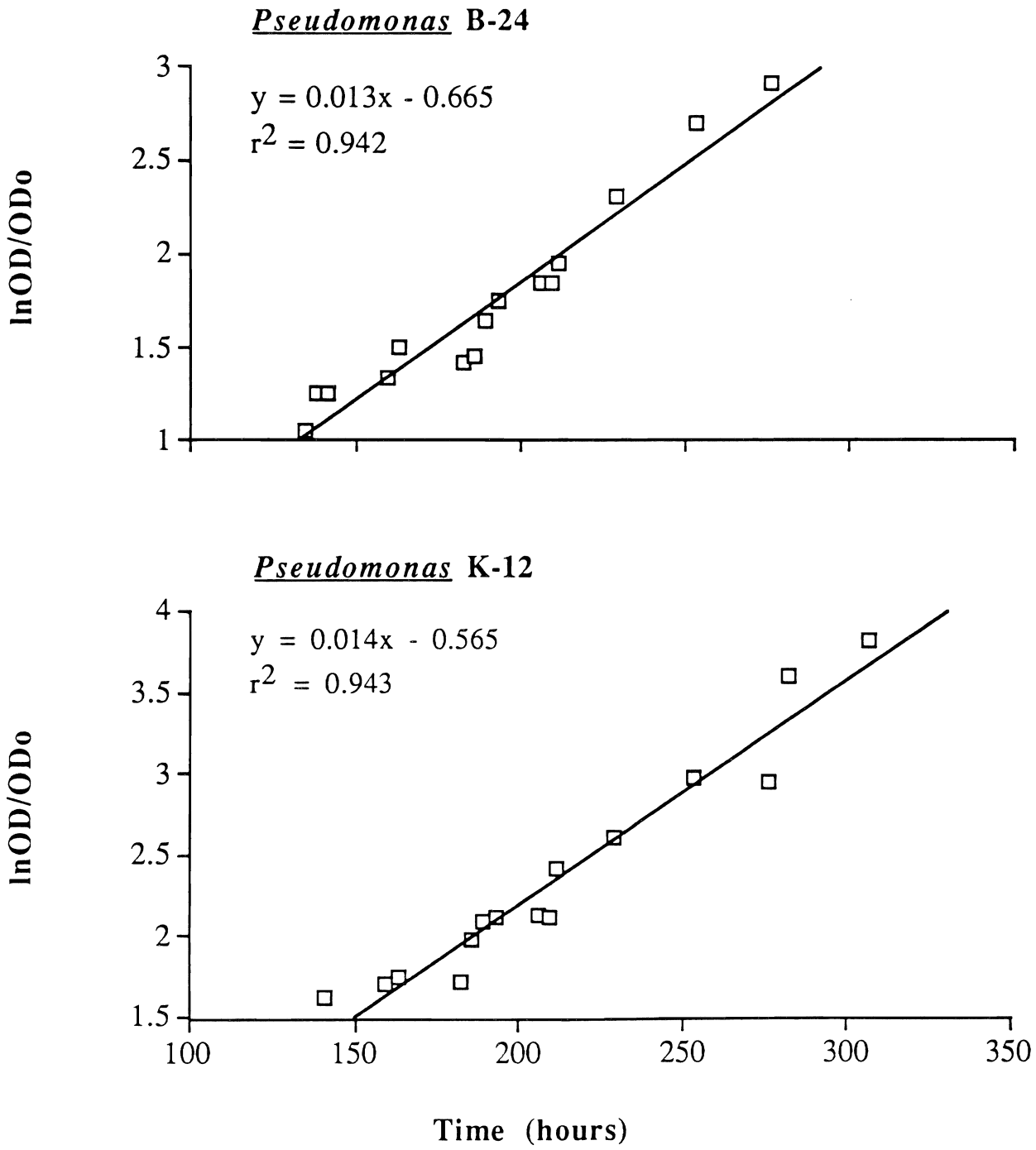

Figure 1. Linear growth curves determined from the natural log of opitcal density (OD) over initial optical density (OD_o) for both isolates, *Pseudomonas* B-24 and K-12.

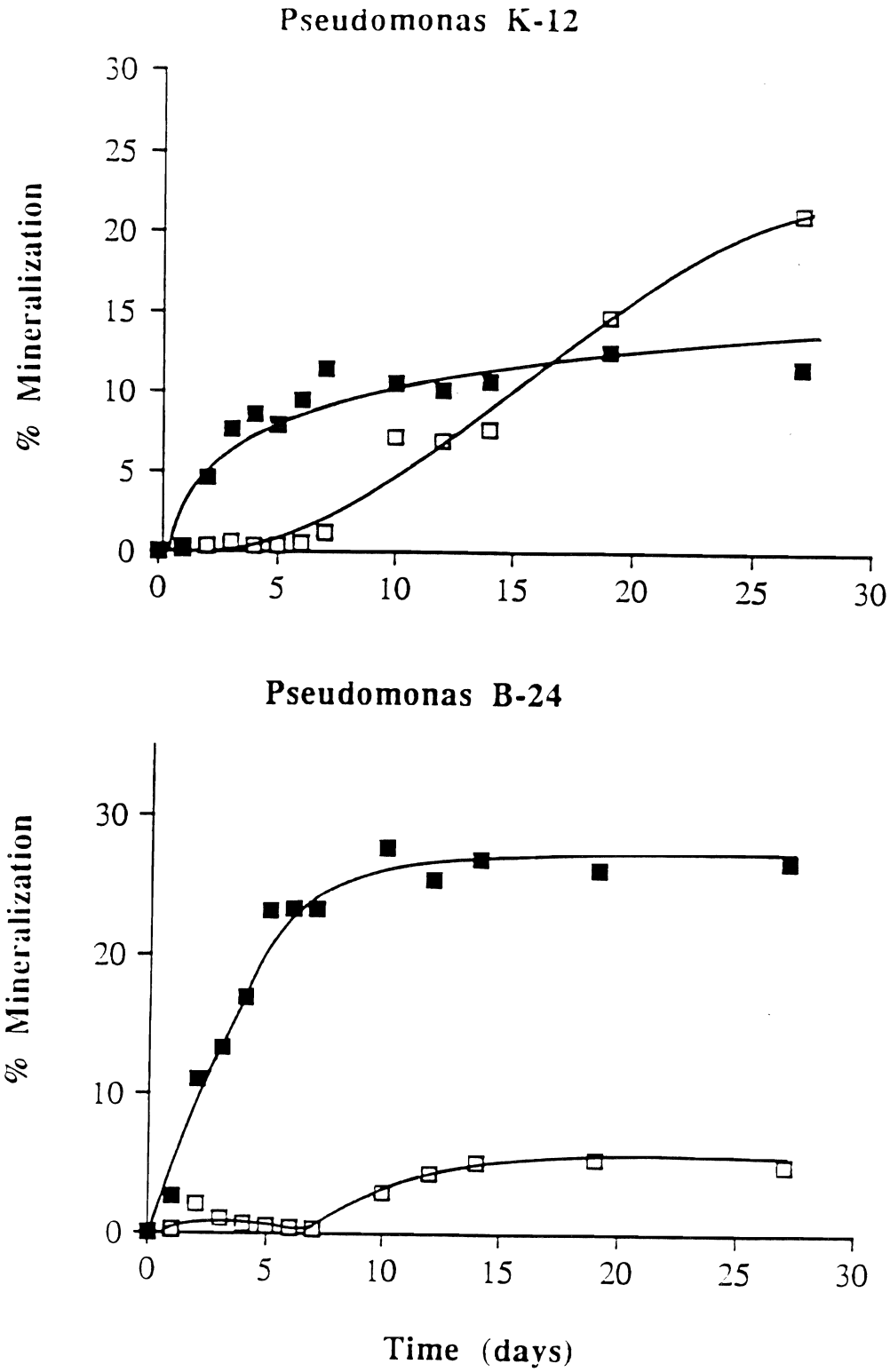

Figure 2. Percent mineralization of ^{14}C-pyrene in culture solutions. K-12 and B-24 isolates pre-grown in the absence of pyrene (-□-) and pre-grown in the presence of pyrene (-■-).

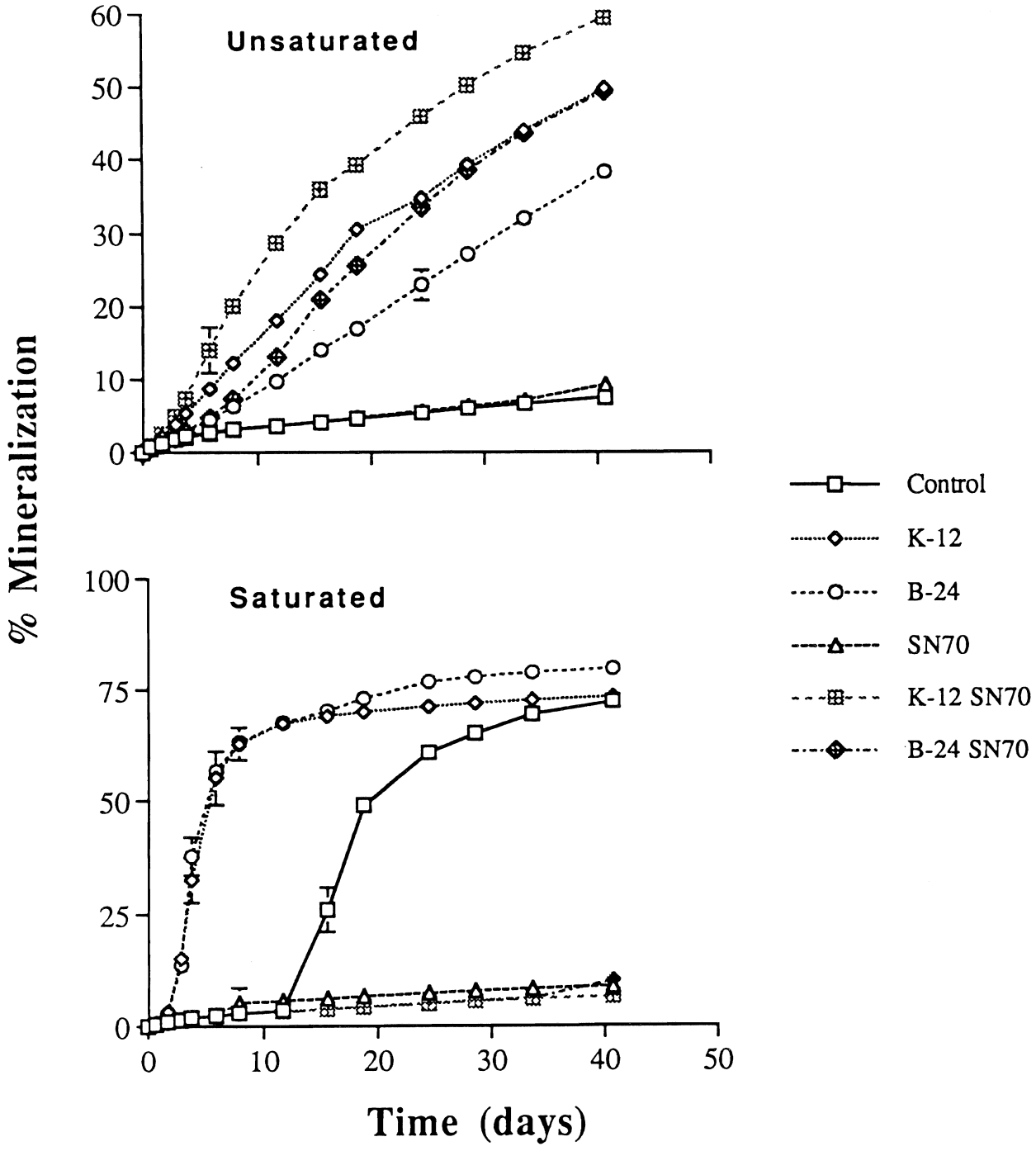

Figure 3. Mineralization of pyrene upon application of bacterial inoculants (K-12 and B-24), addition of surfactant (Witconol SN70), or the combination of treatments in unsaturated and saturated B soil.

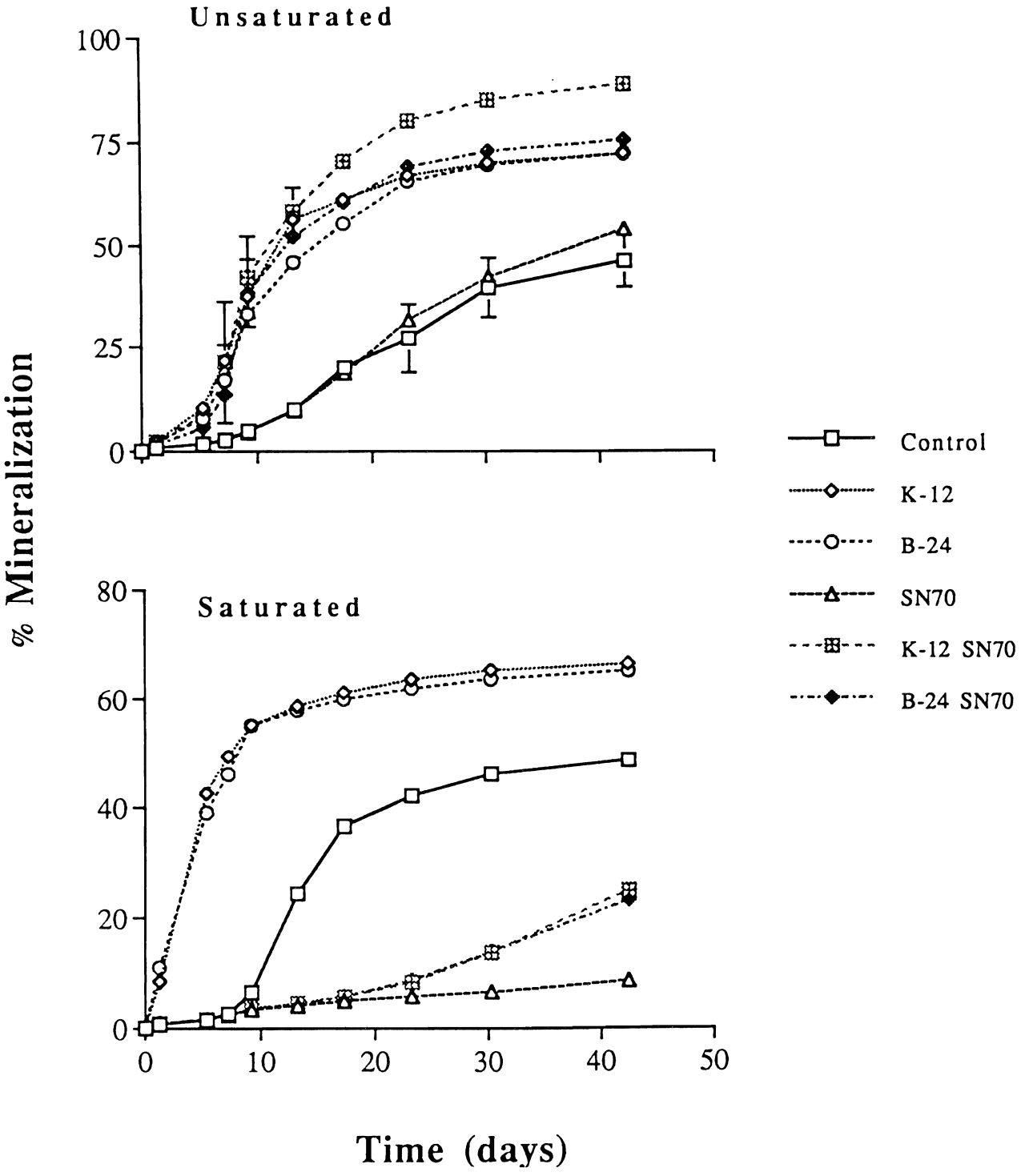

Figure 4. Mineralization of pyrene upon application of bacterial inoculants (K-12 and B-24), addition of a surfactant (Witconol SN70), or the combination of treatments in unsaturated and saturated K soil.

An Integrated Approach to Bioremediation of Pesticide-Contaminated Hazardous Waste Sites.

ARTHUR L. CRAIGMILL[1], DAVID E. CROWLEY[2], MICHAEL STIMMANN[1], DAVID HINTON[3], PETE CLARK[2], MARCIA SALAZAR[2], SCOTT WETZLICHS[1], TIM ARNDT[1], CAROL FRATE[4], AND STEVE WRIGHT[4]

[1]*Department of Environmental Toxicology, Davis Campus;*
[2]*Department of Soil and Environmental Sciences, Riverside Campus;*
[3]*Department of Veterinary Medicine, Medicine, and Epidemiology, Davis Campus;*
[4]*University of California Cooperative Extension, Tulare County*

Summary

Laboratory and field studies were initiated to evaluate the efficacy of specific bioremediation treatments for cleanup of a highly contaminated pesticide waste site in Tulare County. The primary contaminants on this site were the organochlorine pesticides, DDT and toxaphene, which occurred at concentrations up to 1%. A large field study was initiated to compare pesticide disappearance and soil detoxification in cattle manure-amended soil under flooded and moist, aerobic conditions. In two flooded treatments, one treatment cell was planted with cattails, and another was left unplanted. In three moist, aerobic soil treatments, one cell was planted with barley, another with horseradish, and another left unplanted. A sixth control treatment cell was not irrigated or planted, but was left subject to natural rainfall conditions. Sample collections and microbiological analyses were initiated to monitor disappearance of the contaminants over time. An interim laboratory study examined the effects of two different organic amendments, rice hulls and sewage sludge, on disappearance of the contaminants in soil microcosms under flooded or moist aerated conditions, compared to moist soil with no organic amendment. Results of this study showed that after 3 months of incubation with rice hulls under aerobic conditions, extractable toxaphene was not significantly decreased, but DDT decreased to approximately 50% of the control treatment. Maintenance of flooded conditions in soil without organic matter amendments further decreased extractable DDT, but did not affect the concentration of extractable toxaphene.

Key Words: biodegradation, DDT, toxaphene, phytoremediation

Project Objectives Addressed in 1994-95

1. Establish small plots at the Harmon Field pesticide waste site in Tulare County in areas with high concentrations (>200 ppm) of DDT and toxaphene, amend the plots with organic material (manure) and lime, and measure the effects of growing plants on subsequent pesticide biodegradation.

2. Determine the effects of carbon/nitrogen ratio and substrate quality of soil organic amendments on organochlorine pesticide degradation in the contaminated soils.

3. Field test bioenhancement procedures for stimulating activity of the pesticide degrading microflora using protocols developed from lab and field experiments.

Research Plan and Procedures

Site Selection

In February 1995, the project personnel traveled to the field study site at Harmon Airfield in Pixley, CA and met with county collaborators to plan the field study. Cooperating personnel include

Jim Waters, Environmental Quality Coordinator, Tulare County
Craig Kiefer, Environmental Quality Technician, Tulare County
Thomas Kovac, California Dept. of Health Services, Fresno
Mike Pfister, California Environmental Protection Agency, Fresno

Laboratory Study

Soil samples from a runoff ditch adjacent to the tarmac in front of the cropduster hangar, which had been used as a spray tank wash area, were collected for preliminary analysis of pesticide content and analysis of spatial variability in soil chemical characteristics in this area. Soil was also collected from the ditch for use in laboratory studies conducted to examine the effect of selected organic amendments on disappearance of the contaminants. After transport to the lab, the soil was mixed thoroughly using a split shell mixer and amended with 2% lime to adjust the pH to neutrality. Soil was then amended with 5% sludge or rice hulls, and placed into glass tubes measuring 2.5 cm x 20 cm, sealed on one end with Teflon mesh screen to hold the soil. The tubes were then placed into two Nalgene containers and embedded with sand to support the tubes and maintain uniform environmental conditions. One of the containers was flooded with deionized water and maintained under these conditions for the duration of the experiment. The other container was maintained under moist aerobic conditions by periodic watering. Several treatments were included to test the effect of plants on pesticide disappearance in these microcosms, but the soil was too contaminated to permit plant growth. After 3 months in a plant

growth chamber maintained in a controlled environment at 25°C, the soils were sampled and analyzed for pesticide content by the U.C. Davis (UCD) lab.

Analytical Methods

Considerable time was spent at UCD working on the methods for simultaneous extraction and analysis of toxaphene and DDT. A modification of the U. S. Environmental Protection Agency (EPA) method used to quantitate toxaphene was finally selected as the best procedure. The extraction requires approximately 70 separate steps and takes 2 days to complete prior to GC quantitation. Toxaphene is a highly complex mixture of chlorinated terpenes, made by chlorinating pine sap. The resulting mixture contains at least 177 different compounds (Saleh et al. 1977). The EPA quantitation compares the peak heights of a toxaphene standard with the same peaks in the unknowns. Three peaks are chosen and the average of the comparison is used to quantitate toxaphene. We used 5 different peaks which were well defined and quite separate from the interfering DDT peaks.

Previous work (Mirsatari et al. 1987) has shown that the profile of toxaphene peaks changes as the compound "ages" in the environment. Aged or degraded toxaphene mixtures contain many of the same peaks as a toxaphene standard, but their ratios are different, usually showing a shift in the proportion of later peaks to earlier peaks. These changes also correspond with a decrease in toxicity. Because the profile of the peaks changes, this can radically affect the quantitation, depending on which peaks are chosen. In all of the samples analyzed in this project, we chose 5 peaks which ranged from very early to very late to "bracket" the effects. The peak heights of all 5 were summed, and each individual peak height was converted to a percent of this total. These same peak heights were compared to a standard to determine concentrations, based on individual peaks. The concentrations calculated from each of the 5 peaks were then averaged to yield a final estimated concentration, which is reported in mg kg^{-1} soil.

Field Study

The principal investigators decided to run the field trial using highly contaminated soils only instead of the original plan described in the research proposal that also included low-level contaminated soil. The complexity of pesticide analysis and the possibility of testing more treatment modes were the deciding factors in dropping the low level contamination plots. On June 11, 1995, under the direction of Jim Waters, Environmental Quality Coordinator,Tulare County Department of Health, the field study was begun with the preparation of the soil for placement into tthe treatment cells. A 6x6 m^2 area adjacent to the hangar tarmac was marked, after which the soil within this area was rototilled extensively using a rear-mounted PTO rototiller with a tractor. A mixture of lime (approximately 2% by weight) and dry cow manure (approximately 5% by volume) was added to the soil, which was then rototilled extensively. The mixing process for this small area required about 4 hours of tractor work and resulted in a finely tilled mixture of soil and amendments.

The sites for the placement of the cells were excavated with a backhoe, after which the cells were placed into the holes, and backfilled. The 2 m^2 fiberglass cells were then filled with the mixed soil to a depth of approximately 40 cm. The layout for the field trial cells is shown in Fig. 2. Initial samples were taken for pesticide and soil parameter analysis. Cells 1-3 were maintained under moist, aerobic conditions; cells 4 and 5 were flooded; and cell 6, the control, was maintained under ambient, nonirrigated conditions. Irrigation in cells 1-3 was controlled by an irrigation controller wired to Irrometer tensiometers set at 40 centibars (-0.04 MPa). Because of the remote location and the lack of a 110V source, the controller was run with a 12V deep cycle battery and an inverter. The battery is replaced every two weeks. Water levels in the flooded cells was controlled by a float valve. One week after filling the cells with amended soil, barley seed was planted in cell 3, horseradish roots in cell 1. Approximately 25 cattail stems were introduced to cell 5 in July 1995. Samples were collected and several environmental parameters (pH, EC, DO, CO_2 respiration) were measured monthly since the study began.

Results and Discussion

The site selected for this study, Harmon Field in Pixley, California, is an old airfield that was used primarily by aerial pesticide applicators since 1952. The site occupies 100 acres and has been under investigation by California State regulatory agencies since 1979. In 1985, the Harmon Field was placed on the state Priority Ranking list of hazardous waste sites, and in 1989, the California Department of Health Services issued a Remedial Action Order for its cleanup. An extensive site assessment by a private contractor, hired by Tulare County, showed that there was heavy surface contamination in the top two feet of soil by persistent organochlorine pesticides. Cleanup costs, using excavation and thermal desorption technology, is estimated at more than $5,000,000. As this site is typical of several hundred small airfields located throughout California, the cost for cleanup is a tremendous burden to local county agencies and airfield owners. The objective of our research was to explore bioremediation as an alternative, in situ treatment for decontamination of these hazardous waste sites, which may be accomplished at much lower cost.

Initial characterization of the soil at this site revealed potential problems that challenge bioremediation technology. Not only does the site contain a mixture of contaminants, but the soil itself has very low organic matter content and natural rainfall is sparse, thus, the soil has inherently low microbiological activity. Moreover, soil samples collected within the drainage ditch area leading from the applicator tank washpad had highly variable pH and salinity, even for adjacent soil samples located within a few meters of each other (Fig. 1). In this location, which was excavated for the treatment cells, soil pH varied from as low as 4.2 to as high as 9.2, and salinity measured from 0.2 to 65 dS M^{-1}. The latter value for soil EC is more salty than sea water. Other patches of the soil were covered with sulfur granules that had been discarded on the ground, and there were many bare places where weed or plant growth was absent. Thus, both

physical and chemical characteristics of the site must be significantly modified to enhance microbiological activity and plant growth for bioremediation purposes. To standardize the initial soil conditions and eliminate spatial variation in the contaminant concentrations, the soil was excavated and placed into treatment cells (Fig. 2). This procedure also precluded any possible problems with leaching of the contaminants under flooded soil conditions.

Given the long history of contamination at this site, we hypothesized that the indigenous microflora had considerable time to adapt to the presence of the pesticides, and possibly may have developed the ability to use them as growth substrates. Mineralization of the contaminants might involve either unique degraders or microbial communities, either of which may or may not be culturable in laboratory nutrient media. Another possible mechanism for microbiologically mediated detoxification of the soil would be covalent binding of the contaminants to soil organic matter. This may be accomplished by a variety of soil enzymes including laccases and peroxidases. In either instance, whether degradation and covalent bonding, addition of organic matter amendments or establishing plants should increase the rate of disappearance of the pesticides from the soil. In one of the treatment cells, we examined the feasibility of using horseradish to produce peroxidase, which then could be released into the soil by rototilling the crop into the contaminated soil.

Analytical Method Development

New methodology was developed to simultaneously extract and quantify DDT and toxaphene in contaminated soils. For quantification of toxaphene, 5 highly reproducible peaks were selected after separation of components contained an EPA toxaphene standard by GC (Fig. 3). As the relative proportions of these components change upon aging of toxaphene in soil, concentrations of total toxaphene in extracts from aged contaminated soils were independently quantified 5 times, based on comparison to each of the 5 reference peaks, after which a final average was calculated for each sample. DDT concentrations were calculated based on the total of 5 peaks corresponding to 4,4-DDE; 2,4-DDE; 2,4-DDD; 2,4-DDT and 4,4-DDD; and 4,4-DDT.

Laboratory Study

After the contaminated soil was incubated in glass microcosms for three months, the levels of extractable DDT and its isomers significantly decreased in soil amended with organic matter and in soil without organic matter maintained under anaerobic conditions (Table 1). Under aerobic conditions in moist soil, addition of rice hulls or sewage sludge resulted in 47 and 54% reductions in total extractable DDT compared to control soil without added organic matter. Simply flooding the soil resulted in a 30% reduction. The greatest effect was achieved in flooded soil amended with rice hulls, which resulted in a striking 65% reduction in extractable DDT.

With toxaphene, sample variability was quite high, and the differences were not statistically significant when tested for by Analysis of Variance. However, similar trends were observed in the soils amended with rice hulls under aerobic, moist conditions, in which there was a 30% decrease in extractable toxaphene compared to soil without added organic matter (Table 2). In soil amended with sewage sludge, extractable toxaphene was 20% less than in the control treatment. In contrast to the results obtained for DDT, flooding the soil had no apparent effect, irrespective of the addition of organic matter. In only one of the flooded, sludge-amended replicates (not shown) was there a noticeable shift in the toxaphene profile consistent with biodegradation. Flooding the soil had little effect on the profiles of the control or rice hull-amended soils (Fig. 4).

Field Study

At the start of the experiment, four samples were taken from each cell and mixed to obtain a uniform sample for each treatment plot. Baseline analyses for toxaphene and DDT are shown in Figs. 5 and 6. Despite the intensive mixing of the soil prior to its placement into the cells, there were relatively large differences in the toxaphene components we chose for quantification, particularly for the lighter peak fractions (Fig. 5). Total toxaphene and DDT concentrations ranged between 250 and 800 mg kg^{-1} for the different cells (Fig. 7).

Samples are being collected monthly for toxaphene and DDT analysis. Microbiological analysis will include measurements of microbial activity using dehydrogenase enzyme assays, biomass measurements, and respiration. Since no toxaphene or DDT degraders have been isolated previously, we do not expect to find individual isolates of degrader organisms that are culturable, but will nonetheless conduct an enrichment culture study to ascertain this possibility.

References

Mirsatari, S. G., M. M. McChesney, A. L. Craigmill, W. L. Winterlin, and J. N. Sieber. 1987. Anaerobic microbial dechlorination: An approach to on-site treatment of toxaphene-contaminated soil. J. Environ. Sci. Health 22:663-690.

Saleh, M. A., W. V. Turner and J. E. Casida. 1977. Polychlorobornane components of toxaphene: structure-toxicity relations and metabolic reductive dechlorination. Science 198:1256-1258.

Table 1. DDT residues (mg kg^{-1} soil) after 3 months of incubation with different organic amendments under flooded and aerobic, moist conditions.

Treatment	4,4-DDE	2,4-DDE	2,4-DDD	2,4-DDT 4,4-DDD	4,4-DDT	Total
no amendment moist	133 (26)	285 (49)	658 (50)	890 (104)	5316 (762)	7281 a (991)
no amendment flooded	117 (3)	225 (8)	501 (22)	663 (6)	3643 (104)	5148 b (143)
rice hulls, moist	77 (19)	175 (30)	333 (41)	515 (62)	2815 (502)	3916 b (653)
rice hulls, flooded	73 (26)	153 (42)	277 (85)	423 (123)	2327 (626)	3253 b (901)
sewage sludge moist	82 (14)	164 (26)	273 (22)	461 (63)	2389 (229)	3369 b (354)
sewage sludge flooded	116 (22)	212 (58)	387 (138)	566 (186)	3111 (1036)	4392 b (1441)

Values in parentheses are standard deviations for treatment means for 3 replicate microcosms. Letters at end of column for total DDT indicate a significant difference ($P>0.05$) by Student-Newman-Keuls All Pairwise Comparison.

Table 2. Soil toxaphene content (mg kg^{-1} soil) after 3 months of incubation with different organic amendments under flooded and aerobic, moist conditions.

Treatment	Mean	
	Flooded	Nonflooded
Control	11,191 (1582)	10,486 (792)
Rice hulls	7,785 (1,536)	7,464 (1,972)
Sewage sludge	9,469 (1,873)	8,907 (2,231)

Values in parentheses are standard deviations for the treatment means for 3 replicate microcosms.

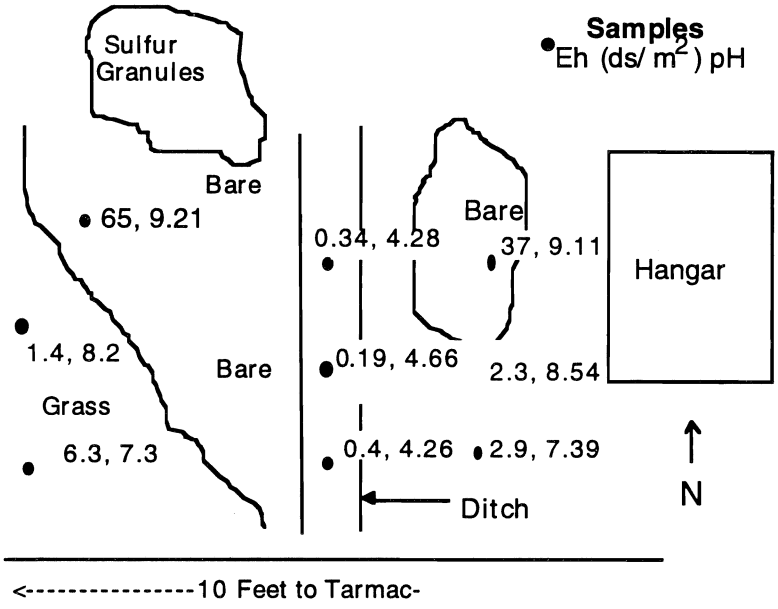

Figure 1. Spatial variability in salinity and pH of soil samples collected in organochlorine pesticide-contaminated soil adjacent to the Earlimart Hangar at Harmon Field, Pixley, CA. Samples taken Feb. 21, 1995.

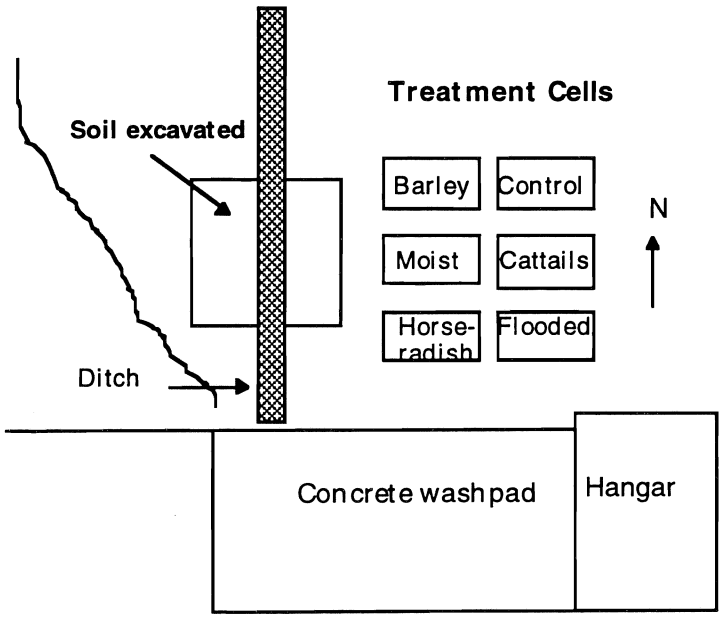

Figure 2. Harmon Field, Pixley California. Treated soil area and treatment cells. Moist cells (barley, horseradish, and no plants) irrigated at -0.04 MPa soil water potential. Cattails and flooded soil cells are continuously submerged.

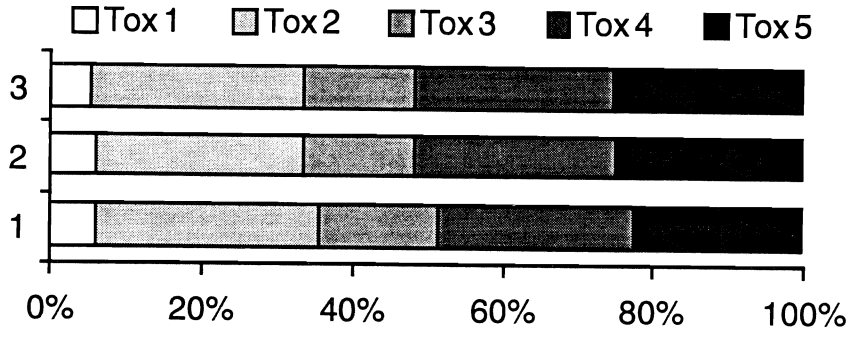

Figure 3. Profile of 5 major components of toxaphene standard assayed for 3 replicate samples.

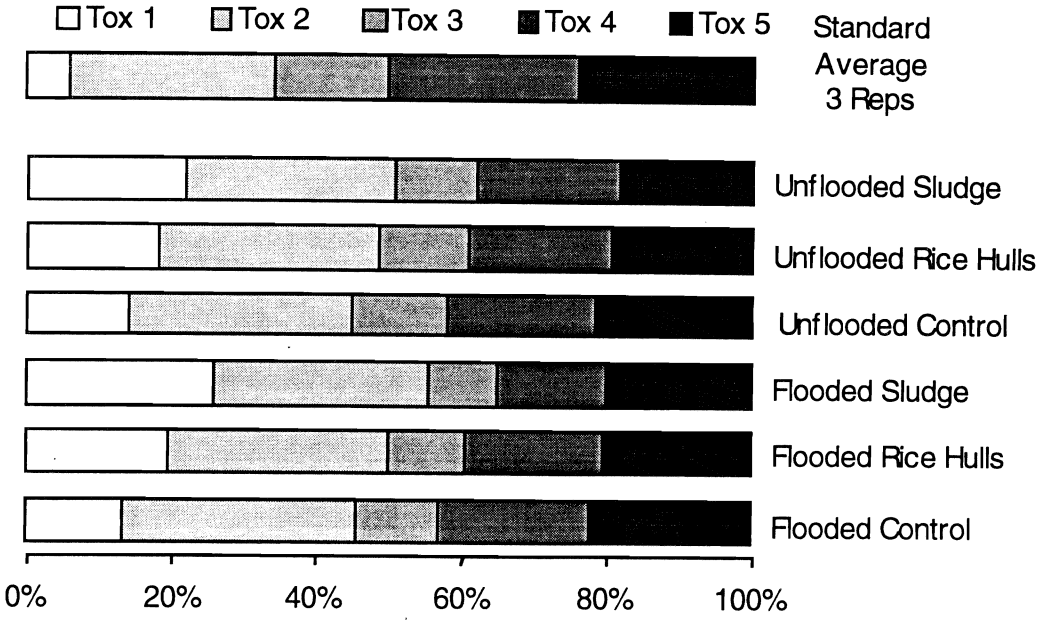

Figure 4. Percent composition of 5 major components of toxaphene after 3 months of incubation with different organic amendments under flooded and aerobic, moist conditions. Shift in composition for lighter molecular weight peak (left) shows aging effect, particularly for samples amended with sewage sludge.

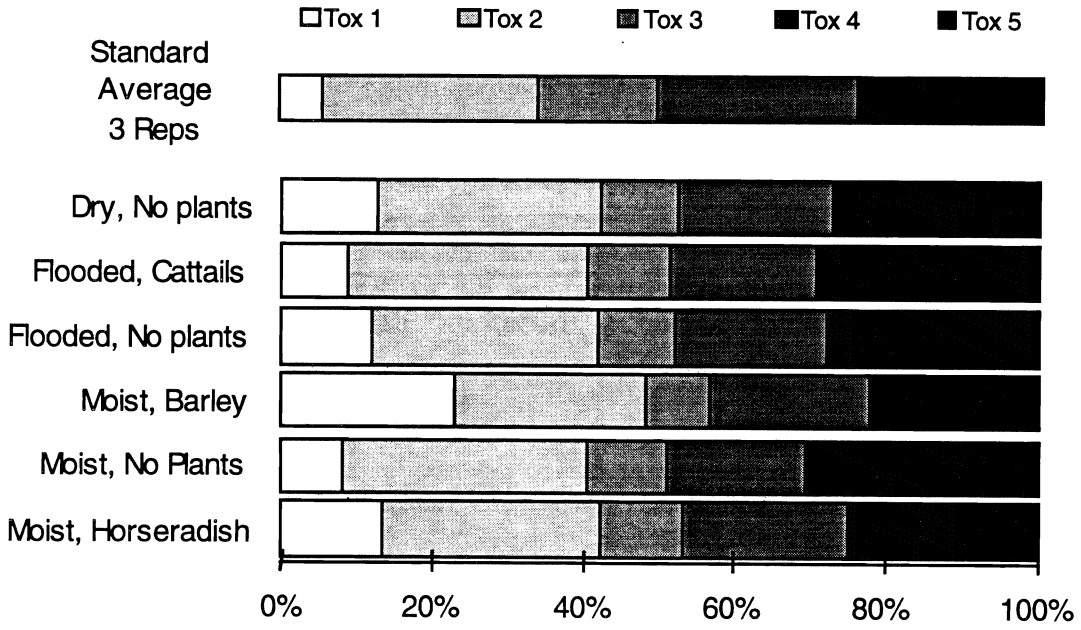

Figure 5. Baseline toxaphene profile (percent composition of 5 major components) for samples from experimental treatment cells at Harmon Field.

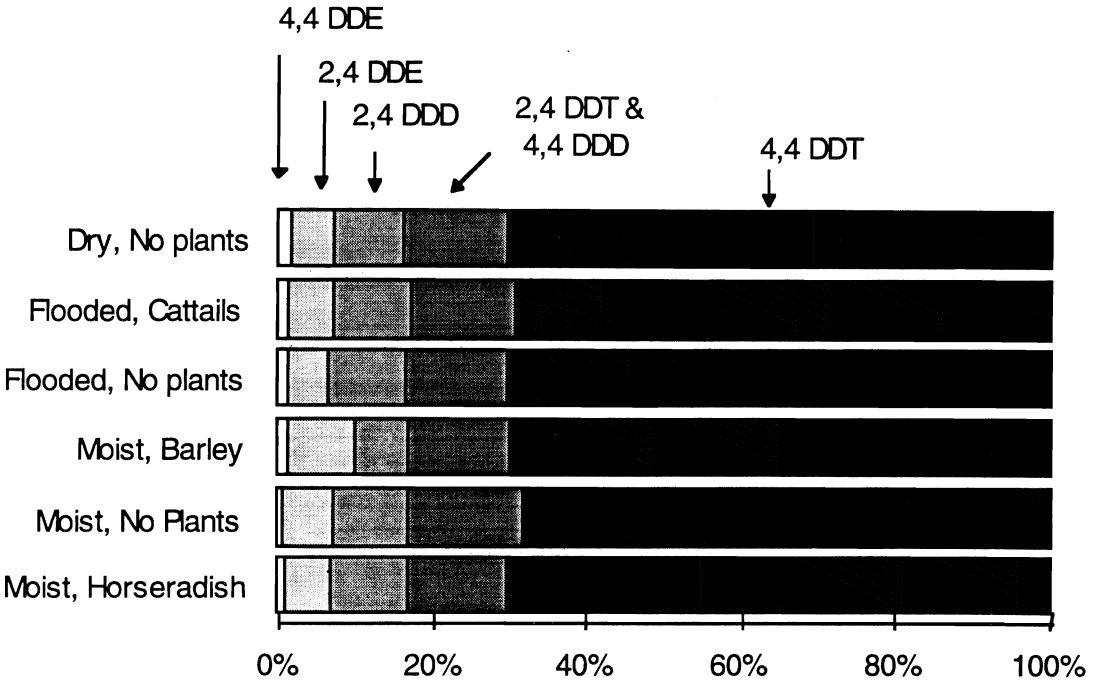

Figure 6. Baseline profile (percent of total) for DDT and selected isomers in experimental treatment cells at Harmon Field.

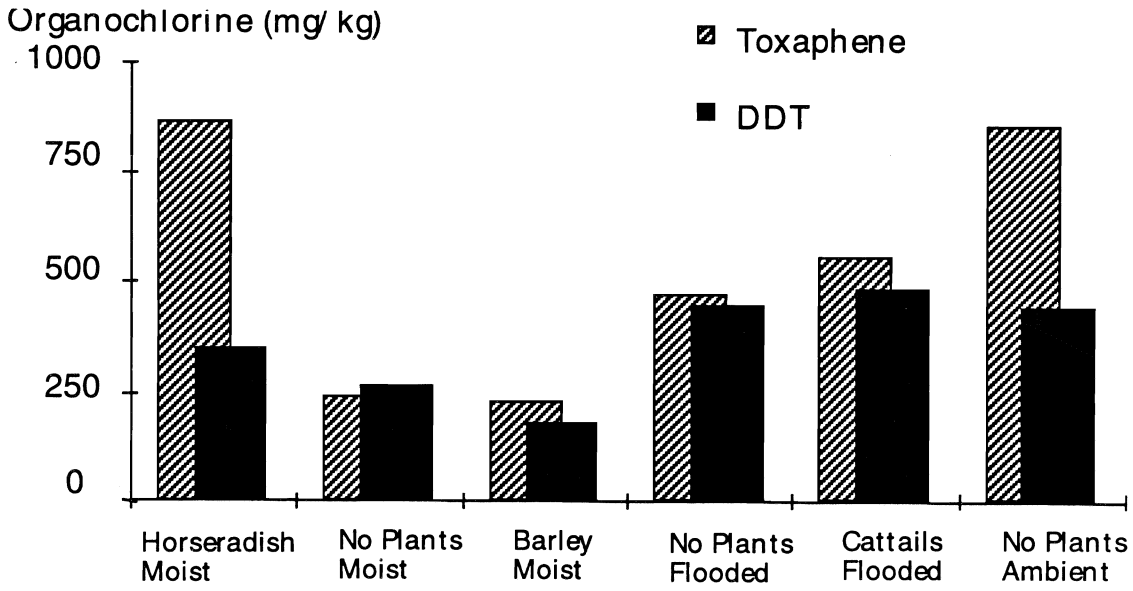

Figure 7. Total toxaphene and DDT in initial soil samples in treatment cells at Harmon Field, Pixley, CA.

Development and Assessment of a Stable Isotope Tracer Method for Determining the Lability of Cadmium Pools in Metal-Contaminated Soils

DAVID R. PARKER AND PAULA J. BOSSERMAN
Department of Soil and Environmental Sciences, Riverside Campus

Summary

The objective of this project is to develop and critically evaluate a stable isotope tracer method for studying the lability of cadmium (Cd) in soils using newly available inductively-coupled plasma mass spectrometry (ICP-MS) technology. Third-year progress includes final optimization of a sequential extraction procedure to operationally define five soil Cd pools. Elemental analyses of the extracted fractions suggest a high degree of reagent specificity. Implementation of a 0.1M NaCl wash between fractionation steps has led to a reassessment of chemical matrix effects on the accuracy and precision of measured isotope ratios (MIRs). The results indicate that three of five fractions are adversely affected by high electrolyte concentrations and that matrix-matched isotope standards do not fully correct for the interferences, particularly at the low Cd concentrations typically recovered. Moreover, the results reveal a previously undetected ^{110}Pd isobaric interference with ^{110}Cd. Preliminary analyses of extracts batch-reacted with Chelex-100 suggest that both matrix and ^{110}Pd interferences are minimized without compromising extracted Cd recovery. Short-term (14 d) incubations have been completed. Most of the tracer disappears from the exchangeable Cd fraction within hours, but continued isotopic exchange with nonexchangeable forms proceeds much more slowly. Long-term (273 d) incubations are nearing completion. Isotopic exchange and equilibration between the operationally-defined Cd pools is evident. Excluding the fractions affected by the ^{110}Pd interference, preliminary results show four kinetically distinctive Cd pools in three of the fractions. The results provide new insights into the reactivity of the various metal pools in contaminated soils and should be useful in situations where cleanup or abatement is required. In addition, these methods represent versatile and powerful new tools for investigating many fundamental aspects of trace element chemistry in the environment and should be applicable to a large number of inorganic soil contaminants.

Key Words: isotopic exchange, isotope ratios, inductively-coupled mass spectrometry, sequential fractionation, matrix interference, isobaric interference, Chelex-100

Project Objectives Addressed in 1994-95

1. To critically evaluate the feasibility and to optimize the experimental design for using stable isotope tracers to study cadmium lability in contaminated soils. Key factors include optimization of the inductively-coupled plasma mass spectrometer (ICP-MS) for measurement of isotopic ratios, and accuracy and precision of these ratios.

2. To conduct analyses for selected elements in the sequential extracts to verify extractant specificity.

3. To optimize sample preparation for MIR analysis by developing protocols to minimize matrix and isobaric interferences by batch reaction with Chelex-100.

4. To conduct short-term (14 d) incubations and long-term (273 d) incubations using four high-Cd soils.

Research Plan and Procedures

All isotopic ratio measurements were made using the VG PlasmaQuad 2 ICP-MS housed in our department. We have found that the following parameters optimized Cd measured isotopic ratios (MIRs) in a 1% HNO_3 matrix: peak jump scan mode, pulse counting detection, a peak dwell of 10.2 msec, and a scan time of 0.18 sec/sweep. All MIRs are based on 10 replicate acquisitions of 30 sec each, such that each determination requires 10 min total (including rinses). Standard ICP-MS protocols are used for measuring natural Cd levels in soils.

We have finalized a protocol for the sequential extraction of the major Cd pools present in each soil (Table 1). Selection of these extractants was largely based on the recent review and evaluation of Shuman (1991), along with a goal of maximizing the specificity of each extraction. The procedure was optimized using the four experimental soils described in last year's report plus two NIST reference soils; basic soil physical and chemical characteristics are reported in Table 2. Following the implementation of a 0.1M NaCl rinse to minimize sample dispersion, we reassessed the effects of "extractant + wash" matrices on the accuracy and precision of total Cd concentrations (Cd_T) and isotope ratio measurements. To establish the validity of the fractionation method, we have conducted selected elemental analyses (Ca, Mg, K, Ti, Al, Fe, Mn, Cu, Zn, Ni, and Cr) of each extracted fraction for each soil to look for "markers" that might indicate poor specificity (e.g., high Fe in the "organic" fraction).

Short-term incubation studies have been completed for each soil. A number of duplicate centrifuge tubes were set up, each containing 2.0 g of soil (ODW basis). A solution containing ^{111}Cd equivalent to 1.0% of the total soil Cd content was added to each tube; the volummetric water content was adjusted to 40% (i.e. field capacity) to limit film diffusion effects. The soils were

incubated at 25°C for 14 d with daily readjustment of water content. After 2, 24, 48, 96, 144, and 336 h, duplicate tubes were extracted with 0.1M $Sr(NO_3)_2$ and the MIRs ($^{111}Cd/^{110}Cd$) determined using ICP-MS.

Long-term incubation studies are nearly complete. For each soil, 300 g of soil (ODW basis) were thinly spread over wax paper and sprayed with a ^{111}Cd solution prepared as above. The soils were thoroughly mixed and quantitatively transferred to uncapped polypropylene bottles. The moisture content was adjusted to field capacity and readjusted every two to three days to simulate field moisture fluctuations. The soils were incubated at 25°C and mixed prior to sub-sampling for sequential extraction. Unspiked, control soils were prepared simultaneously.

Results and Discussion

Finalization of SIT protocols

As reported last year, in order to maximize accuracy and precision in measured isotopic ratios (MIRs), we optimized a number of instrumental and chemical parameters (Janghorbani and Ting, 1989; Russ, 1989). Using the results of whole soil analyses obtained by microwave digestion (Milward and Kluckner, 1989), we identified candidate Cd isotopes for use as the tracer (i.e., the "spike") and as the reference isotope: ^{110}Cd (12.4% natural abundance [NA]), ^{111}Cd (12.8% NA), and ^{112}Cd (24.1% NA). Based on a number of criteria (including absence of isobaric interferences from ^{112}Sn) and experimental results, we had selected ^{111}Cd as the tracer isotope, and ^{110}Cd as the reference.

During the past year, isotope ratio measurements conducted on sequentially-extracted soil fractions revealed a ^{110}Pd isobaric interference with ^{110}Cd, which was previously undetected in the whole soil digests. The interference, which is manifested as a MIR < 1.029 (the value for natural Cd), seems to affect only the oxide and residual fractions for all soils. To test the feasibility of separating Cd from Pd using a cation exchange resin, a sequentially-extracted oxide fraction was batch-reacted with Chelex-100. The MIRs before and after treatment were 1.001 and 1.030, respectively, indicating successful elimination of the ^{110}Pd interference. An analogous method for the purification of the residue fraction is being evaluated.

Following the implementation of the 0.1M NaCl wash used in the sequential extraction procedure, the effects of high electrolyte matrices on the accuracy and precision of measured isotope ratios (MIRs) were reassessed. Whereas matrix-matched standards are satisfactory for correcting matrix/electrolyte interferences and instrumental mass bias for Cd_T analyses, similarly prepared isotope ratio standards do not yield acceptable MIR results. Figure 1 illustrates the nonlinearity of response, and the poor accuracy and precision observed in dilute ^{nat}Cd solutions in a $Sr(NO_3)_2$-NaCl matrix. Similar results are obtained for the carbonate and oxide fractions; the organic and

residual fractions are unaffected. Batch-reaction of the exchangeable and carbonate fractions with Chelex-100 to minimize electrolyte interferences has been optimized, and is now routinely employed.

Optimization of the Sequential Fractionation Procedure

Last year, we adopted a tentative protocol for the sequential extraction of the major Cd pools present in each soil (Table 1). Further investigations and refinements to this procedure were made during the past year and include the following:

1. Prior to fractionation, the soils are air-dried overnight at room temperature and ground to pass through a 150 mm screen.

2. Analysis of ashed filter papers has demonstrated that as much as 9% of extracted Cd may be bound and "lost" to the papers following filtration of high-Cd fractions (e.g. organic). Therefore, following a thorough rinsing with distilled water, we now routinely rinse with 1% HNO_3 to release any adsorbed Cd. Presently, the minimal (< 2%) Cd recovered from ashed filters is reported in the "residue" fraction.

3. To inhibit the formation of a precipitate in the oxide fraction, the volume of 0.1M NaCl employed as a "flocculating wash" has been reduced by half.

4. The exchangeable and carbonate fractions are routinely batch-reacted with Chelex-100 to improve the accuracy and precision of $^{111}Cd/^{110}Cd$ MIR's.

5. Reassessment of the number of treatments with NaOCl required for the optimal removal of soil organic C and recovery of Cd indicate that three rather than five treatments is sufficient for fractionating oxidizable Cd in these soils.

Table 3 summarizes the results of the sequential extraction of the four experimental soils and the National Institute of Standards and Testing (NIST) Certified Reference Material (CRM) soils. The sampling means and standard errors of three extractions (except for Palmerton, n=1) are reported. All soils were extracted in triplicate. The sequential extraction yields consistently good Cd recoveries, and the low standard errors indicate excellent precision.

To establish the validity of the sequential extraction method, the specificity of the extractants was examined. A complete suite of sequential extracts for each soil was analyzed by inductively coupled plasma-absorption emission spectrometry (ICP-AES) for eleven elements (Ca, Mg, K, Ti, Al, Fe, Mn, Cu, Zn, Ni, and Cr). The results are summarized in Fig. 2, and suggest a high degree of specificity. For example, the "carbonate" fraction is high in Ca and Mg, the metals expected to dominate carbonate minerals. Similarly, the majority of the Fe and Al are recovered in the "oxide" fraction, corresponding to hydrous oxides of these metals. Pending mineralogical investigation, we

suspect that the high Zn levels observed in the "organic" fraction of the Penn Mine soil are actually ascribable to the oxidation of Zn-sulfide minerals.

Short-term incubations with stable isotope tracers

Short-term incubation studies using the four experimental soils were completed this year, and measured $^{111}Cd/^{110}Cd$ isotope ratios exhibited similar trends for all soils. After just 2 h of incubation, the measured $^{111}Cd/^{110}Cd$ ratios had declined dramatically (Fig. 3). The results indicate an initially rapid isotopic equilibration with a large fraction of the native soil Cd not extractable with $Sr(NO_3)_2$. Following this initial decrease, a much slower rate of decline (approximately exponential) continued and, after 14d incubation, the $Sr(NO_3)_2$-extractable Cd pool was still quite far from isotopic equilibrium with the entire native Cd pool. These results suggest that each soil contains at least two nonexchangeable Cd pools of differing lability.

Long-term incubations with stable isotope tracers

Long-term incubations are nearly complete and, despite the isobaric and electrolyte interferences, the isotope ratio measurements of the fractions obtained thus far have provided some insight into the kinetics of Cd isotopic exchange and equilibration. As was suggested by the isotopic equilibration kinetics of the short-term incubations, there is evidence for several kinetically distinctive Cd pools. Isotope ratio measurements for the first six weeks of the incubation using the Moreno Valley and Penn Mine soils are shown in Fig. 4, but only the exchangeable, carbonate, and organic fractions are given. Until the ^{110}Pd isobaric interference has been minimized or eliminated in the oxide and residue fractions, the isotopic equilibration kinetics of these two fractions cannot be accurately assessed.

The MIRs change most dramatically in the exchangeable and carbonate fractions (for all soils), suggesting these two fractions are rapidly labile. As with the exchangeable fraction in the short-term incubations, there was an initially rapid decline followed by a period of slow isotopic equilibration. The rapid decline observed for the exchangeable fraction is complemented to some extent by a rapid rise in the carbonate fraction, suggesting that the carbonate fraction is a labile (albeit temporary) sink for the tracer introduced into the exchangeable fraction. Not readily apparent in the graphs is a subsequent, slower decline in the MIRs of the carbonate fraction indicative of isotopic equilibration with more inert fractions. By week six, neither the exchangeable or carbonate fractions had reached overall isotopic equilibrium.

Differences in the rates of isotopic equilibration in the "organic" fraction indicate that two kinetically distinctive sub-fractions are extractable with NaOCl. For the soils containing $\leq$ 2% organic C (i.e. Moreno Valley, Millsholm and Palmerton), the isotope ratios rose relatively rapidly (though more slowly than the exchangeable and carbonate fractions) and approached the new equilibrium value within six weeks (Fig. 4). The Penn Mine soil, however, which

contains very little organic C (0.7%), exhibited sluggish enrichment of the "organic" fraction with ^{111}Cd. These differences in equilibration rates in the "organic" fractions indicate that the NaOCl extraction may oxidize two distinct pools of Cd in these soils, one dominated by organically bound Cd and the other by Cd-sulfide minerals. Based on these results, we would recommend that the "organic" fraction be referred to as "oxidizable". Mineralogical analysis of this fraction before and after treatments with NaOCl is pending and may confirm the presence of sulfides in the Penn Mine soil.

Anticipated Final Results

Because empirical tests of plant uptake of metals, their mobility in soils, and lability during cleanup and remediation efforts are inherently time-consuming and inefficient, greater predictive capabilities are needed. A fundamental understanding of kinetic processes governing metal redistribution and removal from the soil system will provide critical knowledge needed for the development of better conceptual and predictive models. Our stable isotope tracer method is designed to investigate the inherent lability of Cd pools in soils and, coupled with a detailed analysis of soil chemical and mineralogical properties, will offer new insights into the chemistry of Cd in contaminated soils. The results should be particularly useful in the context of highly contaminated soils or sediments for which clean up or abatement is deemed necessary.

References

Gibson, M. J., and J. G. Farmer. 1986. Multi-step sequential chemical extraction of heavy metals from urban soils. Environ. Pollut., Ser. B 11:117-135.

Janghorbani, M., and B. T. G. Ting. 1989. Stable isotope trace applications of ICP-MS. p. 115-140. In A. R. Date and A. L. Gray (ed.) Applications of inductively coupled mass spectrometry. Blackie & Son, London.

Milward, C. G., and P. D. Kluckner. 1989. Microwave digestion technique for the extraction of minerals from environmental marine samples for analysis by inductively coupled plasma emission spectrometry and atomic absorption spectrometry. J. Anal. Atomic Spectrom. 4:709-713.

Russ, G. P. 1989. Isotope ratio measurements using ICP-MS. p. 90-114. In A. R. Date and A. L. Gray (ed.) Applications of inductively coupled plasma mass spectrometry. Blackie & Son, London.

Shuman, L. M. 1983. Sodium hypochlorite methods for extracting microelements associated with soil organic matter Soil Sci. Soc. Am. J. 47:656-660.

Shuman, L. M. 1985. Fractionation method for soil microelements. Soil Sci. 140:11-22.

Shuman, L. M. 1991. Chemical forms of micronutrients in soils. p. 113-144. In J. J. Mortvedt (ed.) Micronutrients in agriculture. 2nd ed. Soil Sci. Soc. Am. Book Ser. 4. SSSA, Madison, WI.

Table 1. Proposed method for sequential, selective extraction of operationally-defined soil Cd fractions.

Extractant	Duration h	Temp. °C	Fraction	Reference
0.1M $Sr(NO_3)_2$	2	25	"soluble & exchangeable"	-
1.0M NaOAc, pH 5.0	5	25	"carbonate & specifically-adsorbed"	Gibson & Farmer, 1986
5% NaOCl, pH 8.5	0.5	95	"organic & sulfides"†	Shuman, 1983
0.4M ammonium oxalate+ 0.1M ascorbic acid, pH 3.0	0.5	95	"Fe/Mn-oxides"†	Shuman, 1985
3:1 HNO_3:HCl	0.3	na‡	"residual"	Milward & Kluckner, 1989

† Three successive treatments

‡ Digestion at high temperature and pressure (150 psi) in a microwave oven.

Table 2. Selected soil physical and chemical properties.

Sample	Cd Source	pH	Carbonates %	Organic Carbon %	Cd_T $\mu g\ g^{-1}$
Moreno Valley	Sewage Sludge	6.04	0.2	7.7	34.0†
Penn Mine	Mine Spoils	3.54	0.0	0.7	21.8†
Millsholm	Natural	7.33	0.6	2.0	26.1†
Palmerton	Smelter emissions	7.02	0.1	3.7	30.5†
CRM 2710	-	5.81	0.3	3.0	21.8‡
CRM 2711	-	8.71	4.4	1.2	41.7‡

† Based on whole-soil digestion using the "residual" HNO_3/HCl microwave method.

‡ Based on certified values.

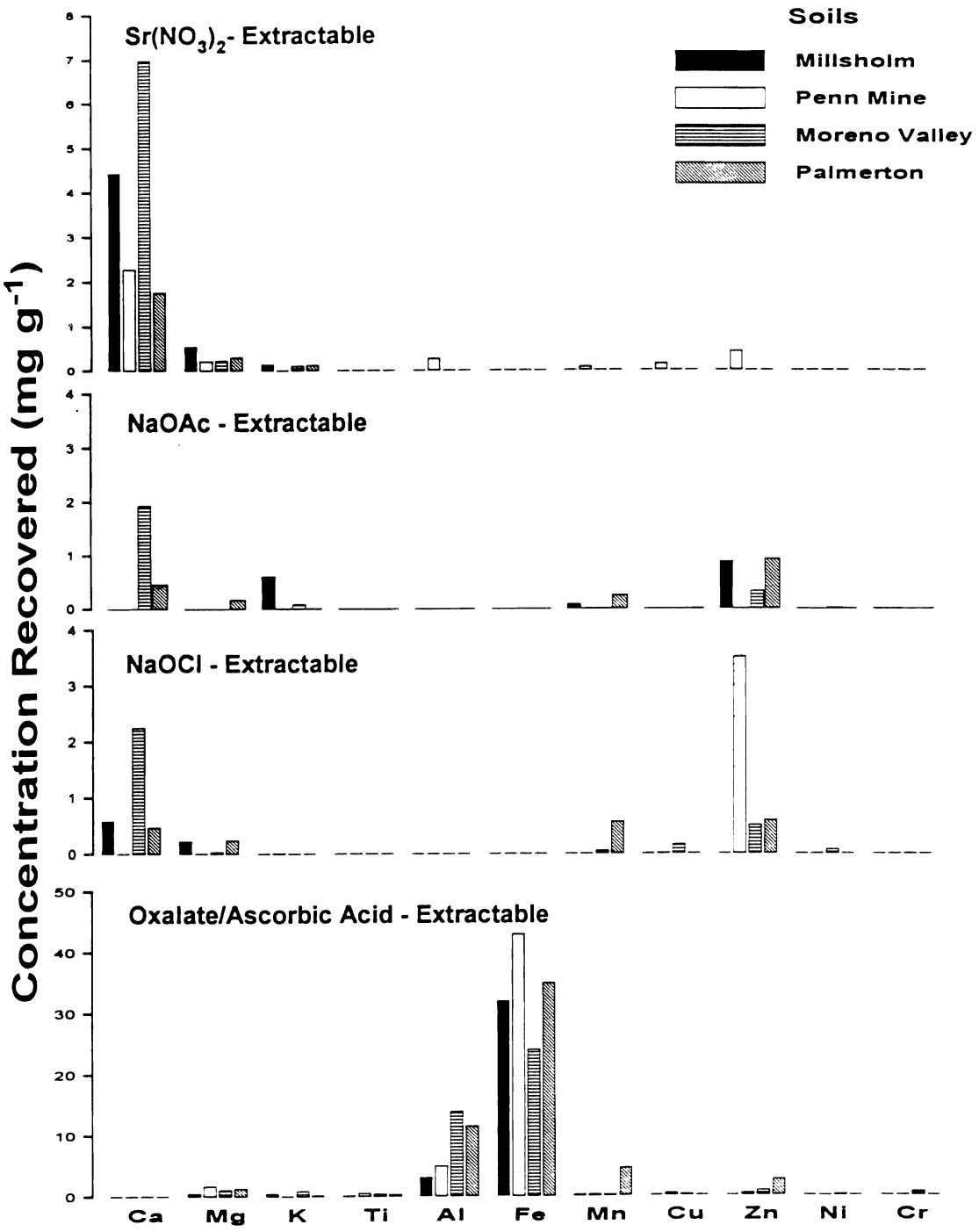

Figure 2. Concentrations of elements (whole-soil basis) recovered in four sequential extraction fractions from the four high-Cd soils under study.

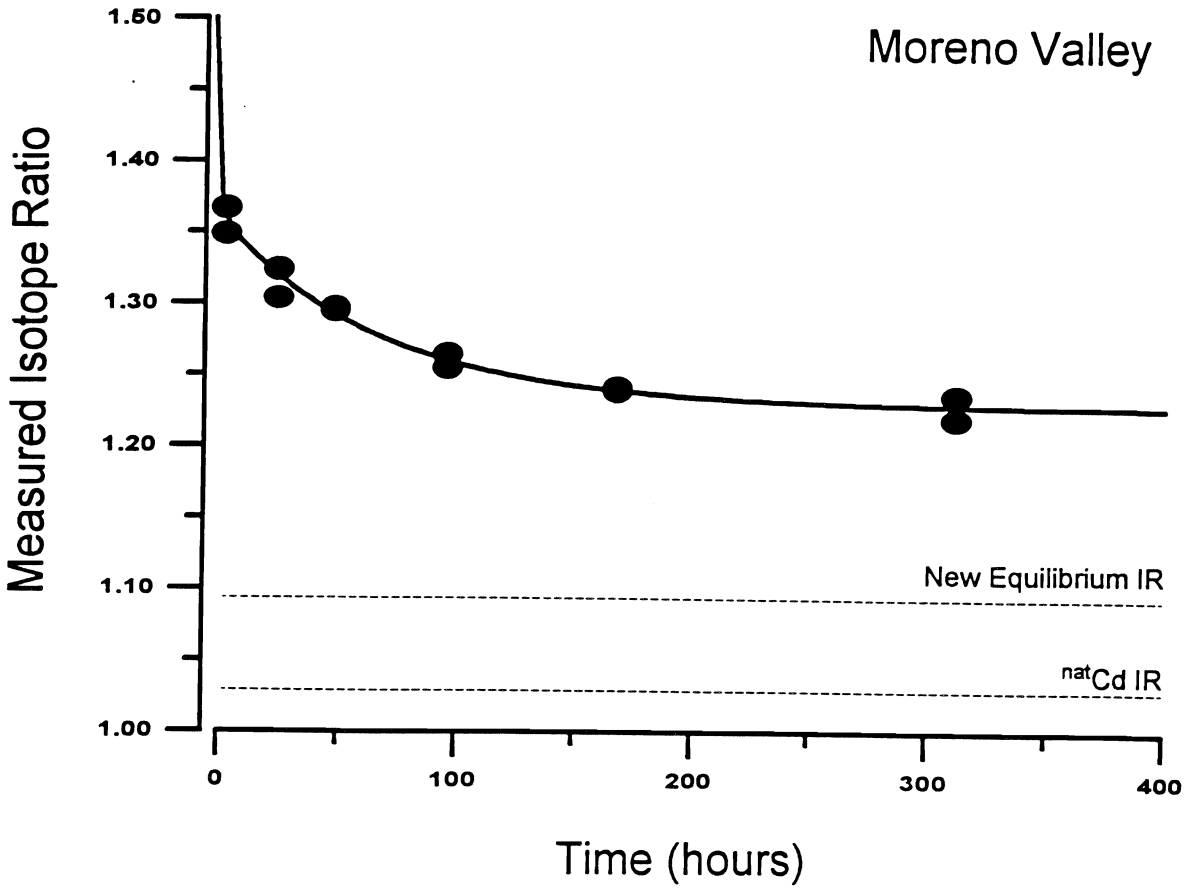

Figure 3. Typical result from the short-term incubation study using the Moreno Valley soil. Horizontal lines indicate the $^{111}Cd/^{110}Cd$ ratios for natural Cd and for isotopic equilibrium; the latter ratio is computed from the size of the ^{111}Cd "spike" relative to the total Cd content of the soil.

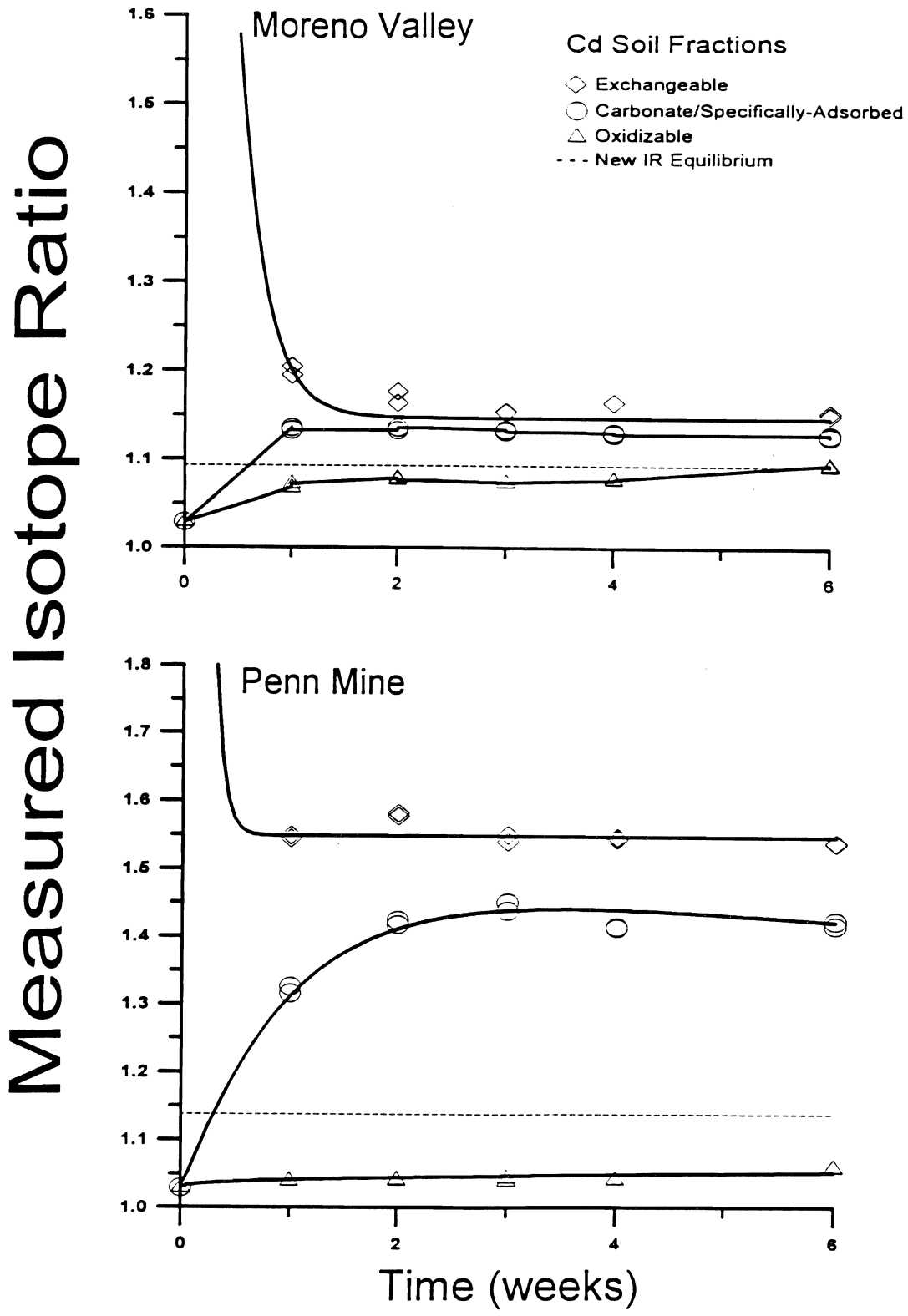

Figure 4. Representative results from the long-term incubations using the Moreno Valley and Penn Mine soils. Horizontal lines indicate the $^{111}Cd/^{110}Cd$ ratios expected once all Cd pools achieve isotopic equilibrium and are computed from the size of the ^{111}Cd "spike" relative to the total Cd content of each soil.

Chemical Factors Affecting Colloid-Mediated Transport of Organic Pollutants in Soils

GARRISON SPOSITO
Department of Environmental Science, Policy, and Management, Berkeley Campus

Summary

Static and dynamic light scattering experiments were performed on suspensions of specimen and Hanford soil illite particles at pH 8 in varying concentrations of NaCl. The critical coagulation concentration (ccc) of specimen illite was found to be 43 mol NaCl m^{-3}, in agreement with literature values and the observed transition from power-law to exponential flocculation kinetics. The fractal dimension of the floccules increased from about 2.14 to 2.25 at the ccc, in contrast with literature data for synthetic spherical colloids. The ccc for Hanford soil illite was around 200-300 mol NaCl m^{-3}, with a fractal dimension near 1.9 both above and below the ccc.

Key Words: colloid stability, flocculation, fractal dimension, groundwater quality, light scattering

Project Objectives Addressed in 1994-95

To perform light scattering experiments on flocculating suspensions of illitic colloids under varying conditions of electrolyte concentration and to evaluate the light-scattering data in terms of transport- or reaction-control kinetics and fractal concepts.

Research Plan and Procedures

Clay stock suspensions

Materials. Silver Hill illite obtained from the Source Clays Repository of the Clay Mineral Society was used as a specimen clay mineral. Its average structural formula is

$K_{1.44}Na_{0.06}Ca_{0.06}\ (Si_{6.8}Al_{1.2})\ [Al_{2.76}Fe_{0.76}Mg_{0.50}]0_{20}\ (0H)_4$

Hanford sandy loam (coarse-loamy, mixed, non-acid, thermic Typic Xerorthent) was used as source of soil illite (Heil and Sposito, 1993).

Colloid surface preparation. Washing procedures are necessary in order to obtain a known surface state of the above materials (saturation of cation-exchange sites and dissolution of surface inorganic coatings). The procedures of Sposito and Levesque (1985) and Heil and Sposito (1993) were used for the Silver Hill and the Hanford soil illite, respectively, but the samples were washed with a mixed solution of NaCl and KCl instead of $NaClO_4$ and $KClO_4$. The KCl is used to prevent desorption of structural K^+ from illite.

Preparation of the colloidal suspension. To recover a colloidal size fraction, the last washing was done at a low (2 mol m^{-3}) concentration of NaCl. The suspension is then centrifuged on a Sorvall SS-3 automatic centrifuge to allow particles larger than 100 nm to settle. The supernatant suspension is then recovered, stored, and refrigerated to reduce microbial activity. Sodium bicarbonate ($NaHCO_3$) is added in order to bring the suspension to pH 8.0.

Dry mass measurement.. The stock suspensions were oven-dried in order to determine the mass-concentration of solid material. Samples for light scattering experiments must be dilute enough to be in the flocculation domain, but not in the gelation domain.

The particle size distribution in the clay stock suspensions, measured by light scattering, was unimodal, with a z-average mean diameter (effective hydrodynamic radius, see below) of 106 nm (Silver Hill illite, kinetics experiments), 345 nm (Silver Hill illite, Stability Ratio experiments), or 140 nm (Hanford illite).

Light scattering experiments

Measurements were performed on a Malvern PCS 100 light-scattering goniometer. The incident light source was a 35 mW He-Ne laser operating at 632.8 nm wavelength with vertical polarization. The temperature was held constant at 25 °C. Flocculation was initiated by mixing 10 ml stock suspension rapidly with 30 ml NaCl solution adjusted to pH 8.0 with $NaHCO_3$. Once mixed, the preparation was poured into a cylindrical Burchard cell (20 ml capacity) used for the light scattering measurement. From mixing to measurement, less than 10 s pass. The data acquisition time was 30 s, but automatic data analysis increases the total measurement time to about 60 s.

The variation of the total scattering intensity with scattering vector **q** was measured between scattering angles of 30° and 150° ($0.00683\ nm^{-1} < q < 0.0255\ nm^{-1}$). The time required for data acquisition was about 5 s, and a measurement was made every 2° to give a total data acquisition time of about 300 s for each intensity [I(q)] curve. Measurements were made continuously during the flocculation process in order to follow the evolution of the apparent fractal dimension of the floccules.

Particle size measurement. The time-fluctuations of light scattered at a given angle by particles in a suspension are autocorrelated. The measured autocorrelation function, $G^{(2)}(\tau)$ is expressed by (Berne and Pecora, 1976; Grabowski and Morrison, 1983):

$$G^{(2)}(\tau) = A\left(1+\beta\left|g^{(1)}(\tau)\right|^2\right) \qquad (1)$$

where $g^{(1)}(\tau)$ is the normalized first-order autocorrelation function at the delay-time τ; A is a "baseline constant"; and β is an "instrumental constant" (Grabowski and Morrison, 1983). If the suspension comprises monodisperse, dilute, optically isotropic scatterers, $g^{(1)}(\tau)$ can be modeled mathematically by the equation (Berne and Pecora, 1976; Ostrowsky, 1988):

$$g^{(1)}(\tau) = \exp\left(-D_T q^2 \tau\right) \qquad (2)$$

where D_T is the particle translational diffusion coefficient; $q=\frac{4\pi n}{\lambda}\sin(\theta/2)$ is the magnitude of the scattering vector; n is the refractive index of the medium; θ is the scattering angle; and λ is the wavelength of the incident light in vacuum. In a polydisperse suspension, $g^{(1)}(\tau)$ takes the integrated form (see, e. g., Ostrowsky, 1988):

$$g^{(1)}(\tau) = \int G(\Gamma)\exp(-\Gamma\tau)\,d\Gamma \qquad (3)$$

where $G(\Gamma)$ is the normalized distribution function for the decay constant, Γ =

$D_T q^2$. In the usual cumulant analysis method, $g^{(1)}(\tau)$ is fitted to a power series in τ (Ostrowsky, 1988):

$$\ln g^{(1)}(\tau) = -\langle\Gamma\rangle\tau + \frac{1}{2!}\mu_2\tau^2 - \frac{1}{3!}\mu_3\tau^3 + \cdots \quad (4)$$

The first coefficient in the expansion is the average decay constant, $<\Gamma>$, determined by the slope at zero-time of the logarithm of the autocorrelation function as a function of τ. A mean hydrodynamic radius R_h (z-average mean particle size) of the scattering particles can be obtained using the Stokes-Einstein relationship:

$$D_T = \frac{k_B T}{6\pi\eta R_h} \quad (5)$$

where η is the viscosity of water, k_B is the Boltzmann constant, and T is absolute temperature.

In our experiments, the influence of rotational diffusion has to be taken into account, because the radius of gyration (R_g) of the floccules will be of the order of or greater than the inverse of the scattering vector (Lin et al., 1990). Thus, an *effective* diffusion coefficient is actually measured, including the effects of rotational diffusion:

$$D_{eff} = \frac{k_B T}{6\pi\eta R} \quad (6)$$

where R is an average size-parameter (an average radius of the floccules, including rotational effects). Rotational diffusion also contributes to the decay of the autocorrelation function; thus, an overestimate of D_T can be obtained, yielding an underestimate of the size parameter. Internal particle modes can also contribute to the decay of the autocorrelation function, but are neglected in this study.

Floccule structure measurement. Figure 1 shows a hypothetical floccule with length scales ranging up to the cluster size. A useful method for probing floccule structure at these different length scales is static light scattering. Figure 2 shows static light scattering data for a flocculating Silver Hill illite suspension (60 mol m^{-3} Na and pH 8.0), where the regions marked 1 to 3 correspond to the spatial scales indicated in Fig. 1.

The average intensity of light scattered by a flocculating suspension can be written as a product of three contributing factors (Teixeira, 1985):

$$I(q) = \phi\, P(q) S(q) \quad (7)$$

where ϕ is the number concentration of individual scatterers (primary particles

or floccules) in the scattering volume; P(q) is the form factor of a primary particle; and S(q) is the structure factor describing the spatial arrangement of the particles in a floccule. If q^{-1} is smaller than a primary particle, S(q) approaches unit value, and the particle form factor is the main contributor to the scattered light (region marked 3). Once q^{-1} becomes larger than an elementary particle, the arrangement in a floccule determines the scattered light intensity, with both S(q) and P(q) contributing notably. The spatial scale probed (region marked 2) could be regarded as a primary particle surrounded by a first coordination shell of other primary particles.

Region 1 is of particular interest because it can be characterized by the fractal dimension of the floccule, giving an indication of how densely it is packed. In a fractal cluster, the particle density-density correlation function, $\rho_2(r)$, has a power-law form (Dale et al., 1984):

$$\rho_2(r) \propto r^{d_f - d} \tag{8}$$

where r is the radial separation (lying between the primary particle size and the cluster size); d_f is the fractal dimension; and d is the Euclidean dimension (d = 3 in our case). In a static light experiment, changing the scattering vector q (by changing the scattering angle) will yield information about the structure factor, S(q), the Fourier transform of $\rho_2(r)$. An equivalent power-law decay in q is then obtained (see, e.g., Teixeira, 1985):

$$S(q) \propto q^{-d_f} \tag{9}$$

This power-law expression is valid over the length-scale range:

$$R_{h1} << q^{-1} << R_g \tag{10}$$

where R_{h1} is the hydrodynamic radius of a primary particle. In this domain, the form factor of the primary particles is equal to 1; the scattered intensity is proportional to S(q) (Teixeira, 1985); and a plot of log I(q) versus log q will give the fractal dimension d_f. Outside the limits of the Inequality in eq. (10), important errors can occur in a fractal dimension measurement.

Determination of the critical coagulation concentration (ccc). We have followed the method of Novich and Ring (1984), wherein the early stage of flocculation is considered, with the average hydrodynamic radius dependent only on the number of dimers and primary particles present in suspension. If a potential barrier to flocculation exists, the initial rate of flocculation is decreased by a factor 1/W relative to the initial rate when no such barrier exists (e.g., Sposito, 1994, §6.5):

$$k_R = \frac{k}{W} \tag{11}$$

where k is the rate coefficient for diffusion-limited flocculation, given at 298 K (for water) by:

$$k = \frac{8k_B T}{3\eta} = 1.233 \times 10^{-17} m^3 s^{-1} \quad (12)$$

and k_R is a rate coefficient for reaction-limited flocculation, given by the model expression (Novich and Ring, 1984):

$$k_R = \lim_{t \downarrow 0} \left[R_{h1} \left(\sqrt{2} - 1 \right) N_o \right]^{-1} \frac{dR_h}{dt} \quad (13)$$

where R_{h1} is the hydrodynamic radius of a primary particle, and N_o is the initial primary particle number concentration. The critical coagulation concentration (ccc) is defined by (see, e.g., Sposito, 1994, p. 251):

$$\lim_{c \to ccc} \ln W = 0 \quad (14)$$

Results

Figure 3 shows a log-log plot of the Stability Ratio against Na concentration for Na-saturated Silver-Hill illite at pH 8.0. All experiments were performed at a clay concentration of 13 mg per kg suspension. The graph in Fig. 3 yields ccc $\approx$ 43 mol m^{-3}. This value is close to that given by Hesterberg and Page (1990), who found ccc = 45 mol m^{-3} for a settling time of 2.2 h using the same clay washing procedure as we did. Sposito (1989) gave 38 mol m^{-3} for the ccc of illite as an average value collected from the literature. A value of 104 mol m^{-3} was given in our 1993-1994 Kearney Foundation Annual Technical Report. In the present set of experiments, the stock suspension contained elementary particles with a mean hydrodynamic size of 345 nm; whereas, in the previous set, a stock suspension with particles of mean size around 100 nm was used. Particles with a larger size are better light scatterers and, therefore, the number concentration in the sample used for ccc experiments can be significantly reduced, in consonance with the condition that mainly dimers form during the flocculation process. At higher concentrations, trimers and multimers also form, which can account for the higher ccc value obtained in the first set of experiments.

In our 1993-1994 Kearney Foundation Annual Technical Report, we described the kinetics of flocculation as exhibiting two limiting régimes. In the first, floccule growth is reaction-controlled and the kinetics is exponential; whereas, in the second, growth is transport-controlled and follows power-law kinetics. These experiments have been repeated at other particle concentrations. Figures 4 and 5 show the evolution in time of the effective diameter of Silver Hill illite floccules at pH 8.0. The experiments have been done with different stock suspensions, but the initial average size of the

particles was identical (around 100 nm). The only difference is the particle concentration. In Fig. 4, the mass concentration is 58 mg per kg suspension; whereas, in Fig. 5, it is 28 mg per kg suspension. It is not clear why plateaus are reached at different effective diameters. One explanation is that the fundamental correlation time, chosen by the apparatus to probe all possible particle diffusion coefficients, was too short because of large polydispersiivity in the sample, such that mainly the smaller floccules were probed and analyzed. In our 1993-94 report, we indicated that the transition from exponential to power-law kinetics occurred at 40 to 45 mol m^{-3} NaCl concentration. This agrees very well with the ccc (43 mol m^{-3}) value stated above.

Figure 6 shows flocculation kinetics data for the Hanford soil illite. In order to observe the same dispersing effect of sodium, the salt concentration had to be much higher than in the case of Silver Hill illite. We interpret this additional stability of the particles in suspension as an effect of natural organic matter coatings on the illite particles (Heil and Sposito, 1993). Soil illite particles are formed in the soil weathering environment, including interaction with organic matter. Partial coating with organic matter and the "rounding effect" of weathering (Heil and Sposito, 1995) also suggest that these particles might have a fractal dimension near that observed for spherical colloids (see below).

Curves similar to that in Fig. 2 were obtained at pH 8.0 for Silver Hill Illite at different sodium concentrations. Figure 7 shows a plot of the evolution of the fractal dimension inferred from those curves (the first 20 data points were chosen, so that the inequality in eq. (10) is met). The vertical line indicates the ccc. Below the ccc, the fractal dimension is 2.14, typical for floccules comprising spherical colloids in the reaction-controlled régime (Aubert and Cannell, 1986). Above the ccc, these latter colloids have a typical value of 1.8 for the fractal dimension (Aubert and Cannell, 1986). In our case, d_f actually increases at the ccc, not decreases. This difference could come from shape anisotropy in Silver Hill illite particles and heterogeneity in the distribution of their surface charge.

Figure 8 shows a static light scattering curve for the Hanford soil illite. Again we see that the three spatial regions described in Fig. 1 are probed. The value of the average fractal dimension was 1.94 $\pm$ 0.11 (90% confidence interval). As before, the first 20 data points were used in the calculation. At a sodium concentration of 500 mol m^{-3} , the fractal dimension is 1.93, with the same confidence interval. From the shape of the curves in Fig. 6, we see that these concentrations correspond to conditions close to or above the ccc for the Hanford soil illite. The exact value of the ccc (for sodium) has not yet been determined, but is estimated to lie between 200 and 300 mol m^{-3}, by comparison with the kinetics data for Silver Hill illite.

Discussion

In order to see if the flocculation process in our experiments involved mainly dimers, we can compare the average size predicted at a time equal to the half-life of a two-particle collision with the size actually measured at the ccc. The half-life is (e.g., Sposito, 1994):

$$t_{1/2} = \frac{1}{kN_o} = 377\,\text{s}. \qquad (15)$$

The kinetics curve obtained at a NaCl concentration of 45 mol m^{-3} (Fig. 9) is that closest to the ccc. After 377 s, the mean hydrodynamic size is 456 nm. After this time, half the primary particles should have disappeared to form dimers. The number concentration of primary particles is thus 1/2 N_o, and the number concentration of dimers is 1/4 N_o, yielding a number distribution of 2/3 and 1/3, respectively. In order to predict the average particle size resulting from such a number distribution, we have to know the contribution of a dimer to the measured size. As mentioned above, dynamic light scattering probes the diffusion coefficients of particles in suspension in order to obtain their hydrodynamic size using eq. (6). If the hydrodynamic radius of a dimer is taken equal to $\sqrt{2}$ that of a primary particle (Novich and Ring, 1984), we can calculate from the number distribution that the mean hydrodynamic radius should be $((1/3) \times \sqrt{2} \times 345) + (2/3) \times 345) = 393$ nm, in reasonable agreement with the measured value (456 nm). Thus, although we have not proven that only dimers occurred, this is suggested by comparison of our data with a simple model approximation.

In Fig. 3, several data points lie below the curve ln W = 0. This result can be explained by considering the following:

- Equation (12) is not accurate for the diffusion-limited flocculation rate coefficient;
- Interparticle forces involve short-ranged interactions between particles that vitiate eq. (12);
- the assumption that only dimers form is not valid.

References

Aubert, C. and D.S. Cannell. 1986. Restructuring of colloidal silica aggregates. Phys. Rev. Lett. 56:738-741.

Berne, B.J. and R. Pecora. 1976. Dynamic Light Scattering. Wiley, New York.

Dale, W., E. Schaefer, P. Wiltzius, and D.S. Cannell. 1984. Fractal geometry of colloidal aggregates. Phys Rev. Lett. 52:2371.

Grabowski, E.F. and I.D. Morrison. 1983. Particle size distributions from analysis of quasi-elastic light scattering data. *In* B.E. Dahneke (ed.) Measurements of Suspended Particles by Quasi-elastic Light Scattering. Wiley, New York.

Heil, D. and G. Sposito. 1993. Organic matter role in illitic soil colloids flocculation: I. Counter ions and pH. Soil Sci. Soc. Am. J. 57:1241-1246.

Heil, D. and G. Sposito. 1995. Organic matter role in illitic soil colloids flocculation: III. Scanning force microscopy. Soil Sci. Soc. Am. J. 59:266-269.

Hesterberg, D. and A.L. Page. 1990. Critical coagulation of sodium and potassium illite as affected by pH. Soil Sci. Soc. Am. J. 54:735-739.

Lin, M.Y., H.M. Lindsay, D.A. Weitz, R. Klein, R.C. Ball, and P. Meakin. 1990. Universal diffusion-limited colloid aggregation. J. Phys. Condens. Matter 2:3093-3113.

Novich, B.E. and T.A. Ring. 1984. Colloid stability of clays using photon correlation spectroscopy. Clays Clay Minerals 32:400-406.

Ostrowsky, N. 1988. Particle characterization by photon correlation spectroscopy. *In* P.J. Lloyd (ed.) Particle Size Analysis 1998. Wiley, New York.

Sposito, G. 1989. The Chemistry of Soils. Oxford Univ. Press., New York.

Sposito. G. 1994. Chemical Equilibria and Kinetics in Soils. Oxford Univ. Press., New York.

Sposito, G. and C.S. Levesque. 1985. Sodium-calcium-magnesium exchange on Silver Hill illite. Soil Sci. Soc. Am. J. 49:1153-1159.

Teixeira, J. 1985. Experimental methods for studying fractal aggregates. *In* E. Stanley and N. Ostrowsky (ed.) On Growth and Form. D. Reidel, Dordrecht, The Netherlands.

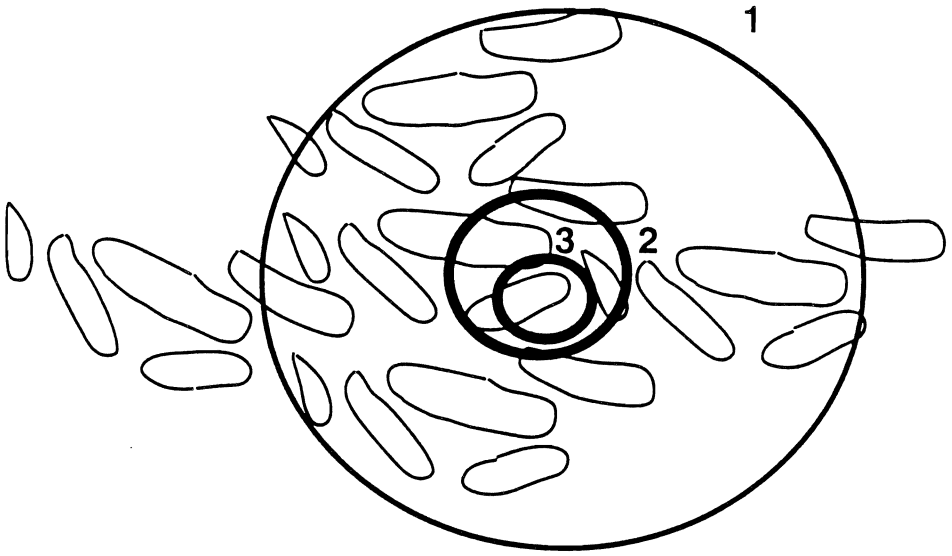

Figure 1. Hypothetical floccule for which three different spatial scales probed by static light scattering are indicated.

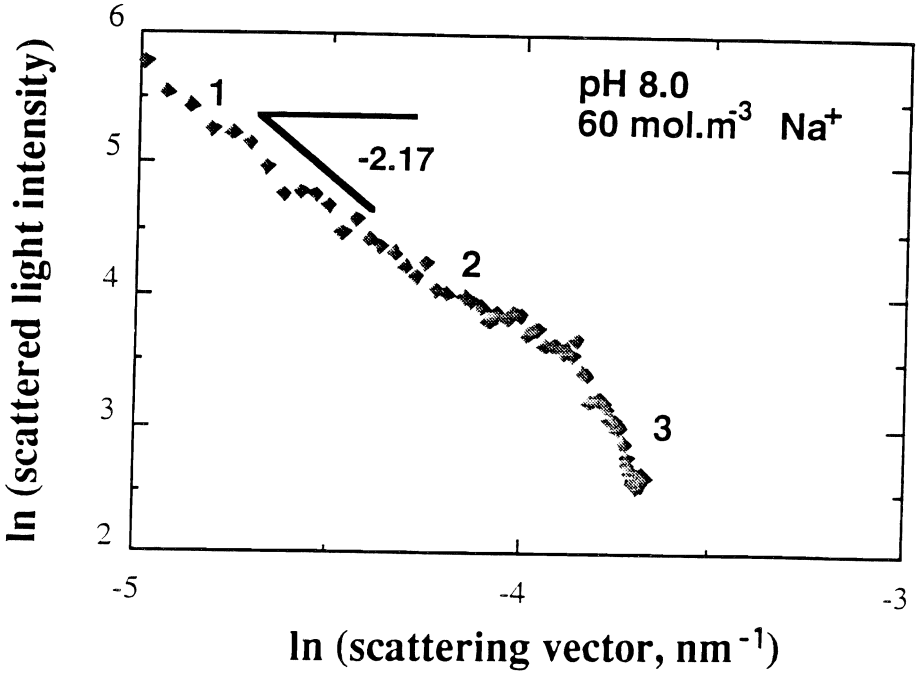

Figure 2. Static light scattering data obtained for a suspension of flocculating Silver Hill illite. Regions 1, 2, and 3 of Fig. 1 are indicated along with the fractal dimension in Region 1.

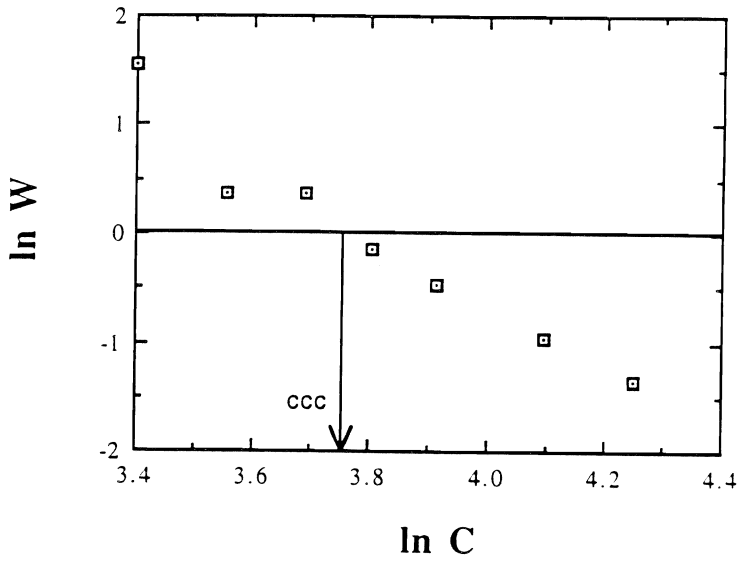

Figure 3. Log-log plot of the Stability Ratio (W) against NaCl concentration (C, in mol m^{-3}) for Na-illite at pH 8.0.

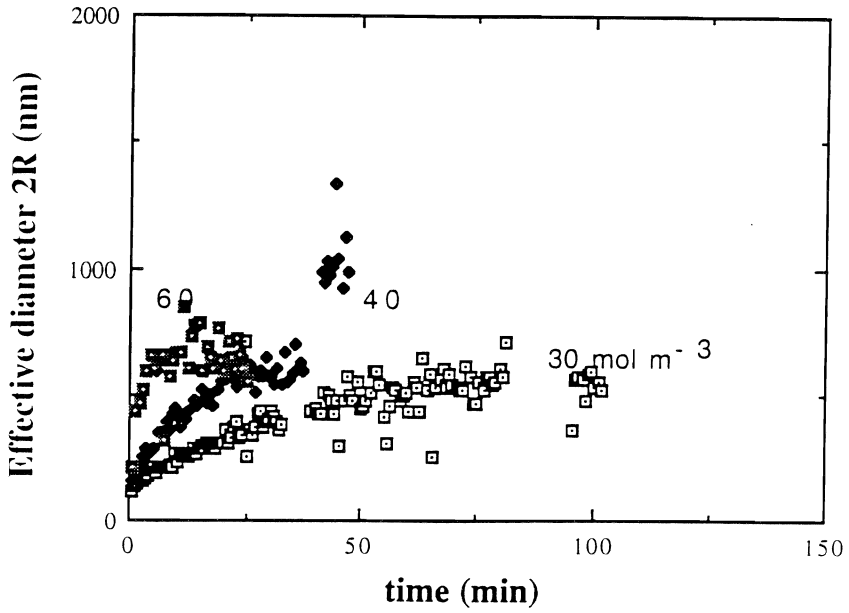

Figure 4. Time evolution of the average effective floccule diameter of Silver Hill illite suspended in different NaCl solutions (concentrations indicated next to the data) at pH 8.0. Clay concentration is 58 mg kg^{-1}.

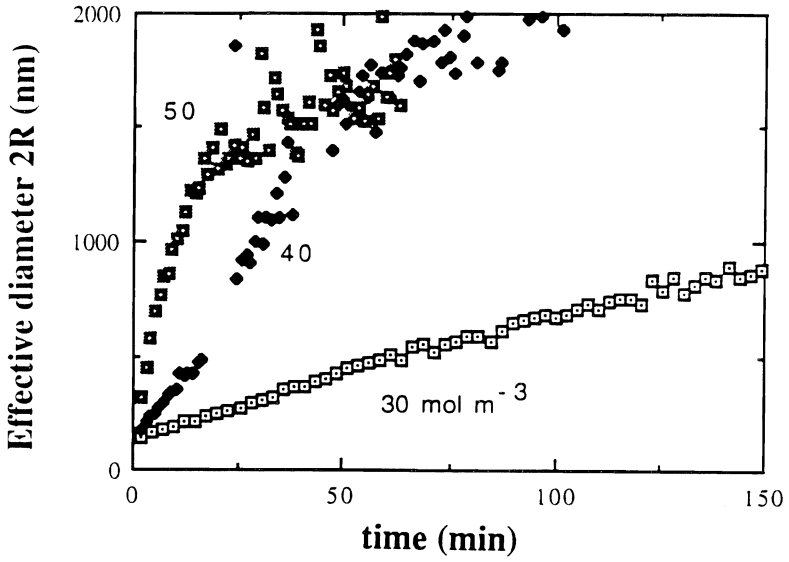

Figure 5. Time evolution of the average effective floccule diameter for Silver Hill illite suspended in different NaCl solutions (concentrations indicated next to the data) at pH 8.0. Clay concentration is 28 mg kg^{-1}.

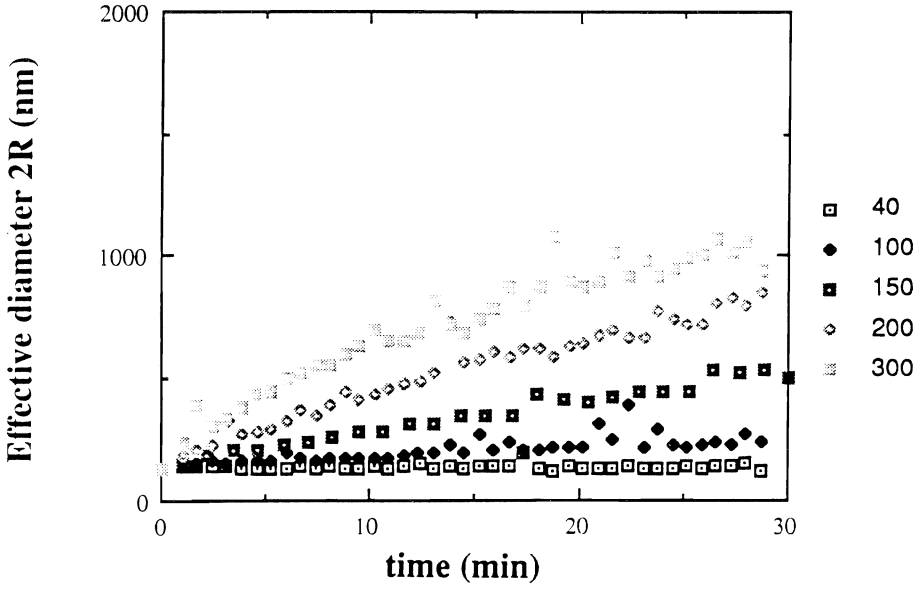

Figure 6. Time evolution of the average effective floccule diameter for Hanford soil illite suspended in different NaCl solutions at pH 8.0 (concentrations in mol m^{-3} are indicated to the right of the figure).

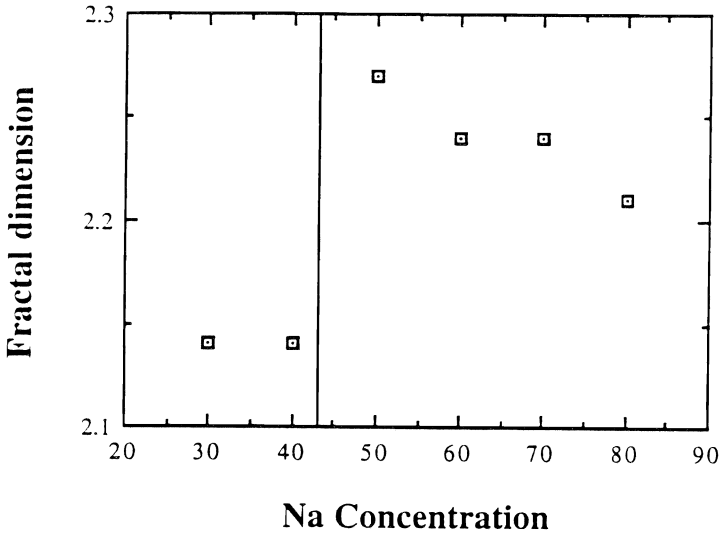

Figure 7. Plot of the fractal dimension of Silver Hill illite floccules against sodium concentration in mol m^{-3}. The vertical line indicates the ccc value.

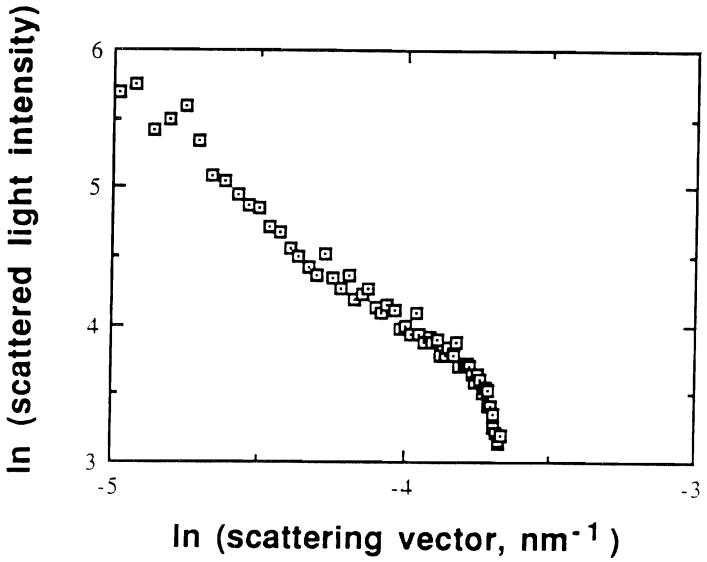

Figure 8. Static light scattering data obtained for a suspension of flocculating Hanfoard soil illite in 300 mol m^{-3} Na at pH 8.0.

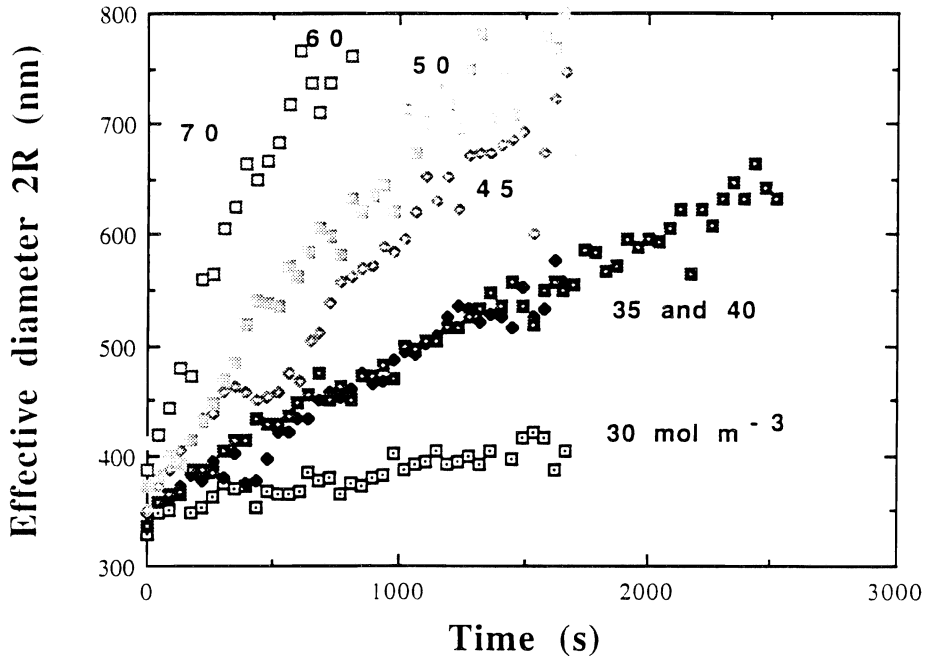

Figure 9. Time evolution of the average floccule diameter for Silver Hill illite in the suspensions used for Stability Ratio measurements (NaCl concentrations indicated near the data).

Interactions of Soil Organic Matter with Aromatic-Amine Pollutants in a Soil-Plant System: Application of Solid-State ^{15}N-NMR

JOHN G. McCOLL
Department of Environmental Science, Policy, and Management
Berkeley Campus

Summary

Regions of intense microbial activity in forest soils, including the rhizosphere and the litter, are very important in the transformation of natural and anthropogenic compounds in soils. ^{15}N-labeled aniline and ammonium nitrate were added to both real forest soils and artificial soils with and without trees or litter cover. ^{15}N-NMR spectra of the soils and litter from the different treatments demonstrated that both ammonium nitrate and aniline were incorporated into the soils and litter by direct reaction and via microbial metabolic pathways. ^{15}N-NMR spectra of soil after three months of ammonium nitrate incorporation promoted the formation of amide, amino-quinone, and amino sugar-N from the ^{15}N added. Spectra of soil after aniline incorporation revealed that most of the aniline is transformed into amide-N and/or anilino-quinone. Whether microbial degradation of aniline occurs or aniline reacts directly with the litter is unclear. However, more common direct-reaction products other than anilino-quinone (which is indistinguishable from amide) are not present, suggesting that the former is more likely. Analysis of the ^{15}N-content of the soils indicated that enrichment was too low for ideal signal-to-noise ratios, but significant signal was detected even at lower enrichment levels, implying that the enrichment technique is effective. The results for this preliminary study clearly demonstrate that solid-state NMR is an extremely effective tool for the analysis of the fate of xenobiotics in soil/plant systems enriched in the labeled contaminant. Additional studies to determine the influence of microbial and abiotic reactions in aromatic amine transformations in soils are required.

Key Words: Organic matter, aromatic amines, soil pollution, ^{15}N-analine, NMR analyses

Project Objectives Addressed in 1994-95

1. Elucidate the reactions between aromatic amines and soil organic matter.
2. Determine the effect of the rhizosphere on aromatic amine reactivity with soil organic matter.

Research Plan and Procedures

Aniline was chosen as a model aromatic amine, and ammonium nitrate was used to determine the relative uptake and speciation of N by plant microbes and soil components with respect to aniline N movement. 99.9% ^{15}N-labeled aniline was diluted to 1 g L^{-1} in distilled, deionized water. Ammonium nitrate with a double (99.9%) ^{15}N-label was diluted into a half-Hoagland solution. Bi-weekly feedings of 10 mL of each solution were added to individual pots containing soil, soil plus litter, soil plus tree, and soil plus tree plus litter. Thus, the effects of a litter layer on an active rhizosphere and their interactions were examined.

The real soil chosen was from the U.C. experimental forest site at Blodgett (properties are presented in Table 1). Two artificial soils were used: the UC mix (a combination of peat and sand) and a mixture composed of coarse perlite, peat, and sand. In this preliminary study, aniline was applied only to the UC mix soil treatments; whereas, ammonium nitrate was applied to all three soils.

Ponderosa Pine trees were purchased from the California Department of Forestry and Fire Protection Service (L.A. Moran Reforestation Project) as 1-year old-bare-root seedlings, and planted into soil pots during January 1993. Application of labeled compounds began in February 1994, after bud-break which indicates active uptake of nutrients by plants, and continued until August 1994. The study began after tree roots had completely filled the volume of the pot. Tree and soil pots were maintained moist such that water was not a limiting factor in plant growth while also maintaining aerobic conditions.

Litter used for surface coverage was collected from a uniform 50-year old ponderosa pine stand at the USDA, Forest Genetics Research Center in Placerville, CA. The litter was characterized before and after treatment.

Pots were sampled by removing three 1/2" diameter soil cores from each pot, freeze-dried, and ground to a fine powder. Cores were taken from stoppered openings in the sides of the pots at a depth of 2 cm. Litter samples were also taken, freeze-dried, and ground to a fine powder. Care was taken to remove all freshly fallen needles from plants so that they did not interfere with the analysis of the "standard" litter layer.

Litter and soil samples were analyzed for total N and ^{15}N enrichment using a Gas Chromatographic Isotope Ratio Mass Spectrometer (GC-IRMS, Europa Scientific). Solid-state nuclear magnetic resonance (NMR) spectra were obtained in Dr. Kevin Thorn's laboratory, at the USGS in Denver, on a ChemMagnetics CMX-200 solid-state NMR spectrometer with a 7.5 and 14 mm broad-band probe. Line broadening (lb) was different for each spectrum based

on the resolution of the results. All spectra were fully decoupled and acquired for 500,000 scans. Parameters are included with the spectra.

Experimental Design

EXPERIMENT 1: Fate of ^{15}N-NH_4NO_3 in a plant-soil system

A replicated pot study was set up to examine the fate of ^{15}N-labelled fertilizer, as a preliminary study to our study of the fate of ^{15}N-labelled contaminants. Four treatments were compared: (1) soil (or artificial media), (2) soil (or artificial media) with a litter layer of pine needles, (3) soil (or artificial media) with Ponderosa pine seedlings, and (4) soil (or artificial media) with a litter layer and pine seedlings.

^{15}N-labelled NH_4NO_3 was applied in solution to soil in five pots of each treatment. Five other pots from each treatment served as a control.

EXPERIMENT 2: Detectability and quantification of ^{15}N-aniline in a soil-plant system

Two treatments, in UC Mix soil described above, were compared: (1) soil (or artificial media); (2) soil with a pine-litter layer and pine seedlings. Replication and sampling followed those outlined above.

EXPERIMENT 3: Fate of ^{15}N-labelled contaminants in a soil-plant system

Based on techniques refined from Experiments 1 and 2, ^{15}N-labelled aniline and picloram will be used as model contaminants added separately in solution to soil-plant systems, using the treaments described in Experiment 1. The pot trial was started January 1996, and will be harvested in October 1996; analyses of soil and plant components will be made thereafter.

Results

^{15}N enrichment was highest for litter and artificial soils (UC Mix and artificial media), where the organic matter content was highest (Table 2). Blodgett soil showed weak enrichment, although overall N content was still relatively high.

^{15}N-NMR spectra for the soils enriched with ammonium nitrate revealed that ammonium (~0 ppm) and nitrate (370 ppm) peaks dissapeared. For the UC Mix soil, peaks were recorded at ~120 (amide), ~75 (amino-quinone-N), and ~40 ppm (amino-sugars, or ammonia salts). Similar spectra were observed for litter from both the UC Mix and Blodgett soils (Figs. 1, 2, and 3). The spectrum of the Blodgett soil showed one broad peak at ~120 ppm, with weak signal-to-noise (Fig. 4).

Aniline-enriched soils and litter showed varied signal-to-noise, depending on the ^{15}N content of the sample. The UC Mix soil spectrum showed weak enrichment with a poorly defined broad peak centered at ~120 ppm (Fig. 5). Litter samples from the aniline reaction study showed one dominant peak at ~120 ppm and smaller shoulder peaks at 150, 40, and 75 ppm (Figure 6).

Discussion

The NMR spectra for the ammonium nitrate study indicate that ammonia and nitrate are quickly taken up by microbes and trees and converted rapidly to amide (~120 ppm), amino-quinone N (~75 ppm), and amino sugars or ammonia salts (~30 ppm). Because these transformations are also seen in the litter layer of the soil, and because the litter shows significant enrichment in ^{15}N, it would appear that microbial transformations are important (bacterial, or more likely fungal hyphae formation). Identification of what is responsible for these transformations is still required. Other studies have analyzed the decomposition of enriched material after being grown in ^{15}N-enriched media. Knicker et al. (in review) composted ^{15}N-enriched wheat and straw and observed only amide formation over time. Comparison with the present study suggests that more available forms of N are incorporated into a variety of materials rather than limited to simply amide formation. The fact that Knicker et al. (in review) did not observe these other peaks may be due to the fact that the smaller peaks are not detectable in their system because of low signal-to-noise. There was not a high enough concentration of many degradation products.

Almendros et al. (1991) did a compost study with ^{15}N-enriched corn straw and found a decrease in all peaks of their composted material, with the main peaks appearing at 87, 55-40, and ~0 ppm. These peaks are attributed to peptide nitrogens in proteinacious material, to $-NH_2$ of nucleic acids, and to free amino groups or ammonia. The differences observed in the peak shifts observed maybe due to the differences in the chemistry of the litters formed or the low concentration of N species formed during the litter degradation by microbes. This is the first study to observe the formation of several different nitrogen species in soils using ^{15}N-NMR, and essential data on the transformation of nitrogen species in soils.

Aniline reactions provide a very interesting picture concerning the transformations of anthropogenic aromatic amines in soils. The implication from this research is that aniline is either rapidly degraded and the N is utilized by microbes, or that aniline reacts to form anilino-quinone with the abundant concentration of phenolic acids in litter and forest soil. The subsequent degradation of the reacted aniline then shows the same characteristic spectra that Knicker et al. (in review) observed with ^{15}N-enriched litter. Given that Almendros et al. (1991) observed no new peak formation in their composting study of corn straw provides insight into why the amide/anilino-quinone peak that forms does not transform into any other structures. Substituted amines (e.g.

aniline or degraded aniline) may be more difficult to degrade completely and therefore result in simple amide formation. Determining the factors influencing the formation of amides is important for predicting the transformations of aromatic amines.

Verifying whether abiotic or biotic processes are responsible for the formation of amides and/or anilino-quinones is essential to determine factors influencing rapid degradation in soils. Therefore, many of the products predicted by monomer studies (e.g. Bollag et al., 1983) do not form. Even a comparison of the present samples with an IHSS peat standard reacted directly with aniline and microbial enzymes reveals the striking difference in products (Fig. 7). In addition, adsorption is not a significant process in the speciation of aniline. Less reactive aromatic amine compounds such as chloro-anilines and a variety of other aromatic amines (e.g. atrazine, picloram) may form a variety of products because degradation will be prevented and various reaction mechanisms may be important.

The weak signal observed in the spectra of the aniline-UC Mix reaction and ammonium nitrate-Blodgett, UC Mix, or artificial media enrichment are expected given the low ^{15}N concentrations in these samples. The preliminary data compiled herein demonstrate that this is an extremely effective technique for determining the reactions of N-compounds in soils, and with the proper level of enrichment, much more information about contaminant reactivity can be obtained.

Conclusions

1. ^{15}N-enrichment coupled with NMR analysis is a powerful tool for following the transformation reactions of contaminants in soils. It provides both a label that can be quantitatively followed by GC-IRMS, and nuclei that can give structural information about the reactants and products using NMR.

2. Ammonium nitrate enrichment demonstrates that several different types of N-compounds form readily in a plant-soil system and that microbial processes appear to dominate the reactions in forest soils.

3. Aniline enrichment with ^{15}N-label provides useful information as to the transformation of aniline in soil-plant systems, and indicates that both abiotic and microbial transformation can account for aniline transformation in soils. A more complete study is required to determine whether biotic and/or abiotic processes are responsible for the transformations.

4. Preliminary results indicate that, with greater enrichment, excellent signal-to-noise can be obtained.

References

Almendros, H. A., R. Fründ, F. J. Gonzalez-Vila, K. M Haider, H. Knicker, and H.-D. Ludemann. 1991. Characterization ^{15}N-enriched litter with ^{15}N-nuclear magnetic resonance. FEBS Letters, 282:119.

Bollag, J.-M., R. D. Minard, S.-Y. Liu. 1983. Cross-linkage between anilines and phenolic humus constituents. Envrion. Sci. and Technol. 17:72-80.

Knicker, H., R. Fründ, and H.-D. Lüdemann. In review. Characterization of the nitrogen in plant composts and native humic material by natural abundance N-15 CPMAS and -solution spectra. Organic Geochemistry

Table 1. Soil Properties

SOIL	C	N	C/N	K	Ca	Mg	Fe	Al
	g kg^{-1}	g kg^{-1}		mg kg^{-1}	mg kg^{-1}	mg kg^{-1}	mg kg^{-1}	mg kg^{-1}
ARTIFICIAL	209.50	3.53	59.38	483.1	1583.8	723.2	2046.1	1958.3
BLODGETT	10.14	0.48	20.82	2677.2	4976.3	3184.8	15809.7	30902.8
UC MIX	18.93	0.74	25.81	427.8	7186.2	2888.5	13576.6	12078.0

Table 2. ^{15}N content of samples used for NMR study.

NMR Spectra	Composition	^{15}N Spike	% ^{15}N	% N
Figure 1	Litter (PL trt)	NH_4NO_3	3.750	0.574
Figure 2	Litter (L trt)	NH_4NO_3	0.555	2.289
Figure 3	Soil (PL trt)	NH_4NO_3	1.050	0.324
Figure 4	Soil (PL trt)	NH_4NO_3	3.250	0.115
Figure 5	Soil (PL trt)	Aniline	0.168	4.732
Figure 6	Litter (PL trt)	Aniline	0.517	3.894

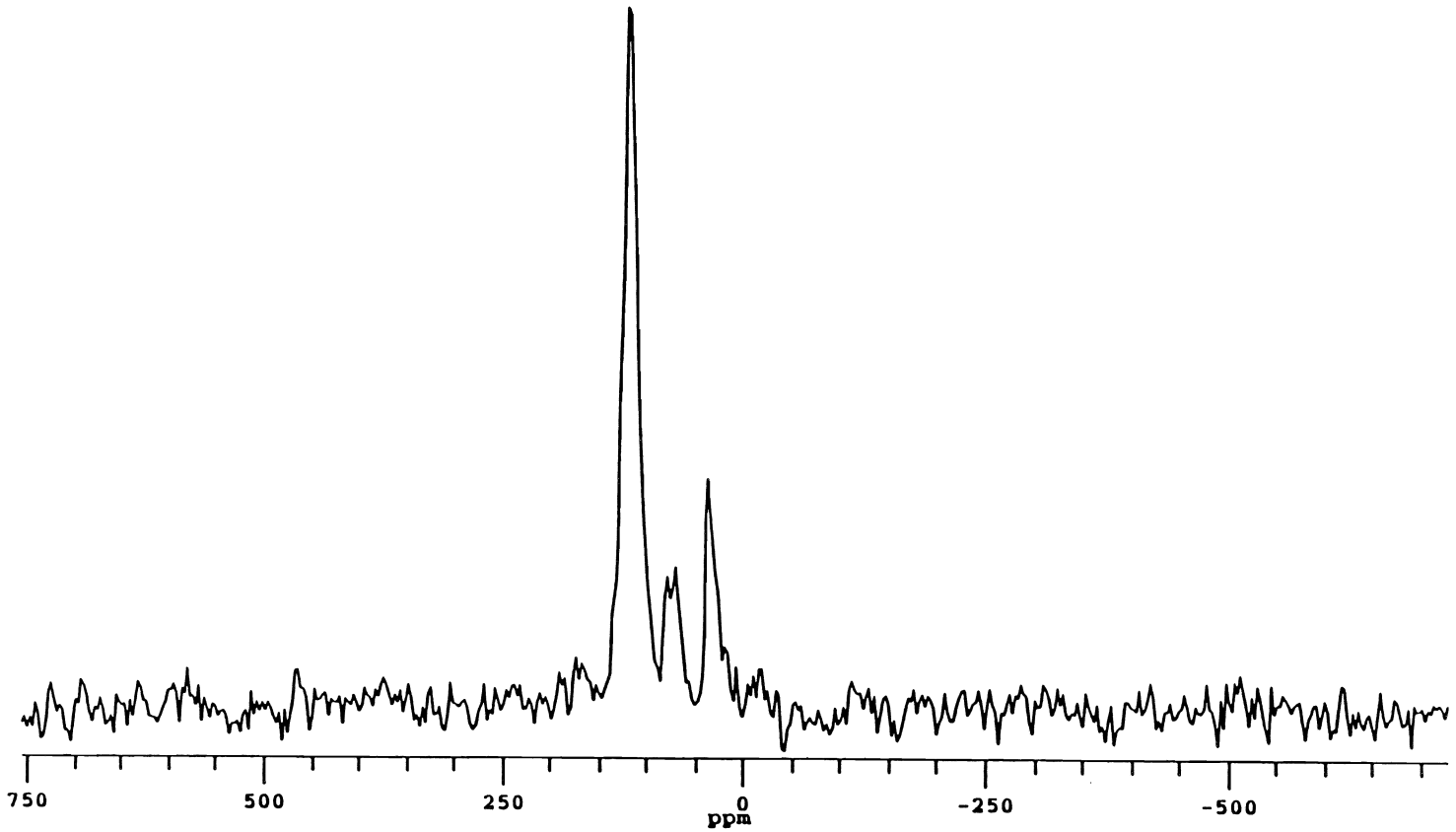

Figure 1. ^{15}N-NMR spectrum of Blodgett soil litter sample after enrichment with labeled ammonium nitrate. Line broadening was 40 Hz.

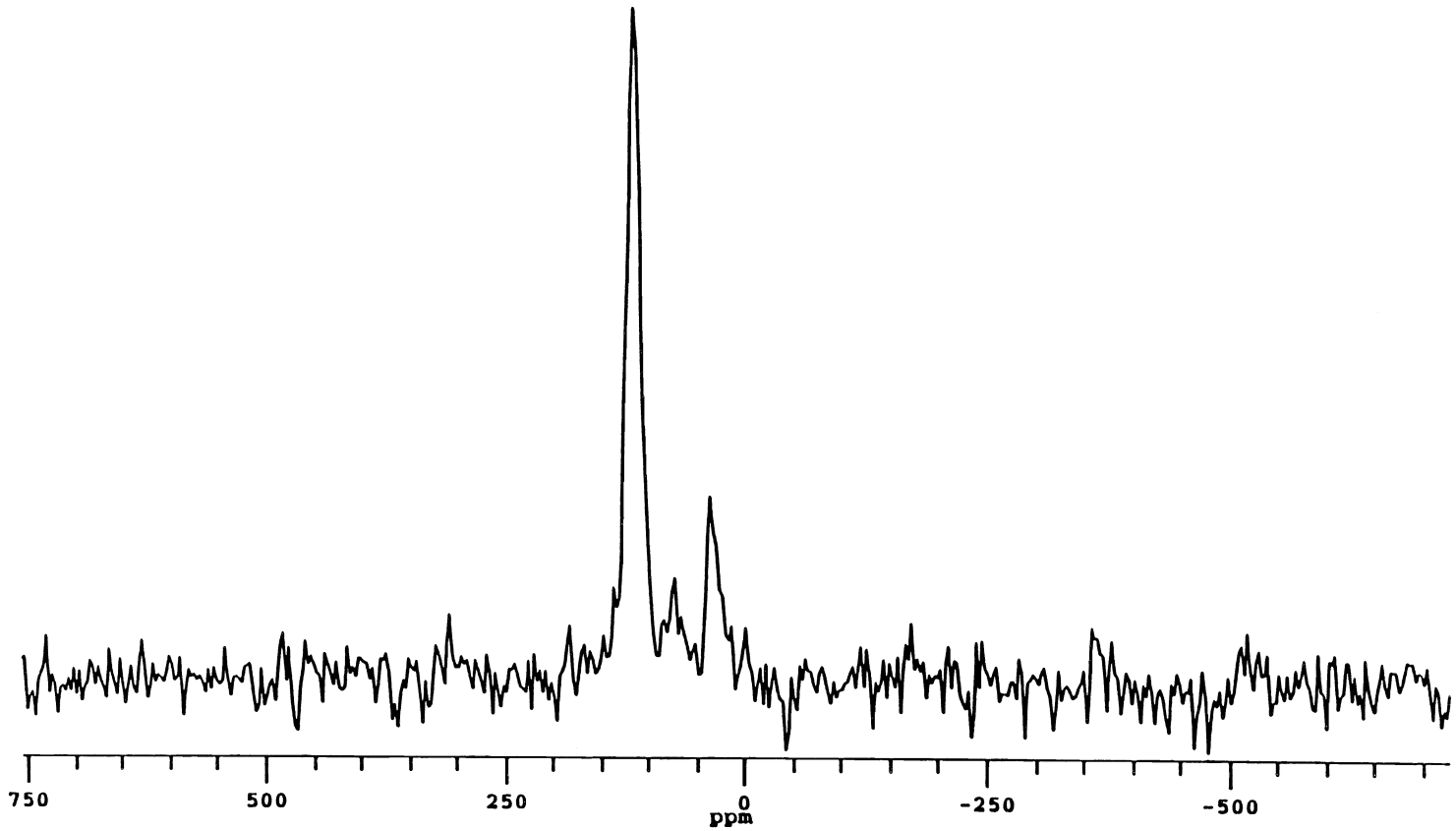

Figure 2. ^{15}N-NMR spectrum of UC Mix soil litter after enrichment with labeled ammonium nitrate. Line broadening was 40 Hz.

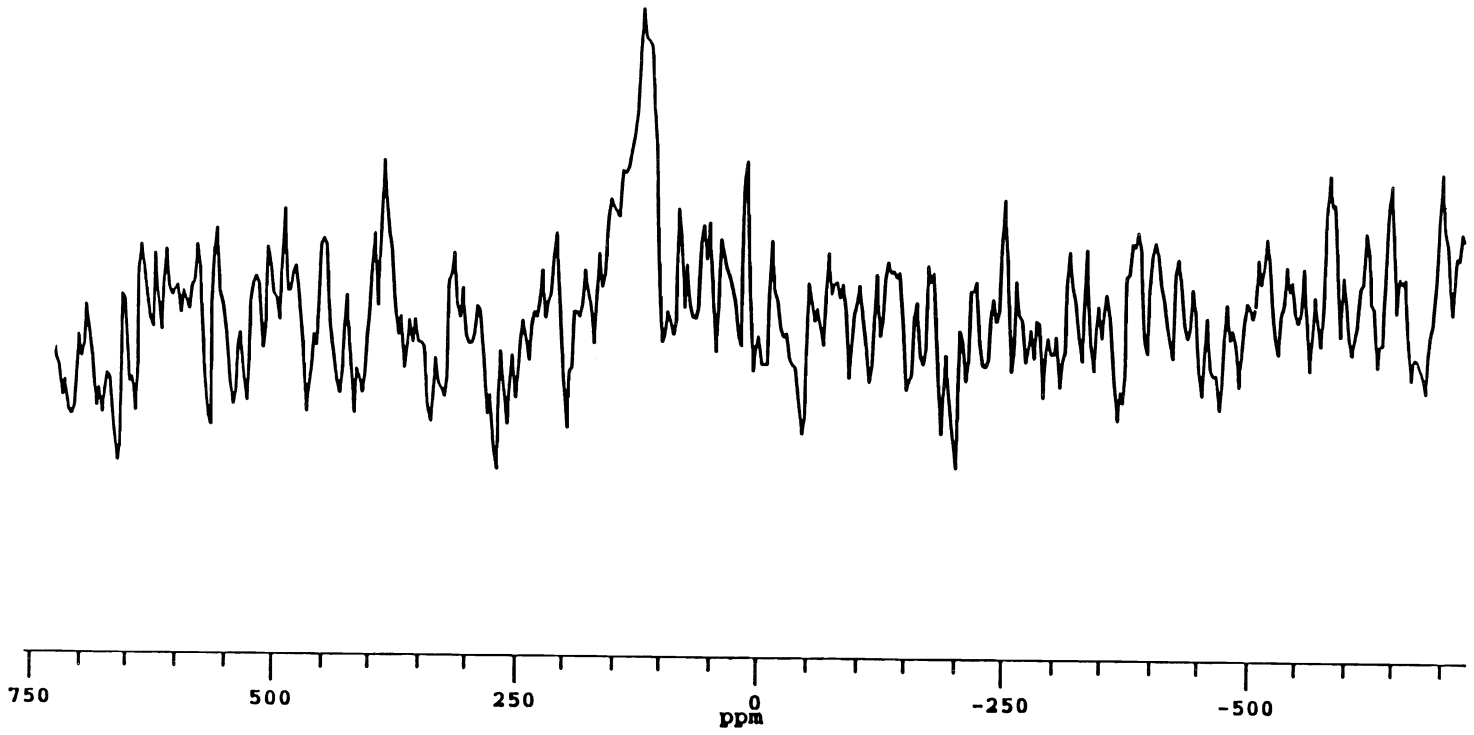

Figure 3. Blodgett soil ^{15}N-NMR spectrum after enrichment with labeled ammonium nitrate. Line broadening was 100 Hz.

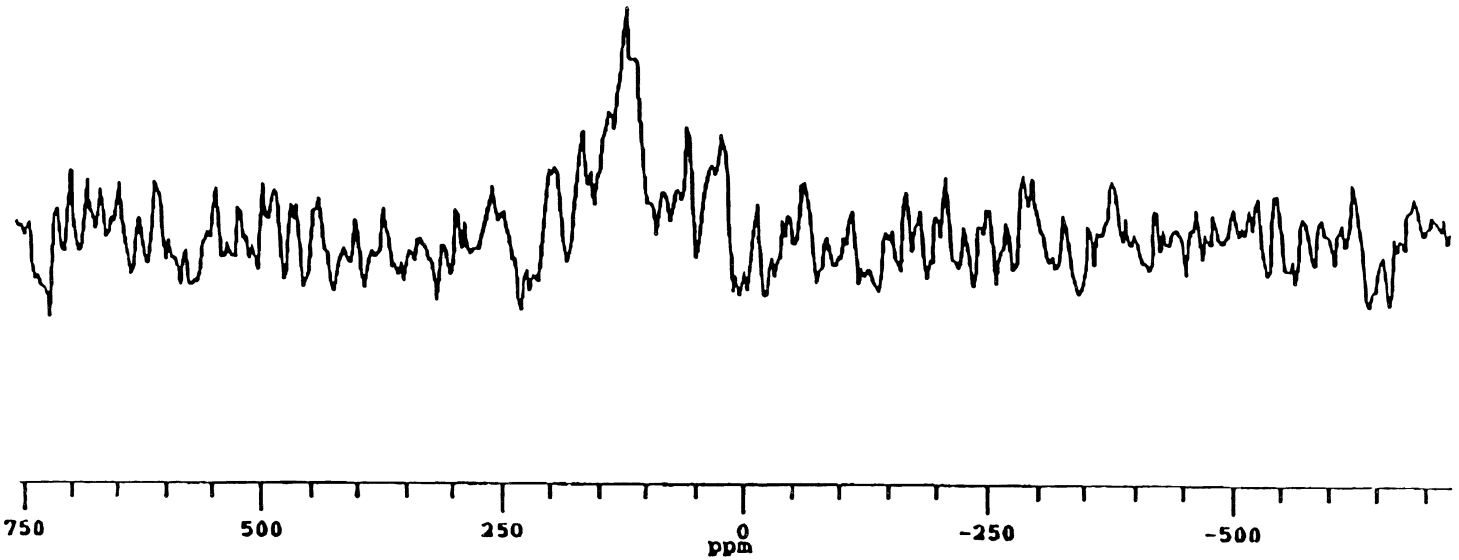

Figure 4. UC Mix soil ^{15}N-NMR spectrum after enrichment with labeled ammonium nitrate. Line broadening was 100 Hz.

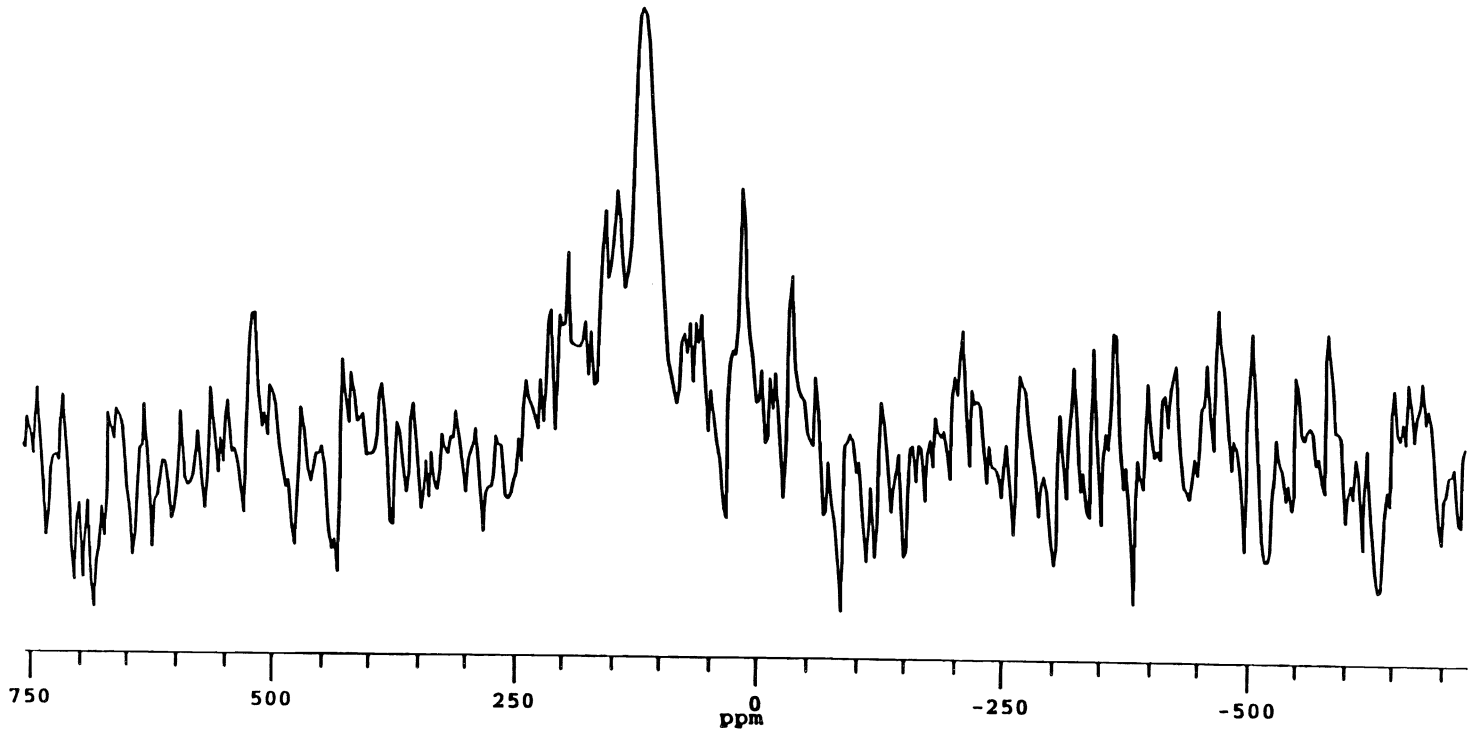

Figure 5. UC Mix soil ^{15}N-NMR spectrum after labeled aniline additions. Line broadening was 100 Hz.

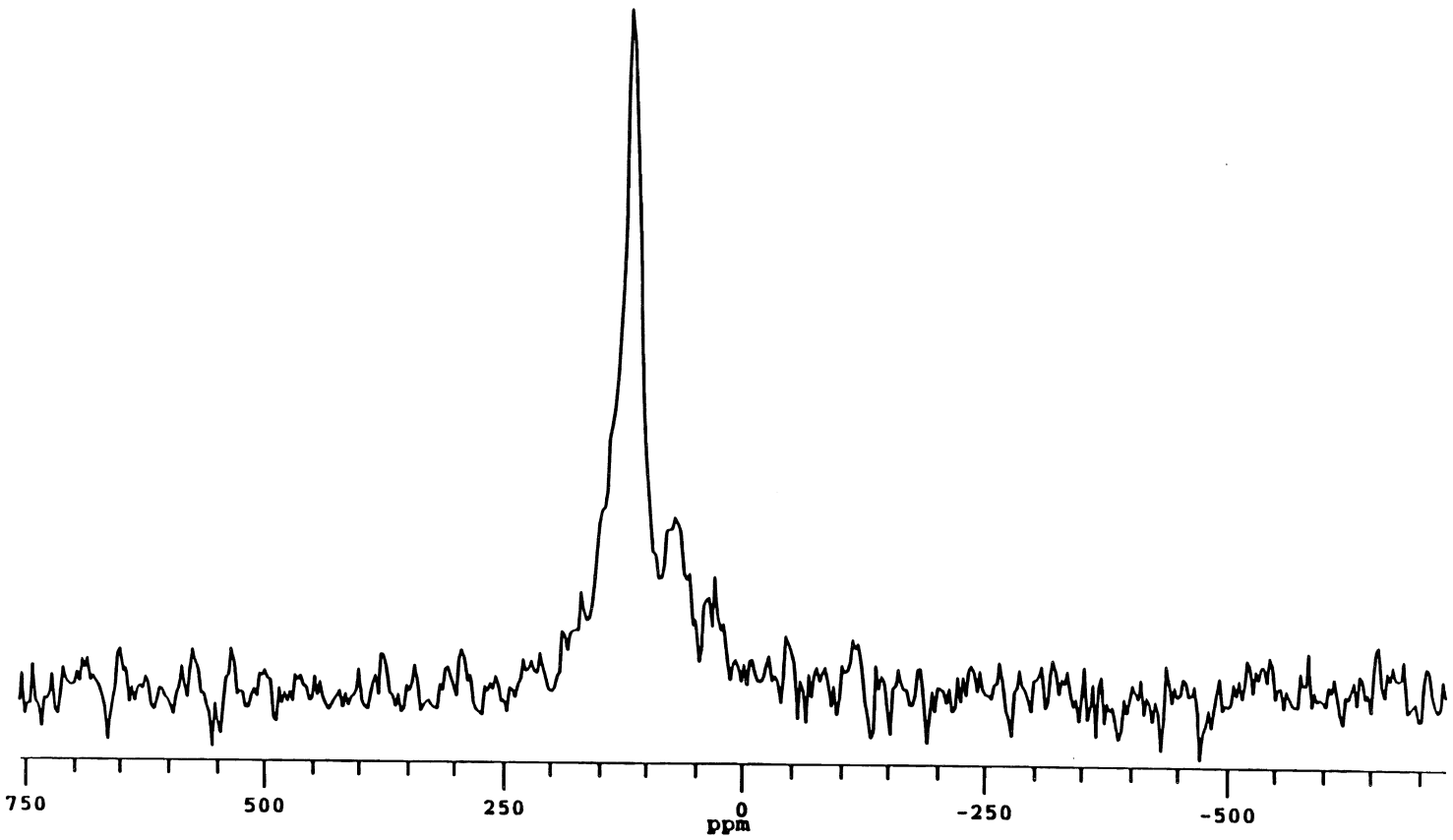

Figure 6. UC Mix soil litter ^{15}N-NMR spectrum after labeled aniline additions. Line broadening was 50 Hz.

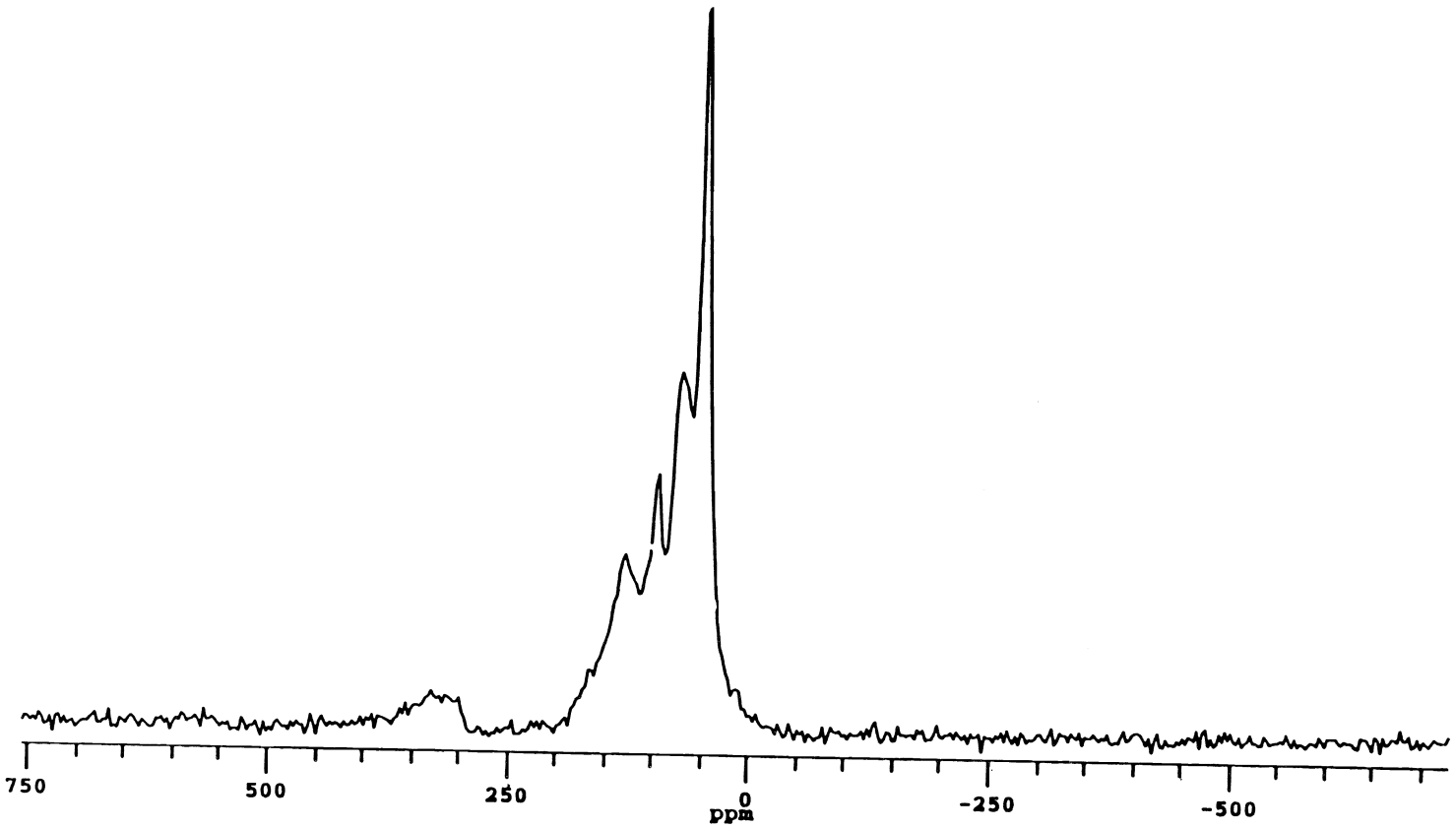

Figure 7. ^{15}N-NMR spectrum of IHSS standard peat after reaction with labeled aniline. Line broadening was 40 Hz.

Pesticide Transport via a Soil Particulate Carrier Mechanism and Interactions with Polymers

JOHN LETEY AND WALTER J. FARMER
Department of Soil and Environmental Sciences, Riverside Campus

Summary

Transport of napropamide was studied in disturbed soil columns in the laboratory. Napropamide was applied to the soil surface followed by water, which was allowed to percolate through the soil and exit the soil column for some period of time. Napropamide was measured in the initial leachate and the concentration decreased gradually with cumulative leaching. No preferential flow occurred in the disturbed soil columns and it was hypothesized that the napropamide moving rapidly through the column was associated with dissolved organic matter. Experiments were conducted comparing napropamide transport in columns with and without organic matter removed. Dissolved organic matter in the leachate was also measured. Effluents have not been completely analyzed at this time. An experiment was conducted on a farmer field who applied kelthane as a miticide in a bean field. Furrow irrigation water with and without addition of a polymer were sampled and analyzed for sediment and kelthane concentration. Polymer treatment reduced total and suspended solids and kelthane leaving the field. Kelthane concentrations in the runoff water in individual furrows were dependent on suspended solid load.

Key Words: napropamide, dissolved organic matter, leachate, erosion, kelthane

Project Objectives Addressed in 1994-95

1. Evaluate the migration of pesticide through soil via clay carrier mechanism for various soil characteristics and water qualities.

2. Evaluate the surface transport of pesticides by particulate movement in furrow irrigation with and without polymer treatment.

Research Plan and Procedures

Objective 1

Last year we reported the results of several experiments investigating thetransport of carbon-14 labeled napropamide through disturbed soil columns in thelaboratory. Carbon-14 was detected in the initial leachate and the concentration tended to decrease with additional leaching. Presence of napropamide in the leachate was verified by GC analysis. No solid particulates were observed in the leachate. However, the leachate had a yellow-orange discoloration. We hypothesized that the transport of napropamide could be attributed to the effect of dissolved organic matter on napropamide mobility, and that the gradual decrease of napropamide concentration with cumulative leachate was consistent with a gradual decrease in leachate discoloration.

Subsequent to the report, a more thorough analysis was conducted on the leachate for C-14 activity and napropamide concentration as measured by the GC. The napropamide had to be extracted from the leachate into hexane for the GC analysis. The C-14 activity was measured in the leachate before hexane extraction, in the leachate after hexane extraction, and in the hexane extract for comparative purposes to the GC analysis. There was close agreement on the napropamide concentration as determined by GC and the C-14 activity in the hexane extract. However, the amount of C-14 activity which was extracted from the leachate into hexane differed tremendously for leachates of the three soils. Essentially all of the C-14 activity (96%) in the leachate was extracted into hexane for the Tujunga soil. In contrast, almost none (4%) of the C-14 activity in the Domino soil leachate was extracted into hexane. Leachate from the Hanford soil was intermediate, with 32% of the C-14 activity extracted into the hexane.

The causative factor for various fractions of the C-14 activity being extracted into hexane had to be identified before further studies could be conducted with confidence. Two explanations for the results were postulated. One explanation is that the napropamide interacted with the dissolved organic matter in a manner which protected the napropamide from extraction into hexane. Another possibility was the presence of C-14 labeled chemicals other than napropamide which would not be extracted into hexane.

Without presenting details of all the studies conducted, it was concluded that the C-14 activity not extracted into hexane was the result of C-14 labeled impurities. Thus, it was concluded that reliable measurements of napropamide in leachate could be accomplished by measuring the C-14 activity in the hexane extract rather than in the total leachate, or that unlabeled napropamide had to be analyzed by other appropriate techniques.

After resolving the analytical technique questions, efforts were renewed to investigate the mechanism by which napropamide was rapidly transported through the soil. The hypothesis that dissolved organic matter (DOM) facilitated the transport was investigated. Hanford sandy loam soil was used in the study. In one case the soil was treated to remove organic matter for comparison with the untreated soil.

Organic matter removal was done by treating the soil with sodium hypochlorite by adding 200 mL of bleach to 100 g of soil. The soil and bleach were mixed for 20 minutes and then centrifuged for 20 minutes at 3,000 rpm and the supernatant was discarded. This procedure was repeated five times. The soil was then washed twice with 0.1 M $CaCl_2$ to replace sodium with calcium on the exchange site. The soil pH was adjusted to 7.1 with HCl. The soil was then dried and passed through a 2-mm sieve.

The treated and untreated soils were packed into plexiglass columns. Napropamide was dissolved in a 50:50 water:acetone mixture. The napropamide solution was applied to the surface of the soil at a rate equivalent to 7 kg ha^{-1}. The water and acetone were allowed to evaporate for 24 hours.

$CaCl_2$ was added to deionized water to bring the electrical conductivity of the solution to 1.0 dS m^{-1}. The water was maintained at the top of the soil column with a constant head of 5 cm. Effluent samples were collected every 15 mL for the first 300 mL of accumulated leachate. Samples were stored at 3°C until analyses were performed.

Dissolved organic matter was determined by oxidation and determination of CO_2 using an infrared detector. Napropamide was determined using HPLC with a UV detector.

The concentration of DOM in the leachate from the untreated columns was high initially (approximately 5,000 mg L^{-1} of C) and decreased to below 100 g L^{-1} C after 200 mL of leachate. Leachate from the columns where the soil had been treated to remove organic matter had DOM concentrations less than 500 mg L^{-1} C which remained relatively constant for 200 mL of leachate and then declined slightly thereafter.

Napropamide concentrations for all samples had not been determined at the time of this report due to instrument problems and time constraints. However, in the few samples that were analyzed, the napropamide concentration in the untreated column was initially high and decreased following the same downward trend as the DOM for the same leachate.

These studies will be continued during the next year to test further the hypothesis concerning DOM-facilitated napropamide transport.

Objective 2

The field experiment was conducted at Patterson, California, to determine the relationship between sediment and kelthane concentration in runoff water and to investigate the effectiveness of applying a polymer in the water to reduce both. The field had a history of kelthane application for the last three years. A lima bean crop was planted on two-row 1.52 m beds. The soil is classified as Capay clay (fine montmorillonitic, thermic Typic Haploxererts) with 45% clay, about 1.5% organic matter, and a neutral pH. The furrows were approximately 243 m long with a gradient of 0.5%.

Kelthane [1,1-bis-(chlorophenyl)-2,2,2-trichloroethanol], commonly known as dicofol, is a sister compound of DDT and used as a miticide in various crops such as cotton, fruits, vegetables and ornamentals. It is slightly water-soluble (0.8 mg L^{-1}) and has a high soil sorption coefficient (K_{oc} = 5,000 mg g^{-1}). It has a half-life of 45 days in soil and a low vapor pressure of 4.0 x 10^{-7} cm Hg (Wauchope et al., 1992).

California Aqueduct irrigation water was pumped through a manifold as schematically illustrated in Fig. 1. One arm of the manifold delivered untreated water to four metered outlets that distributed water to individual furrows. The other arm of the manifold contained a solution injector apparatus through which a concentrated polymer solution was injected at a rate to achieve a 10 mg L^{-1} concentration of polymer in the irrigation water. The polymer was a long-chain (high molecular weight), moderately charged, anionic polyacrylamide manufactured by Allied Colloids, Inc. with a trademark of SOILFIX G1. The polymer solution was passed through four metered outlets to individual furrows that were randomly selected. The flow rate of water to each furrow was adjusted to 2.25 m^3 h^{-1} for the first irrigation and 3.38 m^3 h^{-1} for later irrigations.

Flow near the end of each furrow was measured by collecting water in a container of known volume for a measured period of time. A 19-L bucket was installed with its top flush with the furrow bottom. An apparatus placed in the furrow funneled the flowing water and sediment into the bucket. Except for when samples were being taken, the water flowed through the funnel into a full bucket that overflowed into the last segment of the furrow. At sampling time, water was pumped from the bucket and water flowing into the bucket through the funnel was collected in containers that were set aside for sediment and pesticide analyses. After the samples were collected, the water in the bucket was again pumped out and the time to fill the bucket was recorded. Samples were collected every 15 min during the first hour after the water reached the sampling site and hourly thereafter. Water collected in the glass sampling bottles for kelthane analysis was stored and transported to the laboratory in ice coolers, and then extracted immediately.

Sampling was done three times during the year. A pre-crop irrigation was applied April 23, 1994 and the sampling represents kelthane background residues before pesticide application or crop planting. The lima beans were planted on May 13, 1994 and kelthane was ground-sprayed at the rate of 1 kg ha^{-1} on June 13, 1994 to control mites. Sampling was done on June 23, 1994 during the first irrigation after pesticide application. An irrigation was applied on July 12 but no water samples were taken during that irrigation. Water samples were collected on the next irrigation, which occurred on July 27. The field had been cultivated prior to the latter irrigation.

Eight randomly-located soil samples (0-15 cm) were collected with a hollow tube auger from the ridges or furrows at different times during the year. The soil sampleswere stored in glass jars and transported to the laboratory in ice coolers.

The 1-L water sample was extracted into a total of 250 mL hexane (100, 75, and 75 mL) by liquid-liquid partitioning. The hexane extracts were dried through anhydrous Na_2SO_4 and concentrated to 5 mL final volume. Thus, the concentration in the water sample was concentrated 200 times before analysis. For soil samples, 50 g of the soil samples were extracted into hexane:acetone (4:1) for 4 h by Soxlet extraction. The extracts were dried and concentrated to 5 mL. Kelthane standard (99% purity) was dissolved in DI water to make a 50 µg/mL standard solution. Three blank 50-g soil samples (5% moisture) were spiked with 2 mL of the prepared standard solution. The spiked samples were mixed thoroughly with a glass rod in 3 minutes. Then 25 g of each spiked soil were transferred to a Soxhlet thimble and stored in darkness in the freezer (0°C) for 24 h. On the next day, the soil thimbles were extracted by Soxhlet method, using 125 mL of hexane and 125 mL of acetone which were poured onto the soil thimbles. The extraction process took 8 h, and the extraction temperature was set at 65°C. When the extraction was finished, the extracted samples were filtered through sodium sulfate and the volumes of the extracted samples were brought down to 25 mL by a roto-vap. Then, the concentrated samples were transferred to vials for analysis by a 5980 Hewlett-Packard gas chromatograph. The GC conditions were as follows: injection temperature, 230°C; injection volume, 2 µL with splitless injection; colulmn temperature, 220°C; column type, DB608 (0.53 mm ID, 30 m length); electron capture detector temperature, 350°C; flow rate of N_2 gas (99.999% pure), 45.5 mL min^{-1}; and minimum detection limit, 1.6 g L^{-1}.

Water samples were analyzed separately for total sediment and concentration of finer particulates, hereafter referred to as suspended solids. The total sediment was determined by filtering the samples through crucibles supported with 2.1 cm GF/glass microfiber Whatman papers, drying the material at 105°C for 1 h and weighing the accumulated sediment. The suspended solids concentration was measured by stirring the sample and allowing the particulates to settle for 5 min. At that time, 6 mL of suspension from the top were siphoned and placed into colorimeter tubes. The optical transmittance was measured at 410 nm wavelength in the colorimeter. A calibration curve

between optical transmittance vs. known concentration of particulates in suspension was created to determine the suspended solids concentration in the sample.

Results and Discussion

The time for water in the furrows to reach the sampling site ranged from 6 to 9 h for the first irrigation. On the latter two sampling dates, the water reached the sampling site in 1-3 h. The more rapid advance during the latter irrigations compared to the first was caused by the imposed higher water in-flow rates and reduced infiltration rate later in the season.

The total sediment concentration in the samples collected at different times for treated and untreated furrows are presented in Table 1. With one exception, the total sediment concentration for a given sampling time was consistently higher in the untreated than the treated furrows. The sediment concentration was much higher during the last sampling date than the first two dates. This result was probably caused by the combination of having the field cultivated prior to the last irrigation and the higher water flow rate. Although the field had been tilled prior to the April 23 test, the lower flow rate and the higher infiltration rate probably contributed to the comparably low sediment concentration on that date. The polymer caused the fine particulates to flocculate and settle, as will be reported below, but the settled floccules were observed to be transported by the flowing water. The capacity to transport floccules is enhanced by the higher water flow rate.

The kelthane concentrations in the various samples are presented in Table 2. The lowest concentrations were measured on April 23, which represented background levels from treatments applied in previous years. The highest concentrations were measured on June 23 during the first irrigation after kelthane application. The kelthane concentrations in the samples were considerably lower on August 27 than on June 23. Two or more factors could contribute to the reduced concentrations. First, much of the pesticide residue on the soil surface would have been removed during the first irrigation or subsequently lost by volatilization. Secondly, a cultivation occurred prior to the July 27 irrigation which could have caused a mixing of the pesticide in the top layer, leaving it less exposed at the surface for transport with the irrigation water.

The kelthane concentration in the polymer-treated water was lower than the untreated water, except for June 23 when the concentrations were comparable for the treated and untreated waters.

The amount of pesticide transported from the field by runoff is a function of the concentration of pesticide in the water and the quantity of runoff. The infiltration rate of the soil was characterized by subtracting the average outflow rate from the average inflow rate. During the June 23 irrigation, the infiltration rates in the treated and untreated furrows were 19.28 and 14.74 L min^{-1},

respectively. During the July 27 irrigation, the average infiltration rates for the treated and untreated furrows were 13.23 and 10.21 L min^{-1}, respectively. Evidently, the added polymer in the water contributed to an increased infiltration rate during both irrigations. There was also an overall decrease in infiltration rate as the season progressed. The losses of kelthane in runoff reported in Table 2 were derived by multiplying the average flow rate between the samples with the respective kelthane concentrations. The amount lost in the runoff from the treated furrows was 67% of that lost in the untreated furrows on June 23. On July 27, the amount of pesticide in runoff in the treated furrows was 27% of that in the untreated furrows. Overall, far less than 1% of the applied kelthane was lost in runoff water.

Agassi et al. (1995) investigated the relationship between soil erosion and napropamide transport. Napropamide transport was linearly related to the amount of fine soil particulates eroded. There was no relationship between napropamide transport and total soil mass eroded. The relationship between kelthane concentration and suspended solids concentration (fine particulates) for the June 23 irrigation are presented in Fig. 2. There was no relationship between the kelthane concentration and suspended solids during this irrigation. However, there was an increasing concentration of kelthane with increasing suspended solids in samples collected during the irrigation on July 27 (Fig. 3). In both cases, the polymer was effective in reducing the concentration of suspended solids. However, during the June 23 irrigation, the reduction in suspended solids was not correlated with reduced kelthane concentration in the runoff.

The field had been irrigated previously before kelthane application. The furrow bottoms are relatively smooth after an irrigation, and kelthane would have been distributed over this smooth surface. Thus, the kelthane would have been readily exposed to the water flowing in the furrow and a small fraction of it would have become dissociated from the particulates and become dissolved in water. On the other hand, the cultivation prior to the July 27 irrigation mixed the surface and made for a rough furrow bottom. Under these conditions, the amount of kelthane adsorbed on the fine particulates transported by water would have been a larger percentage of the total kelthane transported. Thus, this resulted in a significant relationship between kelthane concentration and suspended solids concentration.

Based on the above analysis, one can conclude that the difference in amount of kelthane lost from the field in the treated and untreated furrows is almost entirely associated with the effect of the polymer in increasing infiltration rate on June 23. On the other hand, the difference on July 27 is a combination of the polymer increasing the infiltration rate and decreasing the amount of suspended solids leaving the field.

The kelthane concentrations in the soil samples taken on different dates are presented in Table 3. Note that the concentrations on April 23 prior to kelthane application were lower than on subsequent dates. The lower concentration in the soil taken at the bottom of the furrow on July 27 compared

to June 23, probably was a result of the mixing associated with the cultivation between those two dates. Note that the concentration in the ridge was about the same for both sampling dates. Since the total amount of kelthane removed from the field through runoff was very small, there is no significant difference between the samples taken from the treated and the untreated furrows.

Conclusion

The use of polymers in furrow irrigated fields can reduce the runoff loss of pesticides such as kelthane via a combination of two mechanisms. The polymers can increase infiltration rates, thus reducing the amount of runoff water which transports pesticides; and the polymer greatly reduces the suspended solids concentration and moderately reduces the total sediment concentration to which pesticide may be adsorbed and carried from the field. The latter mechanism is particularly important when the pesticide is mixed into the soil by cultivation following pesticide application. Unfortunately, the farm management practices did not allow us to check the effect of cultivating after pesticide application but before irrigation or cultivating the soil immediately before pesticide application. Both of these practices may lead to reduced pesticide removal by runoff and also may enhance the relative effectiveness of the polymer treatment.

References

Agassi, M., J. Letey, W. J. Farmer, and P. J. Clark. 1995. Soil erosion contribution to pesticide transport by furrow irrigation. J. Environ. Qual. 24:892-895.

Wauchope, R. D., T. M. Buttler, A. G. Hornsby, Augustun Beckers, and J. P. Burt. 1992. The SCS/ARS/CES pesticide properties database for environmental decision making. Rev. Environ. Contam. Toxicol. 123: 120 .

Table 1. Total Sediment Load in Runoff Water from Polymer Treated and Untreated Furrows

Sampling time (min)	Total sediments* (g L^{-1}) Treated 4/23	Treated 6/23	Treated 7/27	Untreated 4/23	Untreated 6/23	Untreated 7/27
0	0.227	0.297	7.393	1.441	0.708	11.334
15	0.533	0.295	6.436	2.699	0.696	18.063
30	0.404	0.339	6.169	4.768	0.858	10.178
45	0.362	0.334	7.208	5.862	0.727	8.096
60	0.321	0.276	6.304	1.479	0.751	10.814
120	0.146	0.319	5.736	1.469	0.512	9.170
180	0.045		1.334			
240	0.049	0.259	6.788	1.380	0.537	9.069
480	0.213	7.931		0.418	7.243	
1260	0.244			0.533		

*Average of four replicates.

Table 2. Kelthane Residues in Runoff Water from Polymer Treated and Untreated Furrows.

Sampling time (min)	Kelthane residues* (μ L^{-1}) Treated 4/23	Treated 6/23	Treated 7/27	Untreated 4/23	Untreated 6/23	Untreated 7/27
0	0.286	10.580	1.157	0.532	9.751	3.256
15	0.220	8.145	1.162	0.396	8.121	3.008
30	0.186	5.029	0.841	0.440	5.970	3.345
45	0.175	6.003	0.855	0.428	5.562	1.929
60	0.230	7.047	0.585	0.387	6.741	2.004
120	0.102	2.285	0.758	0.365	4.993	1.854
180	0.122			0.188		
240	0.076	3.692	0.417	0.234	3.958	1.085
480	3.451	0.329		4.842	1.085	
Runoff loss (g ha^{-1})		1.761	0.234		2.608	0.861
(percent)		0.140	0.021		0.244	0.076

Table 3. Kelthane Residues in Soil During Different Runoff Sampling Dates

Sampling date	Kelthane residues* ($\mu g\ g^{-1}$)	
	Treated	Untreated
4/23/94 (ridge)	0.062	0.050
6/23/94 (furrow)	0.273	0.318
7/12/94 (ridge)	0.193	0.198
7/27/94 (furrow)	0.095	0.103
8/18/94 (ridge)	0.196	0.214

*Average of four replicates.

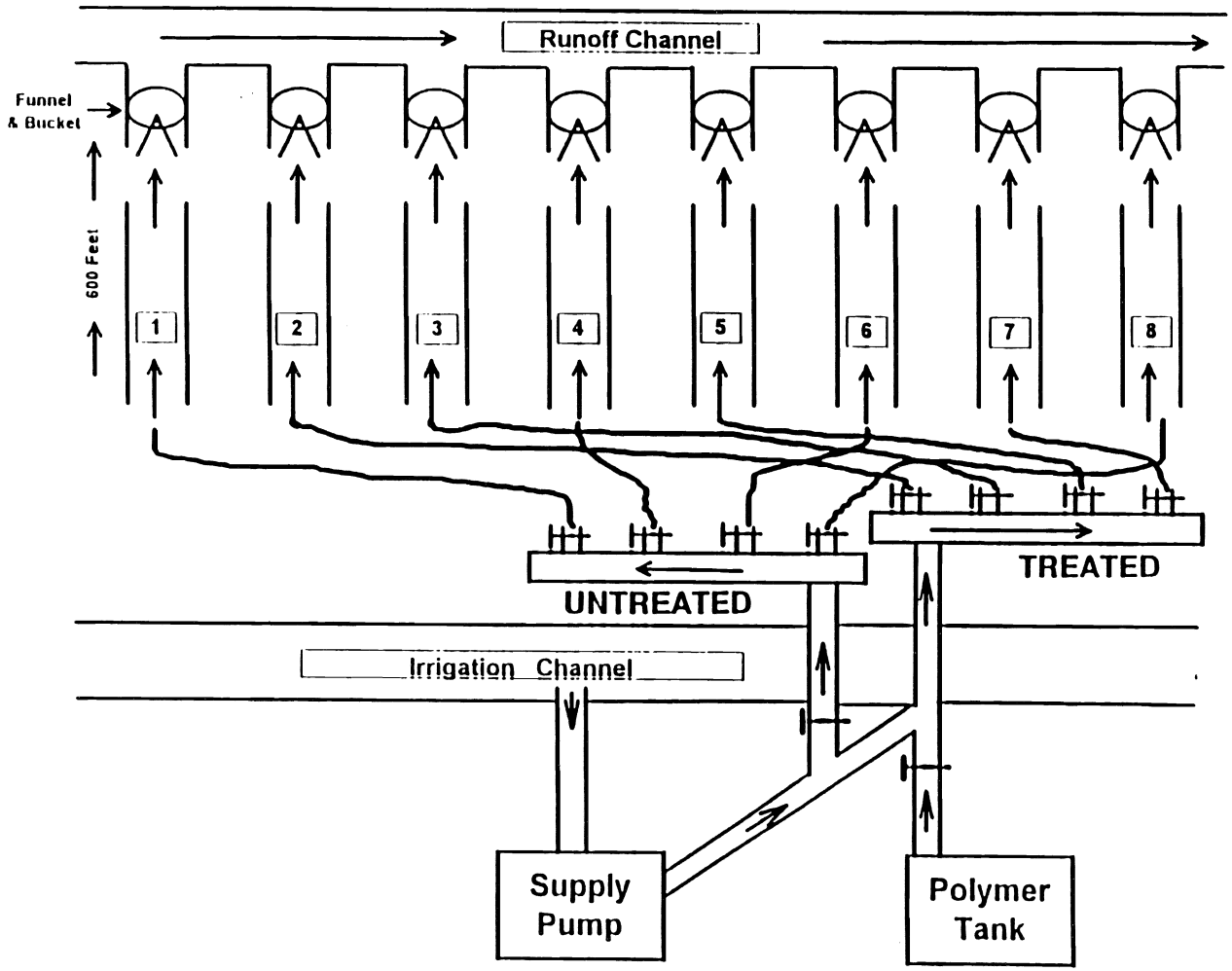

Figure 1. Diagram of field experimental setup and design.

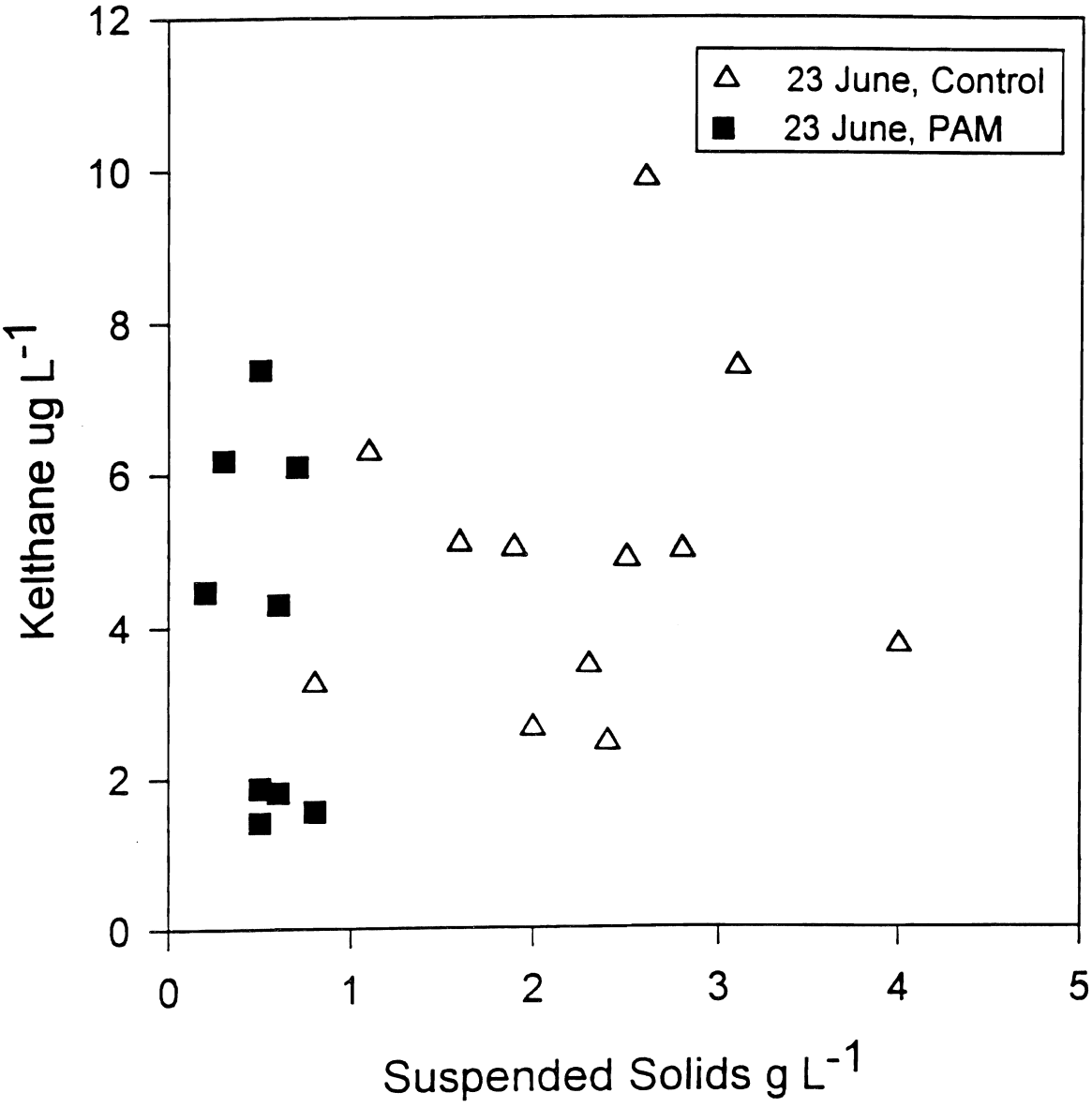

Figure 2. Relationship between kelthane concentration and suspended solids concentration in runoff water for the June 23 irrigation.

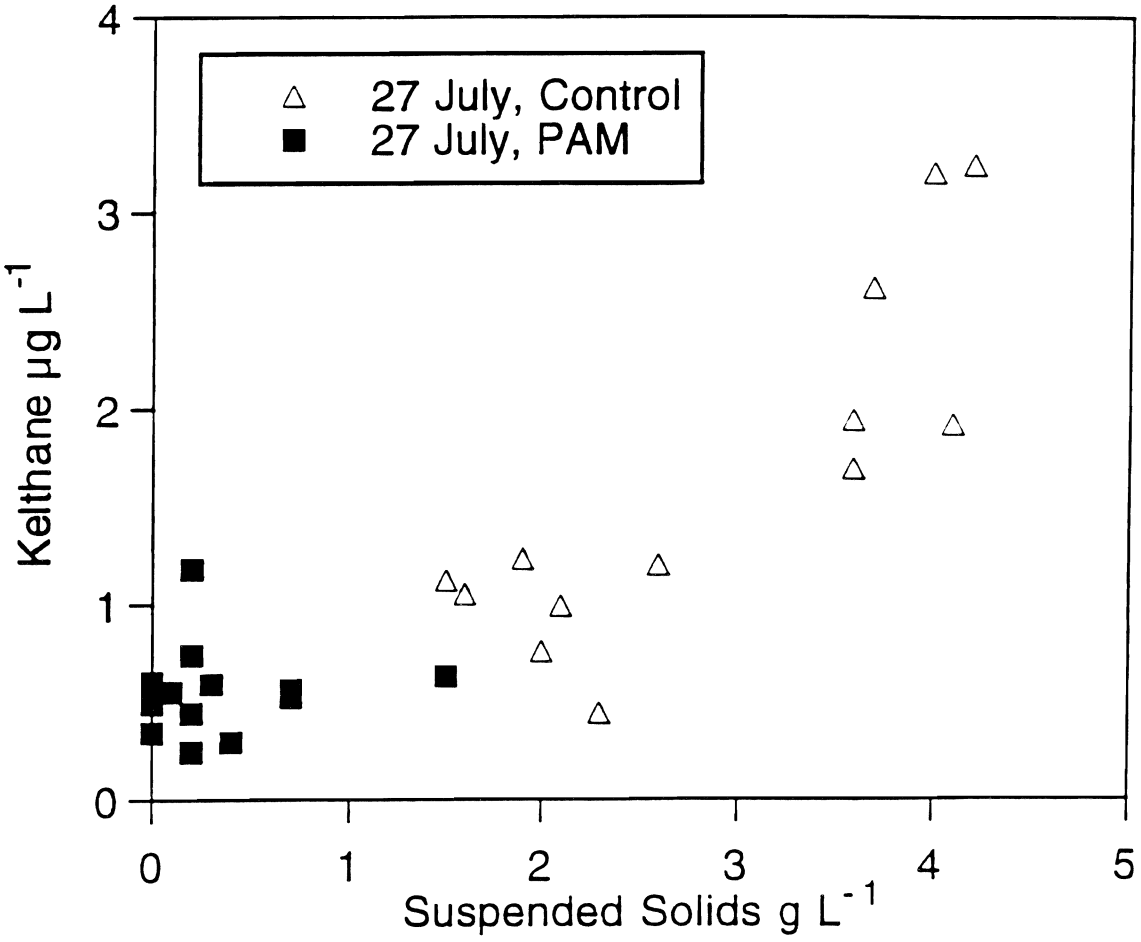

Figure 3. Relationship between kelthane concentration and suspended solids concentration in runoff water for the July 27 irrigation.

An Evaluation of Solute Movement and Porosity in Weathered Granitic Rock

ROBERT C. GRAHAM
MICHAEL A. ANDERSON
Department of Soil and Environmental Sciences, Riverside Campus

Summary

Weathered granitic rock is widespread in upland areas of California where increasing development for various land uses presents the potential for subsurface contamination. We previously reported that the saturated hydraulic conductivity of weathered granitic rock is well within the range found for soils and is, in fact, greater than that of local Bt horizons. Research reported here shows that transport, as indicated by dye and Br^- tracers, is relatively uniform through the bedrock joints and matrix when solute is delivered at less than the infiltration rate, but that ponded conditions lead to channeling through joint traces. This preferential flow is attributed to the greater abundance of macrovoids (pores >0.1 mm diam.) in the joints compared to the rock matrix. Pore continuity is created by woody roots penetrating nearly exclusively through the joint traces. As a result, deep transport of solutes into bedrock occurs in a finger-like pattern coinciding with the distribution of joints. While joint traces become narrower with depth, they extend many meters into the bedrock, providing both vertical and lateral flow paths for solutes, including potential contaminants, to reach surface and ground waters.

Key Words: weathered granitic rock, porosity, preferential flow, solute movement

Project Objective Addressed in 1994-95

To determine the relationship between tracer movement and the morphology of weathered granitic bedrock.

Research Plan and Procedures

Field Experimental Site An experimental site was established on a nearly level hill summit within the U.S. Forest Service North Mountain Experimental Area in the foothills of the San Jacinto Mountains in southern California. The granitic bedrock is tonalite of the late Mesozoic Peninsular Ranges batholith, one of the larger bodies of granitic rock in the United States. In general, the rock contains 50 to 55% plagioclase (An_{30-40}), 20 to 30% quartz, 1 to 8% K-feldspar, 10 to 15% biotite, and 0 to 5% hornblende (Hill, 1988). It is weathered to a depth of several meters, yielding a substrate with 25 to 30% porosity through which water flows at rates of up to 5 cm h^{-1} under saturated conditions (Johnson-Maynard et al., 1994). The bedrock, typically encountered within the upper 40 cm, is generally friable such that it can be chopped and dug using a pick and shovel, and chunks of it can be broken or crumbled by hand. For the most part, it matches the criteria for weathering classes 5 or 6 of Clayton and Arnold (1972), but is not sufficiently weathered to be considered saprolite (weathering class 7). The soils on the site are coarse-loamy, mixed, mesic Typic Xerorthents. Natural vegetation at the site consisted of dense chaparral.

Methods A 2.4 m deep trench was excavated to evaluate the bedrock morphology, particularly in regard to identifying potential preferential flow paths. Morphologic features, including roots, were mapped using a portable frame grid comprising 10 cm x 10 cm cells. *In situ* measurements of saturated hydraulic conductivity (K_{sat}) were made using a compact constant-head permeameter (Amoozegar, 1989). Particle-size analysis was determined by pipette (Gee and Bauder, 1986) for samples from the profile morphologic horizons. Samples for micromorphological analysis were taken by horizon from three separate vertical profiles on the trench face. Thin sections (27 mm x 46 mm) of undisturbed fabric impregnated with blue-dyed plastic resin were examined with a petrographic microscope and described using the terminology of Bullock et al. (1985). Macrovoids (used here to mean pores >0.1 mm in diameter) were quantified using the triplicated horizon samples and point-count transects (Drees and Ransom, 1994) with 1000 counts per thin section. Clods taken from randomly chosen cells of each regolith morphologic class (e.g., C, Cr/C, Cr horizons) were used to determine bulk density by the paraffin-coated clod method (Blake and Hartge, 1986). Total porosity was calculated from bulk density and particle densities measured for each regolith type using a gas pycnometer (Accupyc 1300, Micromeritics, Norcross, GA) (Blake and Hartge, 1986).

Tracer experiment A miniature spray boom (Ghodrati and Jury, 1990) was used to apply tracers to an area of 1.6 m x 1.6 m, which encompassed a 1 m x 1 m plot and a buffer zone. Two tracers, blue dye (7 g erioglaucine/ liter solution) and bromide (20 mmol KBr/liter solution), were applied simultaneously in a 0.5

cm-thick pulse within a time span of 10 minutes. Water to drive the tracer pulse was applied under two different conditions. An "unponded" condition was established by uniformly applying water as a spray across the surface of the plot such that the infiltration rate was not exceeded and ponding did not occur. A total of 7.9 cm of water was applied at a rate of 1.75 cm h^{-1}. A "ponded" condition was established by ponding water on the surface of the plot to a depth of ~1 to 2 cm. To minimize variations in water head pressure across the sloping (~10%) plot surface, aluminum flashing was used to divide the plot and buffer area into 28 cells, within each of which water was ponded. A total of 7.9 cm of water was used at a rate of 3.8 cm h^{-1}.

After application, the plots were covered with plastic sheeting to minimize evaporation until they were sampled about 24 h later. Sampling was conducted from a series of six vertical faces, spaced 20 cm apart, cut through each plot using an electric jackhammer. As each face was exposed, a 1- x 1-m-grid divided into 10 cm x 10 cm-cells was used to guide the mapping of morphologic features and the distribution of the blue dye. Soil and rock samples were collected from 40 cells on each face, distributed such that major features (e.g., joint traces, rock matrix) were well represented throughout the profile. Samples were collected into foil-lined bags and sampling equipment was cleaned with moist paper towels between each sample to avoid contamination. In the laboratory, samples were first air-dried and then 1:1 (by weight) water extracts were obtained using a vacuum extraction apparatus. These extracts were analyzed directly for Br^- using the phenol red method modified for an Alpkem segmented flow analyzer.

Results

Bedrock morphology Weathered rock usually dominates the regolith below the 35 cm depth, although it may begin at depths ranging from 10 to 50 cm. The bedrock mass ("Cr material") is divided into blocks by joint sets spaced 10 to 80 cm apart. Joint traces account for about 20% of the Cr/C horizon (35-85 cm depth). They average 6 cm in width (ranging from 0.1-15 cm wide) and are filled with sandy loam material ("C material") that lacks both rock and soil structure. In the Cr horizon (85-220 cm depth), the average joint trace width (2 cm) is less, although the range in width is the same. The C material filling the joint traces in the Cr horizon has a loamy sand texture, lacks structure, and constitutes <5% of the volume. Both the C and Cr material can be crushed easily by hand, but harder Cr material becomes more prevalent at greater depths. Chaparral roots penetrate deep into the weathered bedrock and are largely confined to the joint traces, resulting in distinct linear patterns in the cross-sectional map presented in Fig. 1. Such roots were found as deep as 4 m in holes augered at the site. In the Cr horizon, where the roots are more narrowly confined, the organic carbon content is considerably higher in the joints (4.0 g kg^{-1}) than in the matrix blocks of weathered rock (0.9 g kg^{-1}) (Table 1). The clay content is <8% for both Cr and C materials.

Porosity Pore space (total porosity) accounts for 36% of the Cr/C horizon volume and 33% of the joint trace material in the Cr horizon, but only 13% of the volume in Cr horizon blocks (Table 1). The Cr/C and Cr horizons have 8 to 9% macrovoid (>0.1 mm diam.) space, except in the Cr horizon joint traces, where macrovoids are 15% by point count (Table 1). By comparison, the overlying soil (AC horizon) has 51% total porosity and 24% macrovoid space.

Original rock fabric is retained in corestone blocks (Cr material), but macroporosity has been generated in the form of fractures both around and through primary mineral grains. Thin laminated clay coatings are common on the fracture surfaces. As indicated by X-ray diffraction, the clay fraction is dominated by a poorly crystalline kaolin mineral. Microporosity has developed as a result of dissolution pitting of plagioclase (Inskeep et al., 1993; Jones and Graham, 1993) and biotite weathering. In contrast, the joint trace material lacks the interlocking grain fabric of rock, having a microstructure similar to that of soil material. Roots penetrate preferentially through this weakly structured material relative to the corestone rock fabric.

Tracer movement Under unponded conditions, the blue dye moved as a continuous front through the thin soil cover and the upper 10 to 20 cm of weathered bedrock (Fig. 2a). No preferential movement along joint traces was observed. The ponded application conditions resulted in dye uniformly penetrating the soil and upper 5 to 15 cm of bedrock, but below this it moved preferentially along both vertical and horizontal joint traces and extended into matrix material only adjacent to the joint traces (Fig. 2b). Fingers of dye penetrated to the 70 cm depth in joint traces; whereas, the bulk of the matrix was unstained below the 20 cm depth.

Under unponded conditions, Br^- occurred in higher concentrations in the rock matrix than within joints in the upper 20 cm of bedrock, but below this, mean concentrations were virtually the same in both joints and matrix (Fig. 3a). Under ponded conditions, mean Br^- concentrations were again lower in the matrix than in joints within the upper 20 cm of bedrock, but below this, concentrations remained higher within the joints to a depth of 90 cm (Fig. 3b).

Discussion

Weathered granitic bedrock is a porous medium through which water and solutes can move readily. Tracers indicate relatively uniform transport through both joints and matrix of the weathered bedrock under unponded application conditions. Flow is primarily via capillary pores with little opportunity for channeling. In the upper part of the bedrock, however, lower Br^- concentrations in the joint material than in the matrix may indicate solute drainage from joint macrovoids, either downward in the profile or laterally into the rock matrix.

Under ponded application conditions, the bedrock morphology has a strong influence on solute movement, since parts of the regolith become saturated and water is able to flow through macrovoids. Preferential flow occurs

in the joint traces, which have nearly 70% more macrovoids than the rock matrix (blocks). Drainage of joint macrovoids, as described for the unponded conditions, may account for the lower Br^- concentrations in joint traces compared to rock matrix in the upper part of the bedrock. In general, channeling of flow is likely promoted by the continuous nature of pores produced by the roots penetrating through the joint traces. As a result, deep transport of solutes into bedrock occurs in a finger-like pattern coinciding with the distribution of joints. While joint traces become narrower with depth, they extend many meters into the bedrock, providing both vertical and lateral flow paths for solutes, including potential contaminants, to reach surface and ground waters.

References

Amoozegar, 1989. A compact constant-head permeameter for measuring saturated hydraulic conductivity of the vadose zone. Soil Sci. Soc. Am. J. 53:1356-1361.

Blake, G.R., and K.H. Hartge. 1986. Bulk density. p. 363-375. *In* A. Klute (ed.) Methods of soil analysis. Part 1. 2nd edition. Agron. Monogr. 9. ASA and SSSA, Madison, WI.

Bullock, P., N. Fedoroff, A. Jongerius, G. Stoops, T. Tursina, and U. Babel. 1985. Handbook for soil thin section description. Waine Research Publications, Wolverhampton, UK.

Clayton, J.L., and J.F. Arnold. 1972. Practical grain size, fracturing density and weathering classification of intrusive rocks of the Idaho batholith. U.S. For. Serv. Gen. Tech. Rep. INT-2, Intermountain For. Range Exp. Stn., Ogden, UT.

Drees, L. R., and M.D. Ransom. 1994. Light microscope techniques in quantitative soil mineralogy. p. 137-176. *In* J.E. Amonette and L.W. Zelazny (ed.) Quantitative methods in soil mineralogy. SSSA Misc. Publ., SSSA, Madison, WI.

Gee, G.W., and J.W. Bauder, 1986. Particle size analysis. p. 383-411. *In* A. Klute (ed.) Methods of soil analysis. Part 1. 2nd edition. Agron. Monogr. 9. ASA and SSSA, Madison, WI.

Ghodrati, M., and W.A. Jury. 1990. A field study using dyes to characterize preferential flow of water. Soil Sci. Soc. Am. J. 54:1558-1563.

Hill, R.I. 1988. San Jacinto intrusive complex: 1. Geology and mineral chemistry, and a model for intermittent recharge of tonalitic magma chambers. J. Geophys. Res. 93:10,325-10,348.

Inskeep, W.P., J.L. Clayton, and D.W. Mogk. 1993. Naturally weathered plagioclase grains from the Idaho Batholith: Observations using scanning electron microscopy. Soil Sci. Soc. Am. J. 57:851-860.

Jones, D.P., and R.C. Graham. 1993. Water-holding characteristics of weathered granitic rock in chaparral and forest ecosystems. Soil Sci. Soc. Am. J. 57:256-261.

Johnson-Maynard, J., M.A. Anderson, S. Green, and R.C. Graham. 1994. Physical and hydraulic properties of weathered granitic rock in southern California. Soil Sci. 158:375-380.

Table 1. Properties of soil and weathered granitic bedrock materials.

Horizon	Depth	Organic carbon	Sand	Silt	Clay	Bulk density	Total porosity	Macrovoids (>0.1 mm)	K_{sat}
	cm	g kg^{-1}	----------%----------			g cm^{-3}	%	%	cm h^{-1}
A	0-5	50.1	75	17	8	ND†	ND	ND	ND
AC	5-20	10.5	75	19	6	1.35	49	24	29
C	20-35	5.6	72	20	8	1.48	44	ND	ND
Cr/C	35-85	2.7	74	19	7	1.72	35	8	4
Cr	85-220								4‡
blocks		0.9	84	14	2	2.34	12	9	
joints		4.0	77	18	5	2.08	21	15	

†ND = not determined

‡Saturated hydraulic conductivity for Cr horizon as a whole (blocks and joints not distinguished).

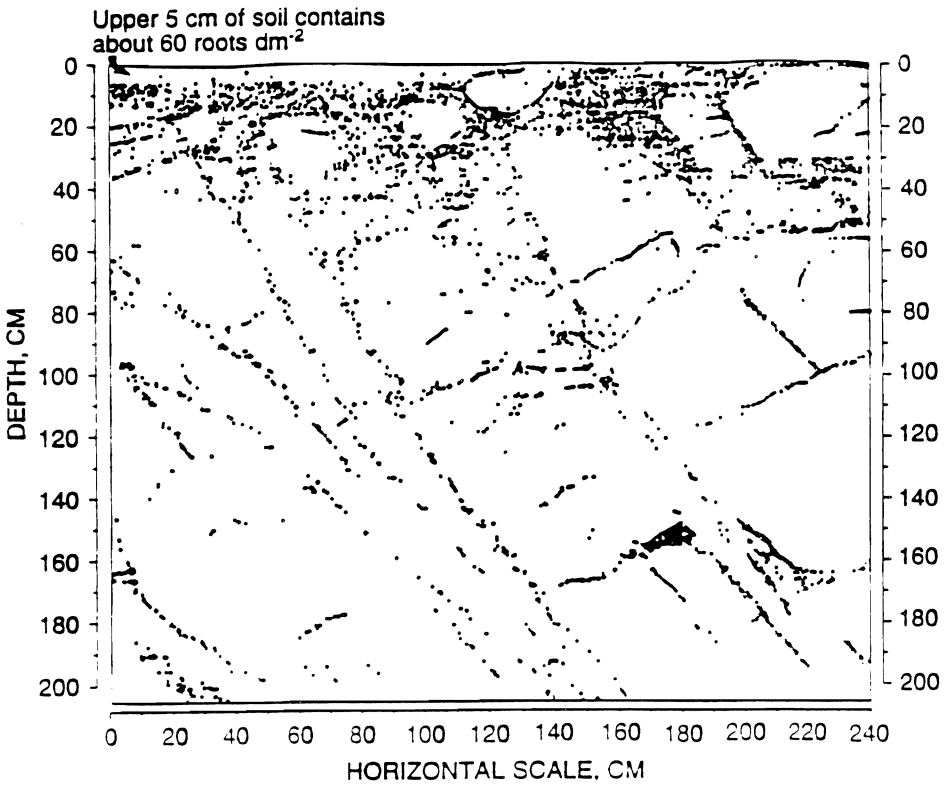

Figure 1. Map of woody (chaparral) root distribution in weathered granitic bedrock. The soil-bedrock boundary is within the 20-40 cm depth. Each point represents a single root intersecting the trench wall. The linear distribution pattern reflects root confinement to joint traces.

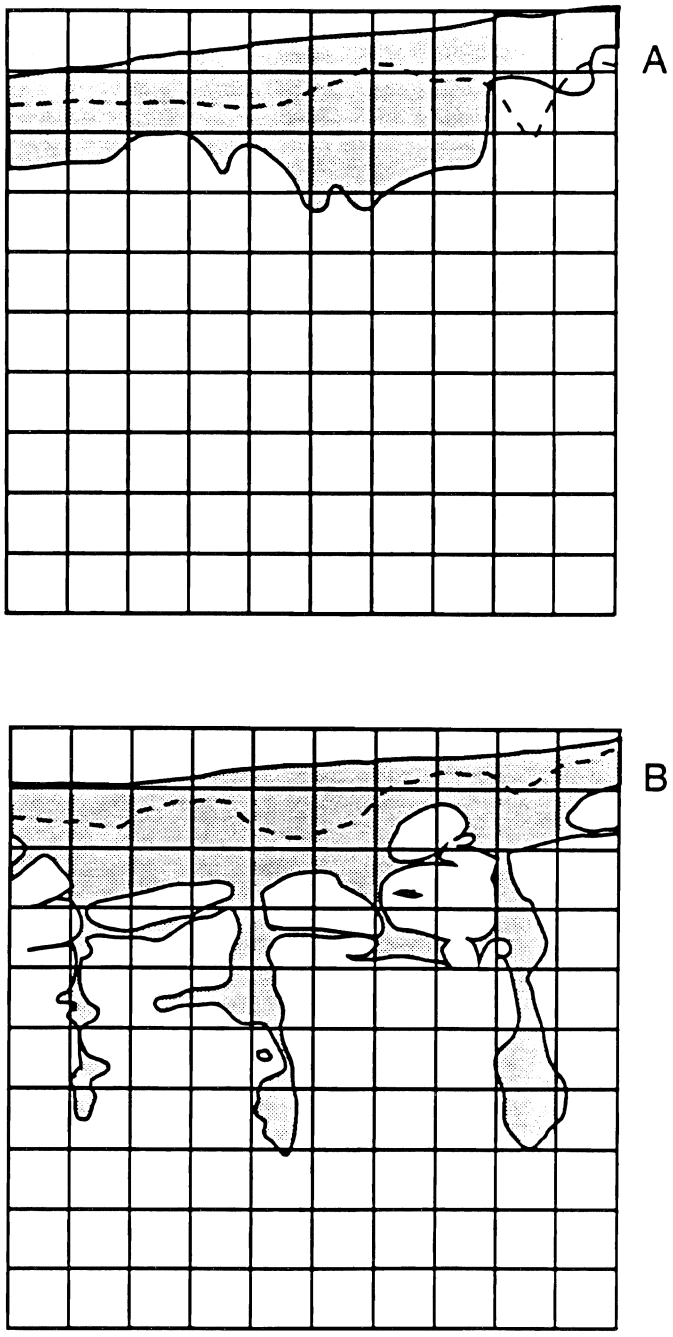

Figure 2. Dye tracer distribution patterns resulting from (A) unponded and (B) ponded water application conditions. Shading depicts the regions stained by the dye. The soil surface slopes gently downward to the left and the soil-bedrock contact is indicated by a dashed line. The grid is composed of 10 cm x 10 cm cells.

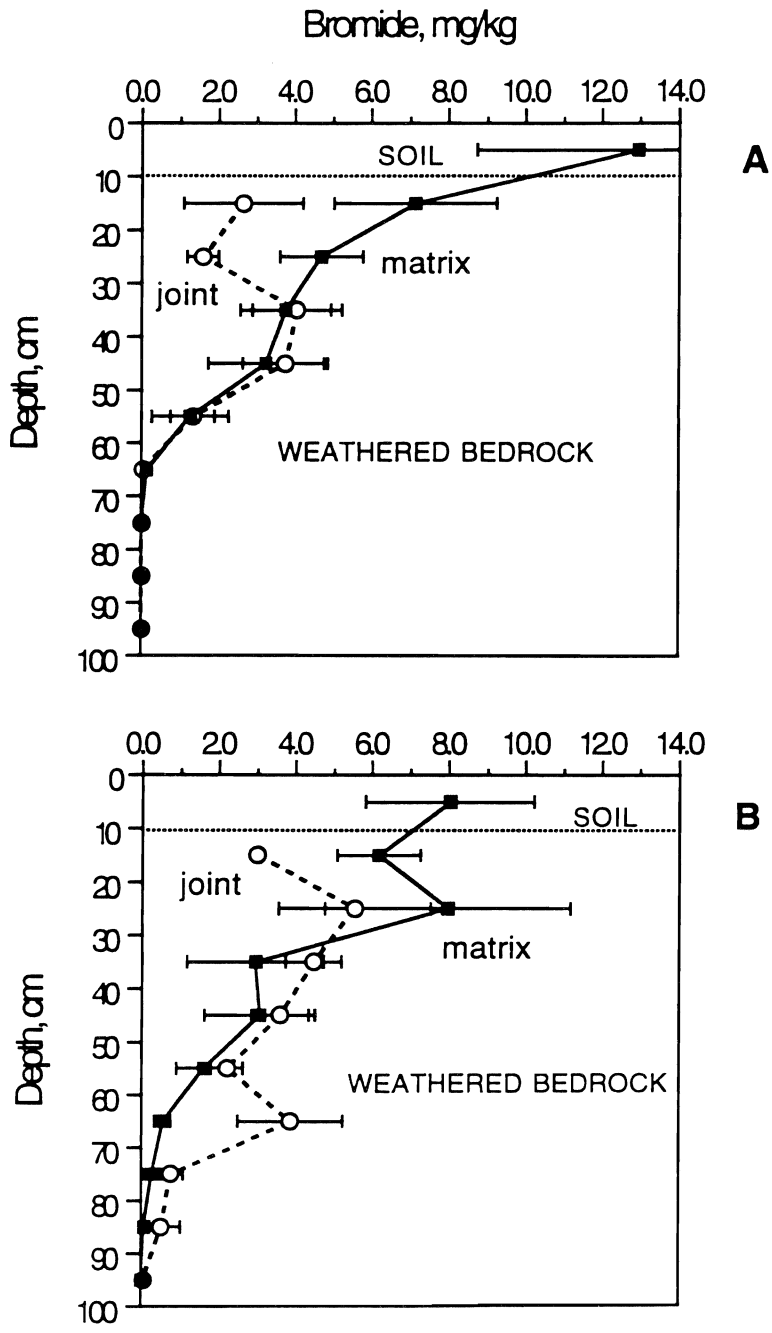

Figure 3. Bromide tracer distributions resulting from (A) unponded and (B) ponded application conditions. Each point represents the mean Br^- concentration (mg per kg of soil or rock) for the plotted 10 cm depth increment from six vertical sampling faces. In all cases, the soil was only about 10 cm thick. Error bars indicate one standard error of the mean.

Water Flow and Virus Transport in Weathered Bedrock

ROBERT C. GRAHAM, MARYLYNN V. YATES, AND MICHAEL A. ANDERSON
Department of Soil and Environmental Sciences, Riverside Campus

Summary

Rural residential developments in California tend to be in upland areas where soils are thin and underlain by weathered, fractured bedrock. These developments typically use septic tanks for on-site waste treatment, but little is known about the potential for contaminant transport or attenuation within weathered bedrock. Of fundamental importance in this regard is the hydraulic conductivity of the weathered rock material. We measured hydraulic conductivity as a function of matric potential for intact cores of weathered granitic rock. The weathered rock contained 84% sand and 2% clay and had a bulk density of 2.34 g cm^{-3}. Saturated hydraulic conductivities ranged from 2-15 cm h^{-1}, while hydraulic conductivity at a matric potential of -3 J kg^{-1} averaged 0.10 cm h^{-1}. Weathered granitic rock can provide unsaturated hydraulic conductivities within the range that is acceptable for on-site wastewater treatment, but saturated conditions resulting from drainfield failures are likely to result in flows that are too rapid for proper treatment of waste water.

Key Words: weathered granitic rock, unsaturated hydraulic conductivity, on-site sewage disposal

Project Objective Addressed in 1994-95

Measure physical properties relevant to contaminant transport in weathered bedrock. Specifically, hydraulic conductivity as a function of matric potential was measured.

Research Plan and Procedures

Intact core samples of weathered rock (tonalite) were taken from a pit excavated about one meter into bedrock. The rock was sufficiently weathered such that it could be broken by hand, but *in situ* it was undisrupted and retained its original fabric. The weathered rock samples contained 84% sand, 14% silt, and 2% clay, and <0.1% organic carbon. The intact samples had a bulk density on the order of 2.34 g cm^{-3}, with 12% total porosity and 9% macrovoids (>0.1 mm diam.). The core samples were 5.35 cm in diameter and 6 cm long. They were taken while the rock material was moist by gently carving around the outsides of metal cylinders as the cylinders were slowly pressed into the bedrock. The weathered rock material fit tightly within the cylinder with no obvious gaps between the sample and the cylinder wall. The cores were mounted in Tempe cells and fitted with micro-tensiometers. The samples, Tempe cell ceramic plates, and tensiometers were saturated with de-aired water. Suction was applied and corresponding outflow water was recorded using transducers connected to a data logger. Suction was applied in steps of 1, 3, 10, 20, and 30 J kg^{-1} increments, allowing us to use a multi-step outflow method, together with the Richard's equation, to determine unsaturated hydraulic conductivity (van Dam et al., 1994). A curve was fit to the hydraulic conductivity - matric potential data using a computer program (van Dam et al., 1990). Volumetric water content was measured at the end of the experiment by oven drying the samples and was recalculated for each equilibrated matric potential using the measured outflow data. Hydraulic conductivity and volumetric water content data were used to estimate the average time required for water-borne pollutants to move a given distance through the rock. This time of travel (TOT) was calculated using the equation:

$$TOT = (L \times \theta) / K(\theta)$$

where L is the distance of transport, θ is the volumetric water content, and K is the hydraulic conductivity (Williams et al., 1994). A unit hydraulic gradient is assumed.

Results

Water retention curves for weathered granitic rock are presented in Fig. 1. They show steep decreases in volumetric water content as matric potential decreases, as is typical of coarse-textured materials. Hydraulic conductivity also decreases sharply with decreasing matric potential as shown in Fig. 2.

Discussion

On-site sewage disposal systems are designed to operate at soil moisture conditions less than saturated, with matric potentials of -2 to -8 J kg^{-1} commonly found below septic drain fields (Williams et al., 1994). Under these conditions, the hydraulic conductivity of acceptable materials must not be so low that unreasonably large land areas are required for disposal, nor so high that waste water flows through the medium too rapidly for effective treatment. A minimum acceptable hydraulic conductivity rate is generally considered to be about 0.07 cm h^{-1} (Williams et al., 1994). The samples we measured all had conductivities at least this high (averaging 0.10 cm h^{-1}) at matric potentials $\leq$-3 J kg^{-1}. When matric potentials were >-4 J kg^{-1}, however, none of the samples had conductivities as high as 0.07 cm h^{-1} (Fig. 2).

Maximum acceptable hydraulic conductivities have been considered to be those resulting in TOT values $\geq$24 h for a 60 cm travel distance (Williams et al., 1994). In this study, all samples had $TOT_{60\ cm}$ values that exceeded 24 h when the matric potential was $\leq$-2 J kg^{-1}. The maximum TOT at -2 J kg^{-1} matric potential was 27 h for a sample with a hydraulic conductivity of 0.5 cm h^{-1}.

Because failure of on-site septic systems is not uncommon, this worst-case scenario, resulting in saturated conditions, must be considered. Saturated hydraulic conductivity ranged from about 2 to 15 cm h^{-1}, which is consistent with values reported for similar weathered granitic rocks (Johnson-Maynard et al., 1994; Graham and Anderson, 1993). These saturated hydraulic conductivities yielded $TOT_{60\ cm}$ values ranging from 1.5 to 13.1 h, substantially less than the recommended TOT of 24 h.

Within the range of high matric potentials associated with septic drainfields, hydraulic conductivities for weathered granitic rock materials in this study are greater than those reported for saprolites in the southeastern United States. For example, we measured an average hydraulic conductivity of 0.029 cm h^{-1} at -4 J kg^{-1} for weathered granitic rock samples (Fig. 2), which is twice the rate reported by Vepraskas and Williams (1995) for granitic saprolites in North Carolina. The finer texture (20% clay) and clay-plugged pores of the saprolites may account for their lower hydraulic conductivities compared to the less intensively weathered bedrock in California.

These results indicate that weathered granitic rock can provide unsaturated hydraulic conductivities within the range that is acceptable for on-site waste water treatment. The relatively high saturated hydraulic conductivity of these materials, however, imparts a concern that if system failure results in saturated conditions, waste water might flow too rapidly for treatment to take place. Water movement under *in situ* saturated conditions may be particularly rapid via preferential flow through joint fissures, as indicated by Graham and Anderson (1996).

References

Graham, R.C., and M.A. Anderson. 1993. An evaluation of solute movement and porosity in weathered granitic rock. p. 135-142. *In* Reactions of Toxic Pollutants in Soil Systems, Kearney Foundation 1992-93 Annual Report.

Graham, R.C., and M.A. Anderson. 1996. An evaluation of solute movement and porosity in weathered granitic rock. (this volume). *In* Reactions of Toxic Pollutants in Soil Systems, Kearney Foundation 1994-95 Annual Report.

Johnson-Maynard, J., M.A. Anderson, S. Green, and R.C. Graham. 1994. Physical and hydraulic properties of weathered granitic rock in southern California. Soil Sci. 158:375-380.

van Dam, J.C., J.N.M. Stricker, and P. Droogers. 1990. From one-step to multi-step determination of soil hydraulic functions by outflow experiments. Dep. Water Resources Report no. 7. Wageningen Agric. Univ., Wageningen, The Netherlands.

van Dam, J.C., J.N.M. Stricker, and P. Droogers. 1994. Inverse method to determine soil hydraulic functions from multistep outflow experiments. Soil Sci. Soc. Am. J. 58:647-652.

Vepraskas, M.J., and J.P. Williams. 1995. Hydraulic conductivity of saprolite as a function of sample dimensions and measurement technique. Soil Sci. Soc. Am. J. 59:975-981.

Williams, J.P., M.J. Vepraskas, and M.T. Hoover. 1994. Quartz vein impact on hydraulic conductivity and solute transport through quartz-phyllite saprolite. J. Environ. Qual. 23:202-207.

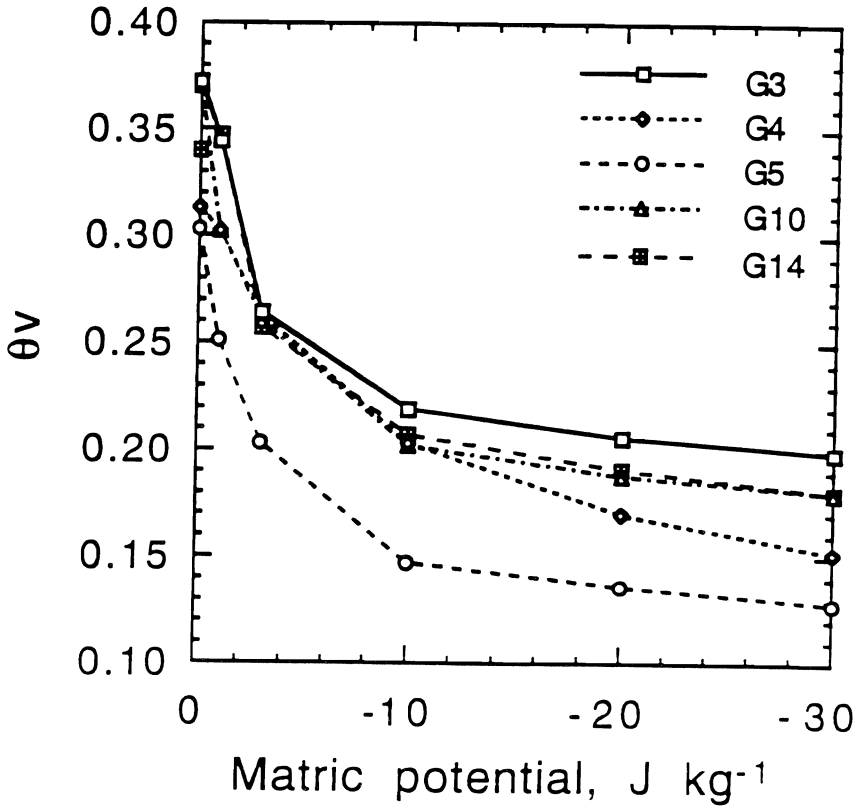

Figure 1. Volumetric water content (θ_v) as a function of matric potential for 5 intact cores of weathered granitic rock.

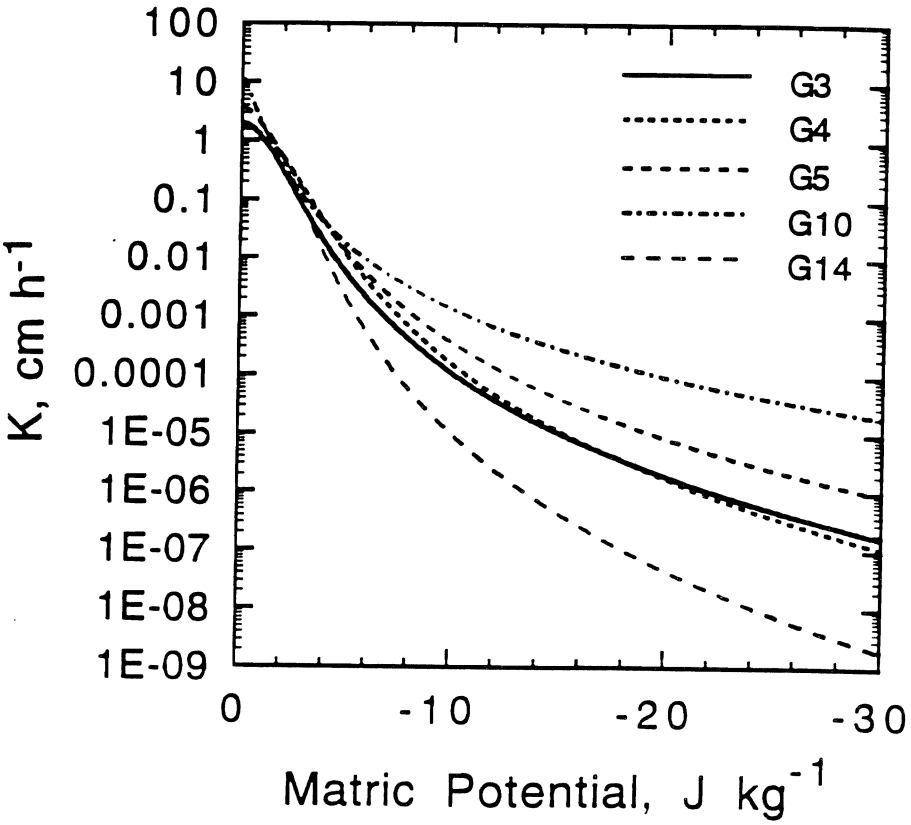

Figure 2. Hydraulic conductivity (K) as a function of matric potential for 5 intact cores of weathered granitic rock.

Metal Fixation at Soil Mineral Surfaces

WILLIAM H. CASEY[1] AND PETER A. ROCK[2]
[1]*Department of Land, Air and Water Resources, Davis Campus*
[2]*Department of Chemistry, Davis Campus*

Summary

Industrial metal extraction releases 7,000 to 70,000 metric tons per year of base metals (lead, copper, zinc, cadmium) to the aquatic environment. Currently there are more than 31,000 metal-contaminated hazardous waste sites in the United States (Moore and Luoma, 1990). The loading to soil from municipal waste treatment is also substantial in the form of incinerator flyash and discarded metal batteries. Much of this metal contamination ends up in carbonate minerals (Fuller and Davis, 1987) because calcareous, western soils are rich in $CaCO_3$ (10-50 weight percent). Understanding the rates and pathways for metal fixation into minerals is important for predicting the environmental fate of metals in soils.

This research project has had two goals. First, we evaluated the rates of incorporation of toxic metals into carbonate mineral surfaces (Rock et al., 1994). Second, we instructed students in an electrochemical approach to determining thermodynamic properties of minerals and aqueous solutions, which avoids many disadvantages of conventional solubility experiments. We accomplished each goal and expanded the research to include thermochemistry of carbonate solid-solution minerals and the electrochemistry of heavy-metal oxalate phases.

Oxalate plays an essential role in nutrient cycling in soil (Jurinak et al., 1986). Calcium-oxalate and calcium-phosphate minerals are relatively insoluble; therefore, biogenic oxalate suppresses the activity of $Ca^{2+}(aq)$ in the soil solution, thereby allowing the phosphate concentration to increase. The high concentrations of oxalate in forest soils ($\approx$90 g/m^2, Cromack et al., 1979) led us to wonder if it plays a similar role in controlling movement of toxic heavy metals. Biogenic oxalates of manganese, copper, and magnesium have been reported to be associated with crustose lichens (Jones and Wilson, 1986). We determined Gibbs energies for forming several heavy-metal oxalate phases to evaluate the role of oxalate solids in the cycling of metals. A new electrochemical cell method is employed in which the solids react with fixed and relatively large concentrations of dissolved oxalate. Three advantages of this cell design are (1) corrections for electrolyte nonidealities can be made directly, without appeal to complicated models of solute speciation; (2) there is no liquid-liquid junction potential; and (3) the possibility of equilibrium is verifiable by Nernstian response of the electrode and by the absence of hysteresis in the relation between cell voltage and current.

Key Words: thermodynamics, electrochemistry, geochemistry, soil chemistry, solubilities.

Project Objectives Addressed in 1994-95

1. Investigate thermodynamic properties of heavy-metal oxalate phases.

2. Investigatge thermodynamic properties of carbonate solid-solution minerals.

Research Plan and Procedures

The Thermodynamic Properties of Heavy-Metal Oxalate Phases

The electrochemical cell method is well suited to examine the hypothesis that cycling of some heavy metals in soils is affected by equilibrium with oxalate solids. The hypothesis was tested using electrochemical cells that allow us to determine $\Delta G^{o}_{f}[PbC_2O_4(s)]$, $\Delta G^{o}_{f}[CdC_2O_4 \cdot 3H_2O(s)]$, $\Delta G^{o}_{f}[ZnC_2O_4 \cdot 2H_2O(s)]$ and $\Delta G^{o}_{f}[Hg_2C_2O_4(s)]$ and, hence, the solubilities in soil solutions. The approach was stepwise. The thermodynamic properties of calcium monohydrate [Whewellite, $CaC_2O_4 \cdot H_2O(s)$] are well known because of the role that this mineral plays in plant nutrition (e.g., Graustein et al., 1977) and in forming kidney stones (Finlayson et al., 1971). We took advantage of this fact to construct an electrochemical cell of the type:

$$Pb(Hg,2\text{-phase})|PbC_2O_4(s),CaC_2O_4 \cdot H_2O(s)|CaCl_2(aq,m)|Hg_2Cl_2(s)|Hg(l) \quad (1)$$

that uses the well-known $\Delta G^{o}_{f}[CaC_2O_4 \cdot H_2O(s)]$ value to determine the relatively poorly known value of $\Delta G^{o}_{f}[PbC_2O_4(s)]$. The postulated electrode cell reactions are:

$$Pb(Hg) + CaC_2O_4 \cdot H_2O(s) \rightarrow PbC_2O_4(s) + Ca^{2}(aq,m)| + H_2O(l) + 2e^{-} \quad (2)$$

$$Hg_2Cl_2(s) + 2e^{-} \rightarrow 2Hg(l) + 2Cl^{-}(aq,m) \quad (3)$$

yielding a net cell reaction of

$$Pb(Hg)+CaC_2O_4 \cdot H_2O(s)+Hg_2Cl_2 \rightarrow PbC_2O_4(s)+CaCl_2(aq,m)+2Hg(l) + H_2O(l) \quad (4)$$

Application of the Nernst equation to the net cell reaction yields:

$$E = E^{\circ} - \frac{RT}{2F} \ln\left[\left(4m^3\gamma_{\pm}^3\right)a_{H_2O}\right] \quad (5)$$

where $\gamma_{\pm}$ is the mean ionic activity coefficient of $CaCl_2(aq)$ in the cell electrolyte at molality m and a_{H_2O} is the activity of water in the cell electrolyte. The values of $\gamma_{\pm}$ and a_{H_2O} are known (e.g., Pitzer and Brewer, 1961). The value of $\Delta G^{o}f[PbC_2O_4(s)]$ was calculated using the relation:

$$\Delta G^{\circ}_{rxn} = -2FE^{\circ} = \sum_{i} \nu \Delta G^{\circ}_{f}[i] \qquad (6)$$

and tabulated values of $DG^{o}f$ for all the species, *i*, in Eqn. (6). These values were $\Delta G^{o}f[Ca^{2+}(aq)]$ = -553.58 kJ·mol^{-1}, $\Delta G^{o}f[Cl^{-}(aq)]$ = -131.228 kJ·mol^{-1}, $\Delta G^{o}f[H_2O(l)]$ = -237.129 kJ·mol^{-1}, $\Delta G^{o}f[CaC_2O_4 \cdot H_2O(s)]$ = -1513.87 kJ·mol^{-1}, $\Delta G^{o}f[Hg_2Cl_2(s)]$ = -210.745 kJ·mol^{-1}, and $\Delta G^{o}f[Pb(Hg, 2\text{-phase})]$ = -1.130 kJ·mol^{-1}.

Once the value of $\Delta G^{o}f[PbC_2O_4(s)]$ is estimated from a cell containing Whewellite, $\Delta G^{o}f$ values for the other heavy-metal oxalate phases, such as $ZnC_2O_4 \cdot 2H_2O(s)$, $CdC_2O_4 \cdot 3H_2O(s)$ and $Hg_2C_2O_4(s)$ can be estimated from electrodes containing the appropriate metal amalgam:

$$Zn(Hg,sat.)|ZnC_2O_4 \cdot 2H_2O(s)|Na_2C_2O_4(aq,m)|PbC_2O_4(s)|Pb(Hg,2\text{-phase}) \qquad (7)$$

$$Zn(Hg,sat.) + PbC_2O_4(s) + 2H_2O \acute{} Zn_2C_2O_4 \cdot 2H_2O(s) + Pb(Hg,2\text{-phase}) \qquad (8)$$

and:

$$Pb(Hg,2\text{-phase})|PbC_2O_4(s)|Na_2C_2O_4(aq,m)|Hg_2C_2O_4(s)|Hg(l) \qquad (9)$$

$$Pb(Hg,2\text{-phase}) + Hg_2C_2O_4 \acute{} PbC_2O_4(s) + 2Hg(l) \qquad (10)$$

Thermodynamic Properties of Carbonate Solid-Solutions

In the course of this research, we designed electrochemical double cells that allow us to monitor the thermodynamic activity of one metal-carbonate component in equilibrium with the aqueous solution and a carbonate solid solution phase. Because the electrochemical cells are novel, we are also conducting high-temperature calorimetric studies to determine the enthalpies of mixing $\left[\Delta H^{mix}_{298}\right]$ end-member components to form solid-solution phases. The $\left[\Delta H^{mix}_{298}\right]$ values for mixing aragonite and strontianite to form $Ca_xSr_{1-x}CO_3(s)$ solid solutions were obtained at 298 K from drop-solution enthalpies $\left[\Delta H^{ds}_{973}\right]$ of pellets of the respective solid solutions into molten $2PbO \bullet B_2O_3$ at 973 K.

The reactions that take place in the calorimeter as a pellet of $CaCO_3(s)$, $SrCO_3(s)$ or $Ca_xSr_{1-x}CO_3(s)$ is dropped into the melt are as follows:

$$Ca_xSr_{1-x}CO_3(s,298\ K) = xCaO(sol.,973K) + (1-x)SrO(sol.,973K) + CO_2(g,973K) \quad (11)$$

Argon was passed ($\approx$1 cm^3/s) through the drop tube and over the platinum crucible during an experiment. This procedure rapidly and efficiently removes $CO_2(g)$ from the calorimeter, ensures that CO_2 does not interact with the solvent, and produces a well-defined final state for the calorimetry. With dissolution of the oxide and degassing of the $CO_2(g)$, the initial and final thermodynamic states are well defined and the experiments yield heats of mixing of strontianite and aragonite to form a solid solution.

Results and Discussion

The Thermodynamic Properties of Heavy-Metal Oxalate Phases

There are surprisingly few thermodynamic data on the stabilities of heavy-metal oxalate solids. Our new estimate of $\Delta G^o_f[PbC_2O_4(s)]$=-758.7 $kJ \cdot mol^{-1}$ differs significantly from values reported in previous work, although few values are available. The critically evaluated compilation of Wagman et al., (1982) reports $\Delta G^o_f[PbC_2O_4(s)]$=-750.1 $kJ \cdot mol^{-1}$, and Naumov et al. (1974) report $\Delta G^o_f[PbC_2O_4(s)]\approx$-750.7 $kJ \cdot mol^{-1}$. The agreement between these two compilations may be misleading, because as the actual datum probably comes from the same single set of experiments. Latimer (1952) estimated $\Delta G^o_f[PbC_2O_4(s)]\approx$-754.4 $kJ \cdot mol^{-1}$, which is closer to the value that we report here. When our value of $\Delta G^o_f[PbC_2O_4(s)]$ is used to establish Gibbs energies for other phases, the agreement with other reported data becomes better. For example, our value for $\Delta G^o_f[ZnC_2O_4 \cdot 2H_2O]$ is -1346.45 kJ mol^{-1} and the value reported by Wagman et al., (1982) is $\Delta G^o_f[ZnC_2O_4 \cdot 2H_2O]$ = -1345.8 kJ mol^{-1}. The solubility products are compared in Table 1.

The possibility that cycling of heavy metals in soils is affected by equilibrium with oxalate solids can be evaluated using the new values of $\Delta G^o_f[PbC_2O_4(s)]$, $\Delta G^o_f[CdC_2O_4 \cdot 3H_2O(s)]$, $\Delta G^o_f[ZnC_2O_4 \cdot 2H_2O(s)]$, and $\Delta G^o_f[Hg_2C_2O_4(s)]$. When the new values of ΔG^o_f are incorporated into multicomponent speciation calculations to examine whether the soil solutions in these oxalate-rich spodosols could reach equilibrium with heavy-metal oxalate solids if contaminated with heavy metals, where we find that $CdC_2O_4 \cdot 3H_2O(s)$ and $ZnC_2O_4 \cdot 2H_2O(s)$ solids are sufficiently soluble that they probably would never form, unless the soils' metal concentrations approach millimolar concentrations of dissolved metal. Such high concentrations are probably not found, even in highly contaminated soils. The soil solutions, however, could easily reach equilibrium with $PbC_2O_4(s)$. Although $Hg_2C_2O_4(s)$ is highly insoluble, it is unlikely to form because most small concentrations of dissolved

chloride ion would lead to formation of calomel, a much more stable solid than $Hg_2C_2O_4(s)$. Heavy-metal oxalate phases could form locally as a result of phytodetoxification of soil; the resulting solids would not be in equilibrium with the adjacent soil solution at reasonable chemical conditions.

The Enthalpies of Mixing in Solid-Solution Carbonate Minerals

When plotted together [Fig. 1], the measured $\left[\Delta H^{ds}_{973}\right]$ values fall significantly below the line corresponding to an ideal mixture of strontianite and aragonite:

$$H^{ds}_{975}[Ca_xSr_{1-x}CO_3(s)] = x\ H^{ds}_{975}[CaCO_3(s)] + (1-x)\ H^{ds}_{975}[SrCO_3(s)] \quad (12)$$

Because the measured enthalpies are endothermic, the distribution of observed ΔH^{ds}_{975} values indicate that values of the enthalpy of mixing $\left[\Delta H^{mix}_{298}\right]$ are positive. Knowledge of the drop-solution enthalpies of strontianite, aragonite and the $Ca_xSr_{1-x}CO_3(s)$ solid solutions directly yields the ΔH^{mix}_{298} values at room temperature:

$$\Delta H^{mix}_{298}\ [Ca_xSr_{1-x}CO_3(s)] = x\ \Delta H^{ds}_{795}[CaCO_3(s)] - (1-x)\ \Delta H^{ds}_{975}\ [SrCO_3(s)] - \Delta H^{ds}_{975}[Ca_xSr_{1-x}CO_3(s)] \quad (13)$$

To within the experimental uncertainties, the measured $\left[\Delta H^{mix}_{298}\right]$ values are positive for all measured values of x [Fig. 2], nearly symmetric around x =0.50, and they reach a maximum value of $+3.82\pm0.94$ kJ mol^{-1}.

Our independent electrochemical studies have reported that ΔG^{ex}_{298} values are also positive over the range $0.0<x<0.9$ and reach a maximum value of $+3.0(\pm1.6)$ kJ mol^{-1} at $x\approx0.7$ (Casey et al., in press). The general similarity between the $\left[\Delta H^{mix}_{298}\right]$ and the ΔG^{ex}_{298} values suggests that the excess entropy of mixing is small or zero, consistent with the regular-solution treatment. With a regular-solution treatment, the interaction parameter is $W = 13.5(\pm1.3)$ kJ mol^{-1}, which yields a very narrow range of stable miscible compositions at Earth surface conditions.

In independent work, we determined the Gibbs energies for this incorporation (Casey et al., in press), so that determination of the enthalpies of mixing allows for a nearly complete set of mixing thermodynamic properties. These thermodynamic data, when considered as a whole, indicate that compositions of aragonite or strontianite, with even a few percent impurity, are not stable and will unmix to form a mechanical mixture of calcium-rich strontianite and a strontium-rich aragonite.

References

Casey, W. H., P. A. Rock, J.-B. Chung, E. M. Walling, M. K. McBeath. 1996. Gibbs energies of formation of metal-carbonate solid solutions 2: The $Ca_xSr_{1-x}CO_3(s)$ system at 298 K and 1 bar. American J. Sci. In press.

Cromack, K. Jr., P. Sollins, W. C. Graustein, K. Speidel, A. W. Todd, G. Spycher, C. Li, and R. L. Todd. 1979. Calcium oxalate accumulation and soil weathering in mats of the hypogeous fungus *Hysterangium crassum*. Soil Biol. Biochem. 11:463-468.

Finlayson, B., L. L. Hench, and L. H. Smith. 1971. *Urolithiasis,* Physical Aspects, National Academy of Science, Washington, D.C.

Fuller C. C. and J. A. Davis. 1987. Processes and kinetics of Cd^{+2} adsorption by a calcareous aquifer sand. Geochim. Cosmochim. Acta 51:241-254.

Graustein, W. C., K. Kromack, Jr., and P. Sollins. 1977. Calcium oxalate-occurence in soils and effect on nutrient and geochemical cycles. Science 198:1252-1254.

Jones, D. and M. J. Wilson. 1986. Biomineralization in crustose lichens. Chapter 6. *In* B.S.C. Ledbetter and R. Riding (eds.) Biomineralization in Low Plants and Animals. Clarendon Press, Oxford. p. 91-105.

Jurinak, J. J., L. M. Dudley, M. F. Allen, and W. G. Knight. 1986. The role of calcium oxalate in the availability of phosphorus in soils of semiarid regions: a thermodynamic study. Soil Sci. 142:255-261.

Latimer, W. M. 1952. The Oxidation States of the Elements and Their Potentials in Aqueous Solutions. 2nd. ed. Prentice-Hall, Englewood Cliffs,N.J..

Moore J. N. and S. N. Luoma. 1990. Hazardous wastes from large-scale metal extraction. Environ. Sci. and Technol. 24:1279-1285.

Naumov, G. B., B. N. Ryshenko, and I. L. Khodakovsky, 1974. Handbook of Thermodynamic Data (translated by G. J. Soleimani, edited by I. Barnes and V. Speltz), U.S. Geol. Survey Water Resources Report. 74-001. p. A-74.

Pitzer, K.S. and L. Brewer. 1961. Revised edition of Thermodynamics by G.N.Lewis and M. Randall, 2nd ed., McGraw-Hill, New York,. 723 pp.

Rock, P. A., Casey, W. H., McBeath, M. M., and Walling, E. M., 1994, A New Method for Determining Gibbs Energies of Formation of Metal-Carbonate Solid Solutions: The $Ca_xCd_{1-x}CO_3(s)$ System at 298°K and 1 bar: Geochimica et Cosmochimica Acta, v. 58, p. 4281-4291.

Vosburgh, W. C. and J. F. Beckman. 1940. The solubility of cadmium and zinc oxalates in salt solutions. J. Amer. Chem. Soc. 61:1028-1031.

Wagman, D. D., W. H. Evans, V. B. Parker, R. H.Schumm, I. Halow, S. M. Bailey, K. L. Churney, and R. L. Nuttall 1982. The NBS tables of chemical thermodynamic properties: selected values for inorganic and C_1 and C_2 organic substances in SI units. J. Phys. Chem. Ref. Data, 11: (Supplement 2), 392 pp.

Table 1. Experimental ΔG^{o}_{f} values at 25.0°C for heavy-metal oxalate solids compared with estimates from selected other studies.

Phase	K_{sp}	ΔG^{o}_{f}(kJ mol^{-1})[1]	Source
PbC_2O_4(s)	$8.3*10^{-12}$	-754.4	Latimer, 1952
	$8.4*10^{-10}$	-750.1	Wagman et al., (1982)
	$2.95*10^{-11}$	-758.70	this study
	$7.2*10^{-11}$	-749.8	Naumov et al., (1971)
$Hg_2C_2O_4$(s)	$1.00*10^{-13}$	-588.7	Latimer (estimate; 1952)
	$1.73*10^{-12}$	-587.51	this study
$ZnC_2O_4 \cdot 2H_2O$(s)	$1.28*10^{-9}$	-1345.95	Vosburgh and Beckman, 1940
	$1.37*10^{-9}$	-1345.8	Wagman et al., 1982
	$1.06*10^{-9}$	-1346.45	this study
$CdC_2O_4 \cdot 3H_2O$(s)	$1.44*10^{-8}$	-1507.66	Vosburgh and Beckman, 1940
	$1.42*10^{-8}$	-1507.7	Wagman et al., 1982
	$1.84*10^{-8}$	-1507.05	this study

[1]The value for $\Delta G^{o}_{f}[CaC_2O_4 \cdot H_2O(s)]$ reported by Wagman et al. (1982) was used in the calculations of ΔG^{o}_{f} values for other phases and is therefore not a new result.

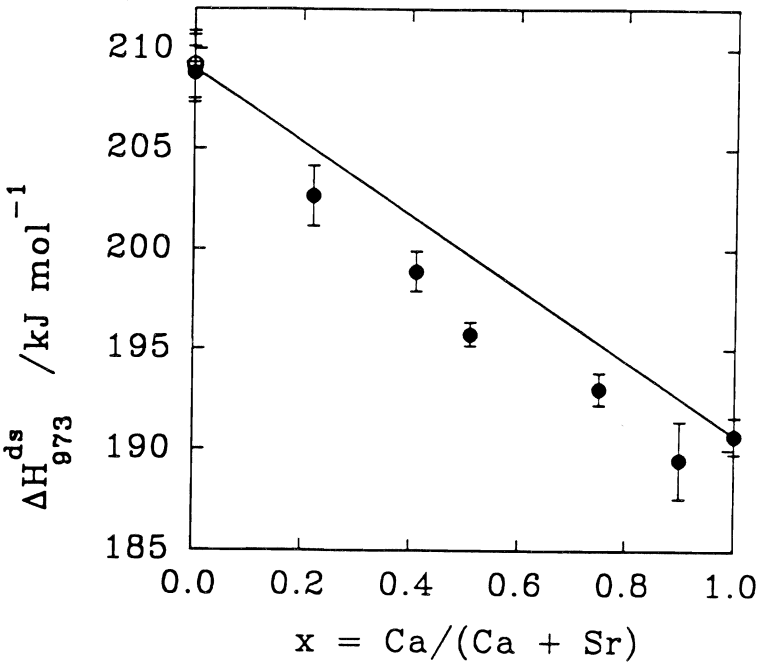

Figure. 1. The ΔH^{ds}_{973} values for $Ca_xSr_{1-x}CO_3$(s) solids. The line corresponds to the values for an ideal solution of aragonite and strontianite.

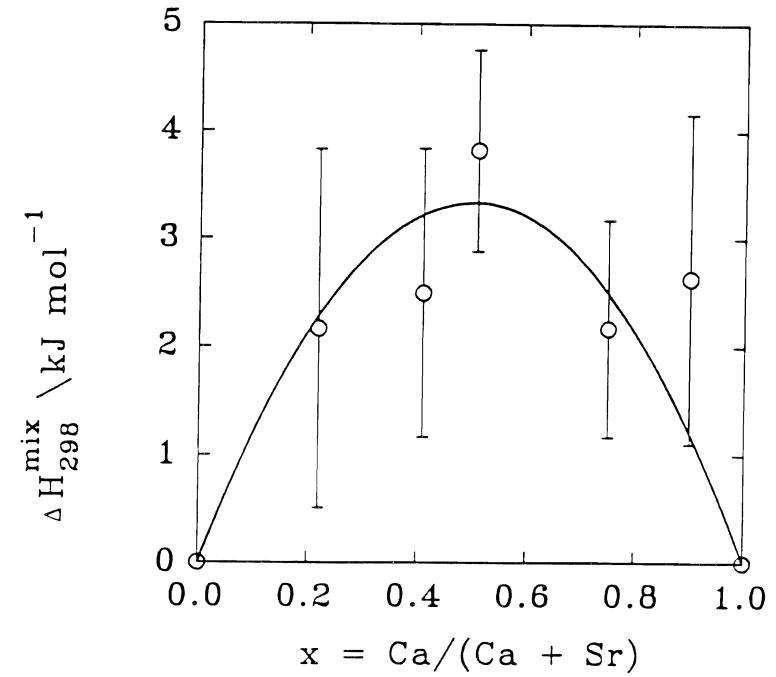

Figure 2. ΔH^{mix}_{298} values for mixing of strontianite and aragonite to form $Ca_xSr_{1-x}CO_3$ solid solutions at 298 K. The line corresponds to the best fit of a regular-solution model to the data using a model interaction parameter of W = 13.5 kJ mol^{-1}.

Spectroscopic Studies of Herbicide-Humic Substance Complexes in Soils

GARRISON SPOSITO
Department of Environmental Science, Policy and Management, Berkeley Campus

Summary

Previous research in this project has indicated proton-transfer and, to a lesser extent, hydrogen-bonding and hydrophobic interactions as principal mechanisms of binding between the herbicide atrazine and humic acids extracted from tropical soils. These results are surprising, in that other *s*-triazines appear to react more by electron-donor-acceptor mechanisms. Two representative temperate-zone humic acids, selected to probe the issue of complexation mechanisms decisively, were reacted at pH< 7 with 140 mmol m^{-3} atrazine solution under exclusion of light. Infrared and electron spin resonance spectra of the resulting complexes gave evidence for proton-transfer (with some hydrogen-bonding and hydrophobic interactions) and, under certain conditions, electron-transfer reactions. These spectroscopic data, taken with many other published studies, suggested a general rule to describe the complexation mechanisms of *s*-triazines with soil humic acids: Proton-transfer is favored, and electron-transfer is disfavored, for humic acids of high acidic functional group content and *s*-triazines of low basicity (e.g., atrazine). The converse of this statement is also true.

Key Words: atrazine, hydroxy-atrazine, humic acid, adsorption, charge-transfer complex, hydrogen bonding, hydrophobic interaction, conformational changes, spectroscopic techniques

Project Objectives Addressed in 1994-95

(1) To apply spectroscopic methods (both optical and magnetic) to characterize the complexes formed between atrazine and humic acids extracted from California soils and other sources.

(2) To interpret the spectroscopic data in terms of surface reaction mechanisms and to compare these mechanisms among the different humic acids investigated.

Research Plan and Procedures

Humic acid samples. The humic acid (HA) samples used in this investigation were extracted from the A horizon of a California Entisol and the Bh horizon of a Canadian Spodosol. Conventional extraction and purification methods (Schnitzer, 1982) were employed to obtain HA products with ash contents < 20 g kg^{-1}. The Entisol from which HA was extracted was Hanford sandy loam (coarse-loamy, mixed, non-acid, thermic, Typic Xerorthents), collected at the Kearney Agricultural Center in the San Joaquín Valley of California. The Spodosol source was a poorly-drained forest soil (Armadale series) in northeastern Canada. Its humic fraction, available commercially (Contech E.T.C. Ltd., Ottawa, Ontario), was analyzed in detail by Sposito et al. (1982), who found its composition to be consistent with typical HA, in contradiction with the supplier, who labeled it a fulvic acid. Further investigation (Maurice-Johnsson, 1993, p. 152) has indicated the essential correctness of an HA attribution for this humic substance. Elemental composition data for the two HA samples are given in Table 1.

Carboxyl content in the HA samples was determined by the modified calcium acetate method of Holtzclaw and Sposito (1979). Briefly, a 100 mg sample of HA is placed into a 125-ml Erlenmeyer flask equipped with a screw cap. The flask is purged with N_2,; 40 ml Milli-Q^{TM} H_2O and 10 ml of 1 mol dm^{-3} $Ca(CH_3CO_2)_2$ stock solution are added, and the flask is closed tightly. Simultaneously, a blank solution is prepared using all reagents other than the HA sample to be analyzed. The flasks are place on an arm shaker for approximately 24 h at room temperature (RT), then are removed and retained for steam distillation. The transfer of the sample for distillation is made by decanting the sample solution from the Erlenmeyer flask into the sample vessel of the steam-distillation apparatus and washing the flask with a few ml H_2O. Steam generation is adjusted to provide a distillate rate of 6 to 8 ml/min^{-1} and a distillate temperature of 22°C upon emergence from the condenser. A 400-ml volume of distillate is collected in a calibrated 500-ml flask, covered, and retained for titration. The sample and blank solution are titrated potentiometrically with standard 100 mol m^{-3} NaOH to pH 8.50. The carboxyl content of the sample is calculated according to the expression:

$$\frac{[\text{volume NaOH(sample)} - \text{volume NaOH(blank)}] \times \text{concentration NaOh}}{\text{ash- and water-free mass of sample}}$$

The steam-distillation step is essential to avoid positive interferences from titrating weakly-acidic functional groups in HA that do not react with calcium acetate (Holtzclaw and Sposito, 1979). Carboxyl contents for the HA samples also appear in Table 1 (sixth column).

Atrazine-humic acid complexes. Reagent-grade atrazine (98.7% purity, Ciba-Geigy, Greensboro, NC) was dissolved in Milli-Q™ water to prepare a 140 mmol m^{-3} solution that was stored in the desk to preclude photoreaction. Exactly 15 mg of purified HA were reacted with 25 ml of this solution at fixed pH values in the range 2-7 (adjusted, as needed, using $HClO_4$ or NaOH). The sample solutions (designated HAAT) were mixed gently at RT for 4 d with exclusion of light to avoid photoreaction (Pelizzetti et al., 1990). Solid-phase reaction products for use in spectroscopic experiments were obtained by freeze-drying these solutions. Reference humic acid solutions without atrazine (designated HA) were treated in the same way.

FTIR spectroscopy. Fourier-transform infrared (FTIR) spectra of the HAAT and HA samples were obtained with a Mattson Cygnus 100 FTIR spectrophotometer using 30-mg KBr pellets. Generally, 2-3 mg of HAAT or HA sample was added to 100 mg of KBr. This proportion of sample to KBr led to spectra with better resolution than samples with the proportion of 1 mg per 100 KBr, which is often used.

ESR spectroscopy. Electron spin resonance (ESR) spectra of the HAAT AND HA samples were obtained with a Brucker ESR spectrometer operating at X-band frequency (9 GHz) with the sample at RT or 123K. At RT, semiquinone-type free radicals were quantitated using the conventional approximation, intensity $\times$ line width^2 (Wertz and Bolton, 1986). The areas of the ESR peaks were calibrated with that corresponding to the ESR signal of a "strong pitch" reference of known free radical content, obtained from Brucker. Saturation curves (Wertz and Bolton, 1986; Czoch and Francik, 1989, Ch. 4) also were obtained for the free radical species to gain information about their interactions with the local molecular environment in the HAAT and HA samples. These curves can have very different forms in two limiting cases (Fig. 1). In practice, however, experimental data fall between the two extremes, and quantitative characterization is best made by calculation of the width parameter, $q_{0.5}$ (Czoch and Francik, 1989, p. 145), as illustrated in Fig. 1b. This parameter has a value near 14 for ideal homogeneous broadening; whereas, for ideal inhomogeneous broadening, it becomes infinite (Czoch and Francik, 1989, p. 145). In the former case, free-radical spins experience the same local effective magnetic field; whereas, in the latter case, each free-radical spin is subjected to a different local effective magnetic field (Wertz and Bolton, 1986, ch. 9).

Results

Infrared spectra of the Hanford HA and HAAT samples appear in Fig. 2. The HAAT samples show a clear relative enhancement in absorbance near 1600 cm^{-1} when compared to the HA samples. This absorbance reflects primarily the antisymmetric vibration of carboxylate groups (Stevenson, 1994, ch. 13; see also Table II in the 1993-94 Kearney Foundation Annual Technical Report), and its enhancement in the HAAT samples can be attributed to proton-transfer reactions between HA carboxyl groups and the 2,4-diamine groups in atrazine (Senesi et al., 1987). At pH > 2, "red shifts" in the spectra near 1100-1200 cm^{-1} occur for the HAAT samples. Given the very low value of 1.68 for the pK_a of atrazine (Weber, 1970), and the assignment of this wavenumber region principally to C-O stretching vibrations in hydroxylated moieties (Stevenson, 1994, ch. 13), these changes in the spectra can be interpreted as the signature of hydrogen-bonding interactions between OH groups and deprotonated atrazine (Senesi et al., 1987).

At pH 2.0-2.5, significant hydrolysis of atrazine to form hydroxyatrazine over the four-day reaction period is likely (Martin-Neto et al., 1994). This derivative of atrazine has a $pK_a \approx 5$ (Clay and Koskinen, 1990). Therefore, it remains protonated at pH 2.0-2.5, with a lesser tendency to form hydrogen bonds with HA than atrazine.

Tables 2 and 3 list ESR parameters measured for the two HA samples and their atrazine complexes at varying pH. An inverse relation between HA carboxyl content and spin concentration (Senesi et al., 1987) is clearly evident on comparison of Tables 2 and 3 with Table 1. No change in spin concentration was observed for the Spodosol HA upon reaction with atrazine; whereas, an appreciable increase in free radical content did occur for the Entisol HA after the reaction. Martin-Neto et al. (1994) observed no significant change in free radical content in HAAT samples comprising humic acids extracted from an Oxisol and a tropical peat. Increases in spin concentration signal the formation of charge-transfer complexes between HA and atrazine (Senesi, 1992).

Power-saturation curves for the Spodosol HA are shown in Fig. 3, and the resulting $q_{0.5}$-values are listed in Table 2 for data at RT and 123 K (columns 5 and 6). The magnitude of $q_{0.5}$ dropped sharply as pH was increased from 2.0 to 3.2, indicating a much greater contribution from inhomogeneous broadening in the HA and HAAT samples at pH 2. The increase in $q_{0.5}$ upon lowering the temperature to 123 K also was much greater at pH 2 than at high pH.

Electron spin resonance spectra of the Spodosol HA at RT, obtained for varying microwave power at pH values below and above 3 (cf. Czoch and Francik, 1989, p. 152), displayed two important effects (data not shown). First, there were two free-radical species at pH 2 and only one species above pH 2 (spectra at pH 3.2, 4.6, and 6.7 were similar). Second, the line width of the principal free radical species at pH 2 increased by a factor of about 1.3 over the microwave power range shown; whereas, it doubled over the same microwave power range at pH > 2. All of these results point to a significantly inhomogeneous relaxation process at pH 2 compared to higher pH values.

Discussion

Infrared spectra of complexes between atrazine and HA extracted from an Oxisol (Martin-Neto et al., 1994, Fig. 4), a Spodosol (data not shown), and an Entisol (Fig. 2) indicate a proton-transfer bonding mechanism is operative at pH < 5 (Fig. 4b). Hydrogen bonding between N in the secondary amino groups or the triazine ring of atrazine and oxygen-containing functional groups in HA also is likely. These conclusions are in accord with many previous experimental studies of the atrazine-HA interaction [for reviews see Hayes (1970), Senesi and Testini (1982), and Senesi (1992)]. Semi-empirical structure-reactivity correlations by Welhouse and Bleam (1993a,b) also lend support, in that they suggest enough delocalization of N lone-pair electron density into the triazine ring to create significant polarity (acidic side-chain NH vs. basic triazine ring), leading to stable hydrogen bond formation. In the same spirit, Gamble et al. (1994) have shown that the atrazine complexing capacity of fulvic acid is strongly and positively correlated with the moles of *protonated* carboxyl groups per unit mass of humic substance.

The Spodosol and Hanford HA samples conform to what may be termed the "Senesi-Testini Rule," that humic substances show an inverse relationship between their content of acidic functional groups and that of stable free radicals of the semi-quinone type (Senesi and Testini, 1982). A corollary of this Rule is that the tendency of a humic substance to complex organic molecules by proton-transfer and hydrogen-bonding mechanisms will be inversely related to the tendency for engaging in electron donor-acceptor mechanisms. This trend is exemplified by the absence of any change in spin concentration after reaction with atrazine for the Spodosol HA, whose carboxyl content is at the upper end of the normal range for HA, while the opposite is true for the Hanford HA, whose carboxyl content is near the lower end of this range [1-6 mol kg^{-1} (Schnitzer and Khan, 1978, ch. 1)]. Thus, well-oxidized HA, such as may be characteristic of highly-weathered soils, is more likely to form proton-transfer complexes than electron-transfer complexes with organic molecules. In the case of the *s*-triazines, both mechanistic options are available simultaneously, making them an especially useful probe of HA reactivity.

Both the Spodosol HA (Fig. 3 and Table 2) and the tropical HA samples investigated by Martin-Neto et al. (1994, Fig. 8 and 10) gave strong evidence of highly inhomogeneous spin relaxation processes at pH < 3. Fundamentally, this means that a distribution of local effective magnetic fields exists among the free-radical species in HA, presumably because of differing molecular environments (Czoch and Francik, 1989, sec. 4.1.2). Martin-Neto et al. (1994) speculated that these environments include protected sites of significant hydrophobicity that disappear at higher pH because of conformational changes in HA induced by functional group deprotonation. These hydrophobic sites would add effectively to the proton-transfer mechanism in binding atrazine and other organic molecules with aromatic character. Their protected existence apparently is the concomitant of a relatively high carboxyl content in HA.

The spin concentration data in Tables 2 and 3, as well as those of Martin-Neto et al. (1994), suggest that electron-transfer mechanisms (Fig. 4c) do not play a major role in the complexation of atrazine by HA. Welhouse and Bleam (1993a) predicted this result from their semi-empirical structure-reactivity analysis, pointing to the low overall basicity of the atrazine molecule. Basicity among the *s*-triazines has long been known to be determined primarily by the substituent at the 6 position on the triazine ring, with lesser effects coming from those on the secondary amino groups at the 2- and 4-positions (Weber, 1967, 1970). Basicity increases as the electronegativity of a substituent decreases. Thus, for example, the order of increasing pK_a (a useful measure of basicity) for the series of *s*-triazines, [6-R-N,N′-(1-methylethyl)-1,3,5-triazine-2,4-diamine], is: 1.85 (Cl), 4.05 (SCH_3), 4.28 (OCH_3), 5.20 (OH), where the 6-position substituent R is shown in parentheses (Weber, 1967). Atrazine differs from propazine, the first member of this series, only by replacement of the 1-methylethyl group at the triazine-ring 2-position by an ethyl group, with the result that pK_a drops slightly to 1.68, in keeping with the decrease in number of C atoms in the alkyl substituent (Weber, 1970). If the Cl at the 6-position on the triazine ring of atrazine is replaced by the less electronegative SCH_3 to create ametryne [6-methylthio-N-ethyl-N′-(1-methylethyl)-1,3,5-triazine-2,4-diamine], the pK_a value rises sharply to 4 (Weber, 1970). With OH in the 6-position to create hydroxyatrazine, it increases to about 5, as noted above.

The low basicity of atrazine inhibits its complexation with HA through electron-transfer mechanisms, unless the carboxyl content of HA is low enough to allow a significant free radical content. Ametryne, being much more basic than atrazine, should not be as unreactive toward electron-deficient HA moieties. Senesi and Testini (1982) found no change in spin concentration, after reaction with ametryne, in two out of three soil HA samples they investigated, but Senesi et al. (1987) observed a large increase in spin concentration for ametryne complexation by a synthetic HA containing almost no carboxyl groups. Senesi et al. (1987) also noted that prometone [6-methoxy-N,N′-(1-methylethyl)-1,3,5-triazine-2,4-diamine], whose 6-position methoxy group renders it quite basic in the series of pK_a (= 4.28) values given above, was highly effective in engaging electron-transfer mechanisms to complex with HA. The same reasoning should apply to hydroxyatrazine, whose production by the hydrolysis of atrazine at $pH < 4$ in the present study may in fact have contributed to the increase in spin concentration observed for the Hanford HA.

These spectroscopic data, taken with other published studies, suggest a general rule describing the complexation mechanisms of *s*-triazines with soil humic acids: Proton-transfer is favored, and electron-transfer is disfavored, for humic acids of high acidic functional group content and *s*-triazines of low basicity (e.g., atrazine). The converse of this rule is also true.

References

Clay, S.A., and W.C. Koskinen. 1990. Adsorption and desorption of atrazine, hydroxyatrazine, and s-glutathione atrazine on two soils. Weed Sci. 38:262-266.

Czoch, R., and A. Francik. 1989. Instrumental effects in homodyne electron paramagnetic resonance spectrometers. John Wiley, New York.

Gamble, D.S., C.H. Langford, and G.R. Barrie Webster. 1994. Interactions of pesticides and metal ions with soils: Unifying concepts. Rev. Environ. Contam. Toxicol. 135:63-91.

Hayes, M.H.B. 1970. Adsorption of triazine herbicides on soil organic matter, including a short review on soil organic matter chemistry. Residue Rev. 32:131-174.

Holtzclaw, K.M., and G. Sposito. 1979. Analytical properties of the soluble, metal-complexing fractions in sludge-soil mixtures: IV. Determination of carboxyl groups in fulvic acid. Soil Sci. Soc. Am. J. 43:318-323.

Martin-Neto, L., E.M. Vieira, and G. Sposito. 1994. Mechanism of atrazine sorption by humic acid: A spectroscopic study. Environ. Sci. Technol. 28:1867-1873.

Maurice-Johnsson, P.A. 1993. Hematite dissolution in natural organic acids. Ph.D. dissertation, Stanford University.

Pelizzetti, E., V. Muarino, C. Minero, V. Carlin, E. Pramauro, O. Zerbinati, and M. Tosato. 1990. Photocatalytic degradation of atrazine and other *s*-triazine herbicides. Environ. Sci. Technol. 24:1559-1565.

Schnitzer, M. 1982. Organic matter extraction. p. 581-594. *In* A.L. Page (ed.) Methods of soil analysis. Part 2. Chemical and microbiological properties. American Society of Agronomy, Madison, WI.

Schnitzer, M., and S.U. Khan. 1978. Soil organic matter. Marcel Dekker, New York.

Senesi, N. 1992. Binding mechanisms of pesticides to soil humic substances. Sci. Total Environ. 123/124:63-76.

Senesi, N., and C. Testini. 1982. Physico-chemical investigations of interaction mechanisms between *s*-triazine herbicides and soil humic acids. Geoderma 28:129-146.

Senesi, N., C. Testini, and T.M. Miano. 1987. Interaction mechanisms between humic acids of different origin and nature and electron donor herbicides: A comparative IR and ESR study. Org. Geochem. 11:25-30.

Sposito, G., K.M. Holtzclaw, C.S. LeVesque, and C.T. Johnston. 1982. Trace metal chemistry in arid-zone field soils amended with sewage sludge: II. Comparative study of the fulvic acid fraction. Soil Sci. Soc. Am. J. 46:265-270.

Stevenson, F.J. 1994. Humus chemistry. John Wiley, New York.

Weber, J.B. 1967. Spectrophotometrically determined ionisation constants of 13 alkylamino-*s*-triazines and the relationship of molecular structure and basicity. Spectrochim. Acta 23A:458-461.

Weber, J.B. 1970. Mechanisms of adsorption of *s*-triazines by clay colloids and factors affecting plant availability. Residue Rev. 32:93-130.

Welhouse, G.J., and W.F. Bleam. 1993a. Atrazine hydrogen-bonding potentials. Environ. Sci. Technol. 27:494-500.

Welhouse, G.J., and W.F. Bleam. 1993b. Cooperative hydrogen bonding of atrazine. Environ. Sci. Technol. 27:500-505.
Wertz, J.E., and J.R. Bolton. 1986. Electron spin resonance. Chapman and Hall, New York.

Table 1. Chemical composition of the humic acid samples.[†]

Humic acid	C	H	N	O	COOH
	---------- g kg^{-1} ----------				mol_c kg^{-1}
Spodosol[‡]	564	46	8.6	380	4.7 ± 0.1
Entisol	438	50	42	470	2.7 ± 0.1

[†] ash- and water-free basis; O calculated as 1000-C-H-N
[‡] data from Sposito et al. (1982)

Table 2. Electron spin resonance parameters for free radicals in the Spodosol humic acid (g = 2.003).

Sample	pH	Spins	Line width		$q_{0.5}$
		10^{17} g^{-1}	G[†]	RT	123K
HA	6.7	6.7 ± 0.5	5.3 ± 0.2	25	32
HAAT	6.7	6.9 ± 0.5	5.3 ± 0.2	25	28
HA	4.6	4.5 ± 0.5	4.8 ± 0.2	22	32
HAAT	4.6	4.3 ± 0.5	4.8 ± 0.2	22	----
HA	3.2	2.4 ± 0.5	3.5 ± 0.2	28	30
HAAT	3.2	3.1 ± 0.5	3.5 ± 0.2	22	31
HA	2.0	2.7 ± 0.5[‡]	3.2 ± 0.2	34	71
HAAT	2.0	2.9 ± 0.5[‡]	3.2 ± 0.2	32	56

[†] 1 gauss (G) = 10^{-4} tesla (T)
[‡] smaller sample volumes than at pH > 2; data for the principal free radical species only

Table 3. Electron spin resonance parameters for free radicals in the Entisol humic acid (g = 2.003).

Sample	pH	Spins $10^{17}g^{-1}$	Linewidth G†
HA	4.5	5.3 ± 0.1	4.5 ± 0.0
HAAT	4.5	5.9 ± 0.3	4.4 ± 0.1
HA	3.5	5.8 ± 0.3	4.3 ± 0.0
HAAT	3.5	7.5 ± 0.3	4.4 ± 0.1
HA	2.5	9.0 ± 1.0	4.0 ± 0.0
HAAT	2.5	13.2 ± 0.8	4.3 ± 0.2

† 1 gauss (G) = 10^{-4} tesla (T)

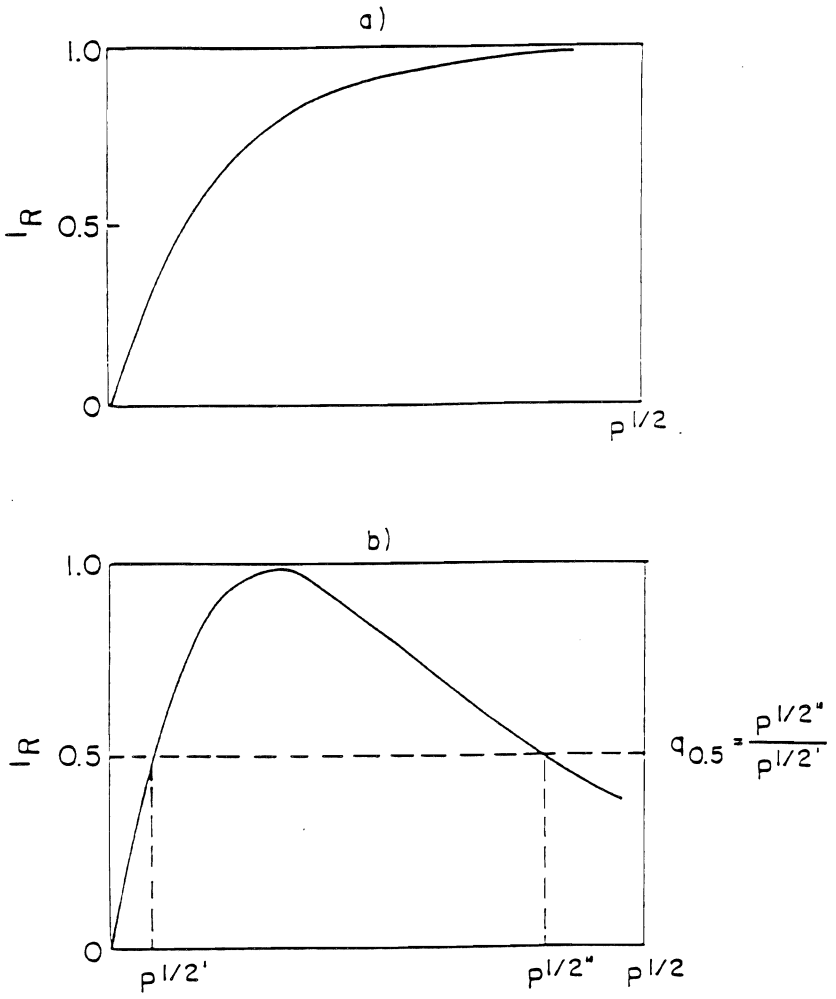

Figure 1. (a) Power saturation curve for ideal inhomogeneous broadening (I_R = relative intensity, P = microwave power). (b) Power saturation curve for ideal homogeneous broadening, showing calculation of the parameter, $q_{0.5}$.

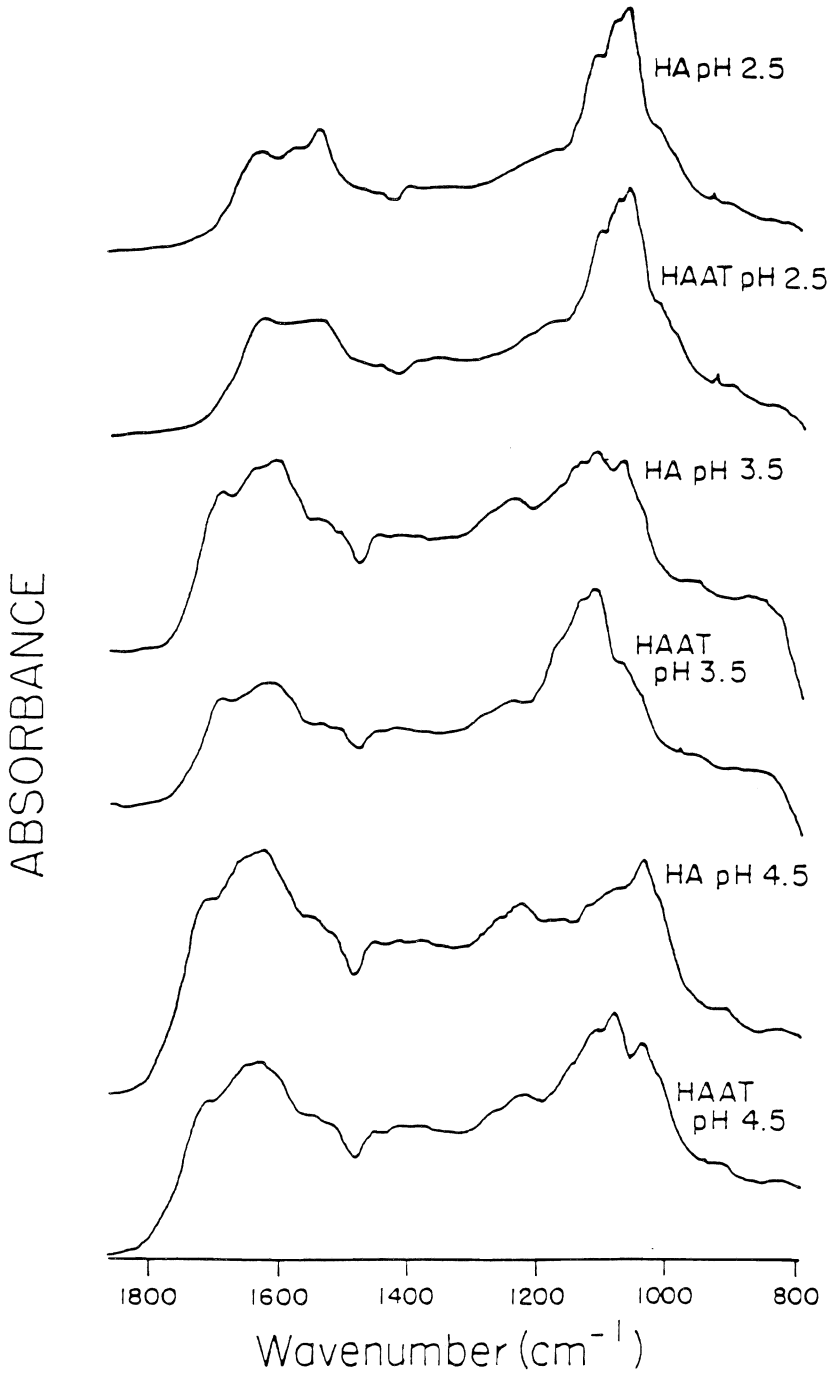

Figure 2. Infrared spectra (2000-800 cm^{-1}) of the Hanford HA and HAAT samples, emphasizing the carboxyl vibrations.

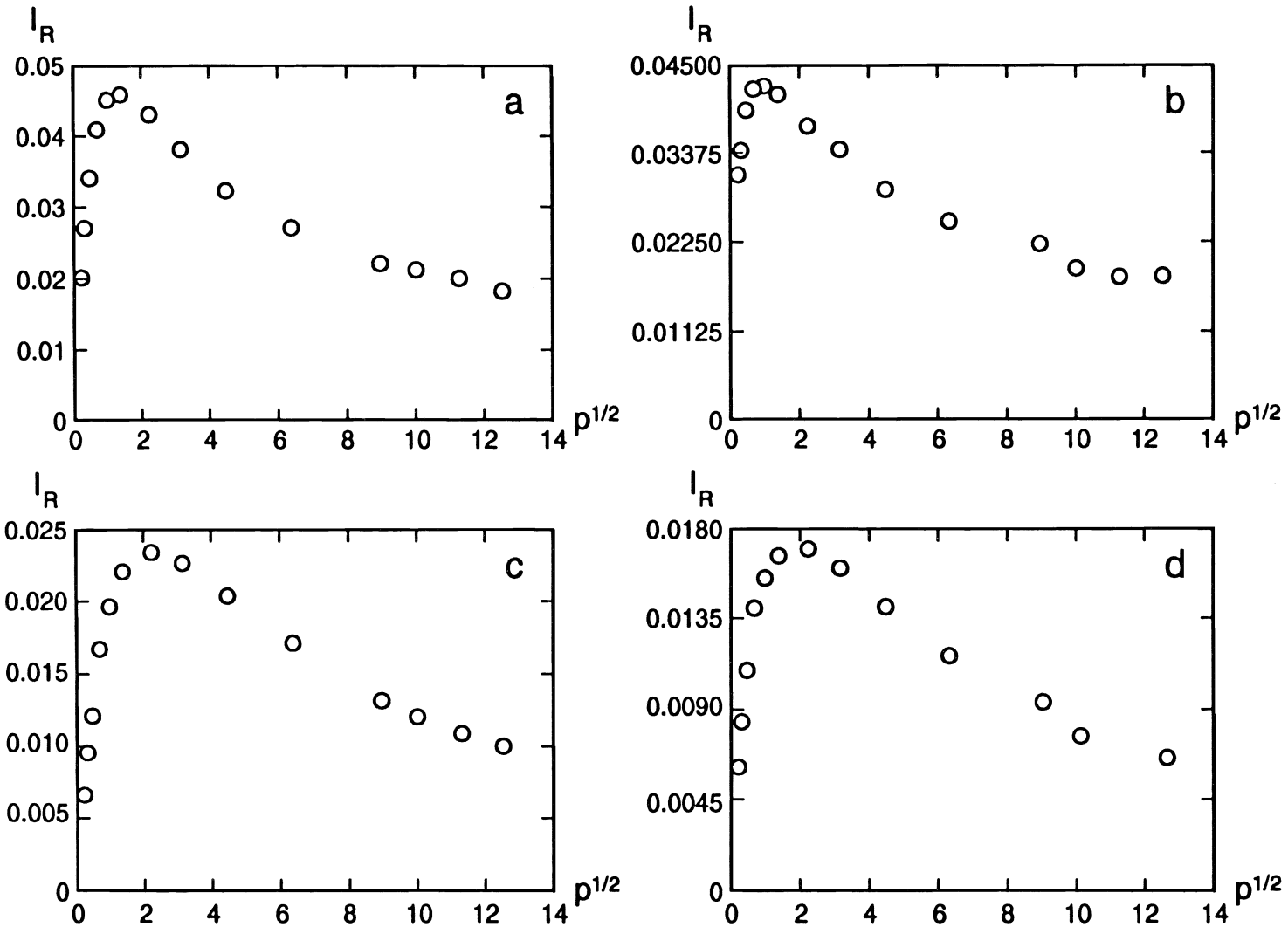

Figure 3. Power saturation curves for the Spodosol HA. (a) pH 2 at RT. (b) pH 2 at 123K. (c) pH 4.6 at RT. (d) pH 4.6 at 123K.

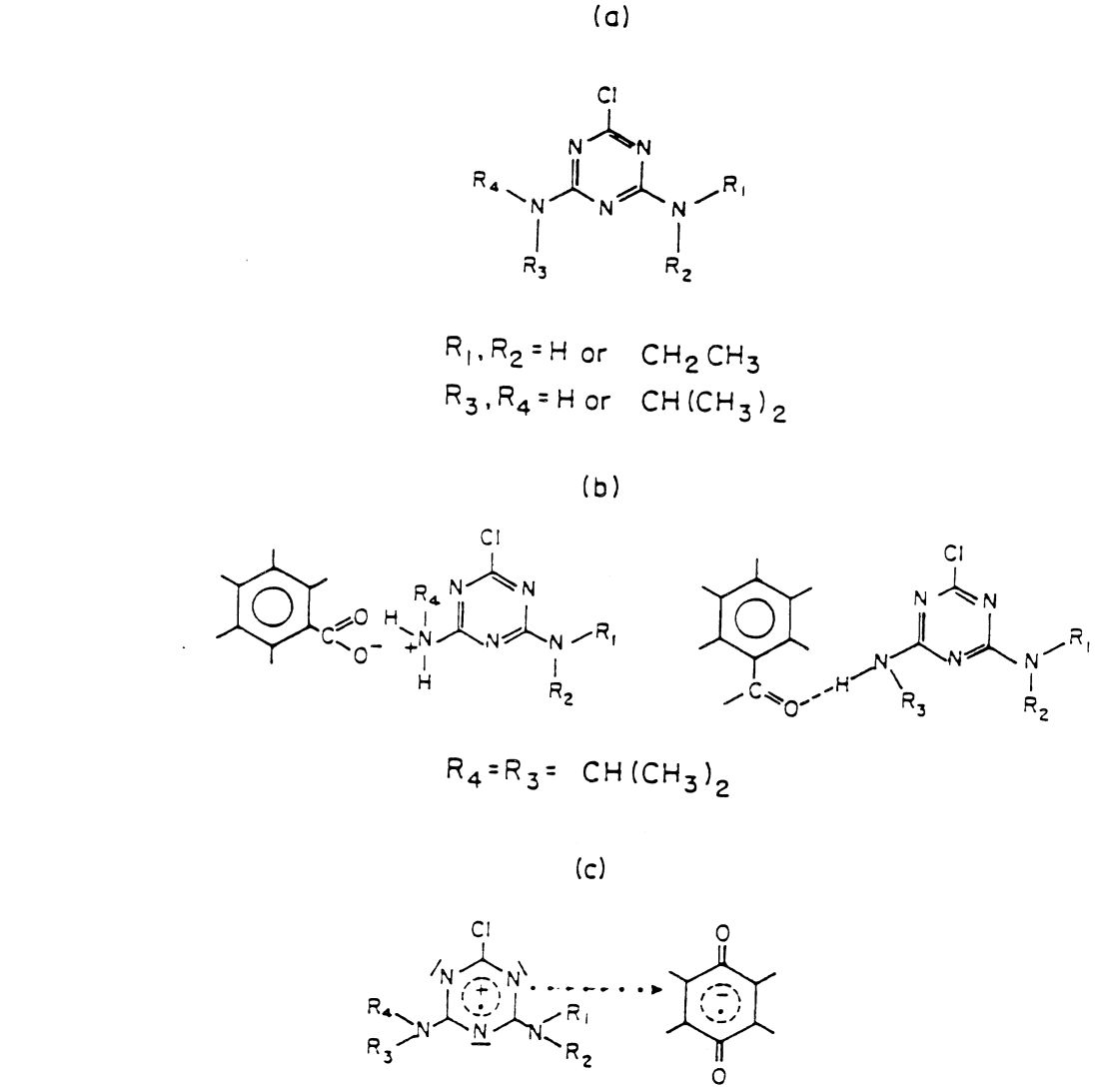

Figure 4. (a) Molecular structure of atrazine. (b) Proton-transfer (left) and hydrogen-bonding (right) mechanisms of bonding to HA moieties. (c) Electron-transfer mechanism of bonding to quinone-like structures in HA.

Rotational Conformers as Molecular Probes of Sorptive Interactions at Mineral and Organic Soil Surfaces

WALTER J. FARMER
Deptartment of Soil and Environmental Sciences, Riverside Campus

Summary

The goal of this research is to enhance understanding of sorption/desorption mechanisms at clay and organic matter surfaces, both singly and in combination in a whole soil, that contribute to the unexplained retention of nonpolar organic chemicals. The use of diffuse reflectance infrared spectroscopy in conjunction with chemicals that exhibit isomerization properties represents a novel approach to the chemicals are uniquely sensitive to the environment in which they exist. This sensitivity is manifested in variations in their conformer populations which can, in turn, be observed in their infrared spectra. A controlled environment chamber allows these variations to be followed *in situ* from a kinetic as well as a mechanistic point of view. These work extend previous studies with clay minerals to humic substances that differ in their origin and properties, and to soils sampled as a function of depth and enable sorption mechanisms at each of these surfaces to be investigated under identical sampling conditions. This methodology provides significant information about preferentially retained species and their importance in the long-term persistence of dihaloethanes and, in addition, mechanistic information about sorbent characteristics that have implications for the sorption of nonpolar organic chemicals in general.

Key Words: humic substances, diffuse reflectance infrared spectroscopy, pollutant persistence

Project Objectives Addressed in 1994-95

Develop a means for comparison of molecular level interaction mechanisms ofnonpolar organics with both mineral and humic substances under dry conditions and in the presence of water vapor.

Research Plan and Procedures

In previous studies conducted in our laboratory, methods were developed using diffuse reflectance infrared spectroscopy (DRIFTS) for the *in situ* investigation of sorption/desorption processes for nonpolar organic chemicals. The methodology as it was utilized with clay mineral sorbents has been described in detail in previous publications (Aochi et al., 1992; Aochi and Farmer, 1993) but a brief description is included here to facilitate the discussion in the remainder of this report. The sorbent of interest is in powder form and is sieved to <45um. It is thoroughly mixed using a mixer mill with a diluent matrix: in previous studies and also in the ones described here, the matrix is KBr. After the mixed sample is packed in the sampling cup of a controlled environment diffuse reflectance cell, the cell is purged using a stream of N_2 gas. The sorption process is initiated by introducing vapor phase chemical into the gas stream and spectra are collected as a function of time. When the selected sorption period has been completed, vapor phase chemical is removed from the flow stream and spectra are once again collected as desorption proceeds. Through the use of spectral subtraction, interferences in each of the collected spectra from absorption bands of the sorbent, unassociated vapor phase chemical in the space surrounding the sample within the chamber, and water vapor are removed. Spectra included in this report, therefore, are those of the sorbed chemical only. For ease of comparison, all of the spectra in the figures have been identically scaled.

It was found in the previous clay studies that the concentration of the sorbents in the KBr matrix had a substantial impact on the resulting spectra. This was also found to be the case for the humic sorbents discussed in this report. In order to obtain acceptable spectra of the sorbed species, the concentration of sorbent had to be greatly reduced from the levels used previously. At concentrations typical of the clay studies, absorption bands were broadened to such an extent that considerable band overlap was occurring. In the clay studies, sorbent concentrations within the KBr matrix ranged from 0.2-2%. For the samples discussed in this report, the concentration used was 0.05%.

The most novel aspect of these experiments is in the use of chemicals, 1,2-dihaloethanes, that exist in multiple conformeric states as molecular probes of the interactions that are occurring. The existence of 1,2-dihaloethanes in two stable rotational conformations, anti and gauche, has been known for some time. Differences in the relative abundance of conformational isomers for these chemicals in different environmental conditions were explained through the use of Onsager relationships (Mizushima, 1954). These relationships describe

mathematically the loss in potential energy for a molecule with a dipole moment when it is transferred from a vacuum to a medium with a different dielectric constant. The higher the dielectric constant of the medium, the greater is the loss in potential energy. Because the gauche conformers of 1,2-dihaloethanes possess a dipole moment but the anti conformers do not, as the dielectric constant of the medium increases, the effect of the potential energy loss is a stabilization of the gauche conformation relative to the anti conformation. Bands characteristic of each conformer are present in the infrared spectra of these chemicals. FTIR can be used, therefore, to monitor any changes in conformer populations that may occur as a function of time and the conditions of sorption.

Our previous spectroscopic investigations of dihaloethane sorption onto clay sorbents (Aochi et al., 1992; Aochi and Farmer, 1993, 1995) provided evidence that the chemicals experience higher effective dielectric fields when they are associated with clay surfaces than when they exist in the bulk state. This conclusion was based on the higher proportion of gauche conformer present in the sorbed chemical relatitve to the bulk state. While the gauche conformer was in each case preferenially retained during both sorption and desorption processes, the degree of preference depended on the clay used. Humic substances, on the other hand, should have the opposite effect when they act as sorbents for dihaloethanes. Instead of providing an environment of higher dielectric field with greater affinities for the gauche conformer, these comparatively nonpolar sorbents should exhibit a preferences for the anti conformer. While sorption/desorption mechanisms should be similar with different humic substances, variations in amounts sorbed as well as rates of accumulation and release were expected.

Results

Spectra are shown in Fig. 1 for 1,2-dichloroethane (DCA) sorbed on soil humic acid as a function of time. During the 22 h sorption period, all the bands in this spectral region are shown to increase in intensity but change very little in the characteristic band shapes. In particular, there are no indications in these spectra of the liquid phase bands that were so prominent in the spectra of DCA sorbed onto clay minerals. Both the 30 min and 6 h sorption spectra are very similar in appearance to that of bulk vapor phase DCA but differ from that spectrum in some important respects. As stated in the methodology section, these spectra are obtained through the use of spectral subtraction of the bulk vapor phase spectrum. The subtraction process is judged complete at the point just prior to the appearance of negative band intensity in the spectrum. The process is illustrated in Fig. 2 showing the 1 h sorption spectrum and, superimposed upon it, the spectrum resulting from an oversubtraction of approximately 5%. It should be noted in the oversubtracted spectrum that the negative band intensity occurs in those regions associated with the gauche conformer. This is particularly interesting since the use of the identical procedure with the DCA/ clay mineral spectra produced the opposite effect, i.e. negative band intensity occurred in the regions where the anti conformer exhibits absorption bands (Aochi and Farmer, 1993). Since this observation

was interpreted in those studies to indicate preferential retention of the gauche conformer, the results shown here indicate that on humic acid the anti conformer is favored. Another way to indicate the preference for the anti conformer is by comparing the integrated intensities of the anti/gauche wag vibrations. Doing so results in a ratio of 6.0 after 30 min which decreases to approximately 4.2 after 3 h of sorption. These values can be compared to 2.7 obtained for the bulk vapor phase species. In the dihaloethane/clay spectra, the preference for the gauche conformer decreased as sorption progressed (Aochi, et al., 1992; Aochi and Farmer, 1993, 1995).

The second important aspect in the sorption series is the delayed appearance of a broad band with maximum intensity at around 1400 cm^{-1}. No similar band can be found in the spectrum of the bulk vapor phase species but one close in both frequency and band shape was observed in the spectra of DCA sorbed onto clay minerals (Aochi and Farmer, 1995). Like the one in the present spectra, it appeared only later in the sorption portion of the experiment and increased in intensity in a manner quite distinct from that of the other bands in the spectra. In contrast, however, the band in the current spectra is not accompanied by the appearance of a second broad band at approximately 1028 cm^{-1}, which, in the case of the DCA/clay spectra, was assigned to the C-C stretching vibration of the gauche conformer in the vapor phase. As can be seen in Fig. 3 for DCA sorbed 22 h onto humic and fulvic acids (HA and FA, respectively), extracted from different sources, the absolute intensity of the 1400 cm^{-1} band as well as its intensity relative to the other bands in the spectrum, varies somewhat depending upon the humic material used as the sorbent. Spectra shown in Fig. 4 demonstrate that this band continues to increase in intensity with longer periods of exposure of Suwannee stream FA to the sorptive chemical while the other bands remain at the same level or even decrease slightly. This activity also mirrors that of what was designated the "persistent band" in the DCA/clay spectra (Aochi and Farmer, in preparation).

Once exposure to the sorptive chemical ceases and only N_2 gas flows through the sample, the vapor phase-type bands rapidly diminish (Fig. 5). The 1400 cm^{-1} band, on the other hand, appears to slightly increase in intensity. In fact, as shown in Fig. 6, it continues to increase in intensity to a significant extent even after 72 h of desorption when all of the other bands in the spectrum have disappeared. After 24 h of desorption, both the intensity and the shape of this band differ with the particular humic substance used as the sorbent (Fig. 7).

Discussion

The chemicals used in these studies are frequently detected as pollutants of groundwater and their retention in soils for periods greater than would be predicted from their physicochemical properties has been documented (Steinberg et al., 1987; Pignatello et al., 1990). Understanding the reasons for the prolonged retention of these particular chemicals, however, is only part of the justification for the investigations discussed here. It is widely held that the persistence of many nonpolar organic chemicals can be attributed

to either hindered intraaggregate diffusion or intraorganic transport, which suggests that the controlling factors lie in characteristics of the sorbent rather than the specific sorbate. Because chemicals with the potential for isomerization exhibit an additional degree of sensitivity to the environment in which they reside, they are also uniquely suited to reveal properties of the sorbents with which they interact that could affect the fate of any chemical that comes into contact with soil materials.

Our previous investigations using these chemicals as sorptives with clay mineral sorbents provided evidence for their rate-limited accumulation during sorption and prolonged retention during desorption. In that case, the formation of the resistant fraction was attributed to the movement of sorbed chemical into a network of narrow pores which restricted transport into and out of the clay particles (Aochi & Farmer, 1995). The ability to observe the status of sorbed species *in situ* and as a function of time was definitely the key to arriving at these conclusions. The goal of the investigations conducted within the last year has been to characterize the sorptive activity of several humic substances using the same experimental conditions used with the clay systems.

The organic carbon matrix has been conceptualized in several different ways. In the most simple view, organic matter is thought to behave much like an organic solvent into which sorbate chemicals actually dissolve (see Chiou, 1990 for a summary). A second view envisions humic macromolecules existing in random coil conformations with extensive inter- and intramolecular bonding. When the humic materials are present in aqueous solution or suspension, the more polar functional groups are oriented toward the exterior of the coils and the more hydrophobic portions toward the interior. This orientation may invert as the amount of water present is reduced, which could account for the difficulty of rewetting dried humic substances (Cameron et al., 1972; Hayes, 1985; Stevenson, 1995). Wershaw (1986, 1993) has proposed a third structural model in which humic substances are comprised of lipid-like amphiphilic molecular fragments originating from partially decomposed plant polymers. In aqueous media, the amphiphiles form micelle structures in which the hydrophobic portions are located in the central regions and the polar heads are present at the exterior surfaces. In association with soil solids, the amphiphile structures flatten to form flexible bilayer membranes that coat the available surfaces. With both the micelle and membrane structures, the central hydrophobic portions are thought to form a liquid-like interior into which nonpolar chemicals can partition. Implicit in both of the latter two models is the presence of discrete regions of both high and low polarity that would differ significantly in their affinity for sorptive chemicals. They also suggest the existence of porous structures through which diffusion of chemicals can occur. Rates of diffusion for chemicals sorbed within these structures could be hindered both by the size of the pores and by interactions with functional groups that comprise the walls.

The broad multiplet shapes of the species sorbed earliest in the sorption process are characteristic of low to moderate resolution spectra of chemicals in the vapor phase. These shapes are actually band contours that extend over a

whole series of bands that are not individually resolved under the spectral conditions (Colthup, 1990). They are only observed for chemicals in the vapor phase because the many bands that comprise them arise from rotational transitions of the molecule. Their presence thus implies a fair degree of rotational freedom for the sorbed molecule. Along with the fact that the band frequencies differ only slightly from those of the bulk phase bands, the spectrum of this species is highly suggestive of pockets of sorbate molecules entrapped within pores of the sorbent. The ease with which this species is desorbed is also consistent with minimal interaction with the sorbent surfaces. The preference for the anti conformer exhibited by this sorbed species with all of the humic sorbents used is consistent with the more nonpolar nature of organic matter compared to mineral surfaces.

It should be noted at this point that the source of these spectral features could be a consequence of the way in which the humic materials were prepared. As a final step in the extraction and purification process, all of the humic materials were subjected to freeze-drying. It has long been recognized that freeze-drying significantly alters the microstructural properties of clay minerals (Murray, 1980). It is thus not improbable that the same treatment could also produce porosity in the organic particles that would not otherwise be present. Such an explanation, however, does not seem appropriate for the persistent band in these spectra.

The band at 1400 cm^{-1} is very similar to the band at 1402 cm^{-1} observed in the spectra of DCA sorbed on clay minerals in band frequency and also in its delayed appearance and its persistence during desorption. The 1402 cm^{-1} band was assumed to arise from combined anti and gauche scissor vibrations of sorbate molecules that had diffused into a network of narrow pores within the clay particles. In these regions, they experienced higher dielectric fields because of the proximity of the walls of the pores that resulted in a predominance of molecules in the gauche conformation (Aochi & Farmer, 1995).

In the current spectra, this band could possibly be accounted for by residual mineral components not removed from the humic materials in the extraction process. The ash content of these materials is, however, extremely low (P. MacCarthy, personal communication). Furthermore, the band is not accompanied by the other persistent band at 1028 cm^{-1} as it was in the DCA/clay spectra. It seems more likely that it is due to the diffusion of sorbate molecules to portions of the organic matrix of greater density, more tightly coiled, or more highly polar. Movement into such regions would certainly be expected to slow the movement of sorbed chemical both into and out of the organic particles.

The intensity of the 1400 cm^{-1} band both in the 22 h sorption spectra (Fig. 3) and in the 24 h desorption spectra (Fig. 7) is fairly well correlated with generally acknowledged properties of these humic substances that could result in the formation of such regions (see Malcolm, 1990; Hayes, 1985 for discussions of properties). In general, FAs are higher in O-containing functional

groups than humic acids and therefore could be expected to provide more extensive areas with high polarity. Stream fulvic acids are believed to be lower in O and N than soil FA and higher in C. Aquatic humic substances such as Suwannee stream FA most likely form by different pathways and from different starting materials than terrestrial ones and should thus differ somewhat in structure and behavior. Peat, on the other hand, is believed to form with soil humates as precursors and thus humic acids from the two sources should be quite similar with that from the peat, exhibiting perhaps more areas of high density.

References

Aochi, Y. O. and W. J. Farmer. 1995. Spectroscopic evidence for the rate-limited accumulation of a persistent fraction of 1,2-dichloroethane. Environ. Sci. Technol. 29: 1760-1765.

Aochi, Y. O. and W. J. Farmer. 1993. Conformational dynamics of 1,2-dichloroethane on illite during sorption and desorption. J. Colloid Interface Sci. 161: 106-114.

Aochi, Y. O., W. J. Farmer, and B. L. Sawhney. 1992. *In situ* investigation of 1,2-dibromoethane sorption/desorption processes on clay mineral surfaces by difffuse reflectance infrared spectroscopy. Environ. Sci. Technol. 26: 329-335.

Cameron, R. S., B. K. Thornton, R. S. Swift, and A. M. Posner. 1972. Molecular weight and shape of humic acid from sedimentation and diffusion measurements on fractionated extracts. J. Soil Sci. 23: 394-408.

Chiou, C. T. 1990. In: *Humic Substances in Soil and Crop Science;* P. MacCarthy, C. E. Clapp, R. L. Malcolm, and P.R. Bloom (eds), Soil Sci. Soc. Am., Madison, WI.

Colthup, M. B., L. H. Daly, and S. E Wiberley. 1990. *Introduction to Infrared and Raman Spectroscopy*, Academic Press, San Diego, CA.

Hayes, M. H. B. 1985. In:*Humic Substances in Soil, Sediment, and Water*, G. R. Aiken, D. M. McKnight, R. L. Wershaw, P. MacCarthy (eds) Wiley-Interscience, New York.

Malcolm, R.L. 1990. In:*Humic Substances in Soil and Crop Sciences*, P. MacCarthy, C. E. Clapp, R. L. Malcolm, and P.R. Bloom (eds) Soil Sci. Soc. of Am., Madison, WI.

Mizushima, S. 1954. *Structure of Molecules and Internal Rotation*, Academic Press, New York.

Murray, R. S. and , J. P. Quirk 1980. Freeze-dried and critical-point-dried clay-a comparison. Soil Sci. Soc. Am. J. 44:232-234.

Pignatello, J. J., C. R. Frink, P. A. Marin, and E. X. Droste. 1990. Field observed ethylene dibromide in an aquifer after two decades. J. Contam. Hydrol. 5:195-214.

Steinberg, S.M., J. J. Pignatello, and B. L. Sawhney. 1987. Persistence of 2,3-dibromoethane in soils: Entrapment in intraparticle micropores. Environ. Sci. Technol. 21:1201-1208.

Stevenson, F. J. 1995. *Humus Chemistry*, John Wiley & Sons, New York.

Wershaw, R. L. 1986. A new model for humic materials and their interactions with hydrophobic organic chemicals in soil-water or sediment-water systems. J. Contam. Hydrol. 1:29-45.
Wershaw, R. L. 1993. Model for humus in soils and sediments. Environ. Sci Technol. 27:814-16.

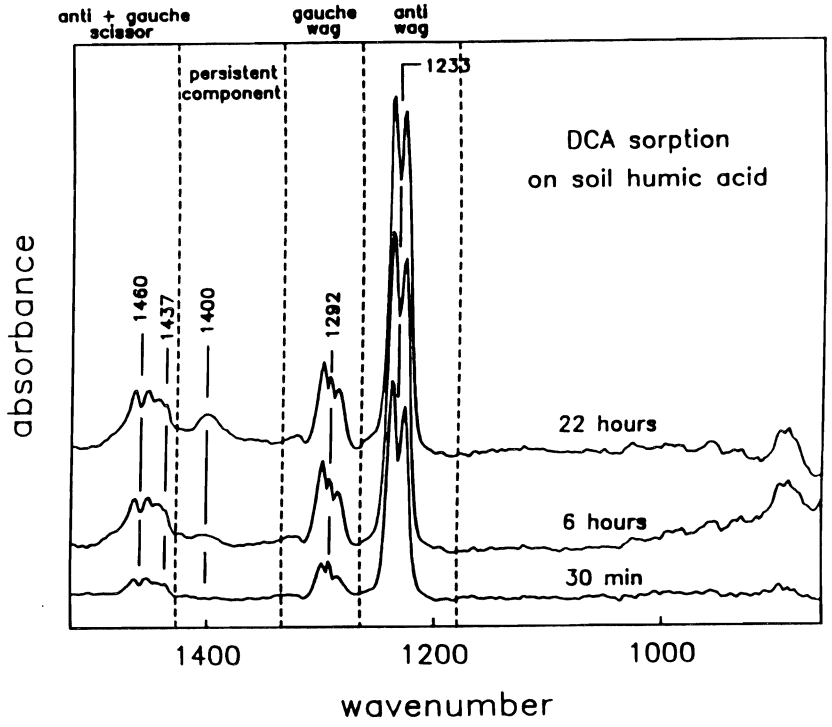

Figure 1. Sorption of DCA on soil humic acid (HA) as a function of time.

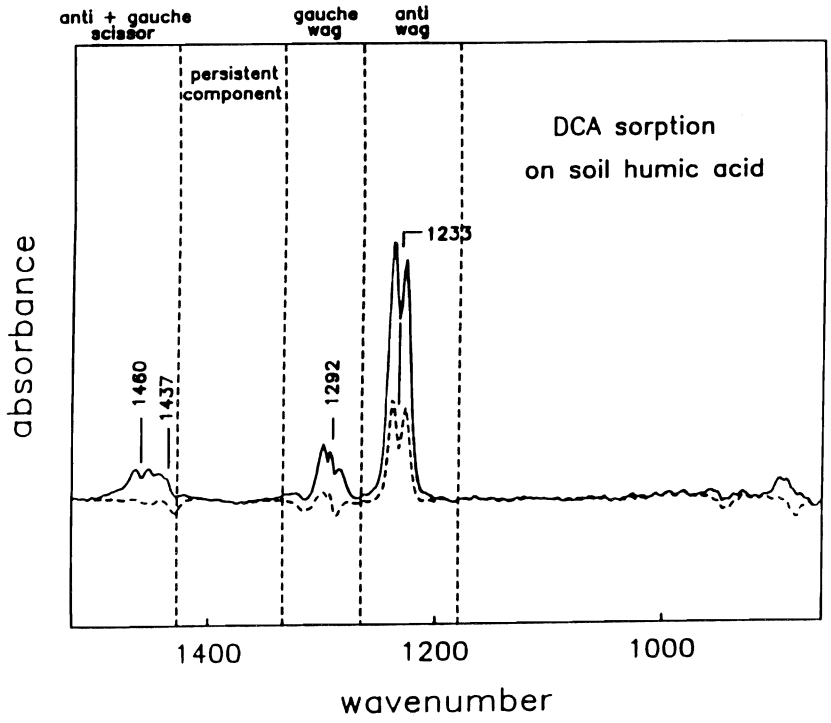

Figure 2. Example of oversubtraction.

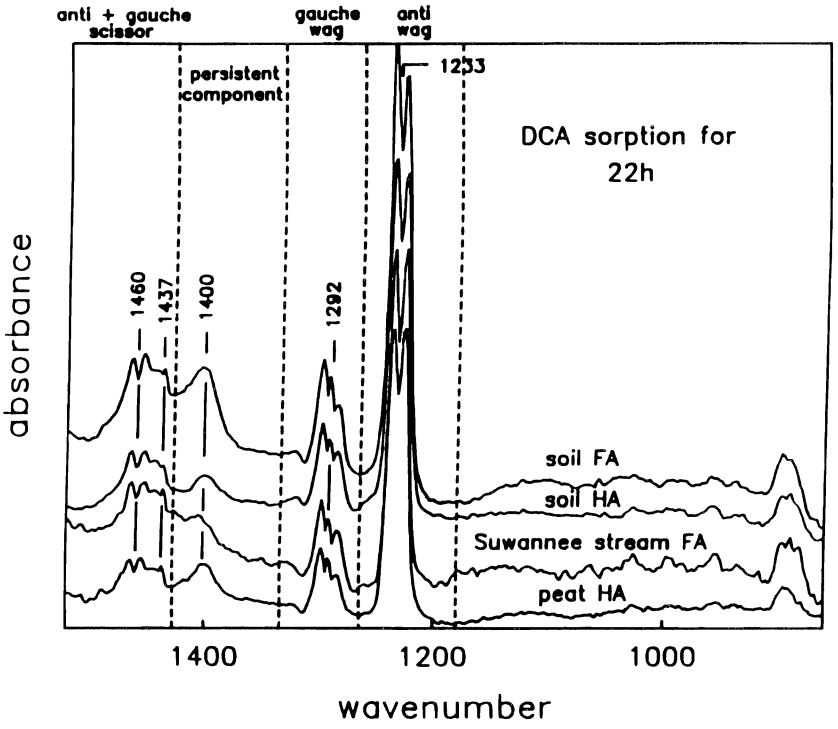

Figure 3. Sorption of DCA for 22 h on four different humic substances (HA = humic acid, FA = fulvic acid).

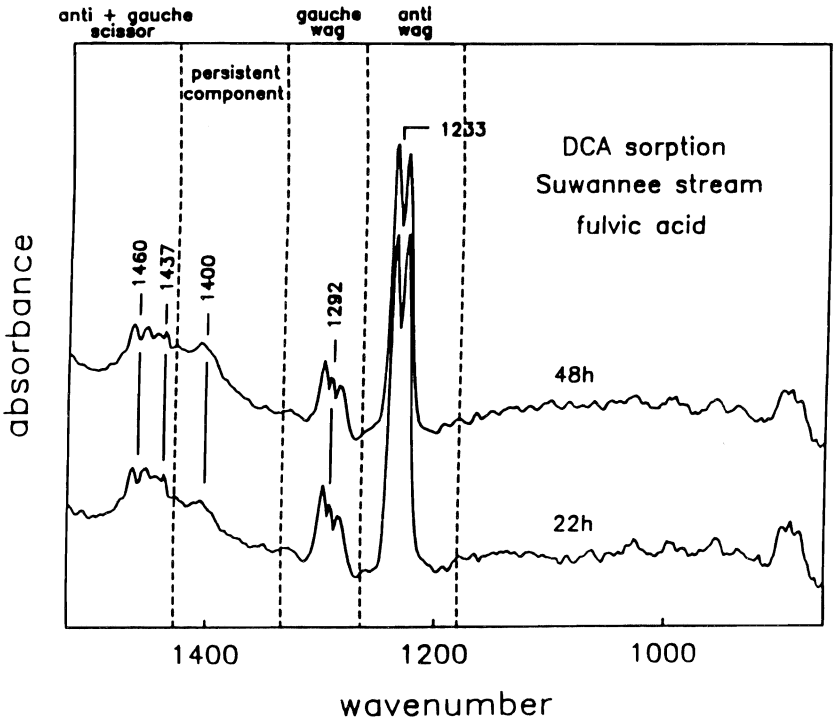

Figure 4. Sorption of DCA on Suwannee stream fulvic acid (FA) for 22 h and 48 h.

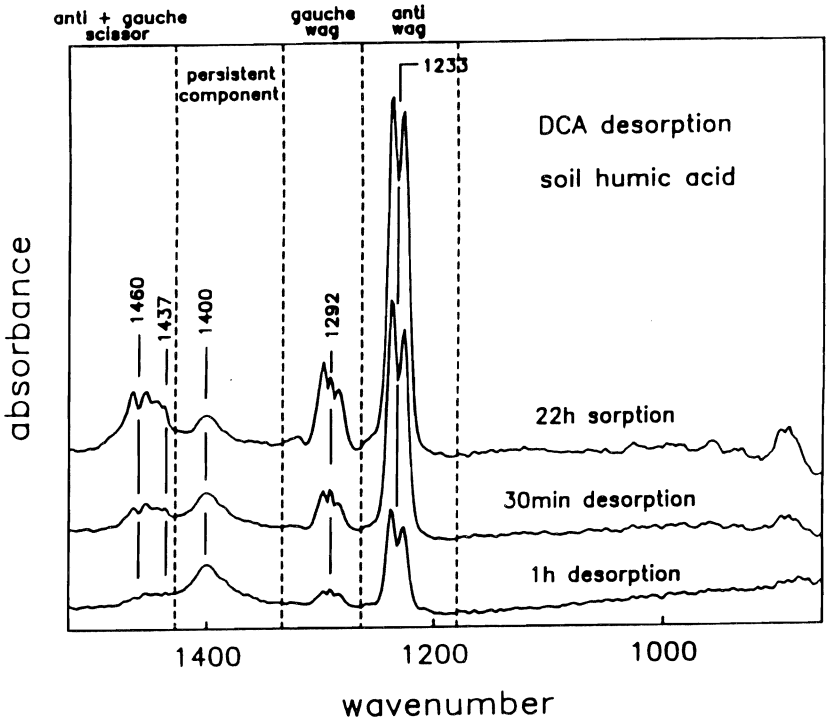

Figure 5. Short term desorption of DCA from soil humic acid (HA).

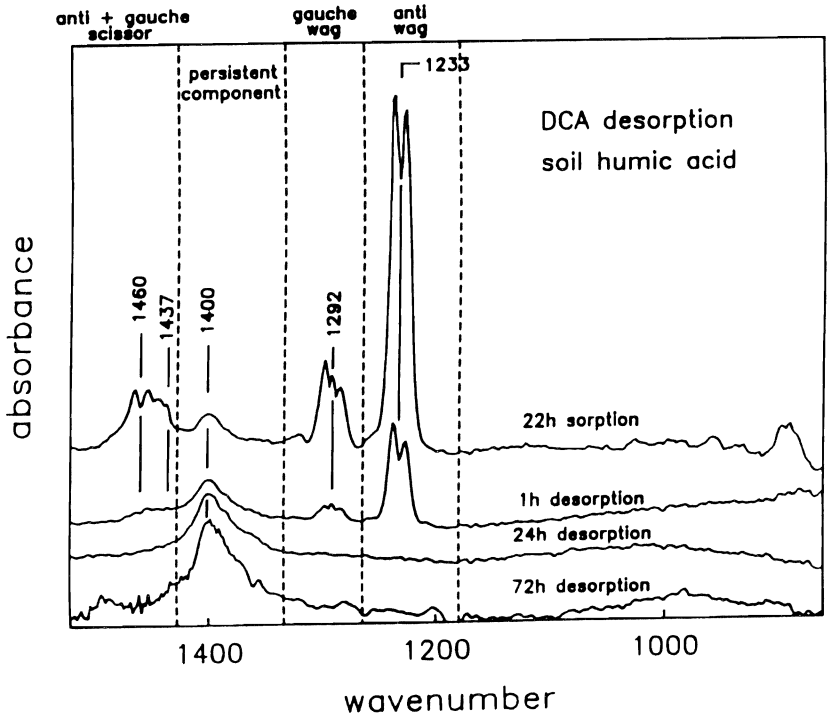

Figure 6. Long term desorption of DCA from soil humic acid (HA).

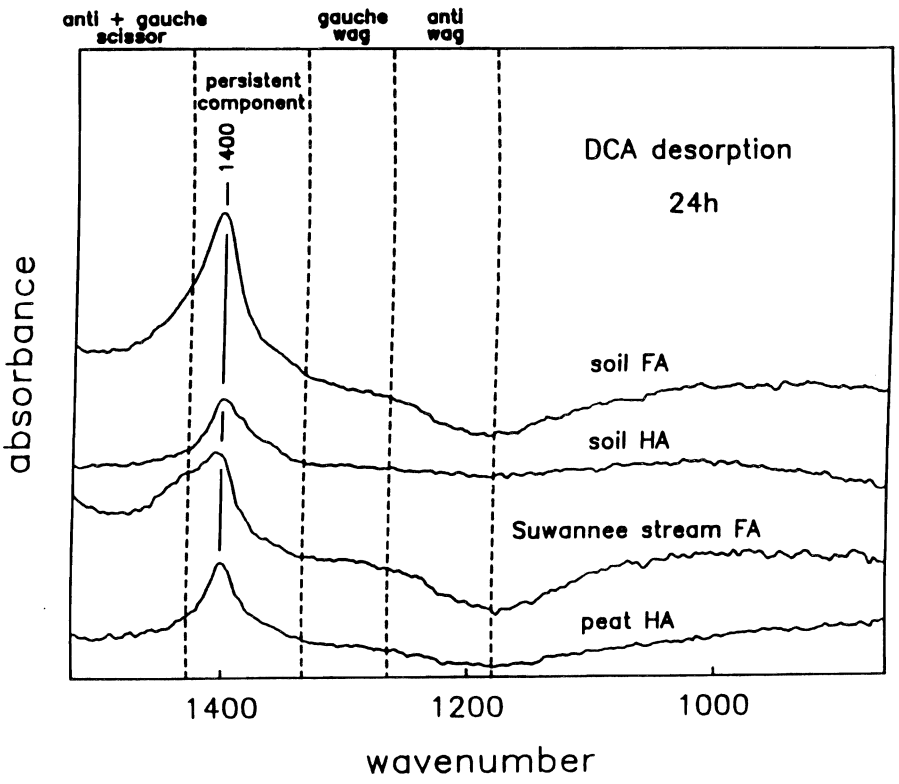

Figure 7. Desorption of DCA for 24 h from four different humic substances (HA = humic acid, FA = fulvic acid).

Factors Influencing Sorptive Properties of Carbonates for Trace Elements in Soils

HARVEY E. DONER[1], MAVRIK ZAVARIN[1], RONALD AMUNDSON[1], AND GORDON E. BROWN, JR.[2]

[1] *Department of Environmental Science, Policy, and Management, Berkeley Campus*

[2] *Department of Geological and Environmental Sciences, Stanford University*

Summary

Extended X-ray Absorption Fine Structure (EXAFS) investigation of selenite coprecipitation with synthetic calcite has shown small variations in the calcite precipitation rate to strongly affect the organization of selenite in the calcite. Additionally, EXAFS analysis of Ni in parent material vs. calcite accumulated Ni from San Joaquin Valley soils has not shown strong variation in coordination structure; this may indicate Ni occlusion rather than coprecipitative accumulation of Ni in the soil carbonates. Soil water extractions of San Joaquin Valley soils indicate either a supersaturated state with respect to calcite or missing complexation reactions involved in the equilibrium state of calcite in soil. Fundamental research into the use of Synchrotron X-ray Fluorescence (SXRF) microprobes for evaluation of trace element accumulation on a micrometer scale in soils has shown that alfa and beta fluorescence energies may be used to determine heterogeneity effects on trace element concentration determination. This new method may help determine the nature of the apparent banding visible by SXRF microprobe in carbonate accumulations on rocks.

Key Words: Selenium, selenite, selenate, nickel, calcite, manganese.

Project Objectives Addressed in 1994-95

The first objective of this two-year research project was to identify the role of carbonates in the immobilization of trace elements and the factors influencing the sorptive properties of carbonates by microscopic and macroscopic means. This was investigated by analysis of natural carbonates from the San Joaquin Valley and by laboratory investigations of the sorptive properties of synthetic calcite by pH-stat and batch sorption methods. Natural samples were tested for total soil and carbonate-associated trace elements. The samples were also investigated for degree of saturation relative to calcite by means of water extracts and for species distribution determination via the equilibration program "HYDRAQL". A pH-stat was constructed and utilized for trace element coprecipitation experiments on synthetic calcite. Selenium, nickel, and manganese were chosen as trace elements of interest--selenium and nickel due to their prevalence at the field site and their potential hazard, and manganese due to its prevalence in natural carbonate and as a comparative element to nickel.

The second objective of this research was to develop the use of synchrotron x-ray techniques in soil science and determine the potential benefits of the new techniques to understand better molecular level trace element interactions in soils. Both natural and synthetic carbonates were investigated by Synchrotron X-ray Fluorescence (SXRF) microprobe and synchrotron Extended X-ray Absorption Fine Structure (EXAFS) to determine the molecular and microscopic organization of trace elements in carbonates. A two-year agreement for support between our research group and the Stanford Synchrotron Radiation Laboratory (SSRL) was made and the first set of natural and synthetic samples were run in June 1995. Similar ties with the synchrotron facilities at Lawrence Berkeley National Laboratory Advanced Light Source (ALS) were made and additional runs were planned at the National Synchrotron Light Source (NSLS) at Brookhaven. A project to develop methods for 2-dimensional mapping of trace element concentrations in natural samples by SXRF microprobe was begun. The effect of sample heterogeneity was investigated and x-ray fluorescence from banded natural carbonates was also investigated.

Research Plan and Procedures

A. Macroscopic Analysis of Trace Element Interaction with Calcite

Soil samples from high terraces near the Panoche Creek, California were collected. The terraces consist largely of fine grained alluvium which is estimated as 100,000 to 200,000 years old. The sediment is primarily derived from the Great Valley Sequence formations in the Silver Creek watershed, a tributary to the Panoche Creek (Amundson, 1992). The soils of this area are well known for their high selenium concentrations but also contain high concentrations of trace elements such as nickel, arsenic, and others. The soils sampled are highly gypsic ($CaSO_4 \cdot 2H_2O$) but also contain carbonate nodules up to 1 centimeter in diameter and clasts in the lower horizons that are coated with carbonate. The gypsum is thought to originate from the high selenium Moreno formation which contains gypsum, pyrite (FeS_2), and other sulfur-containing minerals.

Detailed wet-chemical analysis of field soils were performed by total acid digestion and by water extraction techniques. Total acid digestion was performed both on the whole soil and carbonate separates to determine the possible accumulation of trace elements in the carbonate relative to the soil. Water extracts were used to determine the equilibrium state of soil, relative to calcite solubility. Figure 1 shows the set-up used for determining the equilibrium solute concentrations in the soil extracts. 0.25% CO_2 was used to mimic the approximate CO_2 concentration in the soil system. Soil:water dilution ratios of 1:2, 1:5, 1:10, and 1:50 were used to evaluate which minerals control the solute content of the solutions. Samples were contained in plastic bottles and the 0.25% CO_2 was bubbled through the solution for 24 hours. The bottles were also kept at 25°C by a shaking, constant temperature bath. After 24 hours, the pH was measured and the samples were extracted, filtered through 0.45 micron filters, and stored. Solutions were analyzed for organic matter and major and minor cations and anions. The equilibrium program "HYDRAQL" was used to determine the saturation state of the extract (Papelis et al., 1988).

Detailed laboratory investigation of trace element accumulation in carbonates was started. The method involves the use of a pH-stat to control the precipitation rate and pH of the growing calcite (Fig. 2). It was first documented by Morse (1974) and has been used extensively (Mucci and Morse, 1983, Berner, 1975, Lorens, 1981). The role of the precipitation rate was investigated using a solution initially supersaturated with respect to calcite and inducing crystal formation by calcite seeds. Briefly, 0.25% CO_2 was bubbled through a $CaCl_2$ solution and adjusted to a constant pH with Na_2CO_3. This supersaturated $CaCO_3$ solution contained 0.1M NaCl to control ionic strength and was maintained at 25°C. When the system reached steady state disequilibrium, 0.05-0.5 g $CaCO_3$ seed was added to the system to induce precipitation. The entire apparatus was monitored by a computer which recorded pH and added titrant every 30 seconds. A plot of the titrant added over time determined the rate of precipitation. To date, selenite accumulation on synthetic calcite has been investigated; these samples were also used to investigate the molecular level structure of accumulated selenite (described in part C of this section). Investigation of Ni, Se, and Mn accumulation will be performed on both synthetic and soil carbonates using this system. Additionally, the effect of competing cations and anions on the coprecipitation rate of these trace elements will be investigated. Natural soil carbonates will be collected with the assistance of Dr. Ronald Amundson.

B. Microscopic Analysis of Trace Element Deposition in Calcareous Soils

Microscopic analysis was performed by electron microprobe and SXRF microprobe studies of soil sections. Carbonate nodules were prepared by drying the soil, placing the sample into a vacuum chamber, and then saturating the system with resin. After the soil-resin block hardened, thin sections were cut to expose the carbonate nodule. The sections were polished and then analyzed by both electron microprobe and SXRF microprobe. Electron microprobe analyses were performed at the Geology and Geophysics Department at U.C. Berkeley and the SXRF microprobe studies were performed at the ALS, Lawrence Berkeley Laboratory and NSLS, Brookhaven. Additionally, some feasibility

studies of SXRF microprobe application to heterogeneous systems were performed. The purpose was to understand the effect of sample particle size and matrix heterogeneity on trace element quantitative analysis.

C. Molecular-Level Organization of Trace Elements in Natural and Synthetic Carbonates

EXAFS was used to determine the molecular-level structure around the trace elements both in natural carbonates and also from the coprecipitation experiments performed by the pH-stat method. Natural carbonates were ground to a fine particle size and then placed into special sample slide holders (Fig. 3). Coprecipitation samples from pH-stat experiments were dried and set into similar sample holders.

Selenium adsorption on calcite was performed to determine whether selenate and selenite sorbed to calcite inner spherically, to determine the sorbability of these anions on calcite, and to investigate surface structural differences between sorbed and coprecipitated anions. Sorption samples were run in a similar manner to the water extraction technique, except that air was bubbled through the samples instead of 0.25% CO_2. One gram of synthetic calcite was added to 10 ml of calcite equilibrated solution. At the start of the sorption experiment, a small amount of concentrated selenite or selenate was added to each tube. After 24 hours, the samples were centrifuged; the supernatant was sampled; and the calcite paste was set into sealed sample holders used for EXAFS. Samples were transported to the Stanford Synchrotron Radiation Laboratory (SSRL) for EXAFS analysis in a wet paste form.

Results

A. Soil and Soil Carbonate Sample Analysis

Two terraces from Panoche Creek have been sampled and one was analyzed for trace element content by standard acid digestion methods. It was found that separated carbonates had up to 3 times higher Se concentration than the bulk soil and up to 5 times higher Ni concentration (Table 1). Both parent rock and separated carbonates were ground for EXAFS analysis. Bulk soil samples were sieved and the <2 mm fraction was separated. These samples were then used for equilibrium studies. Carbonate accumulations on bottoms of rocks and carbonate nodules were sampled and later thin-sectioned for electron microprobe and SXRF microprobe analysis.

B. Wet-Chemical Studies of Equilibrium State of Soils from Panoche Creek

If the chemical properties of soil carbonates are dissimilar to synthetic carbonates, one may not be able to model trace element mobility in calcareous soils using synthetic calcite sorption data. One property which has been known to vary greatly between synthetic and soil carbonates is solubility. Previous investigators have found that soils are often supersaturated with respect to calcite and have argued that this is a function of Ca-silicate solubility control,

carbonate surface poisoning, and organic matter coatings on carbonates. We set up an experiment to determine whether the Panoche Creek soils are generally supersaturated with respect to calcite and if this property influences the sorptive properties of soil carbonates (Fig. 1). As a system check, equilibration studies using pure calcite showed that samples reached theoretical equilibrium; all dilution ratios had Ca concentrations varying by less than 10% from the average, and all were near the equilibrium Ca concentration expected. A first set of soils from Panoche Creek were run and equilibrium calculations indicate that more than 80% of the calcium in solution should have precipitated as calcite. Also, the system was found to be supersaturated with respect to barite ($BaSO_4$). About 80% of the Ba should have precipitated as barite.

C. Analysis of Factors Affecting Trace Element Coprecipitation by the pH-stat Method

The first set of experiments examined the effect of pH and supersaturation state on precipitation rate of carbonate on synthetic carbonate nucleation sites. Supersaturation state is defined as the ratio of the ionic activity product of calcite to the Ksp for that system. Figure 4 is a graph of the precipitation rate experiments for pH's 7.5, 7.75 and 8.0 and supersaturation states 1-10. The precipitation rate increases exponentially with supersaturation state and the precipitation rate seems to be unrelated to pH. This fits the empirical relationship which predicts precipitation rate to follow the equation:

$$V = k(S-1)^2$$

where V is the growth rate, K is a constant, and S is the supersaturation state (Stumm, 1992). Our results were plotted using the above equation, resulting in a slope of 0.240 and an R^2 of 0.97 (Fig. 5).

The second set of experiments investigated the effect of SeO_3 on the precipitation of calcite. The calcite precipitation rate with selenite in solution was compared to the calcite precipitation rate from the model equation fit. Table 2 lists the concentration of selenite, the saturation state, the precipitation rate from the experiment, and the expected precipitation rate calculated from the model. Clearly, the difference between the precipitation rate of the sample and the model increases with the increasing concentration of selenite.

The third experiment determined the rate of incorporation of selenite as a function of precipitation rate. Table 3 lists the saturation state, calcite precipitation rate, selenite coprecipitation rate, and the ratio of calcite to selenite precipitation rates. For this experiment, the concentration of selenite at the beginning of the experiment was 1 ppm and was allowed to decrease to 0.75 ppm before the experiment was halted. Although more data are required to confirm the results, it seems that the relative amount of selenite incorporation increases as the precipitation rate increases. This might indicate that at least 2 types of incorporation may exist: site specific selenite coprecipitation and disordered incorporation. EXAFS analysis of the same samples was performed and results are described in the following section.

D. Electron Microprobe Analysis of Soils and Carbonate from Panoche Creek

Electron microprobe scans of carbonate crusts on parent material rocks revealed accumulations of Sr in the carbonate relative to the parent rock (Table 4). Scans also revealed a mineral with Ni as the dominant cation within the parent rock and secondary carbonate. The mineral (or conglomeration of various minerals) has the approximate formula $Ni_{1.5}Fe_{0.26}Mg_{0.21}Si_{2.0}O_{6.4}H_x$. The particles are on the order of 20 micrometers in diameter (Fig. 6). Although the particles are very small, they may persist in the soil and be a significant contributor to the high Ni concentrations. An attempt is being made to isolate and characterize the mineral but, due to the small particle size, it has been difficult to isolate a pure enough sample for x-ray diffraction.

E. SXRF Microprobe Studies of Natural Samples and Theoretical Modeling of X-ray Behavior in Heterogeneous Systems

SXRF microprobe results have revealed bands in the carbonate crusts which may be formed as a function of changing environmental conditions (Fig. 7). The calcite bands are on the order of 70 microns in width. The rather slow decrease of Ni fluorescence across the rock-carbonate boundary (Figs. 8 a, b) seems to indicate possible diffusion or mixing of Ni into calcite.

Due to the relatively young age of the Panoche Creek soils, accumulation of pedogenic carbonate is relatively low. For this reason, older soils with thicker pedogenic carbonate accumulations have been gathered and prepared for SXRF microprobe analysis at the ALS. These samples will be used to look at possible variation of trace element accumulation rates over time.

Determination of trace element concentration in natural samples is very difficult due to the effect of particle size and matrix effects on the fluorescence. For this reason, experiments were performed to try to take those effects into account when determining the concentration of trace elements in heterogeneous systems. The initial experiments were set up to understand the effect of heterogeneity on trace element fluorescence. Figure 9 shows the side view of constructed samples used to test the effect of depth on fluorescence yield from a constant concentration of trace element. Although the figure presents the trace deposit to be Cu, Sn also was deposited on some samples. The Sn and Cu samples were then compared to determine the effect of high versus low energy fluorescences on heterogeneity. Figure 10 presents results from the Sn deposited calcite wedge; the sample was scanned from the thin end (~0 microns, left side) to the thick end (~200 microns, right side). The relative fluorescence of Ca, Fe, and Sn is shown; Fe is relatively homogeneously distributed in the calcite. The calcite thickness does not seem to influence the Sn fluorescence very strongly on this scale. We would, therefore, expect that the quantitative analysis would not be disturbed by heterogeneity effects in this system. When the same calcite wedge is made with Cu as the trace element (Fig. 11), the relative fluorescence of Cu drops by 2 orders of magnitude over the same calcite thickness range. In this case, the quantitative analysis would be strongly affected by heterogeneity in the sample. Note, on the other hand, that there is a very strong change in the relative fluorescence between the Cu-alfa

and Cu-beta intensities as the thickness of overlaid calcite increases. This can be more clearly shown by looking at the difference between the logarithms of the Cu-alfa and -beta fluorescences (Fig. 12). Clearly, the thickness of calcite can decrease the relative intensity of the Cu-alfa peak more than the Cu-beta peak because the mass absorption coefficient for calcite at those two energies is different. This effect is potentially useful for determining heterogeneity effects in natural samples.

To further explore the possibility of using alfa/beta fluorescence ratios to determine the heterogeneity of samples and to explore the matrix effects on fluorescence intensity, a computer program was written to mimic SXRF microprobe scans. The program theory and method are found in Appendix 1. A model scan of the above sample was run and the relative fluorescence of Cu is shown in Fig. 13. The model clearly shows the 2 orders of magnitude change in fluorescence as the calcite wedge thickness is increased.

F. Extended X-ray Absorption Fine Structure (EXAFS) Studies of Synthetic Sorption Samples and Natural Carbonates

The first set of samples was run at SSRL the week of June 23, 1995. Samples from selenite pH-stat experiments, selenite and selenate sorption experiments, Ni in natural carbonates from Panoche Creek, and some standard minerals were analyzed. Because the data analysis is in preliminary order at this time, only raw Fourier transforms with variable k-windowing will be shown here for pH-stat samples and sorption samples.

EXAFS of three pH-stat coprecipitation samples were run, saturation states 2.3, 4.0, and 5.8, to determine if precipitation rates altered the configuration of selenite in the calcite system. Figures 14-16 show the three Fourier transforms from these samples. Selenite coprecipitated at the lowest saturation state (Fig. 14) has peaks at 1.4, 3.2, 3.8, and 5.1 angstrom. It is important to note that these transforms were not corrected for phase shift; the distances, therefore, cannot be related to real bond distances at this time. The peak at 1.4 is clearly due to the Se-O distance of selenite. The peaks at 3.2 and 3.8 are most likely second shell bond distances which may be Se-Se, Se-Ca, Se-C, or Se-O. The peak at 5.1 is most likely a scattering peak which cannot be deconvoluted to give bond distance information but can be used as a characteristic scattering peak. Figure 15 shows the Fourier transforms of the mid-range precipitation rate sample. In this case, we see the characteristic Se-O peak, another peak at 3.2, and very faint peaks at 3.8 and 5.1, which suggest that the coprecipitated Se was beginning to lose some of its ordering due to the increased rate of precipitation and that the atom related to the 3.2 angstrom peak is more likely to be well coordinated than the atom related to the peak at 3.8. Figure 16, the transform for the sample at the fastest rate, indicates that at this rate, most of the coordination beyond the first shell is lost.

EXAFS of the selenate and selenite sorption samples are shown in Figs. 17-20. Figure 17 is for 1 mM selenite sorbed onto calcite. The equilibration program "HYDRAQL" was used to make sure the system was undersaturated with respect to all known solids. The Fourier transforms show peaks at 3.2 and

3.8 angstrom; these distances are equivalent to those found in the slow precipitation rate pH-stat sample. This suggests that the structure around sorbed and coprecipitated selenite is equivalent. Figure 18 shows the Fourier transform of 10 mM selenite sorbed onto calcite. From equilibration studies, it is expected that calcium selenite should precipitate. Clearly, the peaks at 2.7 and 3.2 do not coincide with the data from Fig. 17. This indicates that neither sorption nor coprecipitation of selenite on calcite below the solubility of calcium selenite is structurally similar to calcium selenite.

Sorption of selenate on calcite with 1 mM selenate (Fig. 19) shows only a single distance for second nearest neighbor at 3.1. Additionally, there seems to be a possible scattering feature which is seen at 5.2 angstrom. Clearly, selenate sorption on calcite is inner sphere as is selenite, although the structural ordering of the two oxidation states is different. Figure 20 shows the Fourier transform for 10 mM selenate on calcite. In this case, calcium selenate is not expected to have precipitated. Instead, we again see the single peak at 3.1 angstrom, although it is not as strong as in the 1 mM selenate sorption transform. Some of the peak damping may be caused by two selenate coordinations in the wet calcite paste. Most likely, some of the selenate in the paste is in the aqueous or outer-sphere form, which reduces the inner sphere peak amplitude relative to the Se-O first shell amplitude.

Although the results will not be presented here, Ni EXAFS of natural carbonate and parent rock from the Panoche Creek soil were run. The technique shows promise in its use for identifying the coordination of trace elements in natural samples. From preliminary analysis of the Ni EXAFS, we find that there is little difference between the apparent structure of Ni in the parent rock versus the carbonate. This would indicate that the high Ni concentration in the carbonates may be due to the preservation of parent nickel by occlusion rather than by dissolution and coprecipitation with calcite.

Discussion

A. Macroscopic Analysis of Trace Element Interaction with Calcite

Solute concentrations from water extracts indicate that soil carbonate solubility was distinctly different from the behavior of synthetic calcite. This may, in turn, alter the sorptive properties of soil carbonates, and we expect to investigate this in the following year. The solubility behavior may also be partly due to our incomplete understanding of the equilibrium constants involved in the soil solution or due to altered carbonate surface structure. As can be seen from the selenite pH-stat experiments, small amounts of trace elements can strongly affect the precipitation rate of carbonates, possibly due to changes in the surface structure of the seed calcite. Similarly, trace elements such as selenite may alter the surface structure of natural carbonate, preventing the surface from catalyzing precipitation of calcite, or altering the equilibrium solubility of carbonates.

Study of carbonate samples for Panoche Creek indicate that carbonates are important in the immobilization of trace elements in two ways. The first is by specific or non-specific incorporation of trace elements into the calcite lattice. The second is by the immobilization of trace elements by the occlusion of other minerals, and, therefore, the removal of that trace element from interaction with the soil solution. Both these processes would produce a net decrease of trace elements available to the soil solution, and, therefore, may be significant in the reduction of soil water toxicity from trace metals.

B. Microscopic Analysis of Trace Element Deposition in Calcareous Soils

Electron microprobe and SXRF microprobe studies show promise in their ability to distinguish between occluded and coprecipitated trace elements in carbonates as well as trace element organization in unaltered soils on a micrometer scale. Electron microprobe study of the carbonates from Panoche Creek indicate that occlusion is the principal mode of Ni retention by calcite. SXRF microprobe studies show some evidence of minor Ni diffusion from parent material to the carbonate crust. EXAFS of the carbonate and parent rock concur with the electron microprobe evidence, showing little change in the molecular level coordination of Ni between the parent material and carbonate. SXRF microprobe studies also show evidence of variable carbonate accumulation patterns over time. This suggests that carbonate bands on rocks may be used to determine trace element accumulation in soil carbonates over time.

C. Molecular-Level Organization of Trace Elements in Synthetic Carbonates

Laboratory studies indicate that calcite removes extensive amounts of selenite from solution. The change in precipitation rate with selenite addition indicates that it is interacting specifically with surface sites that are important in the precipitation process. Precipitation rate experiments indicate that the incorporation rate increases with increasing precipitation rate and that selenite second shell coordination is prevalent only under slow precipitation rates. Additionally, EXAFS of adsorbed and precipitated selenite suggest that both processes involve the same structural ordering, which is different from the ordering of calcium selenite. The calcite structure, therefore, forces selenite into an alternate coordination habit.

Selenate sorption EXAFS indicate a possible inner sphere adsorption process for this anion. This would indicate that there exists a relatively strong interaction between selenate and the calcite surface. It is also clear that selenate and selenite are not organized on the calcite surface in the same manner, which may indicate two different coordination sites on the surface of calcite.

Acknowledgments

We wish to thank the many people involved in this research project. Tim Teague and John Donovan of the Geology and Geophysics Department, U.C. Berkeley, helped with running the electron microprobe, preparing thin sections, and preparing calcite wedges. Hau-Wai Wong conducted most of the solubility studies. Karen Chapman and Al Thompson of the ALS, Lawrence Berkeley Laboratory, and Patt Nuessle of the NSLS, Brookhaven, helped set up SXRF microprobe scans. We wish to especially thank Andrea Foster, as well as others in Gordon Brown's research group, for assistance in running our first samples at SSRL and assistance with the EXAFSPAK and FEFF software.

References

Amundson, R. 1992. [Panoche Creek Soil for Trace Elements, personal report].

Berner, R.A. 1975. The Role of Magnesium in the Crystal Growth of Calcite and Aragonite from Sea Water, Geochimica et Cosmochimica Acta 39:489-504.

Lorens, R. B. 1981. Sr, Cd, Mn, and Co Distribution Coefficients in Calcite as a Function of Calcite Precipitation Rate, Geochimica et Cosmochimica Acta 45:553-561.

Morse, J. W. 1974. Dissolution Kinetics of Calcium Carbonate in Sea Water. III: A New Method for the Study of Carbonate Reaction Kinetics, American Journal of Science 274:97-107.

Mucci, A. and J. W. Morse 1983. The Incorporation of Mg^{2+} and Sr^{2+} into Calcite Overgrowths: Influence of Growth Rate and Solution Composition, Geochimica et Cosmochimica Acta 47:217-233.

Papelis, C., K. F. Hayes, and J. O. Leckie 1988. HYDRAQL: A program for the computation of chemical equilibrium composition of aqueous batch systems including surface-complexation modeling of ion adsoprtion at the oxide/solution interface. Technical Report No. 306, September 1988, Environmental Engineering and Science Department of Civil Engineering Stanford University, Stanford CA 94305.

Stumm, W. 1992. Chemistry of the Solid-Water Interface: Processes at the Mineral-Water Interface in Natural Systems. John Wiley & Sons, Inc. New York. 428 pp.

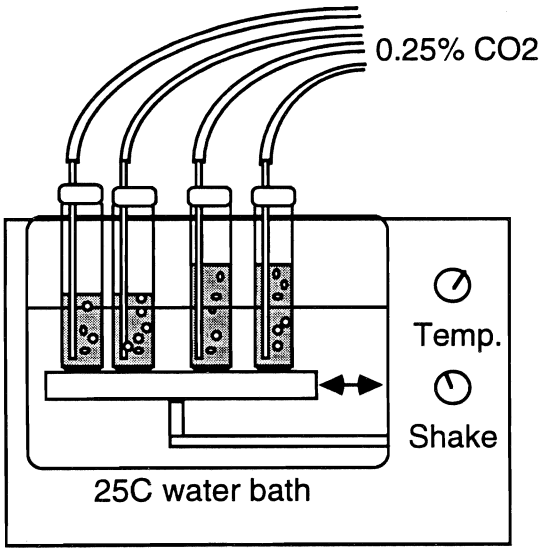

Figure 1. The constant temperature shaking bath used for soil water extract equilibration with 0.25% CO_2.

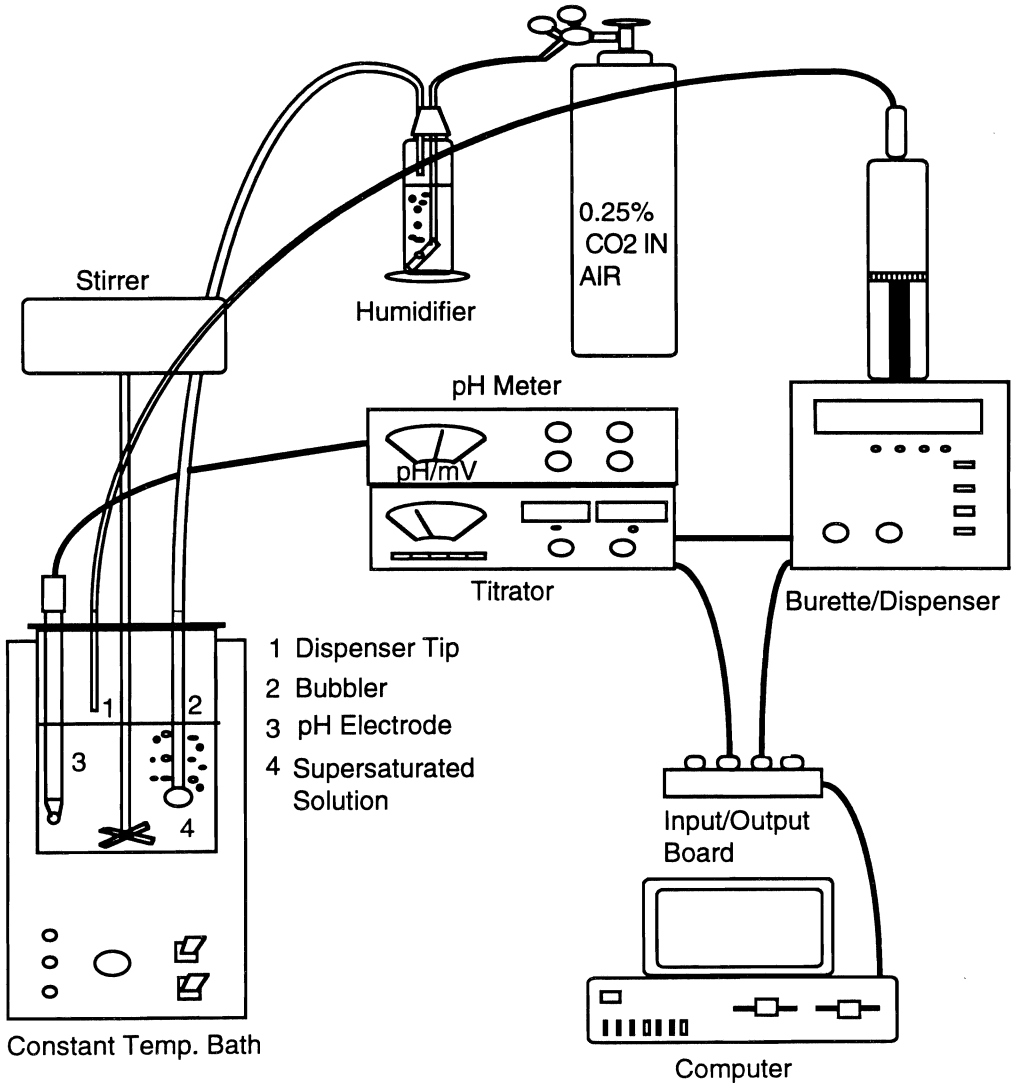

Figure 2. Diagram of the pH-stat setup.

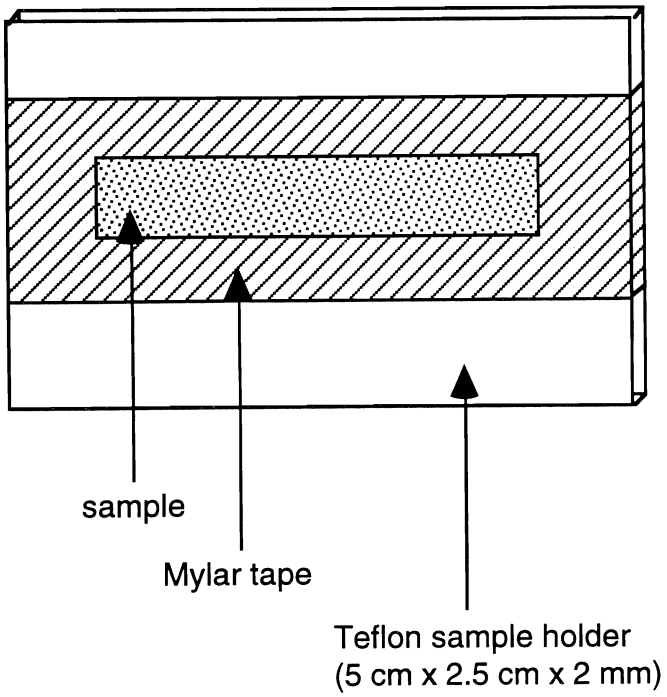

Figure 3. Sample holder for EXAFS samples.

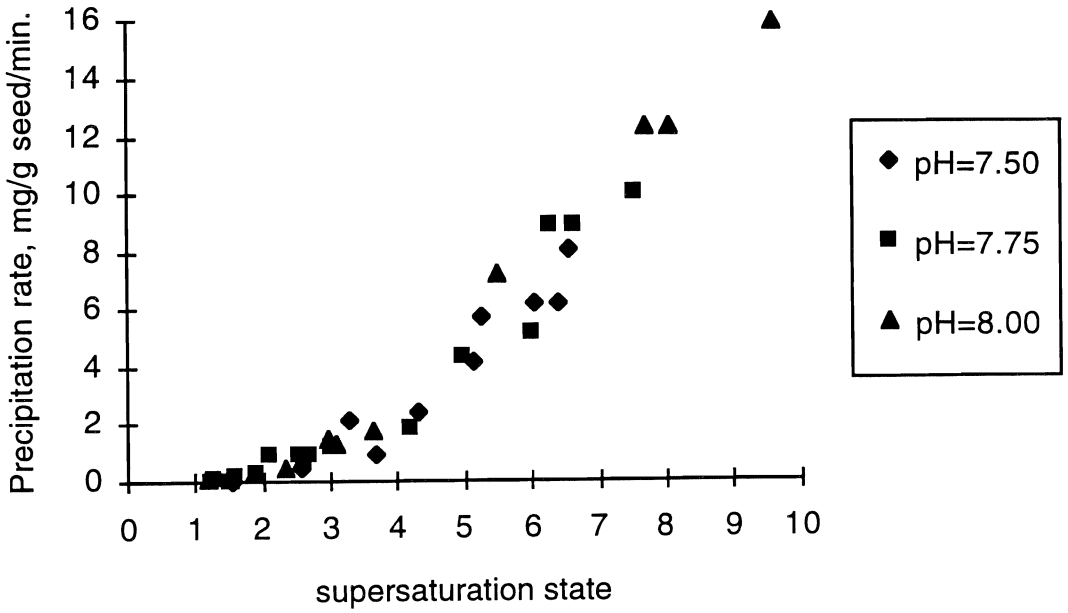

Figure 4. Precipitation rate as a function of supersaturation state at various pHs.

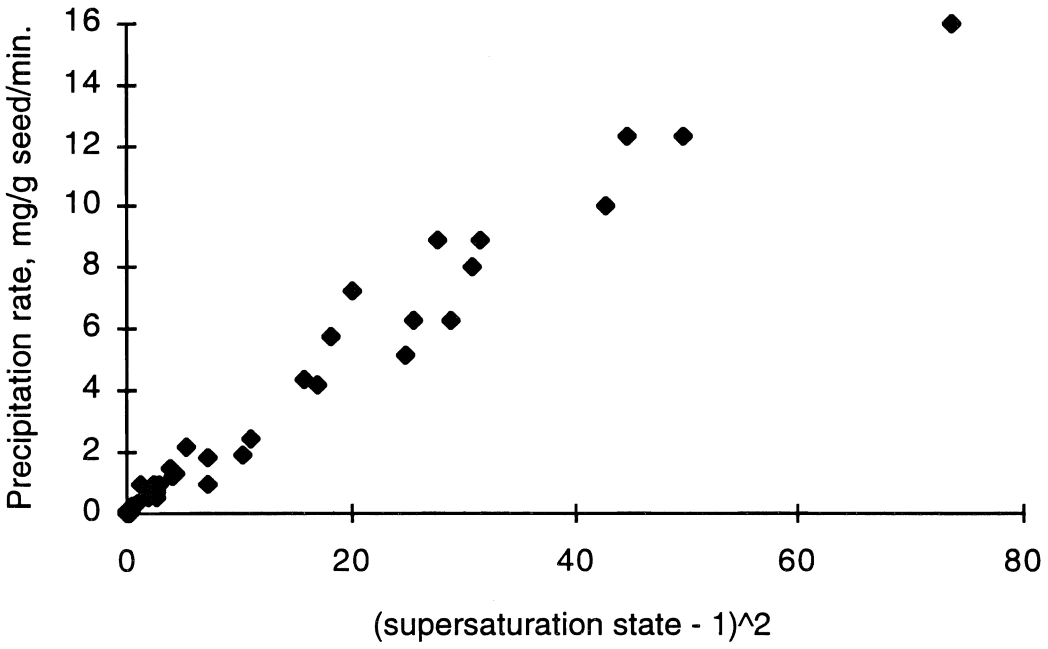

Figure 5. Modeling precipitation rate as a function of supersaturation state.

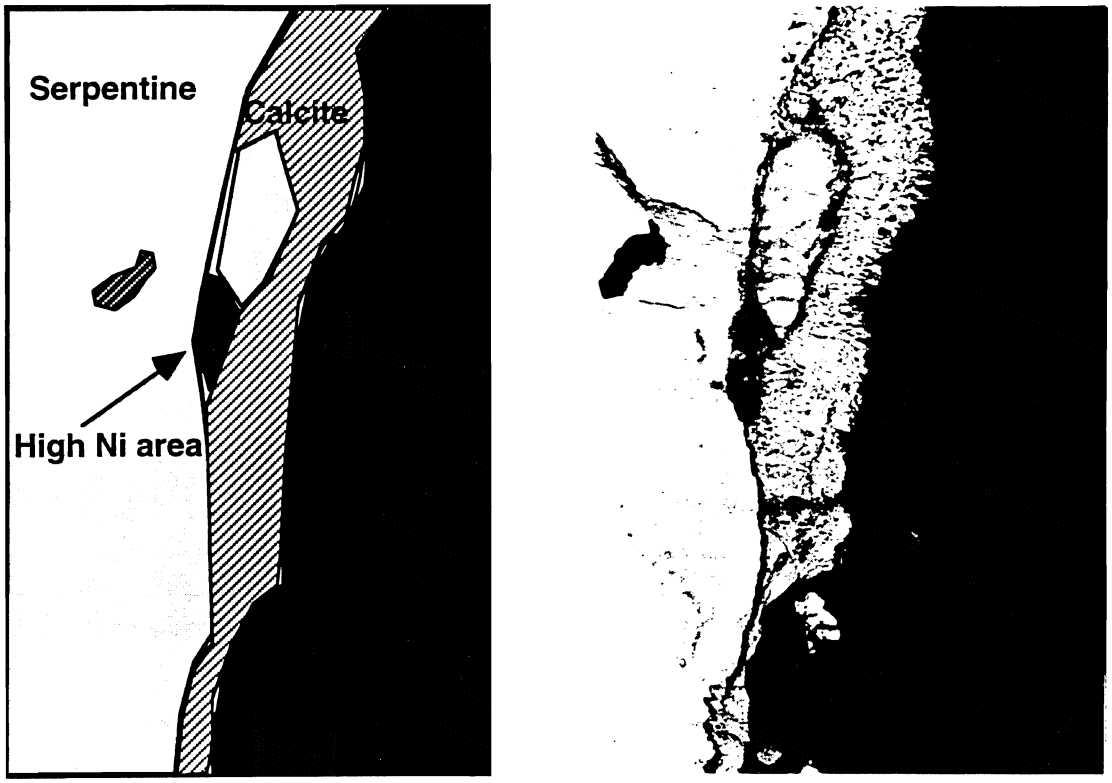

Figure 6. Thin section image of calcite accumulation on serpentine. Calcite accumulation is approximately 200 microns wide.

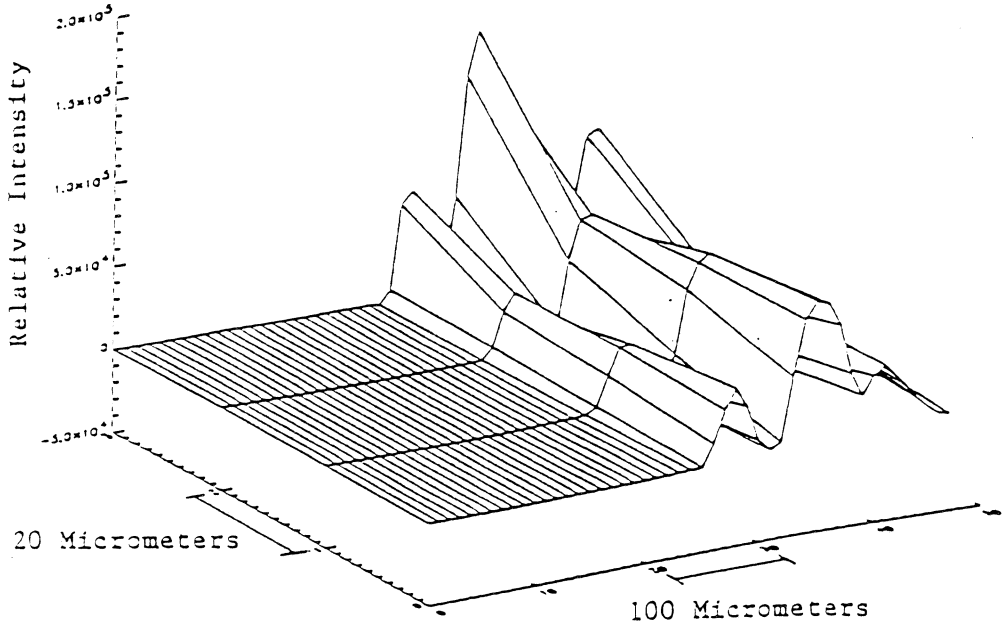

Figure 7. Distribution of Ca as determined by SXRF microprobe in a thin section of $CaCO_3$ coated clast (similar to the one shown above).

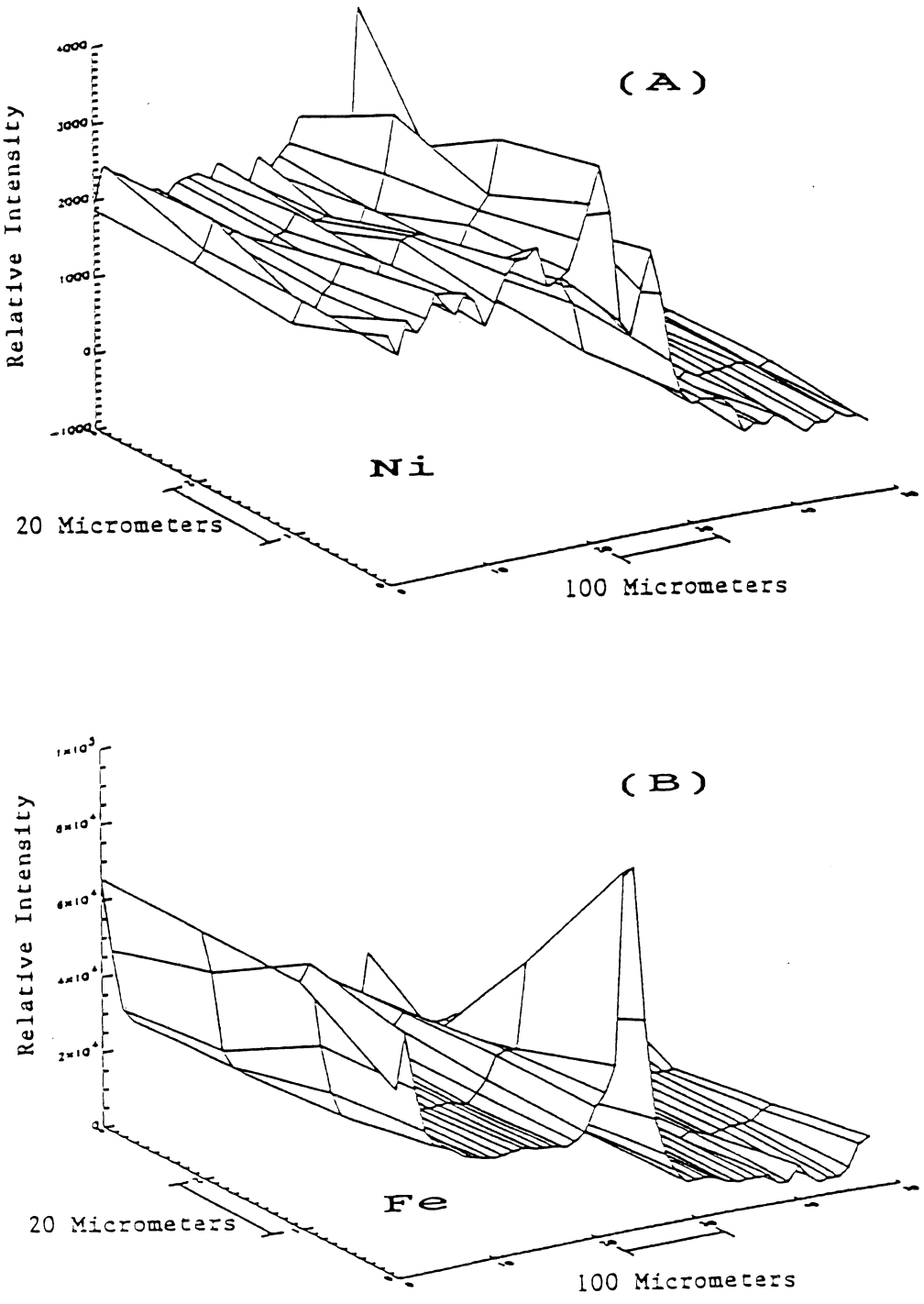

Figure 8. The distribution of Ni (A) and Fe (B) as determined by SXRF microprobe in a thin section of $CaCO_3$ coated clast. The carbonate coating begins at about 240 μm.

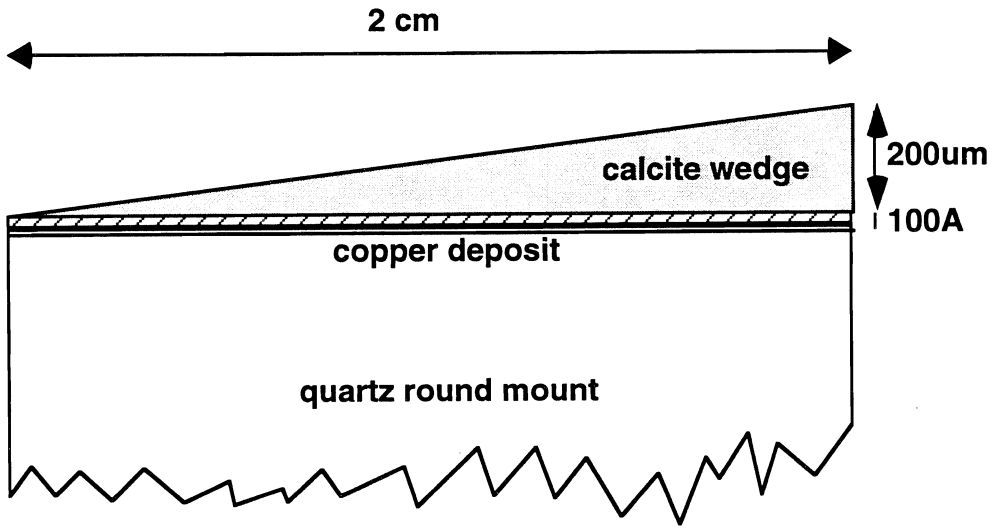

Figure 9. Diagram of the calcite wedge constructed for modeling heterogeneity effects

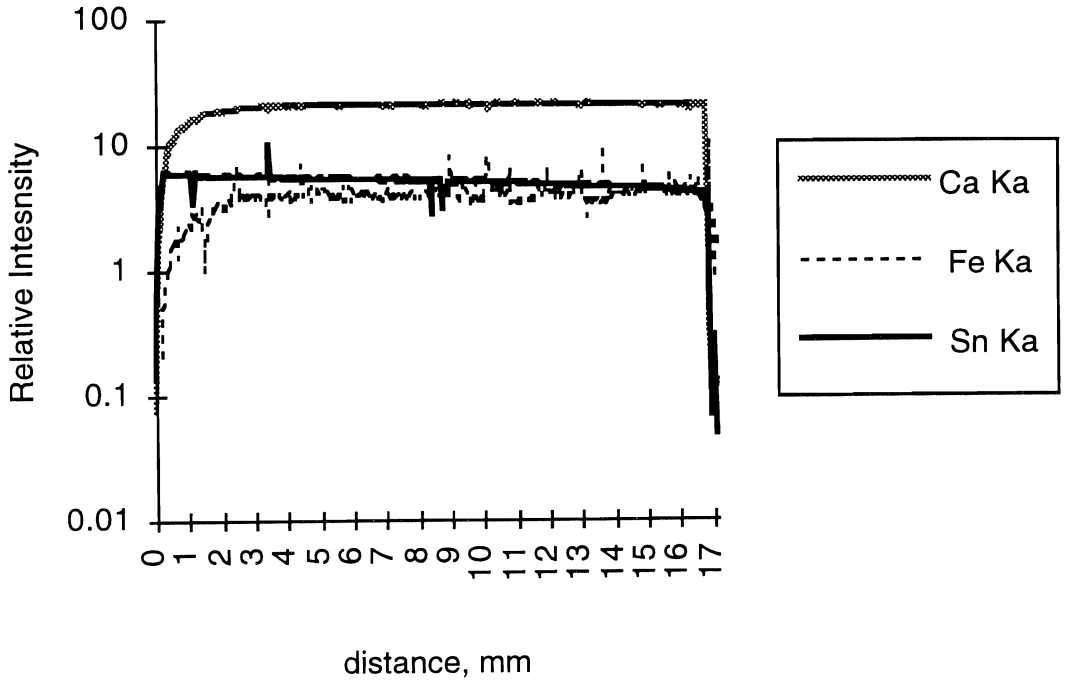

Figure 10. Fluorescence across calcite wedge.

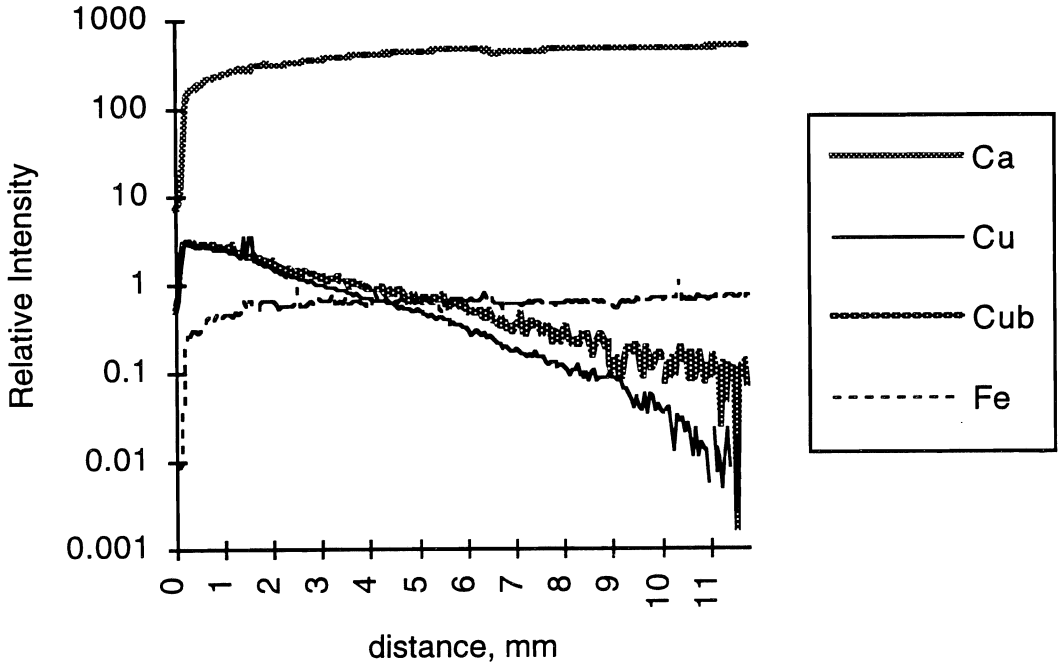

Figure 11. Fluorescence across calcite wedge.

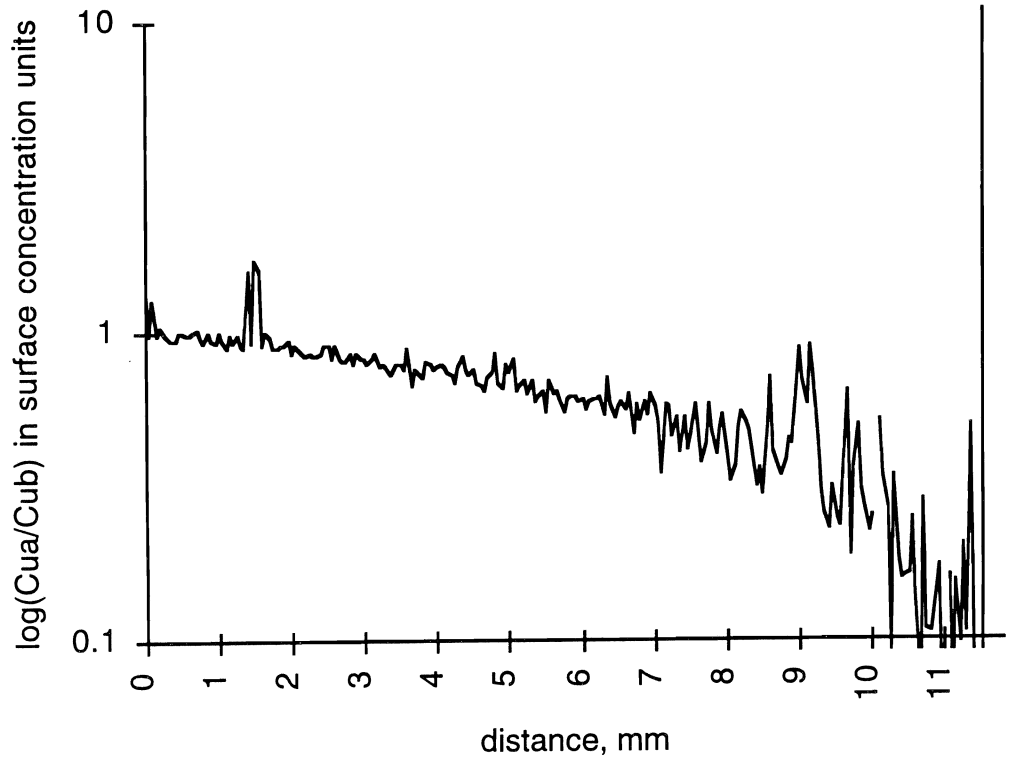

Figure 12. Cu-alfa and Cu-beta fluorescence difference across calcite wedge.

Figure 13. Model of Cu fluorescence across calcite wedge.

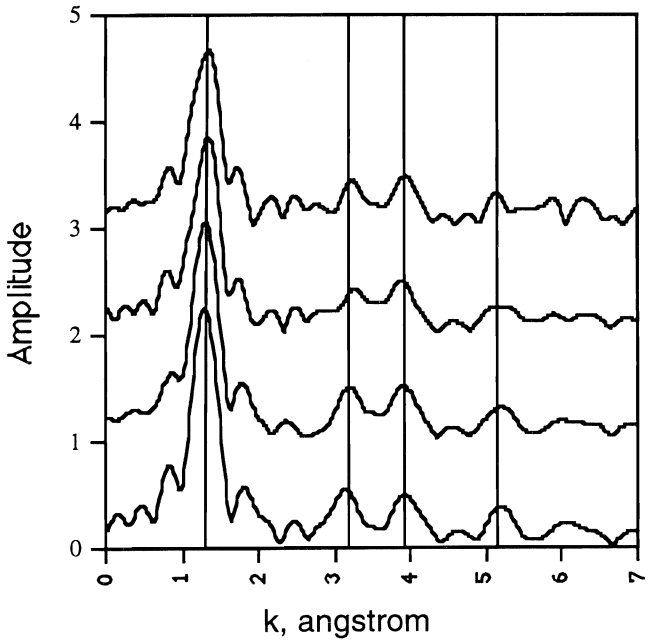

Figure 14. Se(IV) (selenite) coprecipitated with calcite at supersaturation state 2.5, pH 7.5.

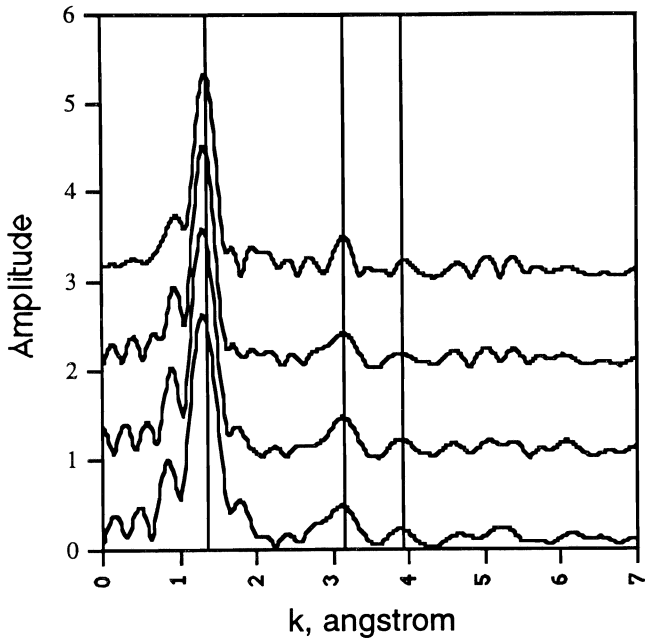

Figure 15. SeIV coprecipitated with calcite at supersaturation state 4.5, pH 7.5.

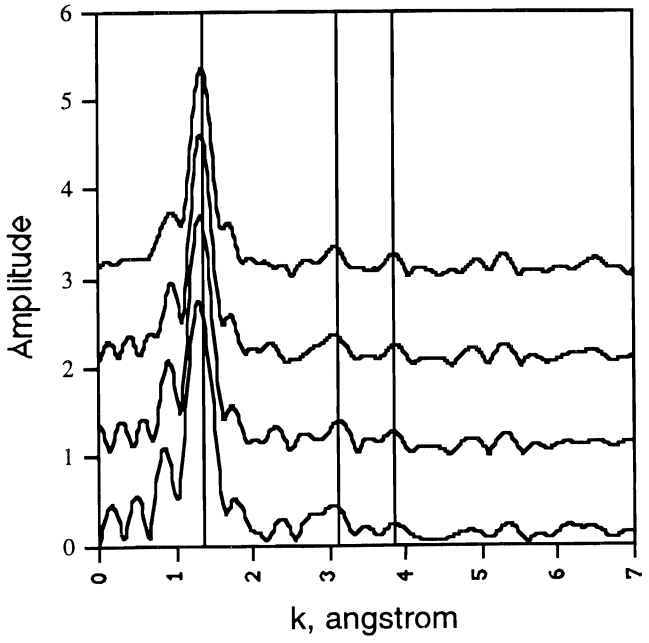

Figure 16. SeIV coprecipitated with calcite at supersaturation state 6.5, pH 7.5.

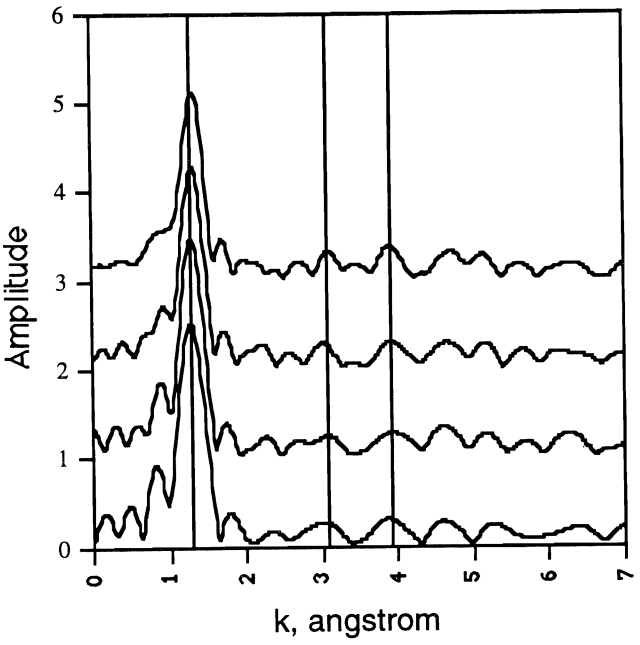

Figure 17. 1mM SeIV sorbed onto calcite, pH 7.5.

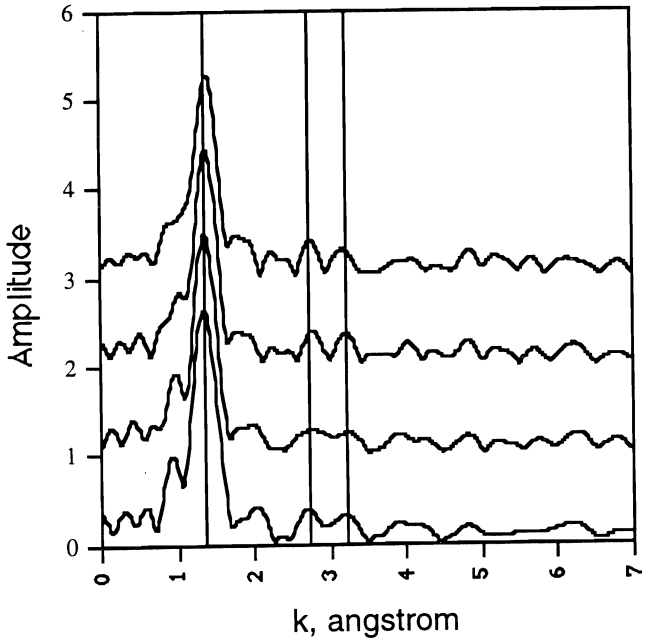

Figure 18. 10mM SeIV sorbed onto calcite, pH 7.5.

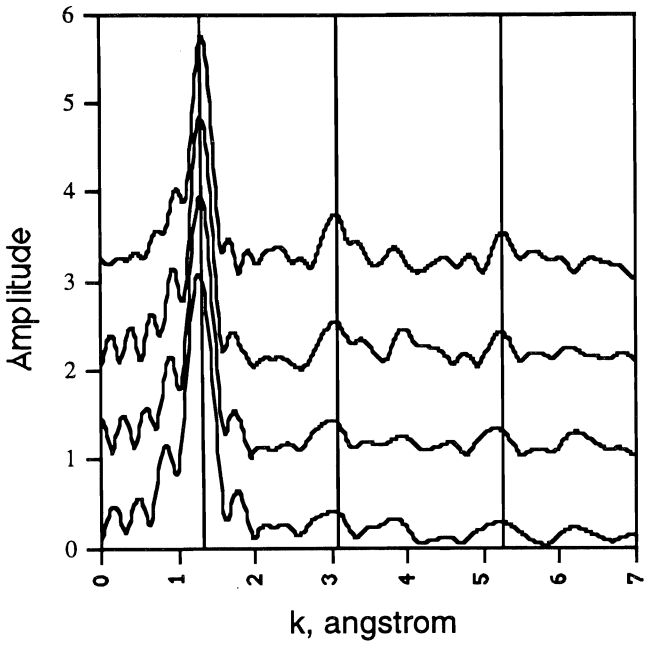

Figure 19. 1mM SeVI sorbed onto calcite, pH 7.5.

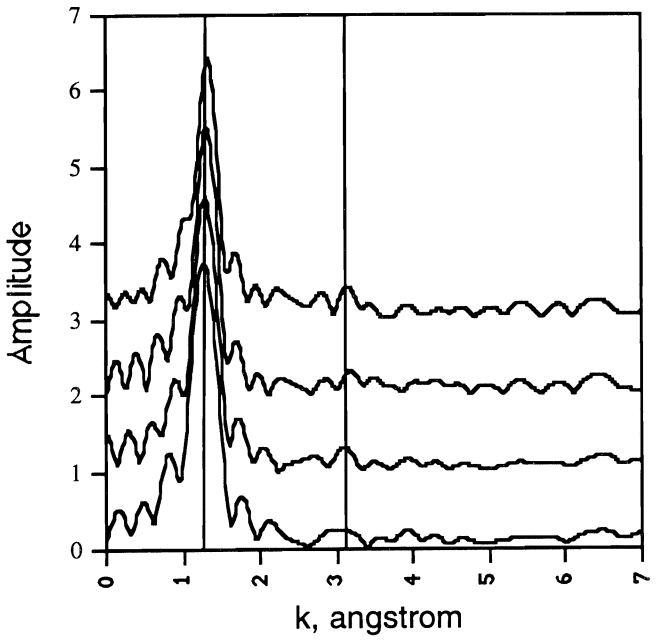

Figure 20. 10mM SeVI sorbed onto calcite, pH 7.5.

Appendix 1. The SXRF Fluorescence Model Program

Modeling 1-D SXRF Scans

This program measures the fluorescence of a particular element across a two-dimensional surface for primary x-rays entering at 45 degrees to the sample and a detector positioned at 90 degrees to the primary x-rays and 45 degrees to the sample (Fig. 1). The solid angle of the detector may be controlled, although it only changes the net fluorescence of the sample and while the effect of angular dependent mass absorption of the secondary fluorescence is not taken into account. The program assumes that the primary x-rays are monochromatic, although the results can often be related to expected results from white beams, depending on the major elements in the sample and element of interest.

The program is constructed with several data and computational files which are tied together via a macro file. Before running the macro, 2 files must be adjusted by the user: the 1-D SXRF DATA file and the SAMPLE file (Fig. 2). The order of adjustment is not important. After the files have been properly set up, the user must save and close all files pertaining to the program, open the SXRF MACRO file, and press ⌘+Option+r to start the program. The program will run through all the computations automatically and will, at the end, graph out the results with x-axis as distance and y axis as fluorescence. A final data file will also be made which contains the fluorescence from each pixel in the sample. These data can be used to determine the minimum thickness of sample which is not affected by sample-thickness effects on fluorescence.

1-D SXRF Scan Input File (Fig. 3)

This file contains all the data required for analysis of the system. Top section of the file contains basic parameters required by the program. The parameters required in this section are the Io value, the pixel size, the mass absorption of the element of interest, and the fluorescence yield of the element. The bottom section of the file is a list of component boxes which can be used to define the composition and mass absorption of each component in your system. For each component, the user must define the density, concentration of the element of interest, and the concentration and mass absorption at primary and secondary energies for each element in the component. To help in determining the mass absorption of samples, a MASS ABSORPTION file is included, which uses an equation modeled by empirical mass absorption data to estimate the mass absorption of elements at various energies. This file consists of a large set of data which contain the mass absorption of most elements between K and Zn at the binding energies, and K-alfa and K-beta fluorescence of each of those elements. One can also add more elements to the bottom of the file simply by filling in the element Z-value, the energy of interest, and then filling the other columns by copying the equations from the above rows. One must then determine which mass absorption line is of interest at that energy (K, L1, L2, L3, M1-5, and N lines are included). When the mass absorption and concentration of each element have been added to the component section, the total mass absorption will be calculated automatically. There are a maximum of 9

components which can be used in the program and a maximum of 8 elements for each component.

Sample File

This file describes the 2-D composition of the sample to be scanned. At the top are 9 pixels which are tied to the 9 components defined in the previous file; they are simply noted by the numbers 1-9. Below the 9 pixel components, there is a large set of pixels grouped into a triangle which defines the sample to be scanned. The user must describe the system by tying each of the pixels to one of the 9 pixels at the top of the file. This is accomplished simply by creating a formula in a pixel, such as "=a2" which ties that pixel to component 1. One can then copy that pixel onto any part of the sample triangle or tie pixels to other component pixels until all the pixels are tied to one of the 9 components. The system and parameters are then fully defined and one can run the program as described above.

Mathematical Aspects of Fluorescence Determination

Part I: General Equation For Fluorescence Of Homogeneous Sample

We will first make the approximation that the characteristic fluorescence of each element is excited by only a specific energy with wavelength λ_p. The wavelength of the characteristic fluorescence is λ_s.

We start with the following equation for calculating the intensity of primary x-rays as they travel through a sample:

$$dI(\lambda_p) = \mu_f(\lambda_p)^*\rho_f{}^*I(\lambda_p,x)^*dx \qquad (1)$$

where

$dI(\lambda_p)$ = change in intensity of primary energy per area

$\mu_f(\lambda_p)$ = sample mass absorption coefficient at primary energy

ρ_f = density of sample

$I(\lambda_p,x)$ = intensity of primary energy at depth x per area.

$\mu_f(\lambda_p)$ can be calculated in the following manner:

$$\mu_f(\lambda_p)= S^*\mu_i(\lambda_p)^*C_i$$

where

$\mu_i(\lambda_p)$ = mass absorption coefficient of element i at primary energy

C_i = concentration of element i w.r.t. mass.

$I(\lambda_p,x)$ can be calculated from Beer's law:

$$I(\lambda_p,x) = I_0{}^*\exp[-\mu_f(\lambda_p)^*\rho_f{}^*x] \qquad (2)$$

where

I_0 = incoming intensity per area.

We are interested in the intensity of the secondary energy; the secondary energy produced will be a function of the intensity of the primary energy, the fluorescence yield, and the fraction of absorption due to the fluorescing compound:

$dI(I_s) = k^*C_e^*\mu_e(\lambda_p)^*[\mu_f(\lambda_p)]^{-1}*dI(\lambda_p)$ **(3)**

where

k = fluorescence yield

C_e = concentration of fluorescing element

$\mu_e(\lambda_p)$ = mass absorption coefficient of fluorescing element.

The actual intensity that makes it to the surface of the sample will be a function of the distance from the point of fluorescence to the surface by way of Beer's law:

$dI_1(\lambda_s) = \exp[-\mu_f(\lambda_s)^*\rho_f^*x]\ dI(\lambda_s)$ **(4)**

Putting together equations 1, 2, 3, and 4, we end up with the following equation:

$dI_1(\lambda_s) = \exp[-\mu_f(\lambda_s)^*\rho_f^*x]^*k^*C_e^*\mu_e(\lambda_p)^*\rho_f^*I_0^*\exp[-\mu_f(\lambda_p)^*\rho_f^*x]dx.$

We can now integrate both sides to get the fluorescence as a function of sample parameters:

$$\int_0^{I_1} dI_1(\lambda_s) = \int_l^0 e^{-\mu_f(\lambda_s)*\rho_f*x} * k * C_e * \mu_e(\lambda_p) * \rho_f * I_0 * e^{-\mu_f(\lambda_p)*\rho_f*x} * dx$$

$I_1 = I_0^*k^*C_e^*\mu_e(\lambda_p)^*[\mu_f(\lambda_p)+\mu_f(\lambda_s)]^{-1}*\{1-\exp[-\rho_f(\mu_f(\lambda_p)+\mu_f(\lambda_s))l]\}$ **(5)**

where

l = thickness of sample.

Note that for an infinitely thick sample, the equation is simplified to:

$I_1 = I_0^*k^*C_e^*\mu_e(\lambda_p)^*[\mu_f(\lambda_p)+\mu_f(\lambda_s)]^{-1}$ **(6)**

Part II. Equation Used in This Program

The program uses the following equation to solve for fluorescence across the sample, the core of which is equation 5. Equation 5 is used to solve the fluorescence from each pixel. To each pixel, one must add a factor which takes into account the path leading to the pixel and the path to the detector. The sum of the fluorescences from all pixels in the linear trajectory of the incoming x-rays is the fluorescence at that point:

$$I = \sum_{i=1}^{m} \frac{I_0 * k * C_e * \mu_{e,i,x}(\lambda_p)}{\mu_{f,i,x}(\lambda_p) + \mu_{f,i,x}(\lambda_s)} * \left\{1 - e^{-\rho_{f,i,x} * (\mu_{f,i,x}(\lambda_p) + \mu_{f,i,x}(\lambda_s)) * l}\right\} \prod_{j=0}^{i-1} e^{-l * (\rho_{f,j,x} * \mu_{j,x}(\lambda_p))} \prod_{k=x+1}^{x+i+1} e^{-l * [(\rho_{f,i,k} * \mu_{i,k}(\lambda_s))]}$$

where the subscripts refer to the positions in the 2-dimensional matrix that describe the sample (filename: SAMPLE), m is the number of pixels in the column of interest, and x is the column number in the matrix.

For additional information, consult Sparks (1980) and Claisse and Samson (1962).

Appendix References

Claisse, F. and C. Samson .1962. "Heterogeneity Effects in X-ray Analysis", Adv. X-ray Analysis, 5:335-355.

Sparks, Jr., C. J. 1980. Fluorescence Microprobe for Chemical Analysis. pp. 459-521. In H. Winick and S. Doniach (eds.) Synchrotron Radiation Research. Plenum Press, 754 pp.

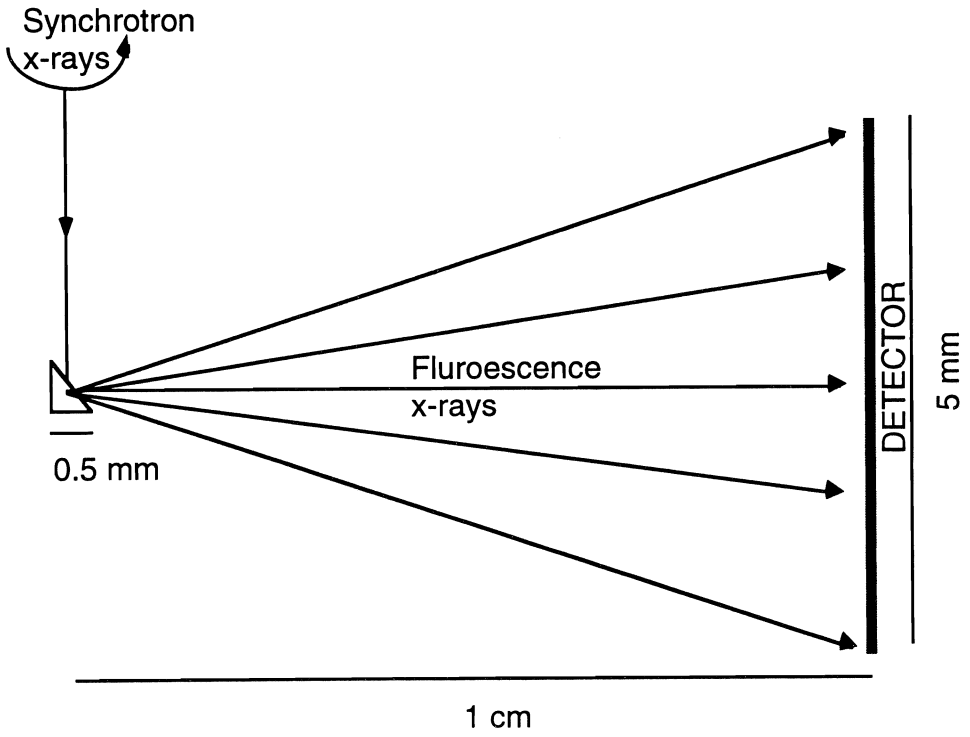

Appendix 1, Figure 1. A diagram describing the SXRF setup assumed by the model.

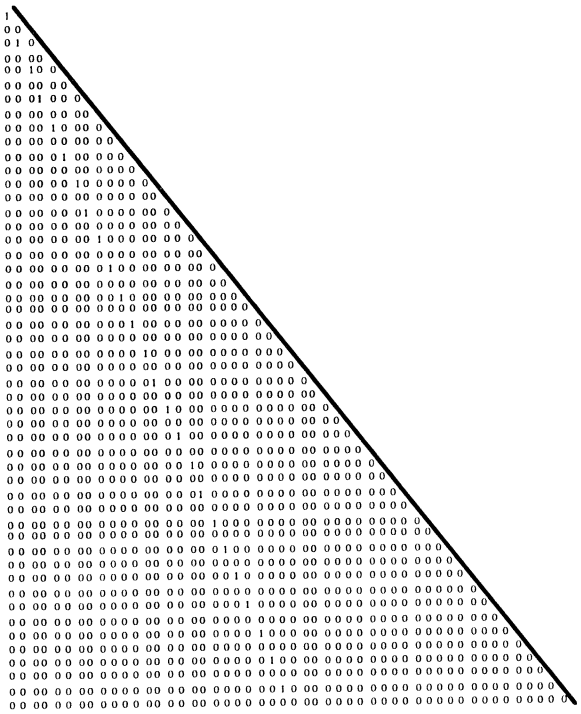

Appendix 1, Figure 2. A diagram of the "sample" file used for SXRF modeling.

Data for calculating 1-DS XRF scan

Io, mass absorption fluorescent element, fluorescence yield, and pixel size must always be filled out.
For each component specified in the sample matrix, at least one value must be prescribed in each boxed area.

Io	PIXEL SIZE, cm
1	0.0005

mass absorption fluorescent el	fluorescence yield
287.8	0.5

COMPONENT 1

DENSITY OF MATERIAL, g/cm^3	CONCENTRATION OF FLUORESCENCE ELEMENT, g/g
2.65	0.001

ELEMENT	PRIMARY ENERGY mass absorption, cm^2/g	SECONDARY ENERGY mass absorption, cm^2/g	CONCENTRATION g/g
Ca	116.7	156.58	0.4
C	7.879	10.57	0.12
O	13.4	17.98	0.48
NET, cm^-1	143.252322	192.20662	1

COMPONENT 2

DENSITY OF MATERIAL, g/cm^3	CONCENTRATION OF FLUORESCENCE ELEMENT, g/g
9.85	1

ELEMENT	PRIMARY ENERGY mass absorption, cm^2/g	SECONDARY ENERGY mass absorption, cm^2/g	CONCENTRATION g/g
Cu	287.8	54.54	1
NET, cm^-1	2834.83	537.219	1

Appendix 1, figure 3. Diagram of "1-dS XRF scan input" file used for SXRF modeling.

Quantifying Mechanisms of Loss From the Chemical Signature of Multicomponent Nonaqueous Phase Liquids in Soils

MICHAEL A. ANDERSON
Department of Soil and Environmental Sciences, Riverside Campus

Summary

Contamination of soils and groundwater by fuels, mixed solvent wastes, and other multicomponent nonaqueous phase liquids (mNAPLs) is a widespread environmental problem. Compositional information (i.e., the chemical fingerprint) of mNAPLs can be used to deduce important information about the processes controlling NAPL fate and persistence in the subsurface. Studies have been completed which quantified activity coefficients in binary and ternary mixtures, as well as experimental and modeling evaluations of volatilization in column systems. Primary emphasis has been placed on mixtures of methyl-*tert*-butyl ether, n-hexane, and benzene. These compounds are present in significant quantities in gasoline and represent a wide range of physico-chemical properties. Activity coefficients for these compounds in ternary mixtures were found to range from 0.7 to 2.0, and were sensitive to mole fraction and composition. Preliminary experimental and modeling results demonstrate chromatographic behavior associated with volatilization. The initial results of this two-year study have implications for *in situ* vapor stripping and enhanced biorestoration techniques.

Key Words: nonaqueous phase liquids, NAPL, volatilization, activity coefficients, solvents

Project Objectives Addressed in 1994-95

To experimentally and theoretically evaluate multicomponent NAPL behavior in soils.

Research Plan and Procedures

Activity coefficients (g_i)) for methyl-*tert*-butyl ether, *n*-hexane, and benzene in mixtures of known mole fraction (c_I) were quantified through headspace analysis based upon solution to:

$$P_i = \gamma \chi_i P_i^0 \qquad (1)$$

where P_i is the vapor pressure of component *i* in the mixture, and P_i^0 is the saturated vapor pressure. Mixtures of known mole fractions were prepared and approximately 10 mL of the solutions were placed in 30 mL headspace vials. The vials were promptly sealed with Teflon-lined septa and aluminum crimp caps. The vials were allowed to equilibrate at room temperature (ª23∞C) overnight. 10 - 100 mL of vapor were withdrawn using a gas-tight syringe fitted with a Teflon stop valve and injected into an HP 5890 GC with 5971 mass spectral detector. Standards were determined from headspace analysis of pure solvents using variable sample injection volumes.

Preliminary studies evaluating resident NAPL contents and vapor flux in columns subject to steady flow of water-saturated air have also been conducted. A well-graded coarse sand was packed to a bulk density of about 1.5 g/cm^3 in 15 cm LC columns fitted with Teflon endcaps, fittings and tubing. The columns were first saturated with water and then drained by gravity and subsequently by vacuum to wet the sand; 0.4 - 1.5 mL of a ternary mixture of methyl-*tert*-butyl ether (MTBE), n-hexane, and benzene (c_I= 0.33) was then added to the top of the column. The columns were then capped and sealed and the NAPL was allowed to redistribute by gravity and vapor equilibration for about 1 h. Fairly uniform and reproducible initial NAPL contents were produced over 70-80% of the column length. Air flow (3.4 cm^3/min) was then applied to the bottom of the columns. Columns were subsampled (1 cm increments), promptly extracted with methanol (2:1 v/v), and analyzed by direct injection of 1mL of the extract into the GC-MS. Vapor flux concentrations were alternately determined by direct vapor injection as described above or by bubbling column outflow through cold methanol for a known period of time, and analyzing the methanol. The latter technique has proven more reliable.

Results

Activity coefficients were found to vary significantly as a function of composition (Fig. 1). Recognizing that the sum of the mole fractions must equal one and that the mole fraction for the chemical given by the activity coefficient is implied by difference, the portion of the figure away from the reader bears no information and is featureless. The activity coefficient for MTBE generally

increased with increasing mole fraction of the other constituent(s), from a value of 1 for a pure liquid to values near 2 for mixtures high in the other constituents. *n*-Hexane activity coefficient values ranged from 0.7 to 1.4, reaching a maximum value in binary mixtures with benzene near a mole fraction of 0.5 and dropping at higher and lower mole fraction values. Similar observations were made for benzene in binary and ternary mixtures (Fig. 1). From Eq. (1), it is readily apparent that without activity corrections, one would potentially substantially underestimate, or in some cases overestimate, vapor concentrations in soils contaminated with a mixture of these three chemicals. Empirical expressions have been developed to estimate activity coefficients, from results like that in Fig. 1, for systems evolving in composition. Assuming that the change in concentration of a NAPL-contaminated soil, which consists of *i* components at mole fractions c_i in the NAPL, is given by:

$$dC_i^{soil}/dt = -(Q_{air}/r_b V)\,(g_i c_i P_i^0/RT) \qquad (2)$$

one can predict a significant influence of activity correction on the NAPL composition over time.

Applying Eq. (2) to a binary mixture of hexane and benzene at initial concentrations of 1.8 $x10^{-2}$ mol/kg in a sand subject to air flow of 4 mL/min, preliminary results suggest that the model will do an adequate job reproducing the vapor phase composition as a functon of time in small flow chambers (Fig. 2). The higher vapor pressure of hexane resulted in more rapid loss than benzene; as a result, the mole fraction of benzene, and thus its vapor concentration (Eq. 1), increased with time. At approximately 80 min, all hexane had been volatilized and removed from the column, which left behind essentially pure benzene, and correspondingly the highest vapor concentration (approximately that equal to a saturated vapor), until all benzene was also lost (after about 120 min). Improvements in analytical techniques and activity corrections are expected to further improve the fit between model and experiment.

It was found, however, that more complicated vapor flux data were observed using ternary mixtures of MTBE-benzene-hexane in somewhat larger samples in 15 cm columns. As a result, resident concentrations were also sampled to quantify behavior in the columns. After approximately one-half of the total mass of mNAPL had been removed from the column by volatilization, flow was stopped and the column was sampled. The column was subsampled lengthwise along the direction of flow in 1 cm intervals, yielding a total of 15 samples for resident concentration analysis. Samples were promptly extracted with methanol to minimize further volatilization losses. Preliminary results indicate redistribution of the components under column conditions, such that benzene concentrations were significantly elevated above the initial concentrations ahead of the volatilization front (Fig. 3). That is, as the lighter components were volatilized away (Eq. 1), a benzene-enriched NAPL phase was left near the inlet; when vapor in equilibrium with that phase was convected through the column, the vapor was then in disequilibrium with respect to the local resident NAPL which bore a different composition (*e.g.*, a lower benzene

mole fraction). Accordingly, the benzene dissolved into the local NAPL phase, thereby enriching it relative to its initial content. The volatilization front for hexane and MTBE were advanced relative to benzene (Fig. 3).

In light of these preliminary experimental observations, a simple 1-dimensional model based on Eq. (2) was developed to take account of volatilization and redistribution along the column length. In this model, the column is divided into 15 1-cm^3 segments for which a mole balance about each segment can be written. Equilibrium partitioning is assumed within each segment.

Results of this simple model (Fig. 4) qualitatively reproduce the experimentally observed trends (Fig. 3). An accumulation of benzene beyond the initial concentration is predicted, with a sharpening front; the model also predicts a very slight buildup of hexane with a more smeared front relative to benzene at any particular simulation time, and most significant removal, with a very broad front, predicted for MTBE.

Predicted vapor flux concentrations are, of course, consistent with this model; significant changes in vapor concentrations were noted at later times (Fig. 5), when the composition of the mNAPL in the final segment deviated from its initial content (in this particular simulation after approximately 60 min) (Fig. 4). The model also predicts a sharp drop in benzene vapor concentration coinciding with loss of the other components from the system. This feature awaits further experimental verification.

Discussion

The results to date imply a type of chromatographic effect within soils contaminated with mNAPLs when subject to one-dimensional vapor flow. Preliminary results are limited to simple cases; in particular, the model developed does not consider dissolution into the aqueous phase or any type of sorption phenomena. Future work during the second year of this project will evaluate more rigorously these reported preliminary results, and extend the results to more realistic situations. The influence of observed chromatographic behavior on interpretation of chemical fingerprints will also be evaluated.

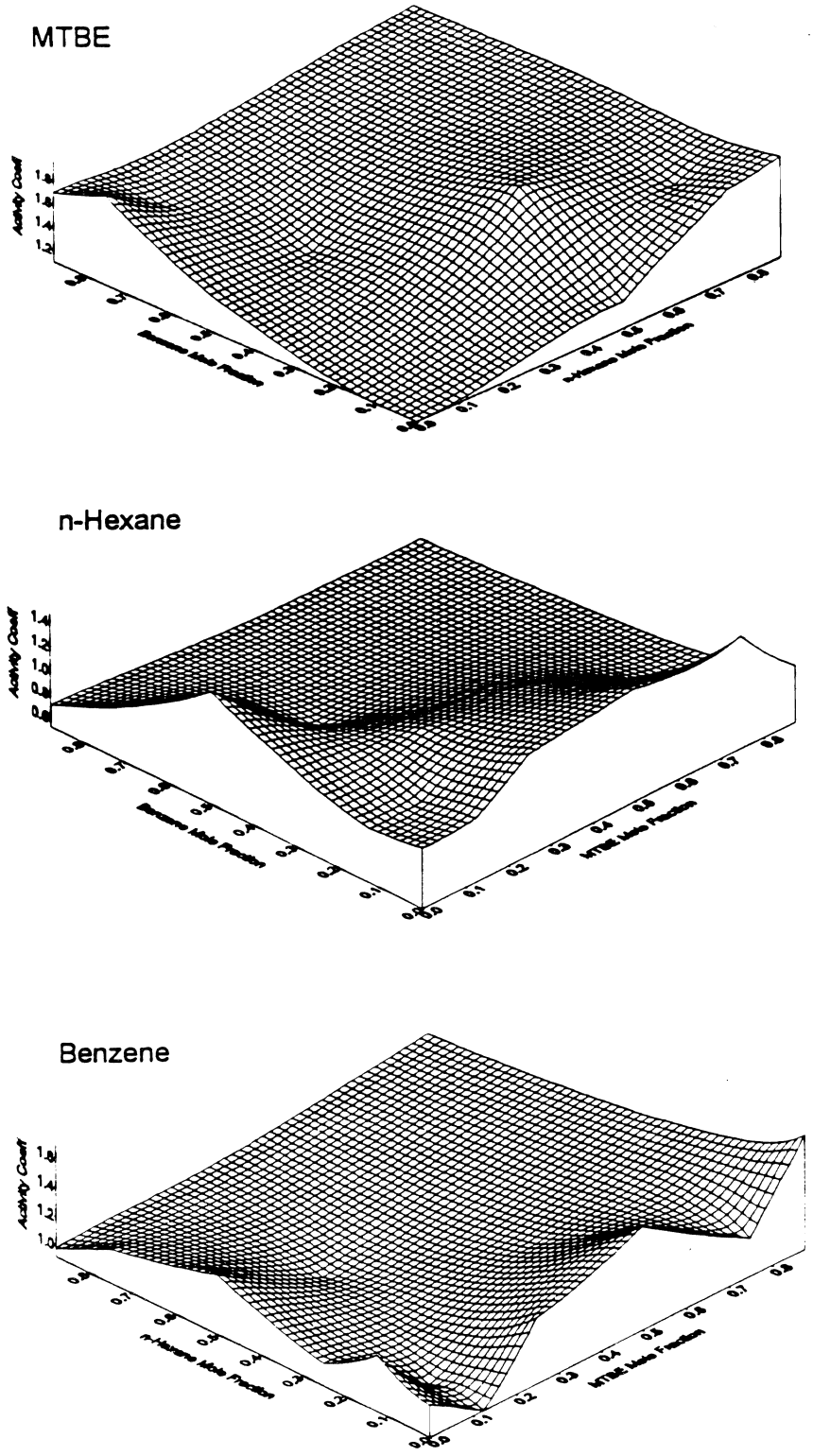

Figure 1. Activity coefficients of methyl-*tert* -butyl ether (MTBE), *n* -hexane and benzene as a function of mole fraction in ternary mixtures.

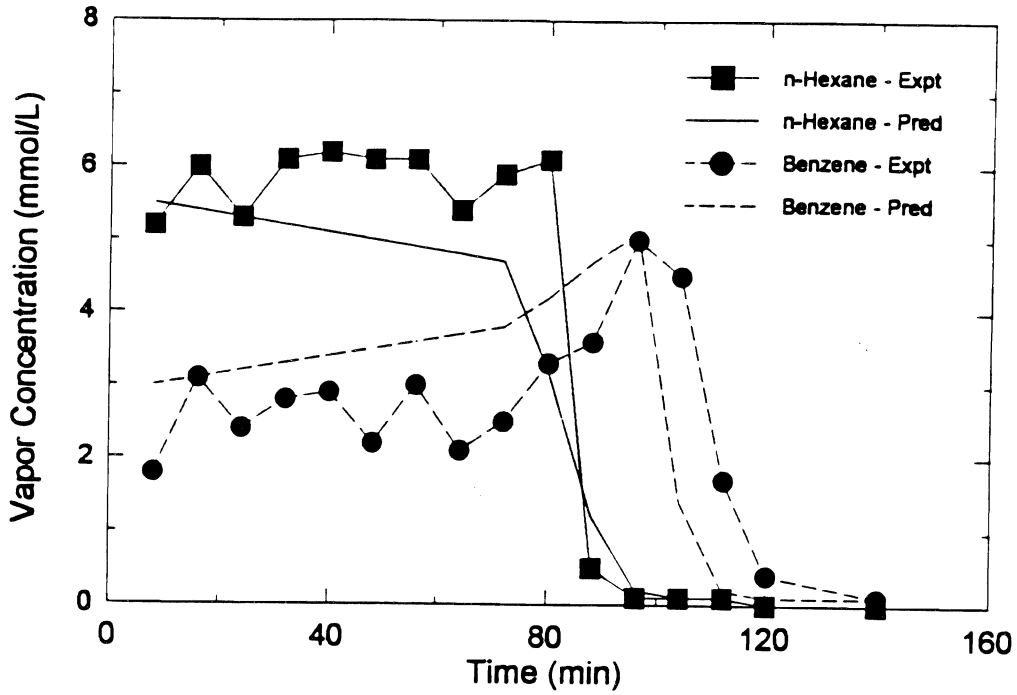

Figure 2. Experimental and model results for benzene-hexane mixture (mole fractions of 0.5) in small flow chamber.

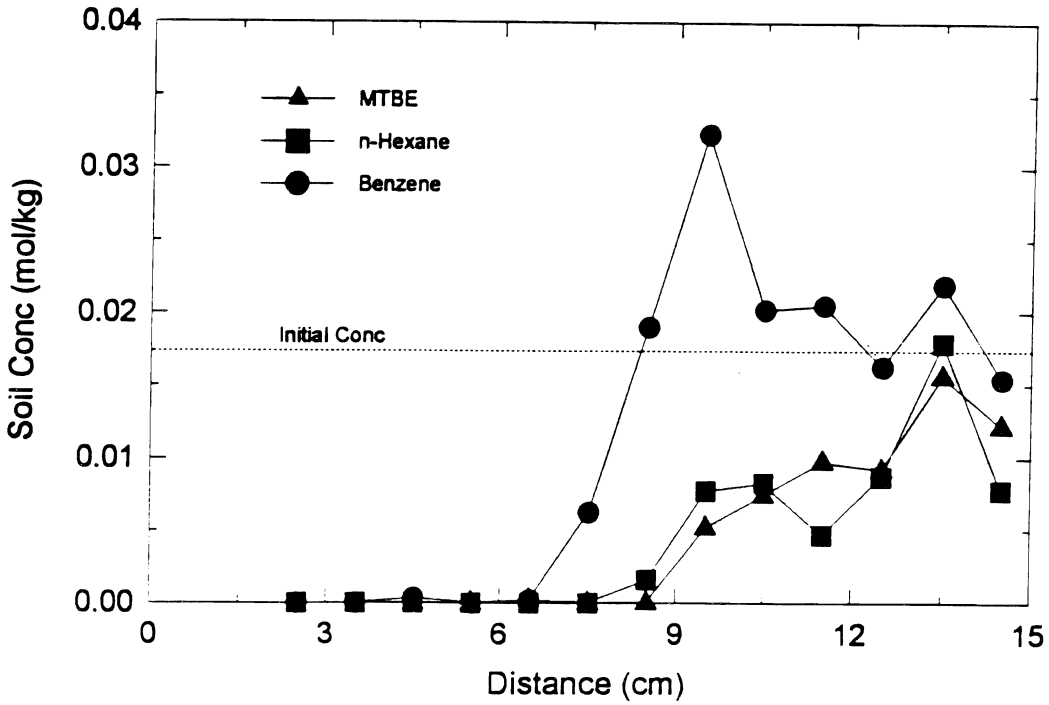

Figure 3. Resident concentrations in 15 cm soil column after 45 min of air flow (initial concentration of 0.018 mol/kg from 6 - 15 cm, air flow of 3.5 cm^3/min) showing benzene chromatographic wave.

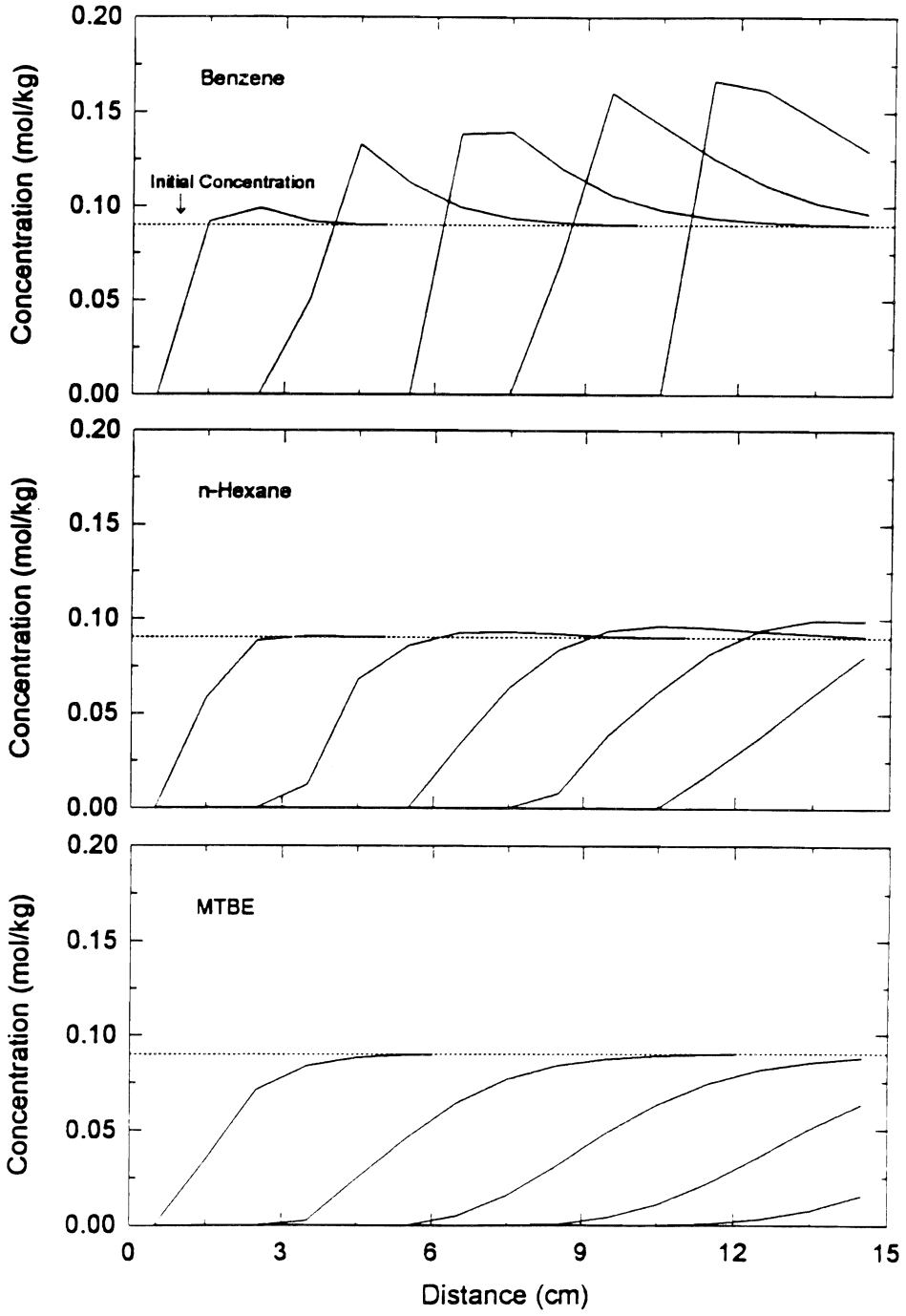

Figure 4. Predicted resident concentrations for a uniform soil concentration as a function of time (after 10, 30, 50, 70 and 90 min of flow, with flow of 3.5 cm^3/min, and an initial concentration of 0.09 mol/kg), showing development of benzene chromatographic wave.

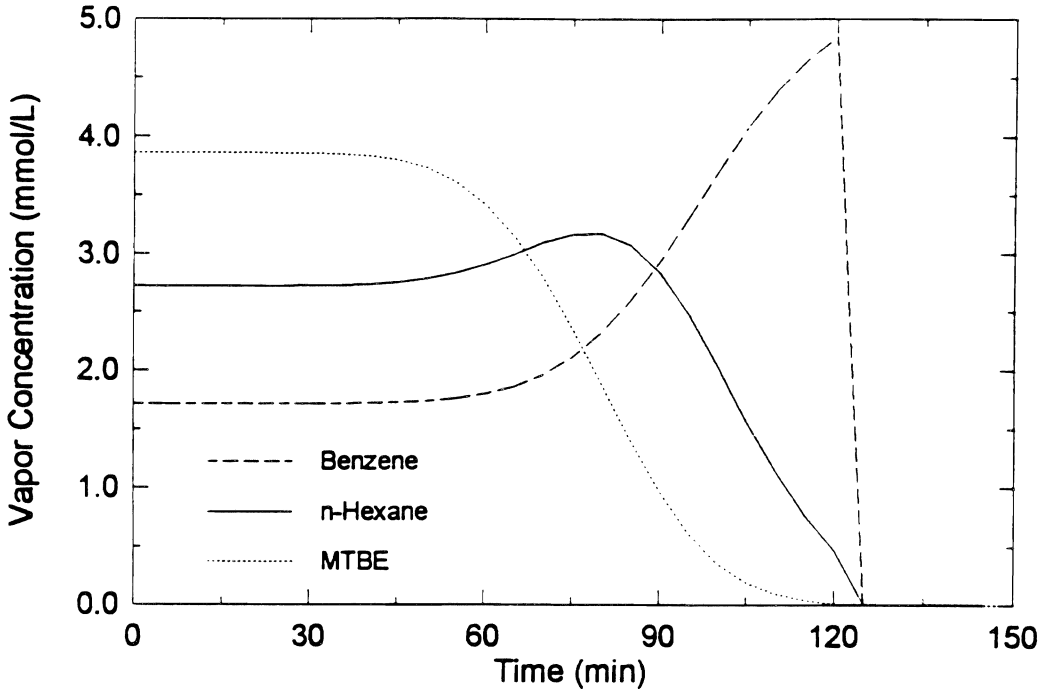

Figure 5. Predicted vapor flux concentrations from Fig. 4, extended in time to 150 min.

Composition and Distribution of Fugitive Dust from Central Valley Crop Management Systems

HEIKE CLAUSNITZER, MICHAEL J. SINGER, AND RANDAL J. SOUTHARD
Department of Land, Air and Water Resources, Davis Campus

Summary

Respirable dust was collected at the implement source from 18 cultural operations for a complete annual crop cycle on twenty-two 4097-m^2 plots 11 km west of Davis, California. (Respirable dust includes particles ≤4 μm in aerodynamic diameter that can reach the alveolar region of the lung.) Plots included conventional and organic corn (*Zea mays*) and tomato (*Lycopersicon esculentum*) fields as well as fields with a winter crop or fallow plots followed by wheat (*Triticum aestivum*). The 266 samples were collected with standard cyclone samplers mounted directly on each implement at an average height of 94 cm above ground. The highest average respirable-particulate level was 10.3 mg/m^3 air from soil ripping and land planing, carried out on dry surface soil. The lowest-ranking operation, disking of corn stubble (0.3 mg/m^3) into soil, was performed during the wet season. The respirable-dust samples in this study were collected very close to their source and therefore cannot describe any distribution over distance and space. Approximately 64% of all operations were performed during hot and dry weather, producing 83% of the annual respirable dust for this three-crop system. Among the measured environmental and implement conditions, air temperature, soil moisture, wind speed and tractor speed were significantly correlated with the dust concentration in an exponential model.

Key Words: Wind erosion, PM-10, PM-3.5.

Project Objectives Addressed in 1994-95

1. Measure PM-10 from an organic and a traditional cropping system.

We made the most progress on this objective. As reported here, we are now in our second season of measuring dust production from all major agronomic systems for tomato, corn and winter wheat.

2. Characterize the inorganic and organic composition of PM-10 from fields in which pesticides are used and from pesticide-free fields.

We have made some progress in determining particle size and composition of dust, especially mineralogy. Some advances are being made on organic characterization.

3. Test the efficacy of winter cover crops in reducing PM-10 levels.

Perhaps the most surprising result from the first crop-year is the increase in dust production from the cover crop plots compared to fallow plots. It is important to understand that we are not measuring ambient levels of dust produced by wind erosion but are measuring dust produced by farming operations. The higher dust production from these cropping systems is due to increased operations during dry parts of the year compared to systems without cover crops.

Research Plan and Procedures

Sample Collection. We provide a somewhat longer than usual discussion of methods here because dust sample collection was a new research area for us and is likely to be a new area for most readers of this report.

Since 1993, the American Conference of Governmental Industrial Hygienists (ACGIH) and the International Standards Organization/European Committee for Standardization (ISO/CEN) have established a unified standard for airborne particulate matter and the associated sampling criteria related to public health. Three particle-size fractions were defined.

(1) The *inhalable-particulate fraction* consists of particles up to 100 μm in diameter, which enter the head through the nose and mouth.

(2) The *thoracic fraction* has a cut size of 10 μm (i.e., 50 % of the particles have an aerodynamic diameter of 10 μm) and is able to enter into the lungs.

(3) The *respirable-dust fraction* with a cut size of 4 μm that is capable of reaching the alveolar region of the lungs.

Of these three, the respirable fraction is the most dangerous in that once it reaches the alveolar region of the lungs, it cannot be easily removed naturally. We collected the respirable-dust fraction, in which 50 % of the particles have an aerodynamic diameter of 4 μm.

We collected respirable dust at the implement source from 18 cultural operations for a complete annual crop cycle on 22 plots measuring 4097 m^2 11 km west of Davis, California. We measured respirable-dust quantities from 22 agronomic operations with 266 samples over the annual crop cycle of 1994 for corn, tomato, and wheat plots. We are continuing to make similar collections from the 1995 cropping season. Data from the 18 operations with five or more samples (a total of 257 samples) are discussed here in Table 1. The sampling site consists of 72 carefully controlled 4097 m^2 -field plots and is part of the Long-Term Research On Agricultural Systems (LTRAS) site located 11 km west of Davis, California. The study was carried out year-round on 22 representative plots, including conventional and organic corn and tomato fields as well as fields with an alternate rotation of a winter legume cover crop or fallow plots followed by wheat. The winter legume cover crop consisted of a mixture of 33% vetch (*Vicia dasycarpa* cv. *Lana*) and 67% pea (*Pisum arvense* cv. *Austrian*). The main soil series found on the site is the Rincon series (fine, montmorillonitic, thermic Pachic Argixerolls), in which the texture of the uppermost horizon is clay loam. Approximately 25% of the area is classified as Yolo series (fine-silty, mixed, nonacid, Thermic Typic Xerorthents) and Brentwood series (fine, montmorillonitic, Thermic Typic Xerochrepts).

The time duration of one sample collection depended on the dust concentration of an operation on one plot. High particle amounts on a filter would result in incorrect post-weighing masses due to particles falling off the filter. For operations with the highest dust levels, such as land planing and ripping, the implement had to be stopped to allow for a filter change. For medium and low dust-yielding operations, the completion of the operation on the plot determined the sampling time. These sample collection procedures are based on experience of the past 18 months.

Samples were usually taken in duplicates with two samplers operating as close as possible and at the same height above ground. This results in 6 possible respirable-dust samples for each operation in each crop and management system with its three replicated plots. We have constructed a six-sampler unit that holds a vertical array of samplers up to 2 m above the implement.

The equipment used for each operation and the operation procedure itself are similar to those employed by farmers in the Central Valley. 1994 was the first year of full operation of the LTRAS plots; thus, we expected few differences in soil conditions among the conventional and organic practices.

From March to September 1994, the respirable-dust sample collection was done with 10-mm-nylon cyclones (Mine Safety Appliances Corp., Simi

Valley, CA; Model No. 456228). Starting in October 1994, the Higgins and Dewer cyclones, (BGI Inc., Waltham, MA; Model No. BGI-4) which are made of stainless steel, were employed for the last two operations of the corn harvest and the disking of corn stubble into the soil. The metal cyclones were chosen because they reduce the risk of losing particles to static charge (Bartley et al., 1994).

The cyclone's collection principle is depicted in Fig. 1 for the nylon cyclone. The applied vacuum causes particulate to enter through the rectangular opening on the side of the vertical cyclone. A tangential channel releases the particulate into the inner cavity, where the cylindrical design results in a spiraling motion of the dust flow. Centrifugal forces separate fine and coarse material. Coarse particulates follow a path of a wider radius, eventually touching the sampler walls and falling down into the bottom collection area. Fine particulates accumulate in the center of the spiral and are pulled up through the center outlet onto the filter on top of the cyclone. The selectivity of a cyclone for a particular particle size is a function of the particle's aerodynamic diameter, defined as the diameter of a sphere whose density is 1 g/cm^3 and whose falling speed in air is equal to that of the given particle (Vincent, 1989).

The metal cyclones were run at a flow rate of 2.2 L/min according to the new international standard for respirable dust with a 50% cut-point size of 4 µm. The nylon cyclones operated at a flow rate of 2.0 L/min which results in a 50% cut-point size of 3.5 µm, the ACGIH standard from 1985 to 1993. This project started sampling with the nylon cyclone when there was still a debate among researchers and limited publications on the relationship between flow rate and cut-point of the 10-mm-nylon cyclone (Bartley et al., 1994). We now use metal cyclones exclusively.

Figure 1 shows the 3-piece filter holder (37 mm diameter cassette) on top of the cyclone that ensures a well-distributed sample over the whole filter area. Teflon filters (2 mm pore size; Gelman Science, Ann Arbor, MI) and PVC filters (5 mm pore size; Gelman Science) were used. Teflon filters were chosen because they retain their physical properties over a wide temperature range and are unaffected by most chemicals. PVC filters were found to have only a limited weight stability. Therefore, we always used them together with control filters that were exposed to identical environmental conditions and were weighed at the same time as the utilized filters. PVC filters were employed in spite of their weight variability because particles on PVC filters were more visible than on Teflon in scanning electron micrographs.

The required flow rates were achieved with low-flow vacuum pumps from Gilian Instrument Corporation (HFS 513 AUP). The flow rate of the pumps was calibrated before each operation and checked afterwards. Custom-made holders for the pumps and the cyclones allowed the length of the tubes (35 cm) connecting the pump and the filter cassette to be minimized on the cyclone and ensured a vertical position of the cyclones at all times.

Soil moisture samples for all machine-soil interactive operations were taken approximately five minutes before the operation and for the first 195 samples afterwards. To compensate for soil variability, five moisture samples of approximately 60 g soil were collected along the NW-SE field diagonal. The soil moisture was gravimetrically determined and data from the five samples were averaged.

Weather data were obtained from the California Irrigation Management Information System (CIMIS) weather station in Davis, 9 km from the sampling site.

Laboratory Analyses. A 6-digit Cahn-25 or Cahn-28 Automatic Electrobalance was used for the pre- and post-weighing of the filter samples. Filters were allowed to adjust to the temperature and humidity in the balance room for at least one day before weighing.

Particle size analyses on source soil were done using the standard pipet method (Janitzky, 1986a). Particle size analysis of dust samples was done by two methods, scanning electron microscopy and laser granulometry. Particle elemental analysis was done using EDAX on the scanning electron microscope. X-ray diffraction analysis of source soil was done using standard methods (Janitzky, 1986b).

Results

Dust amounts. The mean-respirable-dust concentration at the source for all operations (96 averaged duplicates and 65 single samples) was 3.6 mg/m^3 air (dotted horizontal line in Fig. 2). Significant differences in the quantity of respirable dust can be seen among farming operations: The two operations with the highest respirable particulate level were *soil ripping* (16) and *land planing* (5), both resulting in an average of 10.3 mg/m^3. In contrast, the two lowest-ranking respirable-dust operations were *disking the winter legume crop* (2) and *corn stubble* (18) *into soil*, resulting in 0.5 mg/m^3 and 0.3 mg/m^3, respectively. For an explanation of the numbering of operations in Fig. 2, see Table 1.

At a 95% confidence level, mean-dust concentrations for *1st finish disking* (3), *2nd finish disking* (4), *land planing* (5), *road rototilling* (11), *tomato harvesting* (15), *ripping* (16), and *harvesting corn* (17) are higher by up to 10 mg respirable particulate per m^3 air than all other treatments, which average approximately 1 mg/m^3. In Fig. 2, the diamond width is proportional to the sample size and the diamond height equals the 95% probability range for the respective means (horizontal bar), assuming normal distribution.

Student's *t*-test with each of the 18 operations is displayed graphically in rings. Cultivation (8) was chosen as the operation having the representative dust amount (thick black ring), because of its proximity to the mean value of most low-dust operations and because of its large number of samples.

Operations are significantly different if their rings intersect at >90° (gray rings). The seven operations in Fig. 2 that are significantly different from the representative appear in italic numbers. Ring size equals the height of the respective operation's diamond.

Mean-normalized standard deviations (coefficients of variation, cv) were found to be within 25% of the average cv of 0.6325, except for the ripping (16) and corn harvest (17) operations. The small cv range indicates that higher dust concentrations spread more widely (see Fig. 2).

The hypothesis that dust production is independent of the operation type was tested by an analysis of variance that included all 18 operations. The hypothesis was rejected at a very high significance level, expressed in the p–value of < 0.0001. To eliminate the strong influence of the operations themselves on dust production, multiple regressions were performed for each single operation (Table 2). The multiple regression was performed for original and logarithmic respirable-dust concentrations. The logarithmically transformed respirable-dust values showed a stronger linear relationship (measured by the adjusted sum of squares and the corresponding p-value) with the considered influencing factors than the original respirable-dust values. The model equation is described as follows:

$$\textit{ln (respirable-dust concentration)} = a_1x_1 + a_2x_2 + a_3x_3 + a_4x_4 + a_5x_5 + a_6x_6 + c \qquad [1]$$

The weighting factors a_i (i = 1,...,6) are used as fitting parameters and have inverse units of the respective x_1. The intercept c represents the natural logarithm of $K_{Operation}$, a factor which can be interpreted as the base amount of dust created by a specific operation. To calculate the logarithm, $K_{Operation}$ must be expressed in the same units as the respirable-dust concentration. A good fit of the model [1] can be interpreted as the individual influences acting in a multiplicative manner via exponentials:

$$\text{respirable-dust concentration} = \exp(c) \times \exp(a_1x_1) \times \exp(a_2x_2) \times \exp(a_3x_3) \times \exp(a_4x_4) \times \exp(a_5x_5) \times \exp(a_6x_6) \qquad [2]$$

$$\text{respirable-dust concentration} = K_{Operation} \exp(a_1x_1 + a_2x_2 + a_3x_3 + a_4x_4 + a_5x_5 + a_6x_6) \qquad [3]$$

Strong collinearity was found between relative air humidity and air temperature. Relative air humidity was discarded because in most operations air temperature was more strongly correlated with the respirable dust concentration. Among all independent variables, air temperature had the strongest relationship with the respirable-dust concentration. In addition, soil moisture, wind, and tractor speed each were found to have a significant effect on respirable-dust production. We present results for the six operations that

have both a representative number of samples and no coincidal (p-value > 0.15) collinearity between variables. Collinearity was defined in a regression where the independence between two factors was tested with higher p-values representing a higher likelihood of independence.

The two operations in which a single environmental variable had the strongest exponential influence on the respirable-dust production are depicted in Figs. 3 and 4. During the tomato harvest, temperatures climbed and the respirable-dust amount increased exponentially (Fig. 3). ,In Fig. 4, the opposite trend can be seen for soil moisture taken before the operation: the respirable-dust production during fertilization decreased exponentially with increasing soil moisture content. We are presently collecting additional data for more operations to see if this trend is reproducible.

All soil-machine interactive operations were done under relatively dry soil-moisture conditions ranging from 1 to 6 % (Table 1), except for the disking of corn stubbles into soil (15%) in fall after the first rain. As a reference for comparison across soils, the average 1.5 MPa moisture content was 13.5 %.

After the first months of the study, we were able to confirm that soil-moisture samples taken before an operation showed a trend similar to the soil moisture samples taken after an operation, but more pronounced. Since mid-August, soil moisture samples for soil-machine interactive samples were taken only before an operation.

Dust characteristics. Two scanning electron micrographs that have been digitized and analyzed are shown in Figs. 5 and 6. Figure 5 illustrates the appearance of mineral particles on a Teflon filter. Table 3 is our interpretation of the mineralogy based on elemental analysis of each particle. Figure 6 illustrates the appearance of organic particles on a Teflon filter. Table 4 is our interpretation of the composition of the particles. We have just begun our SEM analysis of filters. One important conclusion from size measurements of numerous particles is that our cut size is accurate, which was confirmed further by laser granulometry.

We have thus far been unable to validate the mineralogy interpretations using x-ray diffraction analysis. The microgram quantity of dust collected on the filters is too small for analysis. We are investigating other methods, including electron diffraction methods.

Source characteristics. We have sampled the surface horizon of soils from the 22 LTRAS plots from which dust is being collected and have completed particle size analysis and some x-ray diffraction analysis of two silt fractions and the clay fraction (Tables 4 and 5). Particle size distribution of the surface horizons is quite uniform across the 22 plots.

Quartz and plagioclase feldspars are the major constituents of the silt fractions from all plots (Table 6). Some kaolinite, mica, serpentinite, vermiculite and complex interstratified minerals were also found. The clay fraction was dominated by smectite and vermiculite with smaller amounts of kaolinite and mica (Table 6).

Humic substances were extracted from several LTRAS plots, and have been separated on the basis of electrophoretic mobility, using polyacrylamide gel electrophoresis (PAGE). Each case resulted in at least four fractions: immobile, smeared, and two well-resolved components. For LTRAS plot #6-8, the smeared and two resolved components were collected over 10 preparative-scale PAGE runs, dialyzed, and freeze-dried for analysis. Pyrolysis-gas chromatography-mass spectrometry (pyGCMS) analysis revealed a number of differences in the PAGE fractions: the smeared components appeared enriched in pseudo-polysaccharide structures, while the resolved components lacked these structures. This technique also revealed that the two resolved components differed dramatically from each other in a number of ways, which are being confirmed by high-resolution homo- and hetero-nuclear magnetic resonance spectroscopy (TOCSY and HETCORR techniques). These structural motif results will be input to energy-minimization humic models being developed by Hinedi, Anderson, and Chang at U C Riverside.

Discussion

Farmers typically prepare their land in fall before winter rains. Based on our sampling site, this practice results in approximately 64% of all operations being performed during hot and dry weather, producing 83% of the annual respirable dust for a typical farming system of tomato, corn, and wheat in a semiarid climate. Aside from environmental influences, we can conclude from our measurements that respirable-dust production from the infrequently disked fallow plots (5 diskings/year) ranked naturally lowest. Taking the fallow respirable-dust production as a baseline for comparison, the dust amount nearly doubled by growing a winter cover crop; increased to two and a half times with the wheat and the conventionally managed tomato crops; increased three times with the cultivation of organically grown tomatoes and conventionally grown corn; and rose up to four times of the fallow-dust production with the cultivation of organically managed corn.

The respirable-dust samples in this study were collected very close to their source and therefore cannot describe any distribution over distance and space. The measured respirable-dust quantities should not be interpreted in terms of off-site environmental damage. The respirable-dust concentrations are one measure to show the impact of each operation and to determine influences originating from the climate, soil, and implement variables.

The differences in respirable-dust production among crops are due mainly to inherent plant-growth habits, their associated number of operations, and the chosen management system. Inherent crop differences are especially well expressed in the comparison of the corn and tomato crops, which had a

similar number of operations. The corn crop produced approximately 20% more respirable dust than the tomato crop, chiefly due to higher plant mass and dryness during harvest and additional post-harvest operations.

Among the crops studied, tomato and corn are the most intensively cultivated; thus, they yield the highest amounts respirable dust. In addition to the number of operations compared to the fallow, the number of operations during the dry season is clearly a major influence on respirable-dust production. Comparing the winter cover crop and the wheat crop with the fallow, approximately 20% more respirable dust was produced during the summer. The combined effects of dry season operations and crop differences are revealed in an evaluation of the respirable-dust production from the wheat and the conventionally-managed tomato crops. Both have a similar respirable-dust concentration even though the wheat crop requires only one-third as many cultivation operations. This result is due to the higher percentage of wheat operations that occur during the summer and due to the increased plant mass and dryness of wheat compared to the tomato crop. The seasonal influence is demonstrated further by the 20% increase in respirable-dust production by the organically grown corn and tomato crops compared to their conventionally grown counterparts. The increase can be attributed solely to the delayed cultivation schedule of the main crop due to the time required for incorporation and decomposition of the winter cover crop as the fertilizer source.

Acknowledgments

Individuals contributing to this work and report include Rick Higashi, Teresa Fan, Bill Hobson, Reena Dahliwal and Liese Schultz. This work was completed with support from the U.S. Department of Agriculture (contract no.: 94-38825-0383, R.G. Flocchini PI). Essential cooperation was provided by the LTRAS-management team and its director, Ford Dennison.

References

ACGIH-ISO/CEN. 1993. Annual reports of committees on TLVs and BEIs. App. Occup. Environ. Hyg. 8(12): 1047-1050.

Bartley, D.L., C. Chen, R. Song, and T.J. Fischbach. 1994. Respirable aerosol sampler performance testing. Am. Ind. Hyg. Assoc. J. 55(11): 1036-1046.

Janitzky, P. 1986a. Particle size analysis. p. 11-16 In. M.J. Singer and P. Janitzky (Eds.) Field and Laboratory Procedures Used in a Soil Chronosequence Study. U.S. Geological Survey Bulletin 1648. U.S. Gov. Printing Office, Washington, DC.

Janitzky, P. 1986b. Preparation of soil samples for X-ray diffraction analysis. p. 16-18 In. M.J. Singer and P. Janitzky (Eds.) Field and Laboratory Procedures Used in a Soil Chronosequence Study. U.S. Geological Survey Bulletin 1648. U.S. Gov. Printing Office, Washington, DC.

Vincent, J.H. 1989. Aerosol mechanical background. p. 23-38. *In* J.H. Vincent (ed.) Aerosol Sampling. John Wiley & Sons, New York.

Table 1. Averages of respirable dust concentrations (sorted) and their sampler locations, implement factors, and environmental conditions for the 18 agricultural operations sampled from March 31 to October 19, 1994.

Operation/Dust source	Operation no.	Respirable dust [mg/m^3 air]	Number of samples	Date	Day time range of sampling	Sampler height above ground [cm]	Tractor speed [m/s]	Engine speed [rpm]	Soil moist. before operat. [%]	Soil moist. after operat. [%]	Air temperature [^{o}C]	Relative humidity [%]	Wind speed [m/s]	Wind direction [0-360]	Soil temperature [^{o}C]
Disking-in corn stubbles	18	0.33	4	19-Oct-94	8-11	95	2.1	-	14.7	-	11.6	70	1.7	297	16
Disking-in vetch/pea	2	0.45	7	9-Apr-94	9-16	106	1.6	1800	-	12.5	20.8	35	5.8	282	17
Cultivation&furrow cutting	9	0.66	8	22-May-94	7-16	81	1.7	1953	5.6	8.9	23.3	56	2.1	179	24
Inject.fertiliz.& furr.cutting	10	0.79	15	4-Jun-94	8-14	64	1.5	2100	5.1	8.1	18.7	62	2.7	189	21
Spring-tooth harrowing	7	1.01	6	28-Apr-94	8-15	41	2.2	2200	5.9	11.3	19.6	50	4.1	271	19
Corn seeding	6	1.02	4	14-Apr-94	9-11	52	1.8	2000	3.0	3.5	19.7	53	3.9	256	16
Wheat harvest	12	1.04	7	17-Jun-94	10-15	241	0.9	-	-	3.3	23.2	44	1.8	205	22
Cultivation for weeds	8	1.09	22	23-May-94	8-17	62	1.7	2045	4.5	11.1	21.6	48	4.3	210	21
Vetch/pea mowing	1	1.25	5	13-Apr-94	8-15	68	1.6	2250	-	11.5	18.6	43	4.8	259	17
Disking-in wheat stubbles	14	2.49	4	3-Aug-94	9-12	108	1.8	-	1.9	5.0	24.2	55	1.5	79	24
Wheat-straw baling	13	2.82	5	30-Jun-94	13-16	142	2.7	1000	-	0.7	30.4	32	3.1	165	25
1st finish disking	3	4.05	23	15-May-94	8-15	77	1.6	2200	2.7	8.1	22.2	45	4.1	301	19
Tomato harvest	15	4.34	6	27-Aug-94	11-17	75	0.9	-	3.1	-	28.5	38	3.7	173	24
2nd&3rd finish disking	4	4.94	13	22-Jun-94	8-15	77	1.8	-	2.7	5.33	22.8	49	2.6	274	21
Corn harvest	17	5.63	10	13-Oct-94	11-15	220	1.0	2300	-	19.5	24.3	24	7.4	342	18
Rototilling road	11	6.69	4	1-Jun-94	9-11	58	1.1	2100	3.3	5.2	21.3	60	3.9	176	21
Land planing	5	10.29	12	20-Ap;19-Se	9-14	98	2.3	-	2.4	-	22.1	55	2.0	224	20
Ripping soil	16	10.34	6	7-Sep-94	10-13	77	1.4	2000	3.5	-	24.4	49	2.1	152	23

Table 2. Summary of multiple regression analysis with logarithmic respirable-dust concentration as the dependent parameter.

Operation	Distribution of dust samples	Sample format for model	Most influencing factor(s) of model	P-value of factor	Adj. R^2 of model	P-value of model
Cultivation & furrow cutting	logarithmic	loga-rithmic	tractor speed air temperature	<0.0001 0.0015	87.7	<0.0001
Land planing	logarithmic†	loga-rithmic	tractor speed air temperature	0.0106 0.0029	65.0	0.0062
Tomato harvest	logarithmic	loga-rithmic	air temperature	0.0257	68.8	0.0257
Wheat-straw baling	logarithmic	loga-rithmic	wind speed soil moisture	0.0112 0.0181	96.4	0.0178
Injection fertilization and furrow cutting	logarithmic	loga-rithmic	soil moisture	0.0007	85.1	0.0007
2nd & 3rd finish disking	logarithmic	loga-rithmic	wind speed	0.0002	75.2	0.0002

†single outlier removed

Table 3. Identification of mineral particles by scanning electron microscopy and elemental analysis by EDAX.

Particle No.	Identification	Diameter [mm] Min.	Max.
1	Organic (Plant Material)	1.3	11.2
2	Mineral (Feldspar ?)	1.4	4.1
3	Mineral (Mica)	2.5	4.5
4	Mineral (Quartz)	1.	2.5
5	Mineral (Pyrophyllite)	1.3	2.0
6	Mineral (Quartz)	1.5	1.8
7	Mineral (Clay ?)	0.8	1.0
8	Mineral (Clay ?)	1.0	2.3
9	Mineral (Clay ?)	1.2	2.4
10	Mineral (Clay ?)	2.5	3.1
11	Mineral (Mica)	1.6	1.8
12	Mineral (Feldspar ?)	2.0	5.3
13	Mineral (Quartz)	1.8	3.7
14	Mineral (Clay)	1.5	4.0
15	Mineral (Clay)	1.3	1.5
16	Mineral (Clay)	1.0	1.6

Table 4. Identification of organic particles by scanning electron microscopy and elemental analysis by EDAX.

Particle No.	Identification	Diameter [mm] Min.	Max.
1	Organic (Bacteria)	7.0	16.6
2	Organic (Bacteria)	5.1	7.9
3	Organic (Bacteria)	1.0	2.3
4	Organic (Bacteria)	1.1	1.8
5	Organic (Bacteria)	0.8	0.8

Table 5. Particle size analysis of A horizons for 22 LTRAS plots.

Treatment	Plot	Sand Fraction (%)					Total Sand	Total Silt	Total Clay
	#	v. coarse	coarse	medium	fine	v.fine	(%)	.05-.002 mm	<.002 mm
		2-1 mm	1-.5 mm	.5-.25 mm	.25-.1 mm	.1-.05 mm	2.0-0.05 mm	(%)	(%)
Conv. Corn/Tomato	1-4	0.2	0.4	0.6	6.4	10.4	18.0	49.5	32.6
Conv. Corn/Tomato	5-4	0.1	0.8	0.8	10.4	14.9	26.9	45.2	27.9
Conv. Corn/Tomato	5-5	0.1	0.7	1.1	10.9	14.9	27.7	45.4	26.9
Conv. Corn/Tomato	7-8	0.3	0.6	0.6	6.1	13.0	20.5	48.9	30.6
Conv. Tomato/Corn	1-3	0.4	0.3	0.5	5.5	10.0	16.7	50.8	32.5
Conv. Tomato/Corn	4-5	0.1	1.1	1.6	13.0	16.1	32.1	41.8	26.2
Conv. Tomato/Corn	8-9	0.1	1.1	1.0	14.9	17.1	34.3	40.0	25.7
Conv. WLCC/Corn/Tomato	2-4	0.3	0.7	0.8	7.9	15.6	25.2	48.9	26.0
Conv. WLCC/Corn/Tomato	4-4	0.3	1.4	2.0	13.6	16.5	33.9	41.4	24.7
Conv. WLCC/Corn/Tomato	6-9	0.1	0.6	0.6	6.4	11.1	18.8	50.9	30.3
Org. Corn/Tomato	1-2	0.2	0.4	0.5	6.0	10.7	17.7	47.9	34.4
Org. Corn/Tomato	6-5	0.2	0.9	1.1	9.5	14.9	26.6	45.8	27.5
Org. Corn/Tomato	8-8	0.2	0.9	1.2	12.9	17.9	33.2	41.3	25.5
Org. Tomato/Corn	2-3	0.2	0.5	0.6	6.9	13.4	21.6	49.4	29.0
Org. Tomato/Corn	6-4	0.1	0.1	0.7	8.6	12.7	22.2	47.3	30.5
Org. Tomato/Corn	6-8	0.1	0.1	0.5	5.2	10.1	15.9	51.9	32.2
Rainfed Fallow/Wheat	1-8	0.1	0.2	0.2	3.5	8.3	12.3	53.0	34.7
Rainfed Fallow/Wheat	3-9	0.2	0.7	0.8	7.9	12.7	22.4	48.6	29.1
Rainfed Fallow/Wheat	6-2	0.2	0.6	1.2	12.6	15.9	30.7	44.2	25.1
Rainfed WLCC/Wheat	2-8	0.3	0.4	0.5	4.7	10.9	16.7	52.2	31.1
Rainfed WLCC/Wheat	3-7	0.2	0.8	0.9	8.5	12.8	23.2	47.4	29.3
Rainfed WLCC/Wheat	8-1	0.2	0.8	0.9	10.0	15.7	27.6	47.3	25.1

WLCC = winter legume cover crop

Table 6. Mineralogy based on X-ray diffraction analysis of three particle size fractions of soil from LTRAS.

	Particle size fraction		
Plot #	50-20 μm	20-2 μm	<2 μm
5-4	q, pf, k	q, pf, s/v, k, m	s, v, k, m
6-4	q, pf, k	q, pf ,s/v, k, m,c	mo, v, k ,m
6-8	q, pf, s	q, pf, v, k, m	m, s/vi, v, k, m
8-9	q, pf, v/c/si, m, s	q, pf, c, v/c/si, v, k, m	s, v, m, k

q = quartz; pf = plagioclase feldspar; k = kaolinite; s = smectite; v/c/si = vermiculite-smectite-chlorite intergrade; s/v = smectite-vermiculite intergrade, m = mica; mo = montmorillonite; c = chlorite .

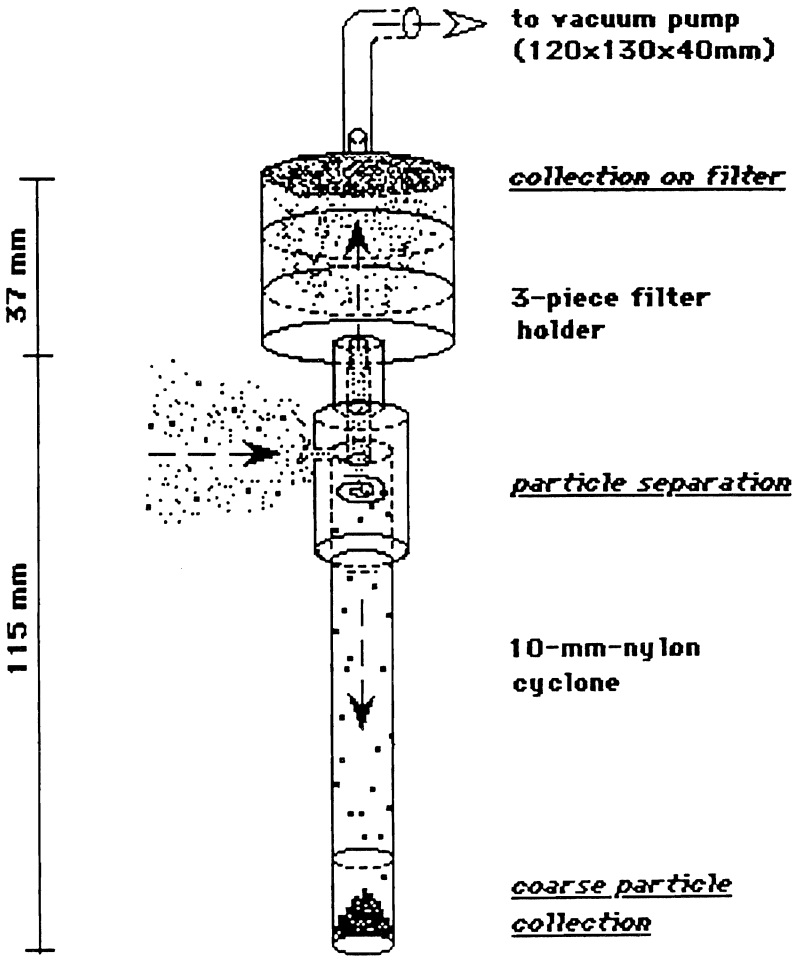

Figure 1. Collection principle of 10 mm nylon cyclone (respirable dust sampler) assembled with dust sample holder and vacuum pump (pump dimensions: L = 120 mm, W = 130 mm, H = 40 mm).

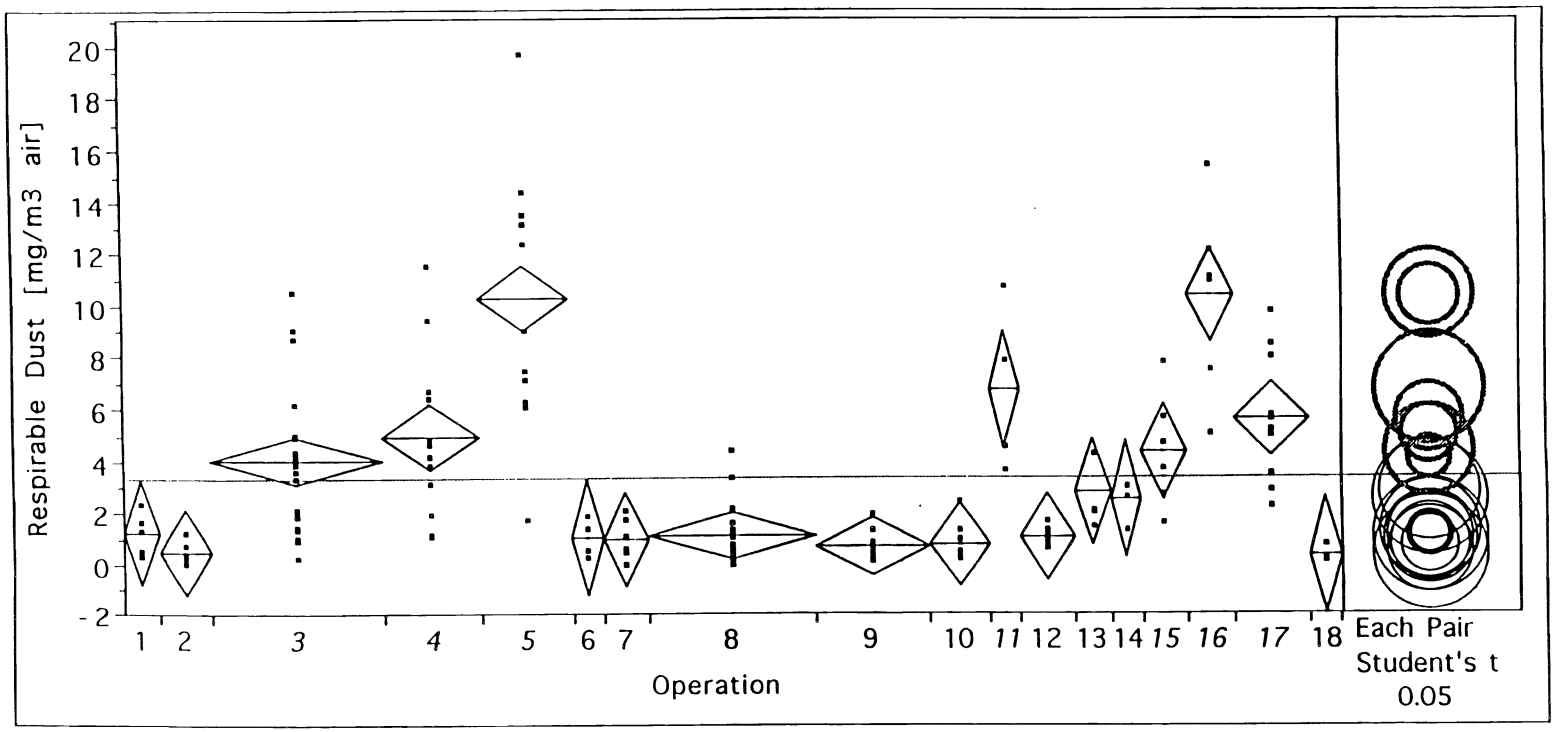

Figure 2. Distribution of all 96 duplicate and 65 single samples within their 18 operations showing respective mean values (horizontal line in diamonds), 95% probability range (height of diamond), oveall mean (dotted horizontal line), and an operation mean comparison for significant differences (rings).

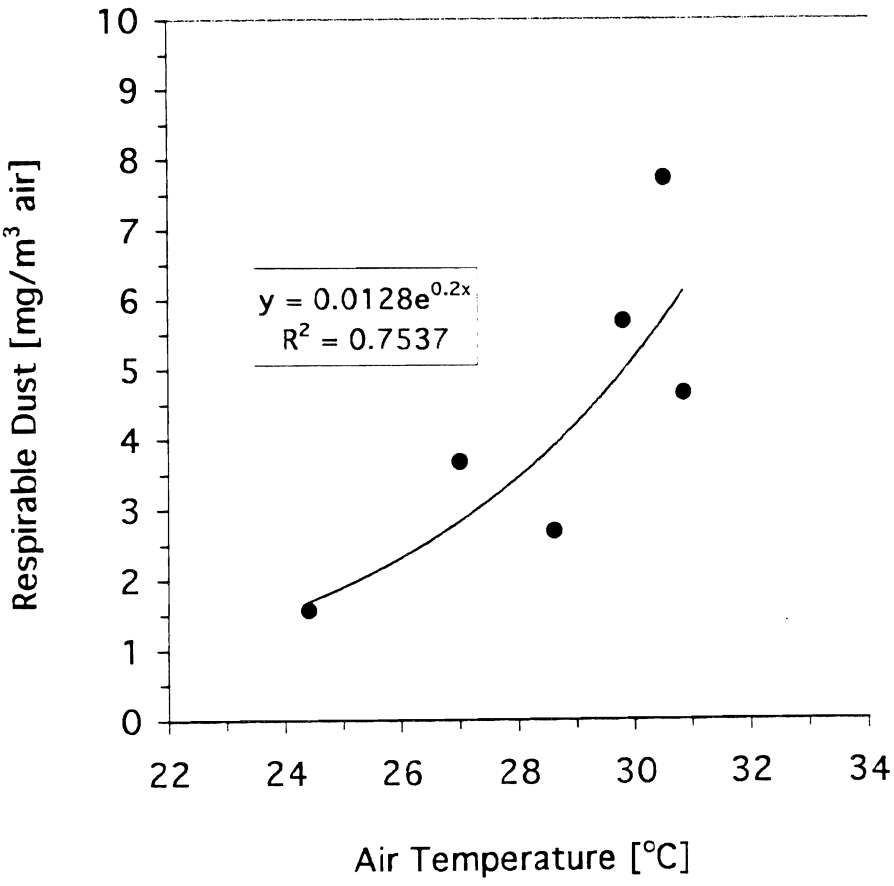

Figure 3. Respirable-dust amounts increase exponentially with air temperature during tomato harvest in August 1994.

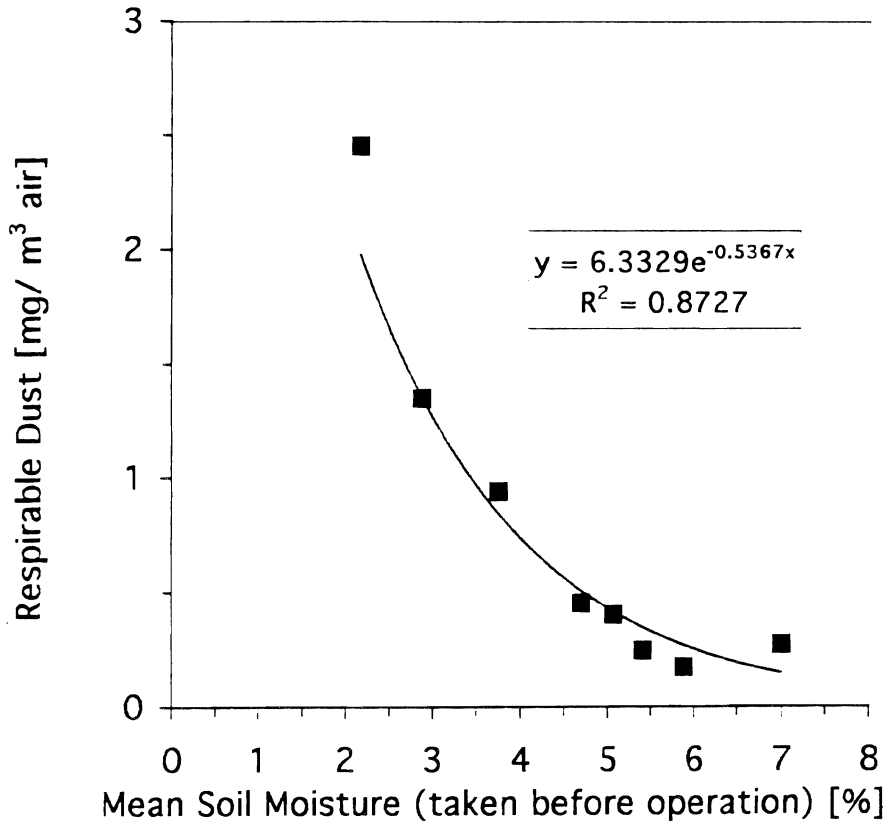

Figure 4. Respirable-dust amounts decrease exponentially with increasing soil moisture in the injected fertilization operation in May 1994.

Figure 5. Digitized scanning electron micrograph of mineral dust particles. Numbers mark particles that were measured and analyzed by EDAX.

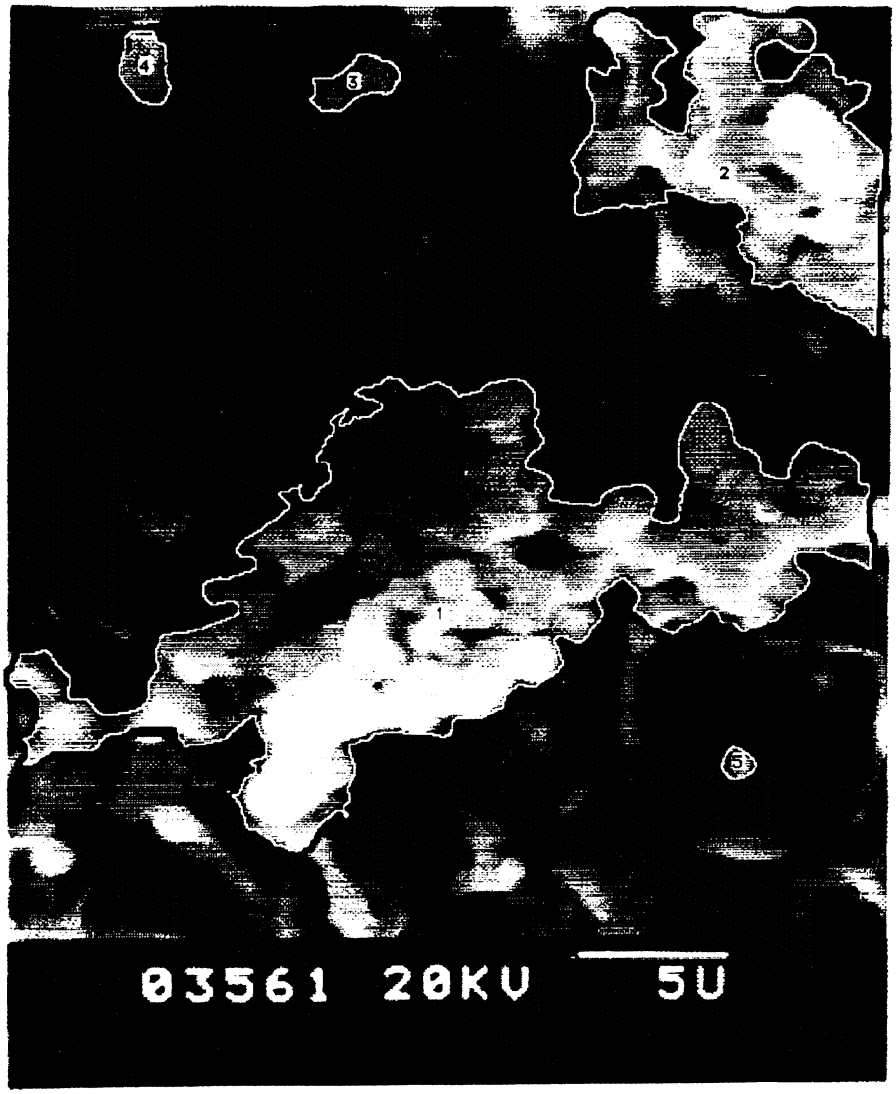

Figure 6. Digitized scanning electron micrograph of organic dust particles. Numbers mark particles that were measured and analyzed by EDAX.

A Geometric Approach to Soil Pollution

CARLOS E. PUENTE
Department of Land, Air and Water Resources, Davis Campus

Summary

This research deals with the geometric quantification of the concentration patterns that are observed when a pollutant migrates within the soil. The objective of this project is to test if the dynamics of actual plumes can be described properly following the time evolution of surrogate parameters that allow a close geometric representation of observed concentration patterns. In particular, this research focuses on the mathematical description of (i) vertically-averaged two-dimensional concentration patterns as seen in actual locations, e.g. the Borden site in Ontario, Canada and the Las Cruces site, and (ii) simulations obtained solving the classical advection-dispersion equations in two dimensions.

Close encodings of the chloride and bromide plumes at the Borden site have been achieved employing the fractal-multifractal framework developed by Puente (1992, 1995). The excellence of the representations is evidenced by close geometric agreements between real and modeled plume snapshots, which in turn result in close correspondence of plume moments of orders one to four, for all times. The plumes' most variable fractal-multifractal parameters are the localization parameters, which basically follow the tracers' centers of mass. These parameters exhibit basically a linear growth with time, which allows the calculation of reasonable predictions for future times.

Key Words: pollution transport, contaminant transport, fractals, multifractals.

Project Objectives Addressed in 1994-95

1. Determination of fractal-multifractal parameters to fit plumes of conservative tracers (chloride and bromide) at the Borden site.

Research Plan and Procedures

Proper description (interpolation, estimation, prediction, simulation, etc.) of hydrologic information in space and time is crucial for the understanding and quantification of the phenomena at hand and its consequences. A common trait of these data sets, typical in pollution studies, is that they are *complex*. They exhibit "heterogeneities", "anisotropies", and "intermittencies" which preclude a simple mathematical description. The typical approach for many years has been to understand such variability based upon well-founded physical principles, i.e. partial differential equations which express conservation laws. When deterministic, physically-based approaches fail (for instance, due to improper knowledge of parameters or boundary conditions), a common technique has been to develop procedures based on probability theory.

Instead of concentrating on data sets per-se, state-of-the art stochastic procedures focus on "relevant statistics" of the patterns at hand (i.e. means, variances, spatial correlations, extremes, etc). Assumptions like stationarity and ergodicity are often used to aid in the development of theories, even though it is common to have phenomena which provide but a single spatial pattern (i.e. as in groundwater properties). Despite substantial progress throughout the years, the problem of understanding and predicting soil pollution still remains. Although state-of-the art stochastic methods provide a viable representation of complex data, more often than not (given their assumptions) they result in "smoothed," "distorted" and/or "unreal" representations of observed patterns. All these approximations may be unacceptable if prevailing dynamic conditions are sufficiently nonuniform and nonlinear.

This work attempts to capture explicitly the geometrical features observed in pollution studies, i.e. "shades of concentrations". The idea is to reproduce the "complex", "jagged", and "intricate" patterns as deterministic, fractal transformations of turbulence-related distributions (multifractal probability measures) (Puente, 1992). The basis for the representation is the belief that the geometric effects may be properly filtered out by proper encoding, which then would allow us to visualize the evolution of the plume based upon few surrogate parameters. Capturing geometry may be the key because, after all, the observed patterns are mere reflections of ongoing physico-chemical mechanisms taking place within the porous medium.

As part of an earlier project funded by the Kearney Foundation of Soil Science, suitable surrogate parameter sets for a fractal-multifractal description of pollution patterns were catalogued. (See Kearney Foundation of Soil Science Annual Reports for 1991-92, 1992-93, and 1993-94.) Observed spatial snapshots are normalized and then interpreted as derived distributions

obtained by transforming a simple (binomial) multifractal measure using a three-dimensional fractal interpolating function whose graph looks like a wire. The surrogate parameters of the fractal-multifractal representation include (a) the points in three dimensions by which the fractal interpolation function passes (localization parameters); (b) the sequences of ups and downs, and the angles that determine the final shape of the fractal interpolating function (scalings and rotations, regularity parameters), and (c) the quantities that dictate how to recursively construct the multifractal measure (*intermittency parameters*). At the end, a compact deterministic description of the derived measure is found despite the complex and seemingly random nature of the target pattern (Puente, 1995).

Results

Surrogate parameters were obtained for 20 snapshots corresponding to the two conservative tracers at the Borden site. Such values were found according to (i) the cataloguing exercise; (ii) an improved preliminary fit based on the multidimensional simplex method (Press et al., 1989), using the catalog as an initial condition; and (iii) a refinement of the previous parameters via simulated annealing (Otten et al., 1989). The objective function, to be minimized, was constructed by finding squared differences between real plumes and fractal-multifractal outcomes in terms of a combination of classical statistical indicators, which included moments of the raw data in both the space axis and the concentration axis.

Figures 1 and 2 exhibit 10 frames of observed and fitted chloride concentration patterns for the Borden site. Figures 3 and 4 provide the corresponding patterns in the bromide plume.

A comparison of the most commonly used statistical moments for both plumes is shown in Tables 1 and 2. The corresponding surrogate parameters for these fits are included in Table 3 and in Fig. 5.

Discussion

As seen in Tables 1 and 2 and in Figs. 1 to 4, excellent agreement was attained for both conservative tracers at all times, when using the fractal-multifractal procedure. The results in Figs. 1 to 4 show that the geometric approach leads indeed to very accurate descriptions of these plumes at the Borden site. As may be seen in Tables 1 and 2, the fit is very good not only visually but also in terms of spatial moments of orders up to four. Figure5, which exhibits the time evolution of the interpolating points for both plumes, shows that the movement and growth of both plumes are captured nicely by means of these surrogate parameters, i.e. as the patterns move and grow, the y-z locations of the plumes' centers of mass also shift accordingly. Observe also that plume dispersion is represented well by these parameters, with more growth in the z direction than in the y direction (see Figs. 1 to 4).

As may be seen in Table 3, there is no significant variability in terms of the scaling parameters (their range is between -1 and 1). When the magnitude of the scaling parameters tends to 1, the derived joint measures may be shown to be Gaussian and therefore elliptical (Puente and Klebanoff, 1994). The obtained values in Table 3, many of which are close to one and all are $\geq$ 0.66, imply a high degree of "ellipticity" for the plumes, which clearly may not be termed Gaussian. The reactor's ratio, defined as the geometric spread of the plume as compared to a Gaussian plume (Thierrin and Kitanidis, 1994)], also gave results that reflect the non-Gaussian nature of the plume, with similar trends in time given by the fractal-multifractal representation. As seen in Table 3, the rotations did not vary greatly as time passed. This fact appears to be in agreement with the observation that the plume center of mass basically travels along a line in space which corresponds to the longitudinal axis of the plumes (Freyberg, 1986).

Simple linear fits for the geometric parameters were obtained in order to test the predictability of the procedure. It was found that such a linear representation results in good fittings for the observed times and in reasonably-looking plumes for intermediate times. When the surrogate parameters were extrapolated into the future, sensible snapshots were also obtained. A test carried for the bromide plume at time 1038 after injection (a snapshot not included in the analysis) revealed that the geometric procedure predicts a pattern similar to that reported by Freyberg (1986). In particular, the plume splitting into two pieces is preserved well by these predictions. These results suggest that the geometric approach may be used to aid in the prediction of the evolution of a plume. Of course, the validity of the linear trends for the Borden site need not be true in general, and other kinds of extrapolations may be needed. Longitudinal variances of extrapolated patterns found via the fractal geometric approach are compatible with the stochastic model proposed by Dagan (1984). This is true, despite an upward trend by the predictions after 1000 days.

When the center of mass and plus-minus one standard deviation are superimposed on the patterns shown in Fig. 5, it is seen that those graphs fit closely within the ranges given in the figure, i.e. the moment values in direction y show a spread which is comparable to the one shown for the localization points Y1, Y2, and Y3. This suggests that a model could be built for which the localization points are uniquely defined by the plume moments of orders one and two. Unfortunately, just replacing the coordinates in y and in z and using the same scalings and rotations, i.e. those of Table 3, do not work. This happens because the needed changes may not be "small", resulting in outcomes that do not resemble the actual plume. The idea of having an explicit model will be tested by considering alternative representations of the localization parameters based on first and second order plume moments, and by optimizing the remainder scalings and rotations. If these parameters show simple behavior (as before), reasonable predictions (forwards and backwards) in time are expected.

References

Dagan, G., Solute transport in a heterogeneous porous formation. 1984. Journal of Fluid Mechanics 145:151-177.

Freyberg, D. L. 1986. A natural gradient experiment on solute transport in a sand aquifer. 2. Spatial moments and the advection and dispersion of nonreactive tracers. Water Resources Research 22(13):2031-2046.

Otten, R. H. J. M. and L. P. P. P. van Ginneken. 1989. The Annealing Algorithm. Kluwer Academic Publishers, Boston.

Press, W. H., B. P. Flannery, S. A. Teukolsky, and W. T. Vetterling. 1989. Numerical Recipes. Cambridge University Press.

Puente, C. E. 1992. Multinomial multifractals, fractal interpolators, and the Gaussian distribution. Physics Letters A. 161:441-447.

Puente, C. E. and A. Klebanoff. 1994. Gaussians everywhere. Fractals 2(1): 65-79.

Puente, C. E. 1995. A new approach to hydrologic modeling: derived distributions revisited. J. of Hydrology In press.

Thierrin, J. and P. K. Kitanidis. 1994. Solute dilution at the Borden and Cape Cod groundwater tracer tests. Water Resources Research 30(11):2883-2890.

Table 1. Lower order moments for chloride at Borden site (measured and fitted).

Day	Measured								
	$\bar{y}$	$\bar{z}$	s_y	s_z	r	g_y	g_z	k_y	k_z
1	0.42	0.47	1.65	1.34	0.13	0.08	0.03	2.28	2.52
9	0.73	0.63	1.86	1.12	0.10	0.20	0.26	2.23	2.72
29	1.45	3.07	2.10	1.59	0.47	0.36	0.76	2.51	3.54
43	1.54	4.10	1.73	1.62	0.34	-0.03	0.47	2.19	2.60
63	1.39	5.19	1.79	1.68	0.15	0.25	0.51	2.42	2.62
259	13.21	23.94	5.33	3.60	0.56	1.11	0.40	3.30	3.15
332	15.16	29.09	3.38	3.78	0.50	1.01	0.28	5.81	2.84
381	15.72	32.42	3.17	3.38	0.66	0.62	-0.03	3.08	2.32
462	16.84	38.51	3.19	4.16	0.63	0.33	0.10	2.69	2.49
647	23.68	52.86	3.18	5.65	0.83	0.11	-0.31	2.54	1.90
Day	Fitted								
	$\bar{y}$	$\bar{z}$	s_y	s_z	r	g_y	g_z	k_y	k_z
1	0.42	0.46	1.63	1.35	0.13	0.09	0.05	2.37	2.55
9	0.71	0.65	1.82	1.12	0.11	0.11	-0.02	2.56	2.64
29	1.29	3.05	1.99	1.50	0.38	0.15	0.41	2.60	3.03
43	1.53	4.08	1.80	1.61	0.36	0.02	0.20	2.67	2.62
63	1.22	5.75	1.99	1.72	0.12	0.06	0.18	2.83	3.15
259	13.03	23.83	3.68	3.53	0.50	0.38	-0.13	3.73	3.05
332	15.02	29.09	2.97	3.78	0.34	0.08	0.22	3.29	2.83
381	15.30	32.87	3.18	3.75	0.65	0.33	-0.22	3.22	2.71
462	16.46	38.11	3.45	4.55	0.59	0.04	-0.17	3.06	2.58
647	23.83	52.95	3.40	5.54	0.79	0.42	-0.14	3.40	2.10

Note: $\bar{y}$, $\bar{z}$, s_y, s_z in meters

Table 2. Lower order moments for bromide at Borden site (measured and fitted).

Day	Measured								
	$\bar{y}$	$\bar{z}$	s_y	s_z	r	g_y	g_z	k_y	k_z
1	0.46	0.47	1.67	1.37	0.14	0.07	0.06	2.30	2.61
9	0.80	0.61	1.84	1.11	0.08	0.22	0.29	2.33	2.81
29	1.63	3.09	2.21	1.61	0.47	0.43	0.64	2.68	3.13
43	1.58	4.13	1.75	1.64	0.33	-0.006	0.46	2.21	2.62
63	1.30	5.29	1.85	1.75	0.16	0.27	0.47	2.53	2.66
259	11.41	23.32	3.35	3.59	0.61	0.38	0.016	2.73	2.99
332	14.91	29.15	3.14	3.94	0.43	0.004	0.29	2.87	2.59
381	16.18	32.16	4.02	4.71	0.44	0.29	-0.69	3.58	4.62
429	17.08	36.27	3.70	4.93	0.62	0.13	-0.08	3.30	2.50
462	17.06	38.91	4.03	5.23	0.51	0.29	0.11	3.05	2.57
647	21.66	50.57	5.78	7.67	0.88	-0.26	-0.08	2.52	1.85
Day	Fitted								
	$\bar{y}$	$\bar{z}$	s_y	s_z	r	g_y	g_z	k_y	k_z
1	0.39	0.47	1.65	1.37	0.18	0.06	0.04	2.34	2.54
9	0.74	0.54	1.84	1.12	0.09	0.08	-0.05	2.57	2.78
29	1.43	3.03	2.02	1.56	0.42	0.26	0.40	2.67	2.80
43	1.60	3.98	1.80	1.61	0.36	0.17	0.22	2.70	2.57
63	0.98	5.01	1.99	1.73	0.11	-0.008	0.19	2.83	3.02
259	12.69	23.67	3.20	3.35	0.45	-0.08	-0.18	2.64	2.81
332	14.85	29.12	3.03	3.91	0.35	-0.01	0.30	2.84	2.62
381	15.53	31.58	3.53	4.25	0.53	0.25	-0.41	3.21	3.41
429	16.85	36.28	3.53	4.55	0.63	0.04	-0.09	2.73	2.55
462	18.66	39.92	3.91	4.83	0.55	0.01	-0.16	2.85	2.50
647	22.39	51.15	5.25	7.40	0.84	-0.02	-0.085	2.49	2.06

Note: $\bar{y}$, . $\bar{z}$, $s_{y,}$,s_z in meters

Table 3. Scalings and rotations for chloride and bromide concentrations at the Borden site.

Day	Chloride							
	Scalings				Rotations (degrees)			
	$r_1^{(1)}$	$r_2^{(1)}$	$r_1^{(2)}$	$r_2^{(2)}$	$q_1^{(1)}$	$q_1^{(2)}$	$q_2^{(1)}$	$q_2^{(2)}$
1	0.94	0.91	0.88	0.92	6.18	-94.0	-6.40	-78.94
9	0.90	0.99	0.87	0.91	-4.55	-105.96	-14.93	-87.85
29	0.93	0.88	0.95	0.99	7.47	-88.34	-2.18	-79.53
43	0.99	0.85	0.99	0.94	-6.68	-80.77	-19.42	-77.77
63	0.99	0.88	0.72	0.87	51.75	-8.14	57.71	-32.62
259	0.98	0.99	0.93	0.97	2.81	-71.14	-16.84	-52.87
332	0.99	0.99	0.91	0.91	10.23	-57.26	-1.76	-63.52
381	0.99	0.98	0.92	0.93	2.21	-57.27	-12.05	-20.16
462	0.95	0.96	0.96	0.91	9.93	-60.84	-7.89	-53.13
647	0.99	0.99	0.83	0.86	2.29	-81.92	-10.88	-62.07
Day	Bromide							
	Scalings				Rotations (degrees)			
	$r_1^{(1)}$	$r_2^{(1)}$	$r_1^{(2)}$	$r_2^{(2)}$	$q_1^{(1)}$	$q_1^{(2)}$	$q_2^{(1)}$	$q_2^{(2)}$
1	0.97	0.92	0.89	0.92	5.63	-98.75	-4.25	-77.99
9	0.92	0.99	0.86	0.94	-5.02	-97.81	-17.02	-93.03
29	0.92	0.89	0.95	0.99	9.15	-91.14	5.05	-81.08
43	0.99	0.85	0.99	0.95	-7.40	-81.18	-18.92	-77.30
63	0.99	0.94	0.66	0.90	49.99	-8.75	65.27	-36.25
259	0.98	0.98	0.93	0.96	2.81	-71.14	-16.84	-52.87
332	0.99	0.99	0.90	0.94	7.87	-55.57	-2.10	-61.21
381	0.99	0.98	0.99	0.93	5.39	-54.32	-14.25	-16.57
429	0.94	0.96	0.98	0.94	94.55	-67.21	-66.96	-44.76
462	0.96	0.98	0.96	0.93	8.61	-60.80	-9.11	-51.89
647	0.98	0.97	0.76	0.91	76.76	-40.02	-89.90	-19.57

Note: parent measures were uniform, i.e. all intermittency parameters equal 1/2.

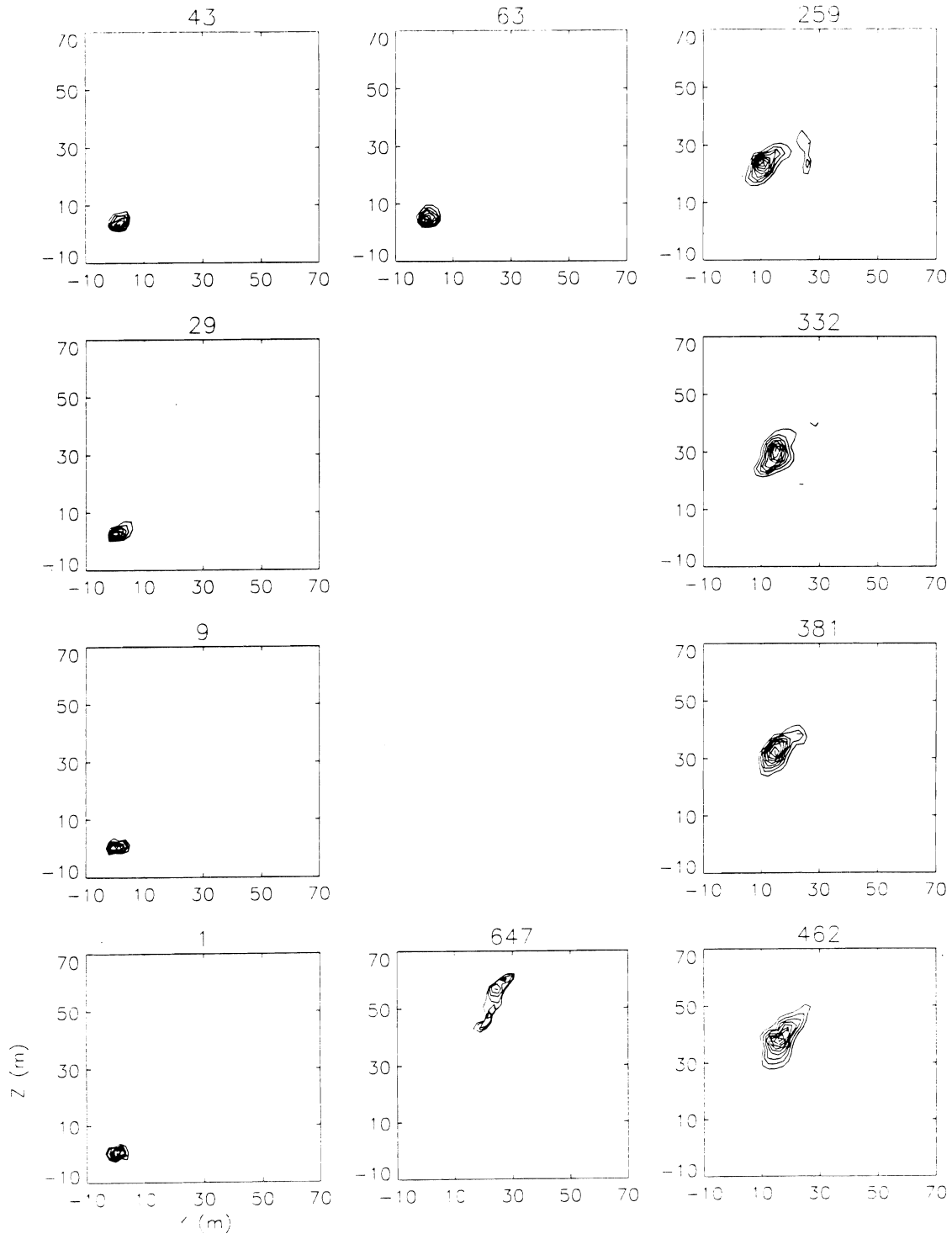

Figure 1. Measured chloride concentrations at the Borden site (clockwise).

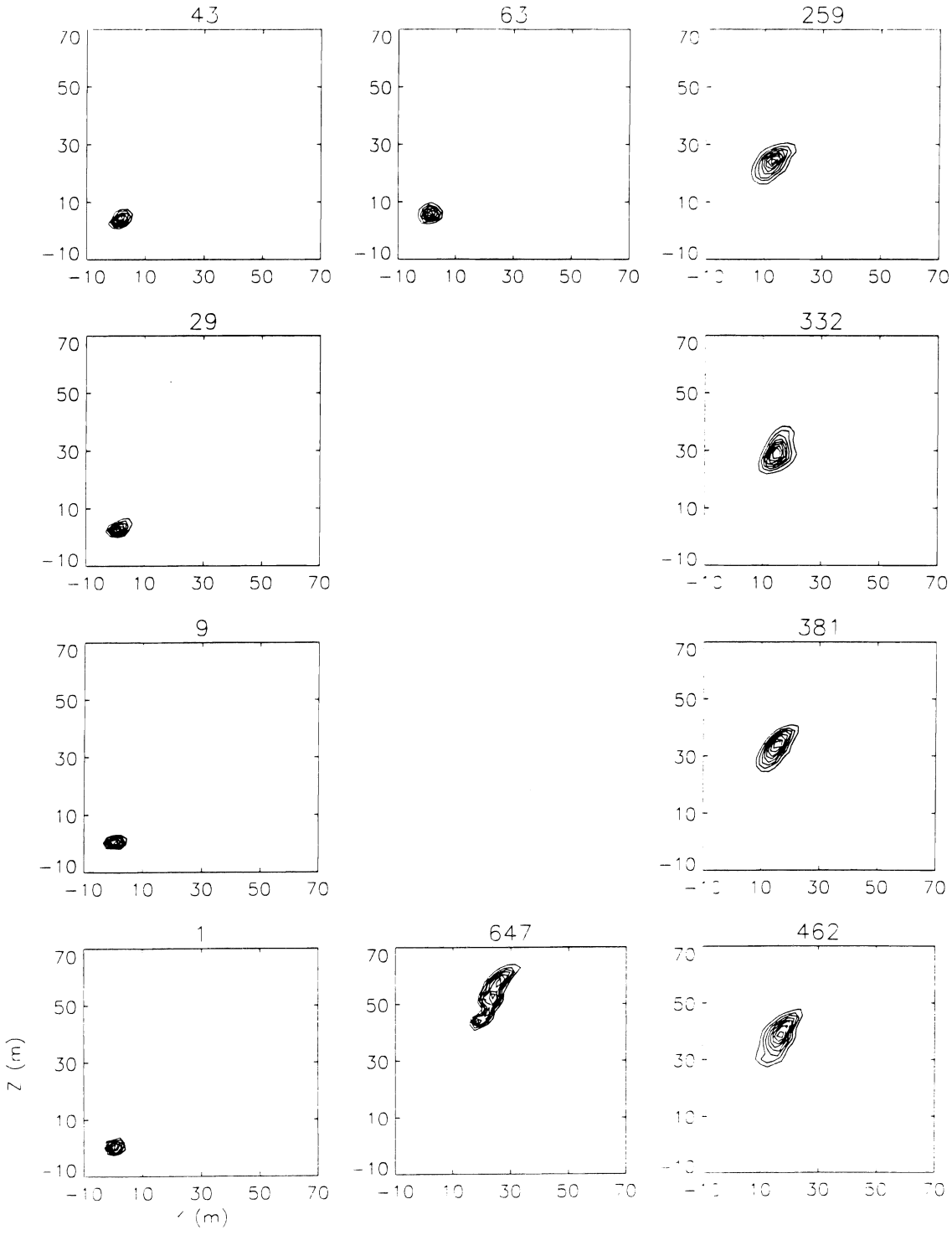

Figure 2. Fitted chloride concentrations at the Borden site (clockwise).

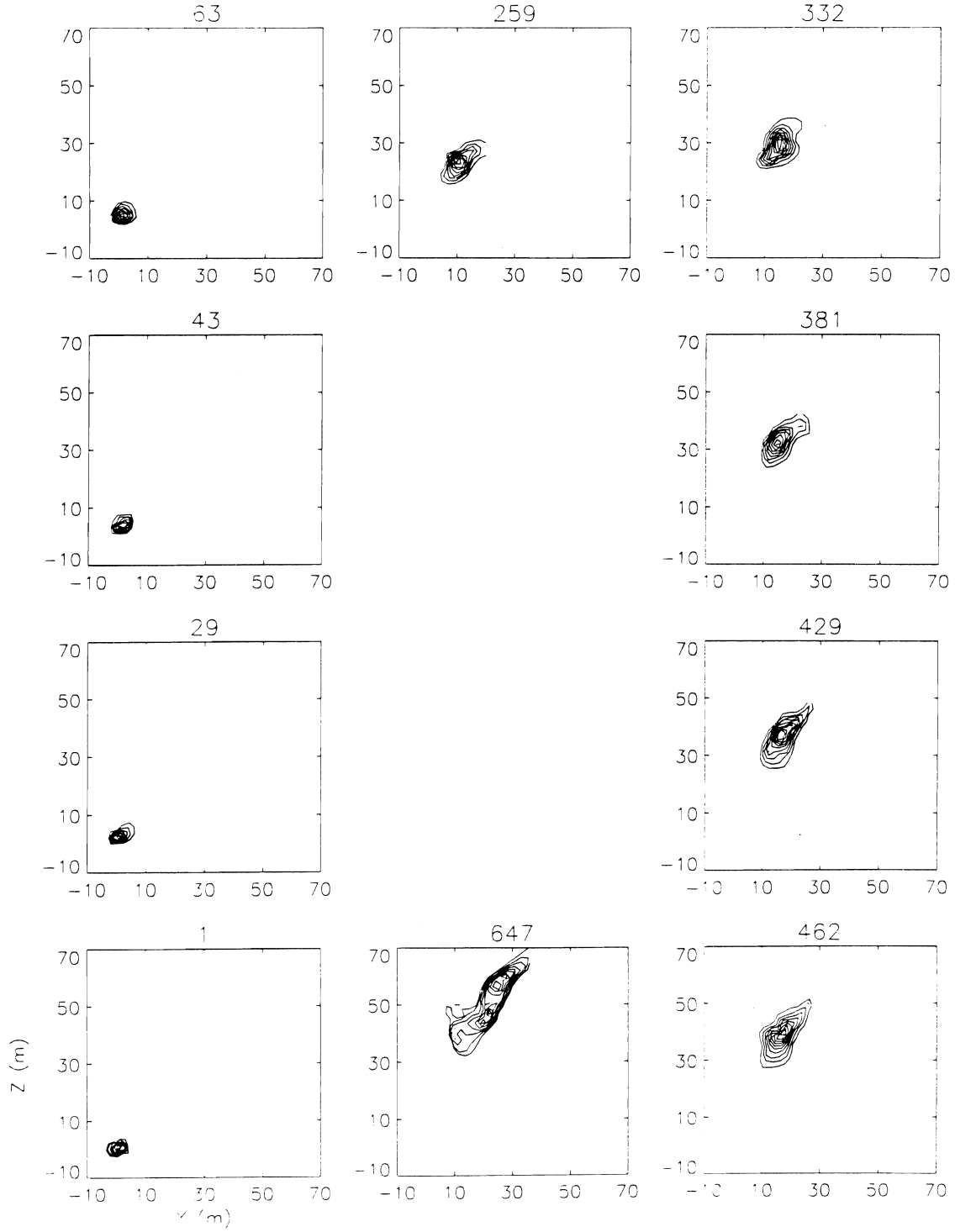

Figure 3. Measured bromide concentrations at the Borden site (clockwise).

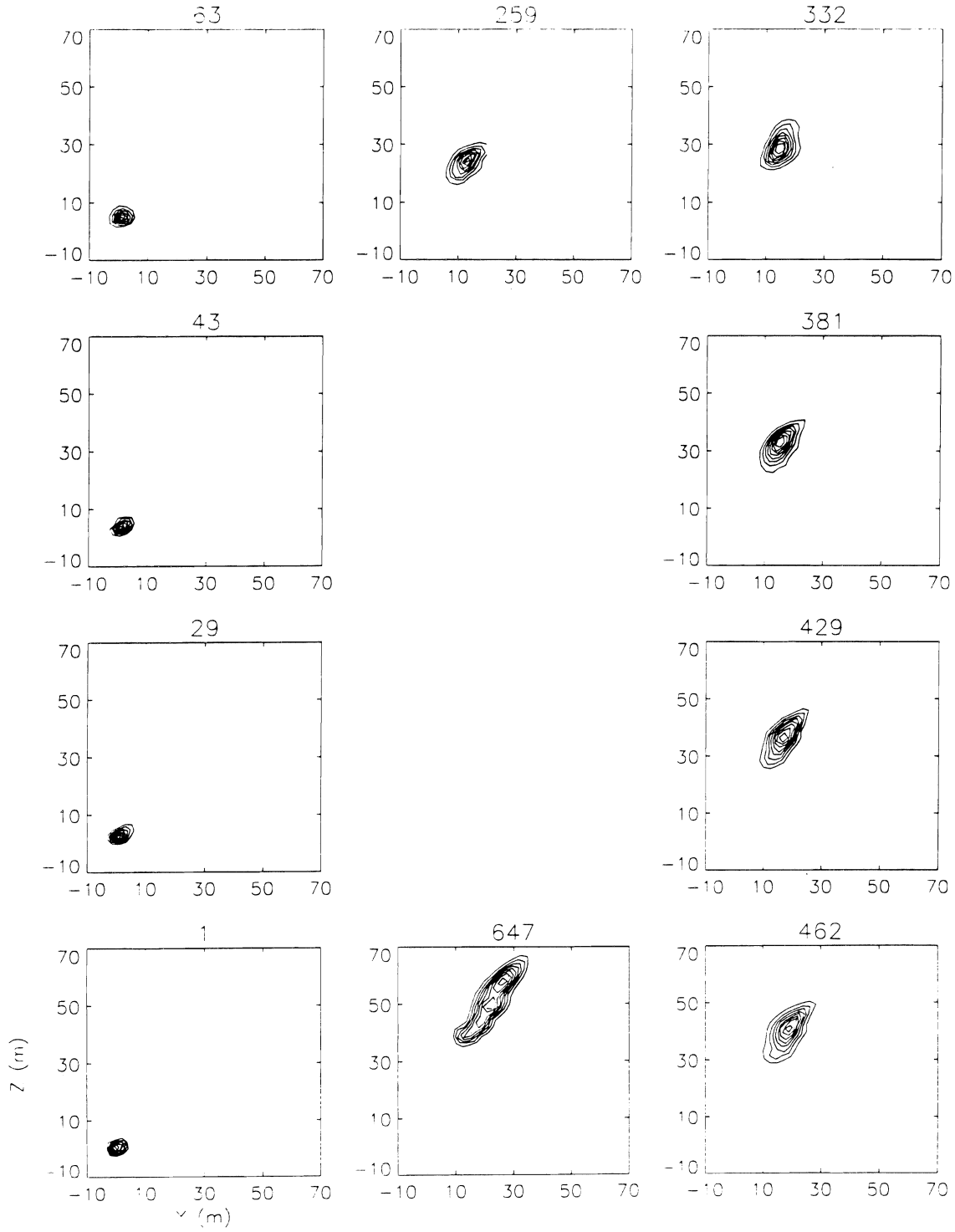

Figure 4. Fitted bromide concentrations at the Borden site (clockwise).

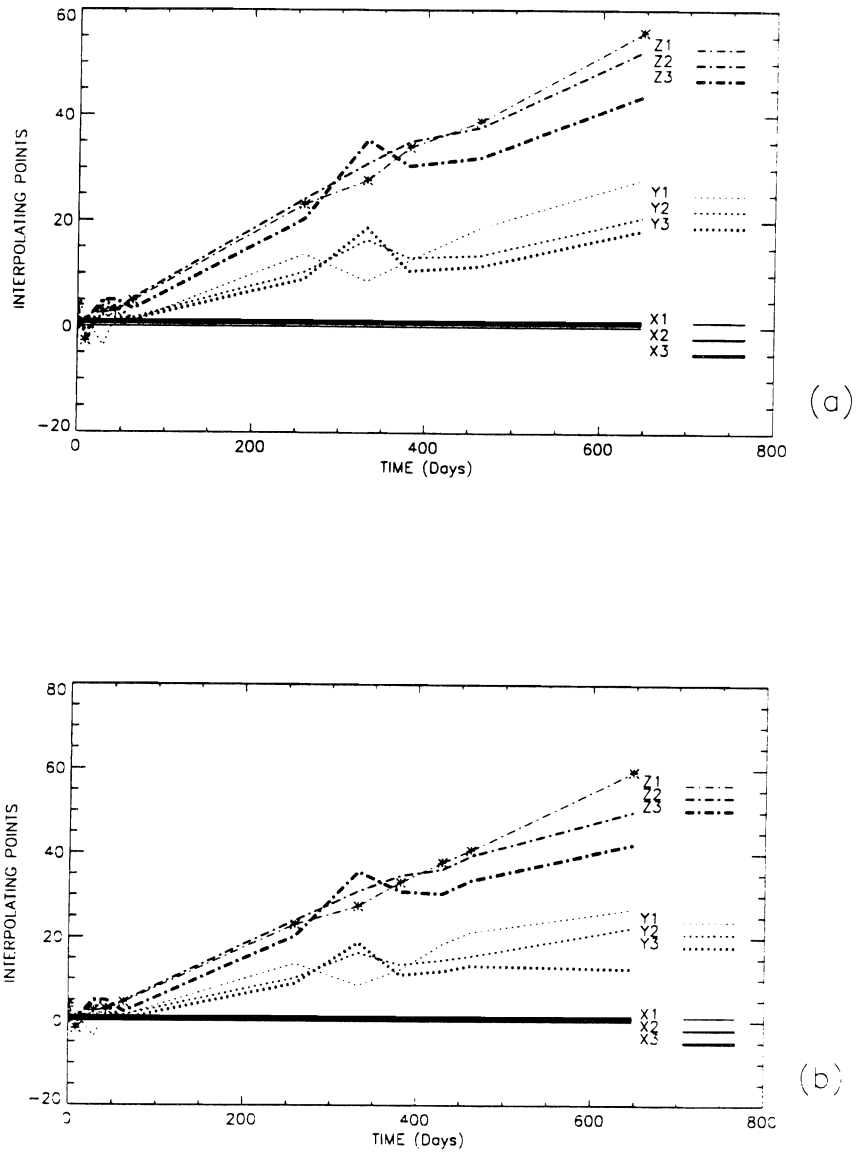

Figure 5. Evolution of fractal-multifractal localization parameters. (a) chloride, (b) bromide.

Simulation of Contaminant Transport in Heterogeneous Soils

M. A MARIÑO[1], H. A. LOAICIGA[2], AND R. B. LEIPNIK[3]
[1]*Department of Land, Air & Water Resources, Davis Campus*
[2]*Department of Geography, Santa Barbarba Campus*
[3]*Department of Mathematics, Santa Barbara Campus*

Summary

The development of effective conductivity in the presence of a deterministically linear trend in the log hydraulic conductivity and a "small" stochastic perturbation has been documented in earlier papers by the project investigators (Loaiciga et al., 1993, 1994). This model is now coupled with the transport phenomena of an ideal tracer to produce equations governing macroscopic dispersivity. Development of these equations includes several manipulations of the Fourier/Spectral transform. To satisfy the formal convergence criteria of these manipulations, an arbitrarily small negative quadratic term is introduced in the log hydraulic conductivity. A general relationship is derived governing the coefficients of the macroscopic dispersivity tensor in terms of an integral equation. Analysis is currently being performed using standard assumptions of the hydraulic parameters. Also, the auto-covariance of the stochastic perturbation in the log hydraulic conductivity is chosen to be Gaussian in nature, as opposed to the usual exponential model. The resulting integrals for the coefficients are Gaussian in nature, as expected. The integrands are expanded in terms of Hermite polynomials and evaluated, with one integral remaining.

Key Words: macroscopic dispersivity, log hydraulic conductivity, stochastic analysis, spectral analysis, hermite polynomials.

Project Objectives Addressed in 1994-95

The transport of particulates via groundwater flow in heterogeneous media is of great interest to environmental protection and water resource management. Due to the variability inherent in a heterogeneous porous medium, its characteristics are modeled as random fields, in particular the hydraulic conductivity. The transport process at large scales (i.e., at field scales of hundreds or thousands of meters) is then characterized by the macroscopic dispersivity tensor through a Fickian law (Gelhar, 1993) Expressions for the coefficients of the macroscopic dispersivity tensor can be derived by coupling the following three stochastic differential equations, having both random variables and a random coefficient (the hydraulic conductivity): (a) the steady-state fluid flow equation; (b) Darcy's equation governing the hydraulic head; and (c) the steady-state transport equation. The steady-state case is assumed, as is normally done, since subsurface groundwater flow occurs at large time scales and has usually evolved into a steady-state. (See Gelhar and Axness (1983) who analyzed the unsteady case and rationalized this assumption.) Also, the particulates are assumed to be ideal tracers (which do not react with the groundwater to produce changes in fluid viscosity or fluid density). Details concerning the case of a non-ideal tracer can be found in Welty and Gelhar (1991).

The heterogeneity of the porous medium is manifested in modeling the logarithm of the hydraulic conductivity as a deterministic mean upon which is superimposed a "small" random field. All other random variables in the stochastic differential equations are modeled in the same fashion: a deterministic mean superimposed upon with a random field. However these other random fields are dependent on the log conductivity field through the stochastic differential equations. In Gelhar and Axness (1983), analysis is performed under the assumptions that the deterministic portion of the log conductivity field is constant and that the random portion is characterized by an exponential model of its auto-covariance function. This constant assumption is apparently too restrictive; experimental results suggest the need for spatial trends in the deterministic portion of the log conductivity field (Rehfeldt et al., 1992).

The technical possibility of including spatial trends is shown by the recent focus on the development of effective hydraulic conductivity in the presence of linear trends (Loaiciga et al. 1993). Recently, macrodispersivity in the presence of a linear trend in the log hydraulic conductivity has been analyzed in Indelman and Rubin (1995). Their method generated moments of the solutions of the stochastic differential equations using Green's functions. The theory of Fourier/Spectral representation, used by Loaiciga et al. (1993) on the first two of these stochastic differential equations, furnishes an alternate approach that allows certain generalizations to be made easily. The spatial trend in the log hydraulic conductivity will be assumed to be dominated by a linear trend within one or two log conductivity scales; the usual distance for field-scale experiments is to be considered essentially infinite. However, a linear trend alone does not fit in well with orthodox Fourier transform analysis, which

requires a degree of decay "at infinity". This point is passed over by Indelman and Rubin (1995) when the Fourier transform is eventually introduced. To satisfy this condition, a small negative quadratic term is also added to the spatial trend, which begins to dominate, after one or two log conductivity scales, preserving the linear structure where needed.

The development of the basic equations has been kept as general as possible. The standard assumptions governing the hydraulic parameters were then applied (e.g., the orientation of the x_1-axis with the direction of the mean fluid flow, the form of the local dispersivity tensor under this orientation, etc.) and the analysis was performed. The hope is that in the future, these standard assumptions can be further generalized. One possible improvement in the stage of explicit calculation, however, was to model the random field in the log conductivity by a Gaussian auto-covariance function, compared to the usual exponential model.

Research Plan and Procedures

The macroscopic dispersivity tensor, $\underline{A}$, having components, A_{mn}, is defined using a version of Fick's Law governing dispersive flux,

$$\sum_{n=1}^{3} A_{mn} G_n = \frac{1}{q} \cdot \overline{c' q'_m} \tag{1}$$

in which the G_n are the components of the mean concentration gradient; q is the mean specific discharge; c' is the random field associated with the concentration field, and the q'_m are the components of the random field associated with the specific discharge vector (Gelhar, 1993). The term $\overline{c' q'_m}$ represents the mean dispersive flux of the tracers in the x_m-direction and can be written as an integral of an expectation value of quantities governed by the three stochastic differential equations mentioned above. This gives

$$\sum_{n=1}^{3} A_{mn} G_n = \frac{1}{q} \int_{\Re^3} E\left[dZ_{c'}\left(\vec{k}\right) dZ^*_{q'_m}\left(\vec{k}\right) \right] d^3k \tag{2}$$

(note: Z^* represents complex conjugation of Z.) The terms $dZ_{c'}$ and $dZ_{q'_m}$ are the spectral representations of the stochastic processes in the concentration field and in the specific discharge vector, respectively. These terms are related to the stochastic process in the log conductivity field through these stochastic differential equations. In particular, Darcy's equation states that

$$q_m = -K \frac{\partial \phi}{\partial x_m} \tag{3}$$

in which q_m is a component of the specific discharge vector represented by a deterministic mean, , plus a zero-mean stochastic process, q'_m; K is the

hydraulic conductivity whose logarithm is modeled as a constant, F, plus a linear trend, $\vec{b}\cdot\vec{x}$, plus a "small" negative quadratic term, $-\sum_{i=1}^{3}\varepsilon_i^2 x_i^2$, plus a zero-mean stochastic process, f; and ϕ is the hydraulic head represented by a deterministic mean, H, (which is assumed to have an essentially constant gradient $-\vec{J}$) plus a zero-mean stochastic process, h. Using these representations in Darcy's equation and dropping terms of second order and higher in the stochastic processes yields the following relationship:

$$q'_m = -\exp\left[F + \vec{b}\cdot\vec{x} - \sum_{i=1}^{3}\varepsilon_i^2 x_i^2\right]\left(\frac{\partial h}{\partial x_m} - J_m f\right) \tag{4}$$

At this point, the spectral representation of the stochastic processes is introduced

$$h(\vec{x}) = \int_{\Re^3} e^{j\vec{k}\cdot\vec{x}}\, dZ_h(\vec{k}) \tag{5}$$

$$f(\vec{x}) = \int_{\Re^3} e^{j\vec{k}\cdot\vec{x}}\, dZ_f(\vec{k}) \tag{6}$$

$$q'_m(\vec{x}) = \int_{\Re^3} e^{j\vec{k}\cdot\vec{x}}\, dZ_{q'_m}(\vec{k}) \tag{7}$$

where $j = \sqrt{-1}$. Using fairly standard manipulations of the Fourier/Spectral transform, (4) becomes

$$dZ_{q'_m}(\vec{k}) = -\frac{e^F}{(2\pi)^3}\left\{\left[\frac{\pi^{\frac{3}{2}}}{\varepsilon_1\varepsilon_2\varepsilon_3}\exp\left(-\sum_{i=1}^{3}\frac{k_i^2}{4\varepsilon_i^2}\right)\right]\otimes\left[jk_i\, dZ_h(\vec{k}) - J_i\, dZ_f(\vec{k})\right]\right\}(\vec{k} - j\vec{b}) \tag{8}$$

where $\otimes$ represents the convolution of the two quantities in square brackets. Before proceeding along these lines, the steady-state fluid flow equation is used to express dZ_h in terms of dZ_f. The steady-state fluid flow equation in three-dimensions can be written in terms of the log conductivity as

$$\sum_{i=1}^{3}\left[\frac{\partial}{\partial x_i}(\log K)\frac{\partial\phi}{\partial x_i} + \frac{\partial^2\phi}{\partial x_i^2}\right] = 0 \tag{9}$$

The same analysis as performed with Darcy's equation can now be applied to this version of the steady-state fluid flow equation to yield the following relationship:

$$dZ_h(\vec{k}) = \frac{j\vec{J}\cdot\vec{k}}{j\vec{b}\cdot\vec{k} - k^2}\, dZ_f(\vec{k}) \tag{10}$$

Loaiciga et al., (1995) derived a similar equation whose denominator was rationalized. Equation (10) is used to eliminate dZ_h in (8). Once this is done, the convolution is evaluated and the following equation is derived

$$dZ_{q'_m}(\vec{k}) = \frac{e^F}{8\pi^{\frac{3}{2}}\varepsilon_1\varepsilon_2\varepsilon_3}\int_{\Re^3}\left(\frac{j\vec{J}\cdot\vec{\xi}}{j\vec{b}\cdot\vec{\xi}-\xi^2}+J_i\right)\exp\left[-\sum_{i=1}^{3}\frac{(k_i-\xi_i-jb_i)^2}{4\varepsilon_i^2}\right]dZ_f(\vec{k})d^3\xi \quad (11)$$

Next, a similar analysis is performed on the steady-state transport equation to express $dZ_{c'}$ in terms of dZ_f. The steady-state transport equation states that

$$\sum_{i=1}^{3}\frac{\partial}{\partial x_i}\left[\sum_{j=1}^{3}\underline{E_{ij}}\frac{\partial c}{\partial x_j}-cq_i\right]=0 \quad (12)$$

in which $\underline{E_{ij}}$ are the coefficients of the local dispersivity tensor (assumed to be constant multiples of the mean specific discharge) and c is the concentration of the tracers (see, for example, Gelhar and Axness, 1983). Let the specific discharge be represented as before, and let the concentration be represented by a deterministic mean, C, plus a zero-mean stochastic process, c'. The mean concentration is further specialized to have a constant gradient, $\frac{\partial C}{\partial x_i}=-G_i$, (Gelhar and Axness, 1983). It is hoped that this restriction may be relaxed in future analysis since the terms introduced in modeling the concentration gradient linearly can be dealt with in the same fashion presented; however, they become rather messy.

The spectral representation of the stochastic processes are introduced, as before, and a similar analysis is performed. This includes using a previous result, (11), to eliminate the dependence on the stochastic process associated with the specific discharge vector. The following equation is then derived

$$dZ_{c'}(\vec{k}) = \frac{e^F}{8\pi^{\frac{3}{2}}\varepsilon_1\varepsilon_2\varepsilon_3}\;\frac{1}{\vec{k}^T\underline{E}\vec{k}+j\vec{k}\cdot\vec{\bar{q}}}\;\bullet$$
$$\int_{\Re^3}\left(\frac{(\vec{J}\cdot\vec{\xi})(\vec{G}\cdot\vec{\xi})}{j\vec{b}\cdot\vec{\xi}-\xi^2}+\vec{G}\cdot\vec{J}\right)\exp\left[-\sum_{i=1}^{3}\frac{(k_i-\xi_i-jb_i)^2}{4\varepsilon_i^2}\right]dZ_f(\vec{\xi})\;d^3\xi \quad (13)$$

Using this result and the complex conjugate of (11), the Fickian relationship governing the coefficients of the macroscopic dispersivity tensor, (2), is manipulated to yield a rather messy equation. This rather messy equation can be simplified first by imposing the orthogonality condition of the spectral process, dZ_f, i.e. that

$$E\left[dZ_f\left(\vec{\xi}\right) dZ_f(\vec{\mu})\right] = \delta\left(\vec{\xi} - \vec{\mu}\right) S_{ff}\left(\vec{\xi}\right) \tag{14}$$

where δ is the dirac delta function and S_{ff} is the spectral auto-covariance function associated with the log conductivity field. Second, the summation can be uncoupled and the messy equation is reduced to the following general relationship governing the coefficients of the macroscopic dispersivity tensor:

$$A_{mn} = \frac{e^{2F}}{64\pi^3 \varepsilon_1^2 \varepsilon_2^2 \varepsilon_3^2} \int_{\Re^3} \int_{\Re^3} \frac{\exp\left[-\sum_{i=1}^{3} \frac{(k_i - \xi_i)^2 - b_i^2}{2\varepsilon_i^2}\right]}{\vec{k}^T \underline{E} \vec{k} + j\vec{k} \cdot \vec{\bar{q}}} \Theta_n^{(m)}\left(\vec{\xi}\right) S_{ff}\left(\vec{\xi}\right) d^3\xi \, d^3k \tag{15}$$

where

$$\Theta_n^{(m)}\left(\vec{\xi}\right) = \left(\frac{(\vec{J} \cdot \vec{\xi})\, \xi_n}{j\vec{b} \cdot \vec{\xi} - \xi^2} + J_n\right)\left(\frac{(\vec{J} \cdot \vec{\xi})\, \xi_m}{-j\vec{b} \cdot \vec{\xi} - \xi^2} + J_m\right) \tag{16}$$

Results

Besides the general relationship given above, any further results require certain choices to be made. The coordinate system is oriented such that the mean specific discharge vector is of the simplified form

$$\vec{\bar{q}} = \langle q, 0, 0 \rangle \tag{17}$$

The local dispersivity tensor under this orientation is assumed to be of the form

$$\underline{E} = \begin{pmatrix} \alpha_1 & 0 & 0 \\ 0 & \alpha_2 & 0 \\ 0 & 0 & \alpha_3 \end{pmatrix} q, \qquad \alpha_1, \alpha_2, \alpha_3 > 0 \tag{18}$$

(See Gelhar and Axness (1983) who worked with the further specialization $\alpha_1 = \alpha_L$, the longitudinal dispersivity, and $\alpha_2 = \alpha_3 = \alpha_T$, the transverse dispersivity.) And as mentioned before, the spectral auto-covariance is chosen to be Gaussian in nature, in particular of the form

$$S_{ff}\left(\vec{\xi}\right) = \frac{\lambda_1 \lambda_2 \lambda_3 \sigma_f^2}{8\pi^{\frac{3}{2}}} \exp\left[-\frac{\lambda_1^2 \xi_1^2}{4} - \frac{\lambda_2^2 \xi_2^2}{4} - \frac{\lambda_3^2 \xi_3^2}{4}\right] \tag{19}$$

which is from the Gaussian auto-covariance function

$$R_{ff}(\vec{x}) = \sigma_f^2 \exp\left[-\frac{x_1^2}{\lambda_1^2} - \frac{x_2^2}{\lambda_2^2} - \frac{x_3^2}{\lambda_3^2}\right] \tag{20}$$

Using these choices, the integrals in (15) become Gaussian in nature and a few are evaluated immediately. The resulting integrand is expanded in terms of the set of classical, orthogonal polynomials created to integrate Gaussian integrals over infinite domains: the Hermite polynomials. Most of the resulting integrals are then evaluated, leaving only one left. It is hoped that this remaining integral can be evaluated in a closed form; otherwise, the leading order asymptotics will be extracted and evaluated numerically.

Discussion

The analysis for a practical case is as yet unfinished; however, the general relationship, (15), looks promising. The results in Gelhar and Axness (1983) can be recovered by setting $\vec{b} = \vec{0}$ and taking the limit of the ε_i to zero from the right, which forms a delta sequence. It also allows the choice of a Gaussian auto-covariance function at little extra cost.

References

Gelhar, L. 1993. Stochastic Subsurface Hydrology. Prentice-Hall, Englewood Cliffs, N. J.

Gelhar, L. and C. Axness. 1983. Three-dimensional stochastic analysis of macrodispersion in aquifers. Water Resources Research 19(1): 161-180.

Indelman, P. and Y. Rubin. 1995. Flow in heterogeneous media displaying a linear trend in the log conductivity. Water Resources Research 31(5): 1257-1265.

Loaiciga, H., R. Leipnik, M. Mariño, and P. Hudak. 1993. Stochastic groundwater flow analysis in the presence of trends in heterogeneous hydraulic conductivity fields. Mathematical Geology 25(2): 161-176.

Loaiciga, H., R. Leipnik, P. Hudak, and M. Mariño, 1994. Effective hydraulic conductivity of nonstationary aquifers. Stochastic Hydrology and Hydraulics, 8: 1-17.

Loaiciga, H., R. Leipnik, P. Hudak, and M. Mariño, 1995. 1-, 2- and 3-dimensional effective conductivity of aquifers. Submitted for publication.

Rehfeldt, K., J. Boggs, and L. Gelhar. 1992. Field study in a heterogeneous aquifer, 3, Geostatistical analysis of hydraulic conductivity. Water Resources Research, 28: 3309-3324.

Welty, C. and L. Gelhar. 1991. Stochastic analysis of the effects of fluid density and viscosity variability on macrodispersion in heterogeneous porous media. Water Resources Research , 27(8): 2061-2075.

Retention and Permeability of Multi-Fluid Soil Systems

JAN W. HOPMANS[1], F.J. LEIJ[2], P.J. SHOUSE[2], AND
M. TH. VAN GENUCHTEN[2]
[1]*Department of Land, Air and Water Resources, Davis Campus*
[2]*U. S.Salinity Laboratory, USDA, ARS, Riverside*

Summary

Liquid retention and permeability functions are crucial for quantifying subsurface flow and transport processes. The direct measurement of these functions is generally difficult and time consuming, especially for permeability. The problem is exacerbated if more than one (immiscible) liquid is present. This is the case for many organic contamination problems. In our 1993- 1994 Kearney Foundation report, we presented retention data for two- and three-fluid systems with different wettabilities. In the first part of this report, we will discuss methods to predict retention curves for three-fluid systems from data for two-fluid media and methods to estimate the various interfacial areas that may occur in multi-fluid soil systems.

Previous research on air-water systems has demonstrated the feasibility of using the multi-step outflow method, which involves numerical simulation of the flow process, to estimate parameters for the hydraulic functions by using experimental data. This report also describes the theory and application of a modified multi-step method for arbitrary two-fluid media; the fluid pairs may consist of air-oil, air-water, or oil-water. Transient outflow experiments will be discussed be discussed first. The inverse modeling and the parameter optimization are reviewed subsequently.

Key Words: hydraulic properties, capillary pressure, NAPL, wettability, interfacial areas

Project Objectives addressed in 1994-1995

1. Transient measurements of water and oil flow properties using a modified version of the multi-step method. Research was codnucted at UC Davis.

2. Measurement of retention curves for air-oil, air-water, and oil-water media for a variety of wettabilities and spreading coefficients using an automated setup. Prediction of retention curves and estimation of interfacial areas. Research was conducted at UC Riverside and the U. S. Salinity Laboratory in Riverside.

Research Plan and Procedures

Multi-step experiments

Multi-step outflow experiments were conducted in a laboratory with a constant temperature of 20°C, using a modified Tempe cell of 7.6 cm high and 6.4 cm in diameter (Figure 1). Colombia sandy loam (Table 1) was air-dried, sieved through a 2-mm screen, and uniformly packed with a soil bulk density of 1.42 g/cm^3 for all experiments. One-dimensional displacement experiments were carried out in three two-phase systems: (1) air-water, (2) air-oil (Soltrol 130), and (3) oil-water. The nonwetting phase was air in the air-water and air-oil systems and oil in the oil-water system. In our experiment, a soil sample was placed in the cell on top of a high flow rate (K_s = 0.0411cm/h) 1-bar ceramic plate. The soil sample was saturated by the wetting fluid from the bottom. Then a multi-step positive pressure of the nonwetting phase fluid was introduced to the soil sample, resulting in wetting phase drainage through the ceramic plate. The outflow was collected in a graduate burette, with a transducer connected to it to monitor outflow level and cumulative outflow (Fig. 1). Hydrophilic and hydrophobic tensiometers were vertically installed in the center of the soil sample to monitor pressure changes of the wetting and nonwetting phases. Transducers, connected to a datalogger, were used for automatic data acquisition of pressures and cumulative outflows during transient drainage.

Positive pressure steps for the air-water system were 60, 80, 120, 200, 400, and 700 mbar. The pressure steps of nonwetting phase fluids for other systems were determined based on the scaled relationship of the interfacial tension between wetting and nonwetting phases (Table 2). The positive air pressure from an air source was directly imposed on the top of the sample (Fig. 1). To obtain different positive oil pressures, a Marriotte bottle filled with oil was connected to a pressurized air source on one side and to the top of the cell. The air pressure was adjusted to impose intended oil pressures. As the wetting phase pressure became relatively constant, the positive pressure was changed to the next pressure step. Final saturation was determined by the oven-dry method at the end of each experiment. The initial saturation was calculated based on final saturation and total outflow. More detailed information on multi-step experiments can be found in Hopmans et al. (1994).

In the original outflow experiments of an air-water system, air pressure was assumed to be constant in the draining soil system, because of its low viscosity and density. In that case, a positive air pressure imposed on the upper boundary was equivalent to a negative water pressure applied at the lower boundary (Kool et al. 1985). Therefore, a one-phase model was conveniently used for the simulation of a draining soil core. If the nonwetting phase is oil as in an oil-water system, the assumption of constant nonwetting phase pressure is not necessarily valid, since the viscosity and density of the oil phase are close to that of the wetting phase (Table 2). Special attention was paid to the oil pressure changes during drainage. In addition, experiments were conducted with different soils and for different time lengths to examine soil physical properties (Table 1) and time influence. The surface tensions of air-water and air-oil were measured by the plate method, while the interfacial tension between oil and water was measured by the ring method (Table 2) (Adamson, 1990).

Parameter estimation

To simulate the transient multi-step outflow experiments, we solved the following system of equations with the appropriate initial and boundary conditions:

$$\phi \frac{\partial S_w}{\partial t} + \nabla . q_w = 0 \tag{1a}$$

$$q_w = -\frac{\kappa_w}{\mu_w}[\nabla P_w - \rho_w g] \tag{1b}$$

$$q_{nw} = -\frac{\kappa_{nw}}{\mu_{nw}}[\nabla P_{nw} - \rho_{nw} g] \tag{1c}$$

$$\phi \frac{\partial S_{nw}}{\partial t} + \nabla . q_{nw} = 0 \tag{1d}$$

where q denotes flux density, S is the degree of saturation, f, k, m, r denoting the porosity, intrinsic permeability, viscosity and density of the subscripted wetting (w) or nonwetting (nw) fluid phase, respectively, and P is the phase pressure. The van Genuchten expressions were used as the constitutive expressions to relate capillary pressure and permeability to degree of saturation for each fluid phase.

We used a one-dimensional two-phase flow model to solve the above flow equations simultaneously. The model was originally derived from a code from the University of Minnesota (Dr. John Nieber), and was adapted to be applicable to our experimental conditions. The model was tested by comparing one-phase simulation results (air-water) with the one-dimensional code used by Eching et al. (1993).

For the optimization, we used the code developed by Clausniter and Hopmans (1995), LM-OPT, which is now available on the Internet using FTP. This optimization code allows the use of various minimization algorithms, and is flexible enough to be interfaced with specified analytical or numerical models. The interplay of optimization with the experimental and numerical results is presented in Fig. 2.

Predicting Three-Fluid P_c-S Relations

Under objective 2 we will outline how capillary pressure (P_c)-saturation (S) data can be used to predict P_c-S curves for other fluid systems and to estimate interfacial areas. The wettability of the porous medium greatly affects the pore-scale distribution of immiscible fluids. It is frequently assumed that the solid has uniform wetting properties and is hydrophilic. However, many porous media may have fractional wettability. Hence, we will pay special attention to the multi-fluid properties of fractional wettability media.

Indirect methods have often been used to predict P_c-S curves from data that are already available or can be measured more easily. For two-fluid systems, scaling of P_c-S data for one fluid pair is used to predict P_c-S curves for other fluid pairs in the same medium, while for three-fluid systems, P_c-S functions can be predicted from corresponding two-fluid P_c-S data according to Leverett's assumption (Leverett, 1941). Such scaling procedures assume that only one fluid wets the solid surface, while Leverett also assumed a continuous intermediate wetting fluid.

Interfacial Areas

The area between two fluids or a fluid and a solid may be important for the mass transfer between two phases or for quantifying the permeability of the porous medium for each fluid. Direct measurements of fluid-fluid interfacial areas have only recently emerged and are likely to remain cumbersome. Indirect methods have therefore also been used for quantifying the area between two fluids. Morrow (1970) demonstrated that for an isothermal system, with incompressible fluid and solid phases, the area under the P_c-S curve (f_{NW}) is related to the solid-nonwetting (A_{sN}^*) and nonwetting-wetting (A_{NW}^*) interfacial areas by

$$f_{NW}(S_W^{NW}) + C_{NW} = s_{NW}\cos(f_{sNW})A_{sN}^*(S_W^{NW}) + s_{NW}\, A_{NW}^*(S_W^{NW}) \qquad (2)$$

where f_{sNW} is the contact angle, the areas are given per unit pore volume, and C_{NW} is the constant of integration. Bradford and Leij (1996b) approximated C_{NW} by assuming that the entrapped nonwetting fluid exists as saturation-dependent spheres; the radii of these spheres are related to the capillary pressure of the primary drainage curve according to the Laplace equation.

Results and Discussion

Multi-step experiments

Figure 3 shows the relation of cumulative outflow and capillary pressure of wetting phase for the three fluid systems with Columbia soil. It can be seen that the same amount of wetting phase flows out of the cell when capillary pressure is about 100, 250, and 400 cm of water column for air-oil, oil-water, and the air-water system, respectively. The relation between capillary pressures for the 3 fluid-pair systems is governed by the interfacial tension ratios (Table 2). Since the interfacial tension between air and water is highest among the three systems, it requires the maximum pressure for an equal volume of water drainage as compared to the two other systems.

Values of initial and final saturation of wetting phase for three systems are tabulated in Table 3. The initial saturation is defined here as the saturation under the negative suction before applying any positive nonwetting phase pressure. The final saturation is measured by the oven-dry method at the end of each experiment. Since the oven-dry method can not be used for the final saturation determination for an oil-water system, the corresponding saturation value is estimated based on the cumulative outflow, with an assumption of 100% wetting phase saturation of the soil sample before any outflow starts.

The optimized retention curves for the 3 fluid systems is presented in Fig. 4a. Using the fluid properties in Table 2, the three retention curves can be scaled to a single curve, with the individual curves derived using the interfacial tension ratios. The correponding relative permeability curves are shown in Fig. 4b, with the parameters describing the van Genuchten functions in Table 3. Similar to the retention curves, the conductivity functions for each specific fluid-pair system can be derived from the fluid-specific viscosity and density values in Table 2.

Pressure changes as a function of time are presented for the oil-water system in Fig. 5, with the jumps in fluid pressures correponding with changing applied oil pressures. As would be expected, the wetting phase (water) pressure goes to zero. However, it appears that the pressure of the nonwetting phase (oil) in the oil-water experiments immediately attains the constant applied oil pressure for each pressure increment. This would indicate that also for the oil-water experiment, a one-phase flow model can be used to simulate flow in the oil-water system, just as is done traditionally for an air-water system.

In summary, experimental data can be used for the inverse modeling and parameter optimization for two-phase systems. Because of the transient flow nature of multi-step outflow experiments, retention and permeability functions can be estimated from experimental data in combination with computer simulation and optimization in a much shorter time frame than conventional methods of steady-state or equilibrium conditions.

Predicting Tthree-Fluid P_C-S Relations

Experimental air (a) and oil (o), air and water (w), oil and water P_c-S data were reported for media of various wettabilities by Bradford and Leij (1995a,b). The P_c-S model of van Genuchten was modified to describe oil-water retention data to account for positive and negative capillary pressure values that may occur in fractional wettability media. For oil-wet and fractional wettability media there may not be a continuous intermediate layer since water does not spread well on oil; three capillary pressures occur, viz. over the oil-water, air-water, and air-oil interfaces. Bradford and Leij (1996a) outlined how the capillary pressure relation for a three-fluid system could be predicted reasonably well from the pressure drop of a two-fluid system. Figure 6 shows the measured and calculated capillary pressure curves for oil-water in a 3 fluid hydrophobic VTS medium (Bradford et al., 1995), as predicted from experimental two-fluid data.

Interfacial Areas

Equation 2 serves as the basis for predicting A_{sN}^* and A_{NW}^* from P_c-S data. Bradford and Leij (1996b) estimated $A_{NW}^*(S_W^{NW})$ and $A_{sN}^*(S_W^{NW})$ by empirically partitioning the area under the P_{NW}- S_W^{NW} curve for a nonzero contact angle. For oil-water media with fractional wettability we separately approximate interfacial areas for water- and oil-wet portions of the P_{ow}-S_w^{ow} relation. Figure 7 shows the calculated curves for A_{NW}^* as functions of the wetting (denser) fluid saturation during drainage. These curves were obtained from P_{ao}-S_o^{ao} data for the untreated sand, and air-water, and oil-water P_c-S data for a hydrophobic 75% OTS medium (Bradford et al., 1995). For the air-oil and air-water systems, A_{NW}^* increases as the liquid saturation increases. The pore-size distribution and wettability determine the magnitude A_{NW}^* at a given saturation.

References

Adamson, A.W. 1990. Physical chemistry of surfaces. John Wiley & Sons., Inc.

Bradford, S. A., F. J. Leij, J. W. Hopmans, P. J. Shouse, and M. Th. van Genuchten. 1995. Retention and permeability of multi- fluid soil systems. Kearney Foundation of Soil Science 1993-94 Annual Report.

Bradford, S. A., and F. J. Leij. 1995a. Wettability effects on scaling two- and three-fluid capillary pressure-saturation relations. Env. Sci. and Technol. 29:1446-1455.

Bradford, S. A., and F. J. Leij. 1995b. Fractional wettability effects on two- and three-fluid capillary pressure-saturation relations.J. Contam. Hydrol. (inpress).

Bradford, S. A., and F. J. Leij. 1996a. Predicting two- and three-fluid capillary pressure-saturation relations in fractional wettability media. Water Resour. Res. (in press).

Bradford, S. A., and F. J. Leij. 1996b. Estimating interfacial areas for multi-fluid soil systems. Water Resour. Res. (submitted).

Clausnitzer, V, and J.W. Hopmans. 1995. Nonlinear Parameter Estimation, LM-OPT. A General purpose optimzation code based on the Levenberg-Margquardt Algorithm. Land, Air and Water Resources Paper 100032. UC Davis.

Eching, S.O. and J.W. Hopmans. 1993. Optimization of hydraulic functions from transient outflow and soil water pressure data. Soil Sci. Soc. Am. J. 57:1167-1175.

Hopmans, J.W., J.C. Van Dam, S.O. Eching, and J.N.M. Stricker. 1994. Parameter estimation of soil hydraulic functions using inverse modeling of transient outflow experiments. Trend in Hydol. 1:217-242.

Kool, J.B., J.C. Parker, and M. Th. van Genuchten. 1985. Determining soil hydraulic properties from one-step outflow experiments by parameter estimation: I theory and numerical studies. Soil Sci. Soc. Am. J. 49:1348-1354.

Leverett, M. C. 1941. Capillary behavior in porous solids. Trans. AIME 142:152- 169

Morrow, N. R. 1970. Physics and thermodynamics of capillary action in porous media. In R. J. M. deWiest (ed.) Flow through porous media. Academic Press, New York.

Table 1. Physical properties of experiment soils

	Sand (%)	Silt (%)	Clay (%)
Columbia Soil	63.2	27.5	9.3
Lincoln Soil	88.6	9.4	2.0
	Bulk Density $(g/cm)^3$)	Saturated K (cm/hr.)	Porosity (cm^3/cm^3)
Columbia Soil	1.42	4.29	0.464
Lincoln Soil	1.69	22.99	0.362

Table 2. Physical properties of fluids

	Air-Oil[1]	Air-Oil[2]	Air-Water	Oil[1]-Water	Oil[2]-Water
Surface Tension (nN/cm)	23.9	25.9	68.1	25.9	36.4
	Oil[1](38°C)	Oil[2](38°C)	Air (18°C)	Water (20°C)	
Viscosity (cp)	1.13	3.61	0.0183	1.00	
Density (g/cm^3)	0.762	0.803	0.0128	1.00	

[1]Soltrol 130 used for Columbia soil experiments.
[2]Soltrol 220 used for Lincoln soil experiments.

Table 3. Optimized van Genuchten parameters for 3 fluid-pair systems of Columbia soil

Parameter	Air-water	Oil-water	Air-oil
q_r (cm^3 cm^{-3})	0.123	0.098	0.053
K_s (cm hr^{-1})	3.00	8.90	2.10
a (cm^{-1})	0.011	0.021	0.029
n	2.23	2.68	2.54
** q_s (cm^3 cm^{-3})	0.464	0.464	0.464

** fixed parameter

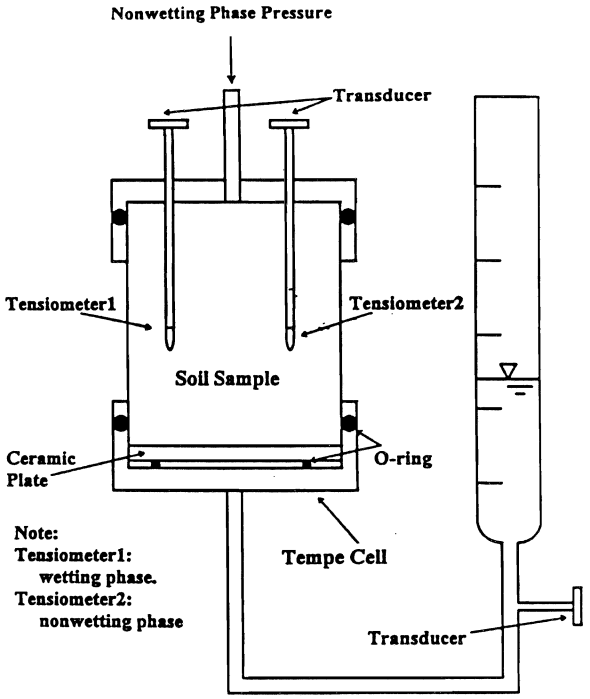

Figure 1. Experimental setup for multi-step two phase-experiments

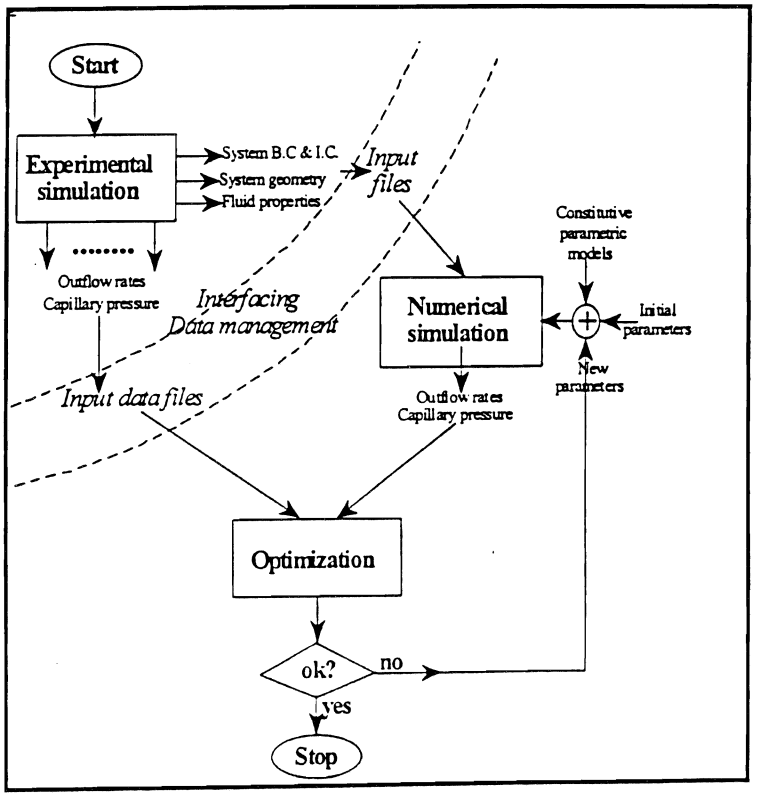

Figure 2. Flow diagram for parameter optimization procedure

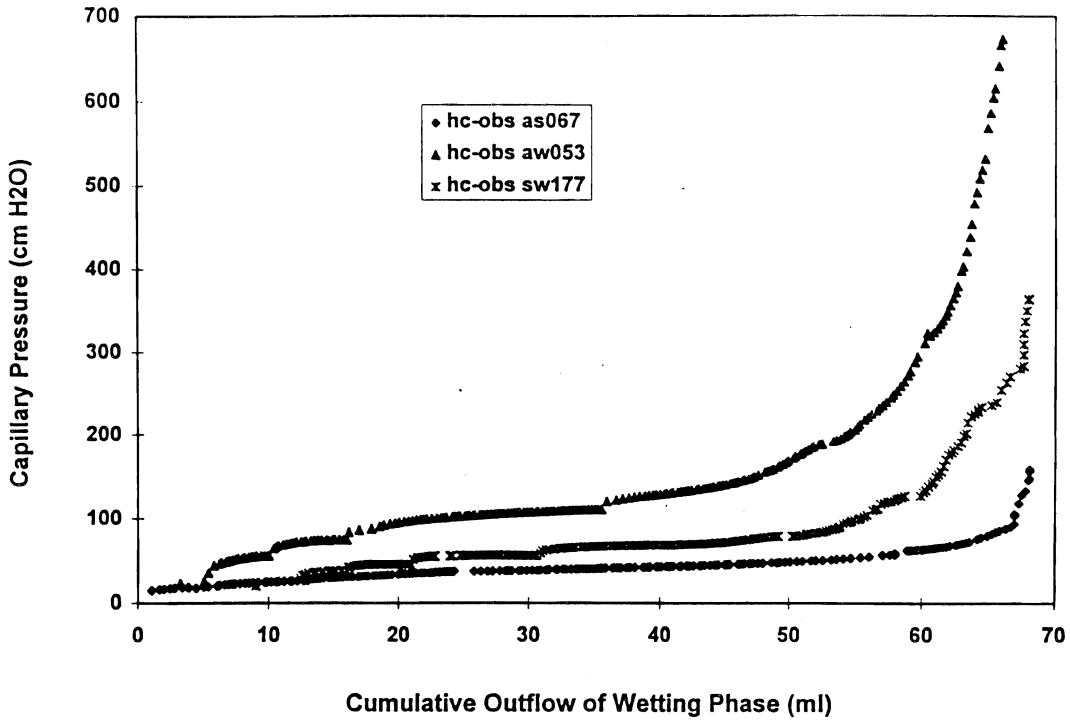

Figure 3. Relationships between capillary pressure and cumulative outflow for air-water (triangles), air-Soltrol (diamonds) and Soltrol-water (crosses)

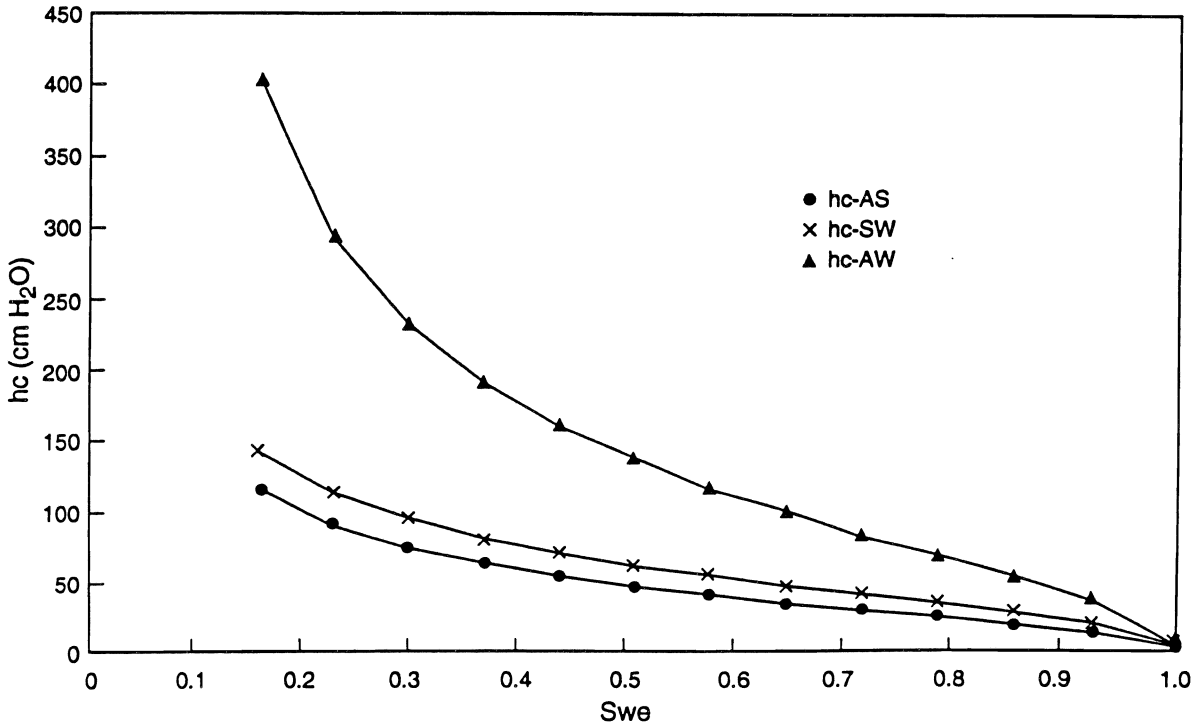

Figure 4a. Optimized retention functions for air-water (AW), air-Soltrol(AS) and Soltrol-water (SW) systems.

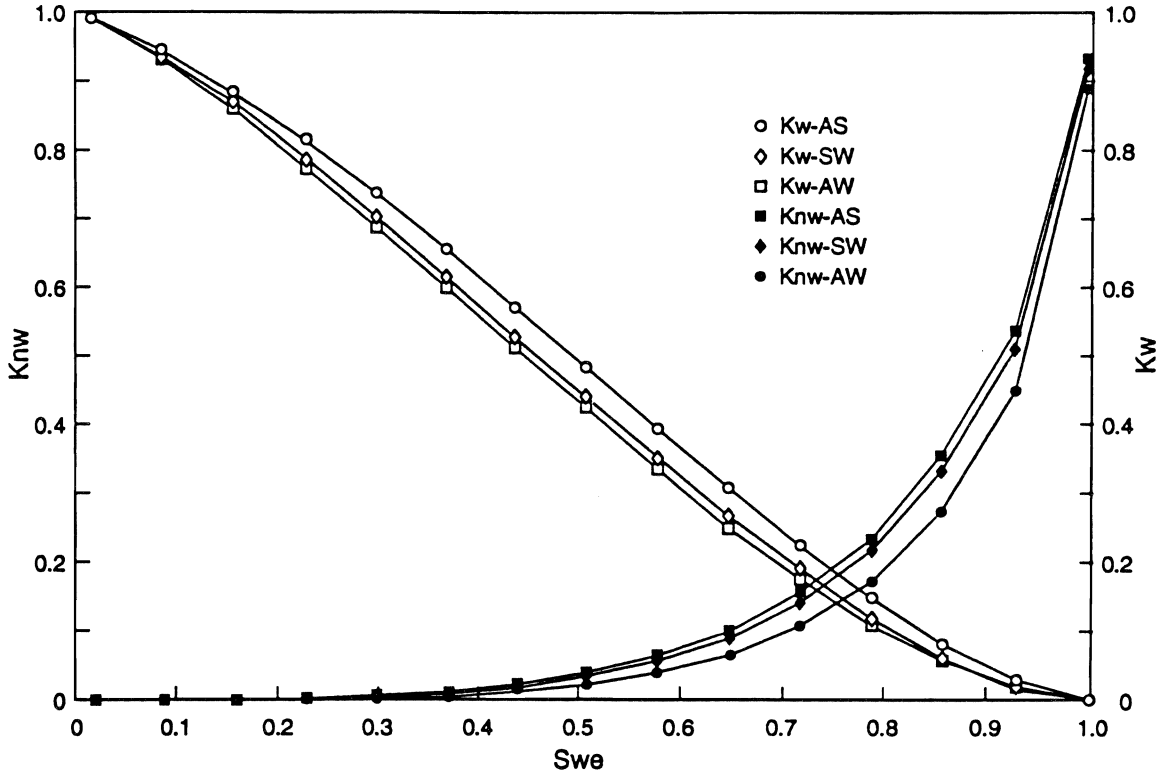

Figure 4b. Optimized relative permeability functions for air-water (AW), air-Soltrol(AS) and Soltrol-water (SW) systems.

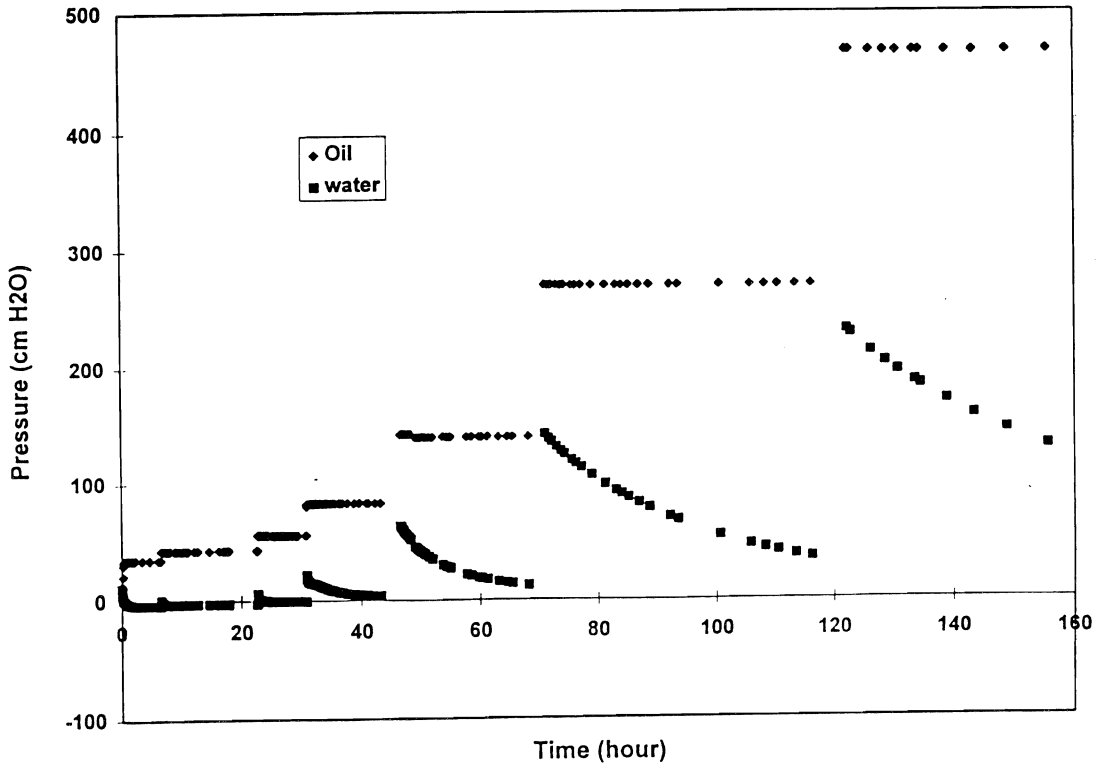

Figure 5. Pressure changes as a function of time for Soltrol-water system

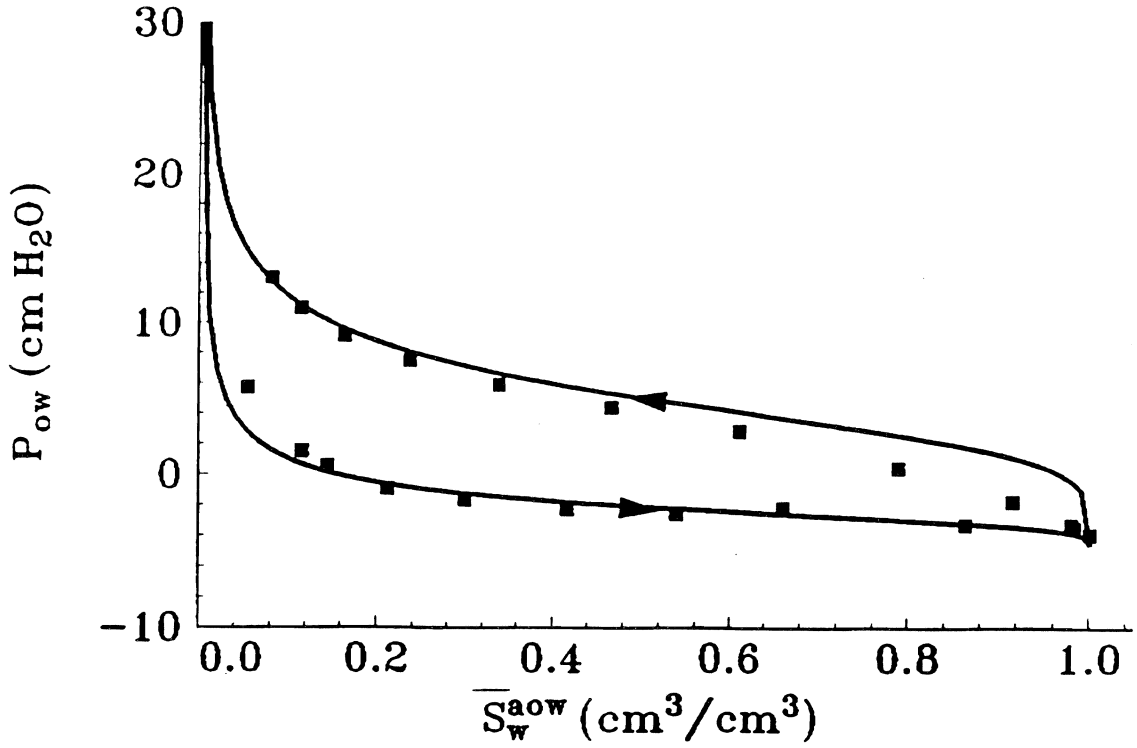

Figure 6. The observed and predicted three-fluid P_c-S curves (oil-water) for the hydrophobic VTS medium.

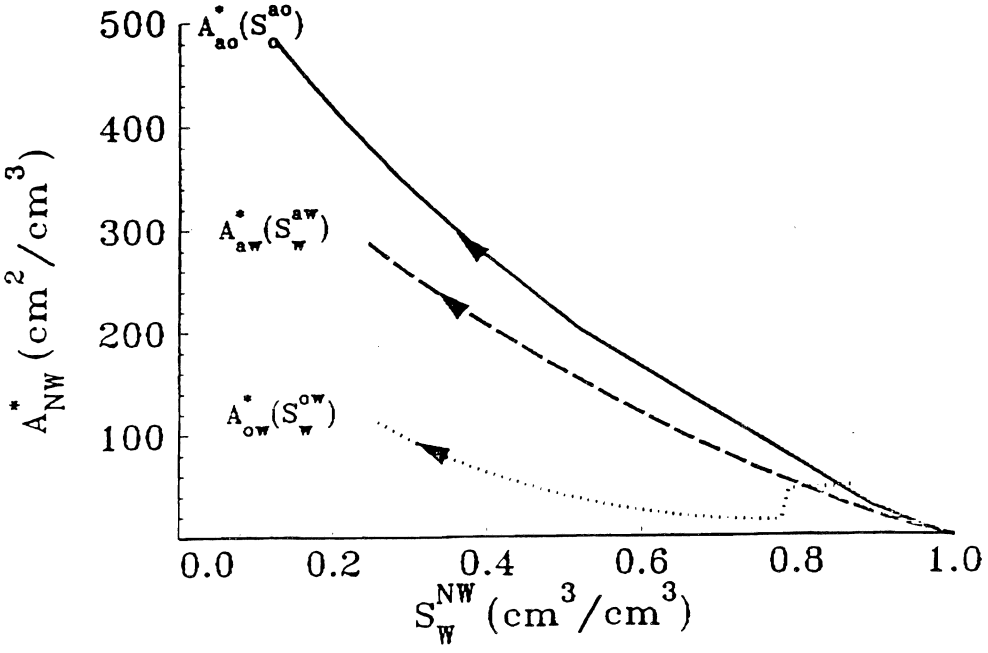

Figure 7. The calculated $A_{NW}(S_W^{NW})$ relations during (a) drainage and for untreated media containing air and oil, and the 75% OTS medium containing air and water, and oil and water.

Groundwater Contamination in Fresno County, California: Simulated Leaching and Transport of DBCP in the Unsaturated-Saturated Subsurface

KEITH LOAGUE
Department of Geological and Environmental Sciences, Stanford University

Summary

The overall objective of this study was to conduct a process-based case study investigation, using a process-based simulation of non-point source induced groundwater contamination that resulted from regional scale application of agricultural chemicals. Such a research design facilitates future investigations of the interplay between near-surface solute transport processes, economics-based regulatory constraints, epidemiologic-based public health constraints, and the constraints associated with the legal and political arenas. The research has focused on simulating the potential vulnerability of groundwater in Fresno County (California) to contamination resulting from long-term, agriculture-related applications of the nematicide 1,2-dibromo-3-chloropropane (DBCP). Regional scale groundwater contamination resulting from the chemical legacies associated with past agricultural practices, is potentially a huge problem. For example, by the mid 1980's more than 50 different pesticides had been detected in California's groundwater. The assessment and remediation of non-point source groundwater contamination can easily pose problems that have significantly greater economic impacts than those which have long been recognized for point sources.

Key Words: Fresno County, California; non-point source groundwater contamination; agriculture; DBCP; PRZM; MODFLOW; MT3D; risk-cost-benefit analysis.

Research Plan and Procedures

1,2-dibromo-3-chloropropane (DBCP) and The San Joaquin Valley

A major chemical soil fumigant used to control nematodes in California, from the late 1950s to the late 1970s, was 1,2-dibromo-3-chloropropane ($C_3H_5Br_2Cl$ or DBCP). The terrestrial fate of DBCP when released in the near-surface includes primarily volatilization and leaching, with the remaining, weakly sorbed residues being very persistent. The positive attributes of DBCP as a nematicide are that (i) it is less volatile than many of the other soil fumigants of the time period, (ii) it remains active in the soil for a long time, (iii) it is very effective in killing nematodes, and (iv) it does not penetrate the roots of plants. The negative attributes of DBCP as a nematicide are that (i) it is relatively mobile in soils, with high groundwater recharge rates, (ii) it is fairly persistent, (iii) there is strong evidence that it causes sterility in human males, and (iv) it is likely to be carcinogenic. DBCP was banned in the United States in 1979 due to the health risks associated with human consumption of foods grown with exposure to the chemical. The maximum contaminant level (MCL) which has been set for DBCP in groundwater in the United States is 0.2 μg/kg. The current detection limit for DBCP is approximately 0.001 μg/kg.

The San Joaquin Valley (SJV) is located at the southern end of California's Central Valley. Between the late 1950s and its statewide cancellation in August 1977 there was widespread use of DBCP throughout the valley. During this period, the typical annual DBCP application rate in the SJV ranged from 22 to 90 kg/ha. The total usage of DBCP in California between 1960 and 1977 has been estimated to be approximately 1,360 metric tons per year. More than 3,000 wells in the SJV were sampled for DBCP between 1975 and 1988; the pesticide was found in 1,280 of the wells. It has been suggested that, within the valley, an area encompassing more than 18,000 km^2 has DBCP-contaminated groundwater.

The possible pathways for DBCP to have reached groundwater in the SJV include (i) non-point source, regional-scale applications of the chemical at label-directed rates, (ii) point source loading in areas used for chemical mixing, and (iii) point source dumping of the chemical after it was banned. Two key and timely questions embedded in the DBCP contamination problem are (i) Is the current DBCP legacy situation in the valley the result of the label-recommended application rate during the time of the chemical use? and (ii) Are there other agriculture related practices, not necessarily covered by the label, which could have led to the DBCP hot spots in the valley's groundwater?

Methodology

The approach used in this study to simulate the fate and transport resulting from multiple applications of DBCP, under changing land use, for a 1172 km^2 area (approximately equal to the east-central part of Fresno County)

for 35 years is summarized in the following twelve-step procedure (see League et al., 1996a,b for complete descriptions):

- Approximate the climatic history from 1950-1994.
- Approximate the distribution of soil types at the order taxonomic category.
- Approximate the land cover history, used here as a surrogate for the DBCP application history, from 1958-1994.
- Approximate the irrigation history from 1960-1994.
- Approximate the water table depth (from the surface) history from 1960-1994.
- Approximate the study area geology, used here as a surrogate for hydrogeologic properties, for a block with a datum 1650 m below the highest surface elevation.
- Approximate the recharge pond history from 1960-1994.
- Approximate the pumping history from 1960-1994.
- Simulate the vertical unsaturated fluid flow (i.e., recharge at the water table) and DBCP transport for 1172 separate 1 km^2 elements for the period 1960-1994.
- Using the simulated, last day of the year, concentration profiles (dissolved phase), pick off the DBCP concentration at the water table for each of the 1172 elements for each year, 1960-1994.
- Simulate tree-dimensional fluid flow (with recharge and pumping), 1960-1994.
- Simulate three-dimensional solute transport (with DBCP loading at the water table and chemical decay), 1960-1994.

The numerical model used for the one-dimensional near-surface fluid flow and DBCP transport simulations in this study is PRZM-2 (Mullins et al., 1993). The numerical models used for the three-dimensional fluid flow and DBCP transport simulations in the saturated subsurface are MODFLOW (McDonald and Harbaugh, 1993) and MT3D (Zheng, 1992), respectively. In this study, PRZM-2 simulations of dissolved-phase DBCP concentration profiles are used to estimate chemical loading at the water table on an annual basis. Each one-dimensional vertical soil column, in a 2-D horizontal grid, requires a separate PRZM-2 simulation. The aggregate of the DBCP concentrations loaded to the water table for each grid element (each year) makes up the annual loading files for the three-dimensional saturated transient fluid flow and solute transport simulations. Figures 1 through 4, respectively, show the soils map, a 1972 land cover map, a 1994 water table depth map, and a geologic cross section.

Results

The 1172 PRZM-2 simulations conducted for this study facilitate the construction of DBCP water table loading maps for the study area for each day of the 35 year simulation period. Figure 5 shows the simulated DBCP loading at the water table, for concentrations greater than the detectable limit (0.001

mg/kg), for the last day of 1980. Figure 6 shows six snap shots of the simulated distribution of DBCP in the saturated subsurface between 1965 and 1990.

The PRZM, MODFLOW, and MT3D simulations conducted in this study lead to the following general comments:

- The area most likely to facilitate DBCP leaching through the entire unsaturated soil profile are targeted.
- The first appearance of DBCP above the detectable limit at the water table is simulated as most likely occurring between 1961 and 1965.
- The estimated DBCP concentrations reaching the saturated subsurface exceed the MCL at several locations at different times. The first appearance of the chemical at the water table above the MCL was between 1965 and 1970. By 1990, the simulated DBCP concentrations loaded to the water table are reduced to below the MCL.
- Relative to the size of the study area, the extent and duration of the estimated contamination is small.
- Concentrations are a function of the pesticide application rates and frequency; the highest estimates are associated with citrus and vineyards, the lowest estimates are associated with cotton.
- Concentrations are a function of the unsaturated profile thickness; the greater the depth to the saturated subsurface the longer the lag time before the impact of the leaching is felt at the water table. Obviously, the longer the residence time the chemical has in the unsaturated zone, the more opportunity there is for decay.
- Concentrations are a function of soil hydraulic properties: the higher estimates are associated with the Alfisols and Entisols soil orders; the lower estimates are associated with the Inceptisols, Mollisols, and Vertisols soil orders.
- Concentrations are a function of near-surface sorption; the higher estimates are associated with the Entisols and Vertisols soil orders, the lower estimates are associated with Mollisols.
- Widespread DBCP leaching is pronounced only when concentrations below the detectable limit are considered. Of course, the detectable limit will continue to be lowered as analytical techniques improve.
- The fate and transport simulations of DBCP in the saturated subsurface show wide-spread occurrence, well below the MCL, only in the more permeable younger sediments.
- The occurrence of DBCP in the saturated subsurface is a complex function of the chemical loading history, the groundwater recharge rates, and pumping rates.

Discussion and Conclusions

The past, present, and future use of agrochemicals in the United States is a major environmental issue. The use of process-based numerical simulation models for assessment of groundwater vulnerability at regional scales, albeit data- and computer-intensive, is perhaps the most effective means of addressing problems that in all likelihood will not be investigated thoroughly

through field study due to lag times associated with the unsaturated zone that can easily span several decades. Simulation facilitates, as in this study, the assessment of agrochemicals long since out of use whose fate and transport is still of great concern. For the agrochemicals currently in use, and those that may be developed for use in the future, simulation allows us to look well into the future and consider alternative management strategies. The goal of the simulation effort reported here is to estimate the possible leaching history of a given pesticide for a large area over a long time with a process-based model using the best available data. Our simulation philosophy in this research is simply to use the best available model, in an uncalibrated mode, to ask "what if" questions at a regional scale that can then be interpreted in terms of the limiting assumptions associated with both the likely model error and data error uncertainties. We believe our simulation results do provide a good starting point for understanding the fate and transport of DBCP in Fresno County. For example, we are able to go back in history (i.e., 16 years of multiple and variable applications) and estimate what the spatially variable DBCP loading rates to the water table would likely have been across the regional scale study area 18 years ago at the time of the chemical's cancellation.

An important legal issue today is whether or not the manufactures of DBCP should have realized, before it was licensed, that the pesticide would leach to groundwater in Fresno County through long-term vulnerability assessments. The simulation approach used in this study can be critical in future characterization and remediation efforts for DBCP in Fresno County as well as for establishing a simulation-based protocol for assessing regional scale groundwater contamination problems that are related to the use of other agricultural chemicals. The objective of this study has been to address, from a simulation perspective, the question of whether (or not) label-recommended non-point source (i.e., agriculture) applications of DBCP are the principal source of groundwater contamination in Fresno County (i.e., the forward simulation problem). In our larger and ongoing effort, we will be investigating various point source scenarios for the same Fresno County boundary value problem (i.e., inverse simulation problems). Finally, the Fresno case study, as well as our earlier work in Hawaii (see Loague, 1994), set the foundation for the quantitative economic-based environmental risk assessment, proposed by Loague et al. (1996c), for non-point source groundwater contamination. The risk-cost-benefit analyses to be conducted for the Fresno case study will provide useful insight into the feasibility of potential remediation strategies (e.g., pump and treat, capture and containment) for existing regional scale non-point source groundwater contamination problems and for designing new regulations to limit future problems.

References

Loague, K. 1994. Risk-Cost-Benefit analysis for groundwater contamination from non-point sources. In Reactions of Toxic Pollutants in Soil Systems. pp. 277–286. 1992–93 Annual Report Kearney Foundation of Soil Science.

Loague, K., R.L. Bernknopf, R.E. Green, and T.W. Giambelluca. 1996c. Uncertainty of groundwater vulnerability assessments for agricultural regions in Hawaii: Review. Journal of Environmental Quality (in press).

Loague, K., D. Lloyd, A. Nguyen, S.N. Davis, and R.H. Abrams. 1996a. A case study simulation of DBCP groundwater contamination in Fresno County, California: Leaching through the unsaturated subsurface. (in preparation).

Loague, K., R.H. Abrams, S.N. Davis, A. Nguyen, and I.T. Stewart. 1996b. A case study simulation of DBCP groundwater contamination in Fresno County, California: Transport in the saturated subsurface. (in preparation).

McDonald, M.G. and A.W. Harbaugh. 1993. A Modular Three-Dimensional Finite-Difference Groundwater Flow Model. Techniques of Water Resources Investigations of the U.S. Geological Survey, Book 6.

Mullins, J.A., R.F. Carsel, J.E. Scarbough, and A.M. Ivery. 1993. PRZM-2, A Model for Predicting Pesticide Fate in the Crop Root and Unsaturated Soil Zones: Users Manual for Release 2. Environmental Research Laboratory, U.S. Environ. Prot. Agency, Athens, GA, EPA-600/R-93/046.

Zheng, C. 1992. MT3D: A Modular Three-Dimensional Model for Simulation of Advection, Dispersion, and Chemical Reactions of Contaminants in Groundwater Systems. Version 1.5, S.S. Papadopulos & Assoc., Bethesda, MD.

Figure 1. Distribution of the five soil orders in the study area (from Loague et al., 1996a).

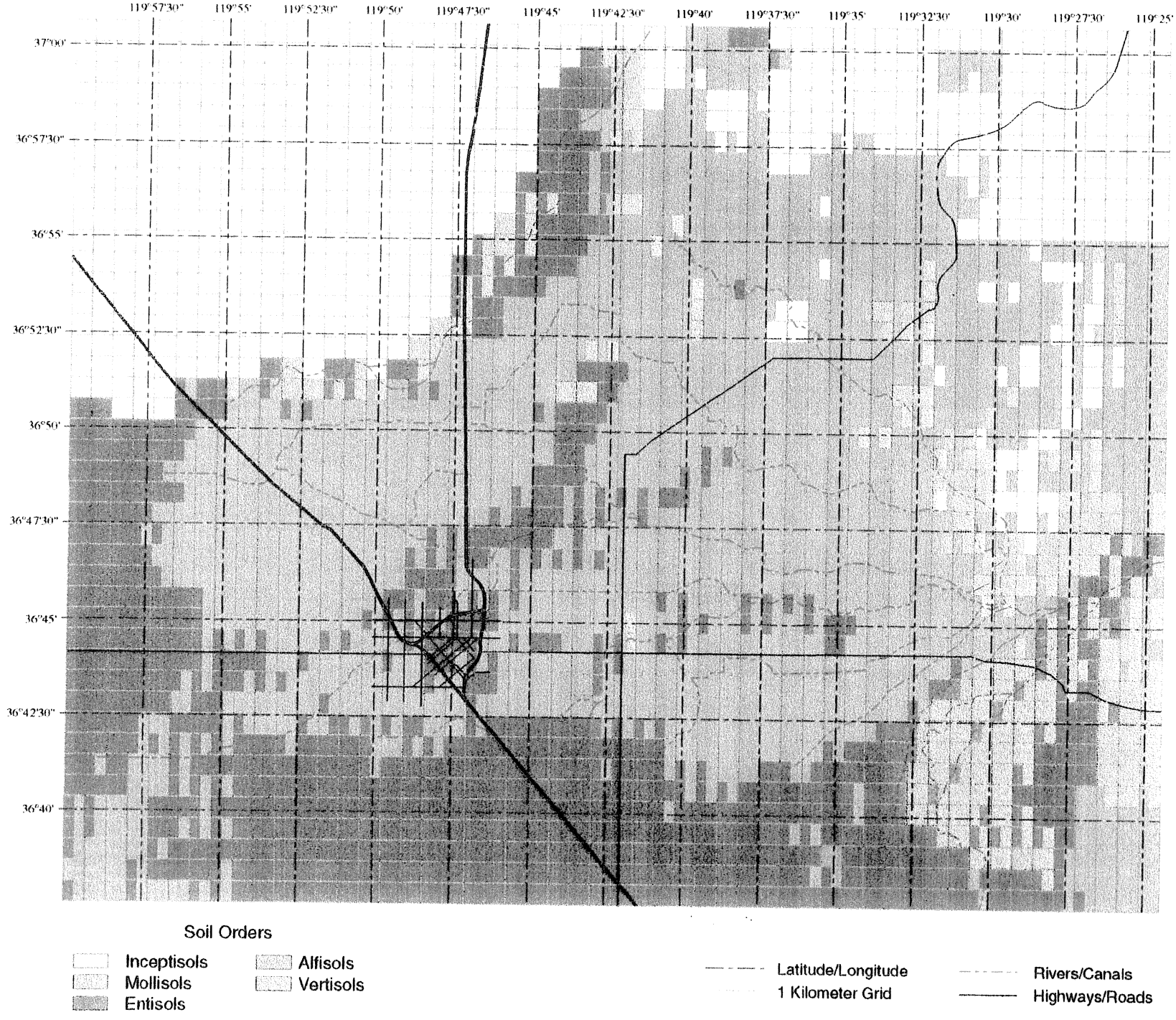
119°57'30"
119°55'
119°52'30"
119°50'
119°47'30"
119°45'
119°42'30"
119°40'
119°37'30"
119°35'
119°32'30"
119°30'
119°27'30"
119°25'
37°00'
36°57'30"
36°55'
36°52'30"
36°50'
36°47'30"
36°45'
36°42'30"
36°40'
Soil Orders
Inceptisols
Mollisols
Entisols
Alfisols
Vertisols
Latitude/Longitude
1 Kilometer Grid
Rivers/Canals
Highways/Roads

Figure 2. Representation of the 1972 land cover for the study area (from Loague et al., 1996a)

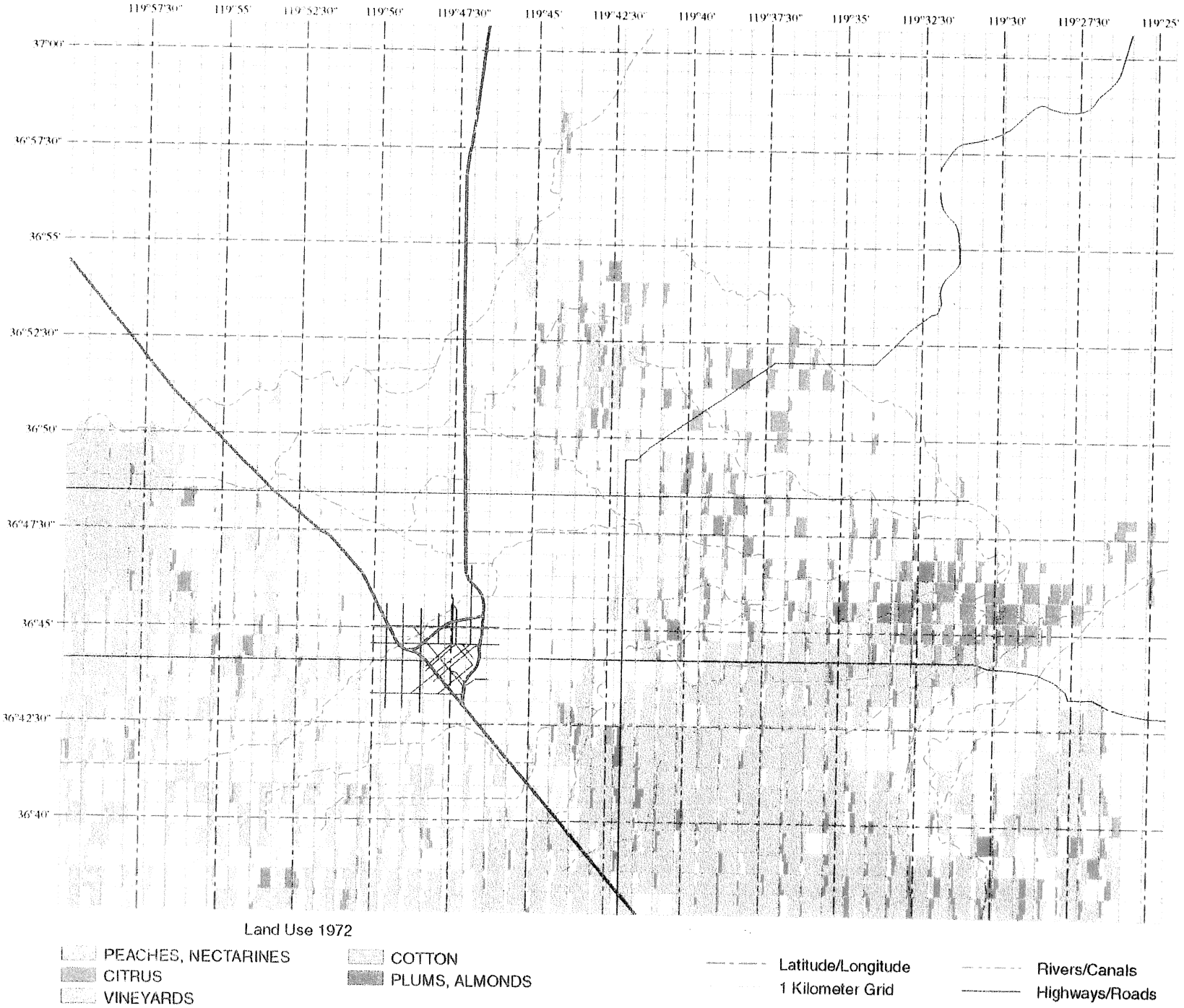
119°57'30"
119°55'
119°52'30"
119°50'
119°47'30"
119°45'
119°42'30"
119°40'
119°37'30"
119°35'
119°32'30"
119°30'
119°27'30"
119°25'
37°00'
36°57'30"
36°55'
36°52'30"
36°50'
36°47'30"
36°45'
36°42'30"
36°40'
Land Use 1972
PEACHES, NECTARINES
CITRUS
VINEYARDS
COTTON
PLUMS, ALMONDS
Latitude/Longitude
1 Kilometer Grid
Rivers/Canals
Highways/Roads

Figure 3. Estimated depth to the water table for the study area in 1994 (from Loague et al., 1996).

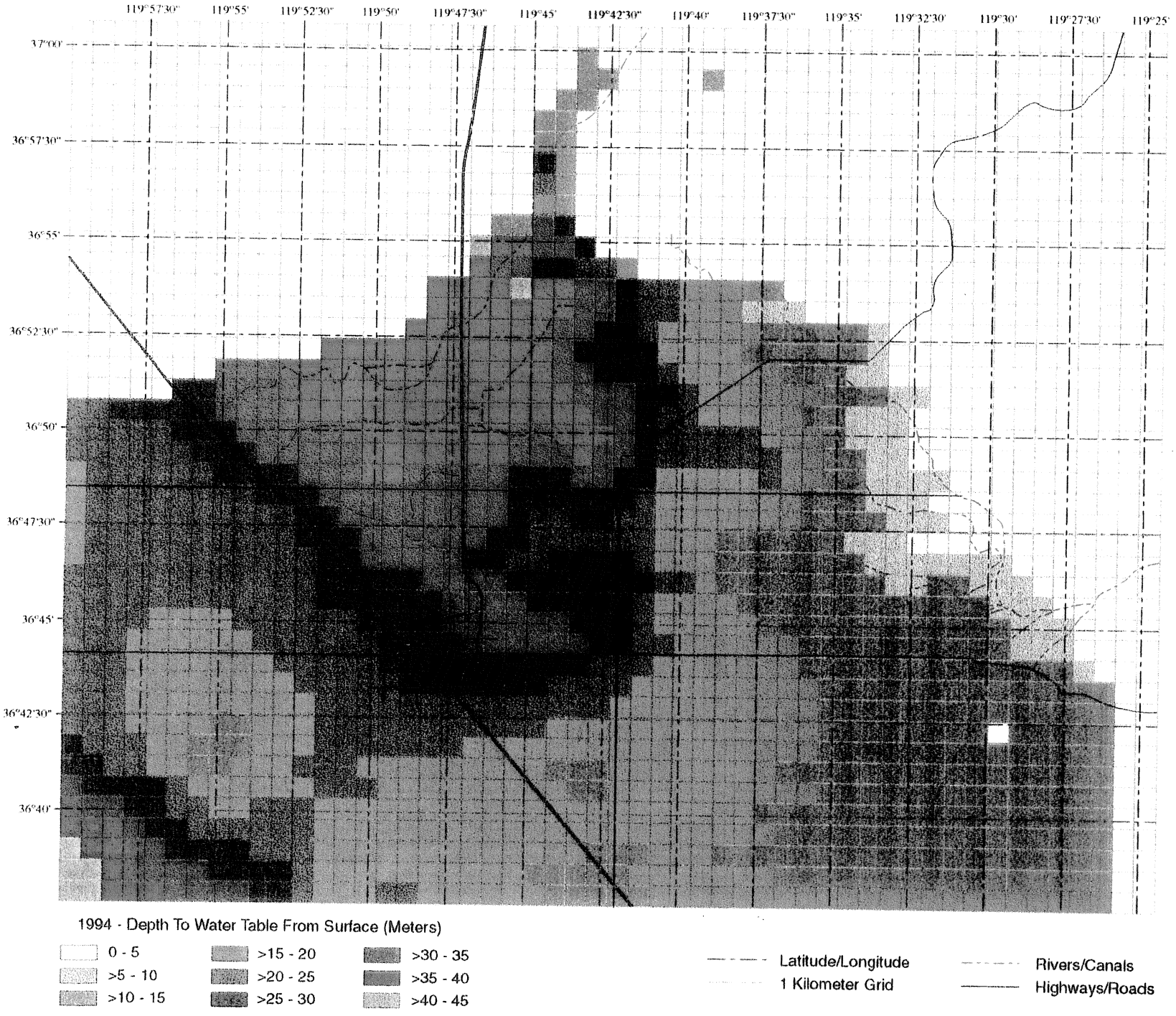
119°57'30"
119°55'
119°52'30"
119°50'
119°47'30"
119°45'
119°42'30"
119°40'
119°37'30"
119°35'
119°32'30"
119°30'
119°27'30"
119°25'
37°00'
36°57'30"
36°55'
36°52'30"
36°50'
36°47'30"
36°45'
36°42'30"
36°40'
1994 - Depth To Water Table From Surface (Meters)
0 - 5
>5 - 10
>10 - 15
>15 - 20
>20 - 25
>25 - 30
>30 - 35
>35 - 40
>40 - 45
Latitude/Longitude
1 Kilometer Grid
Rivers/Canals
Highways/Roads

Figure 4. Geology of the study area (from Loague et al., 1996b)

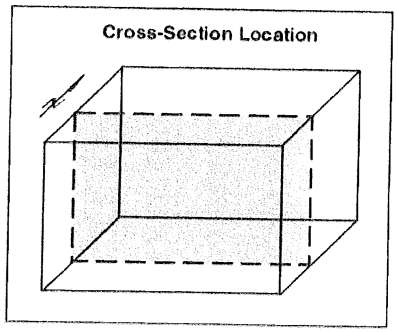

Geologic Cross-Section B

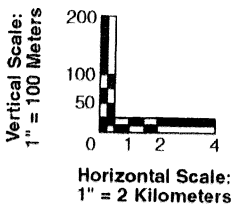

Legend

- Above the Surface
- Outside the Study Area
- Younger Sediments
- Older Sediments
- Bedrock

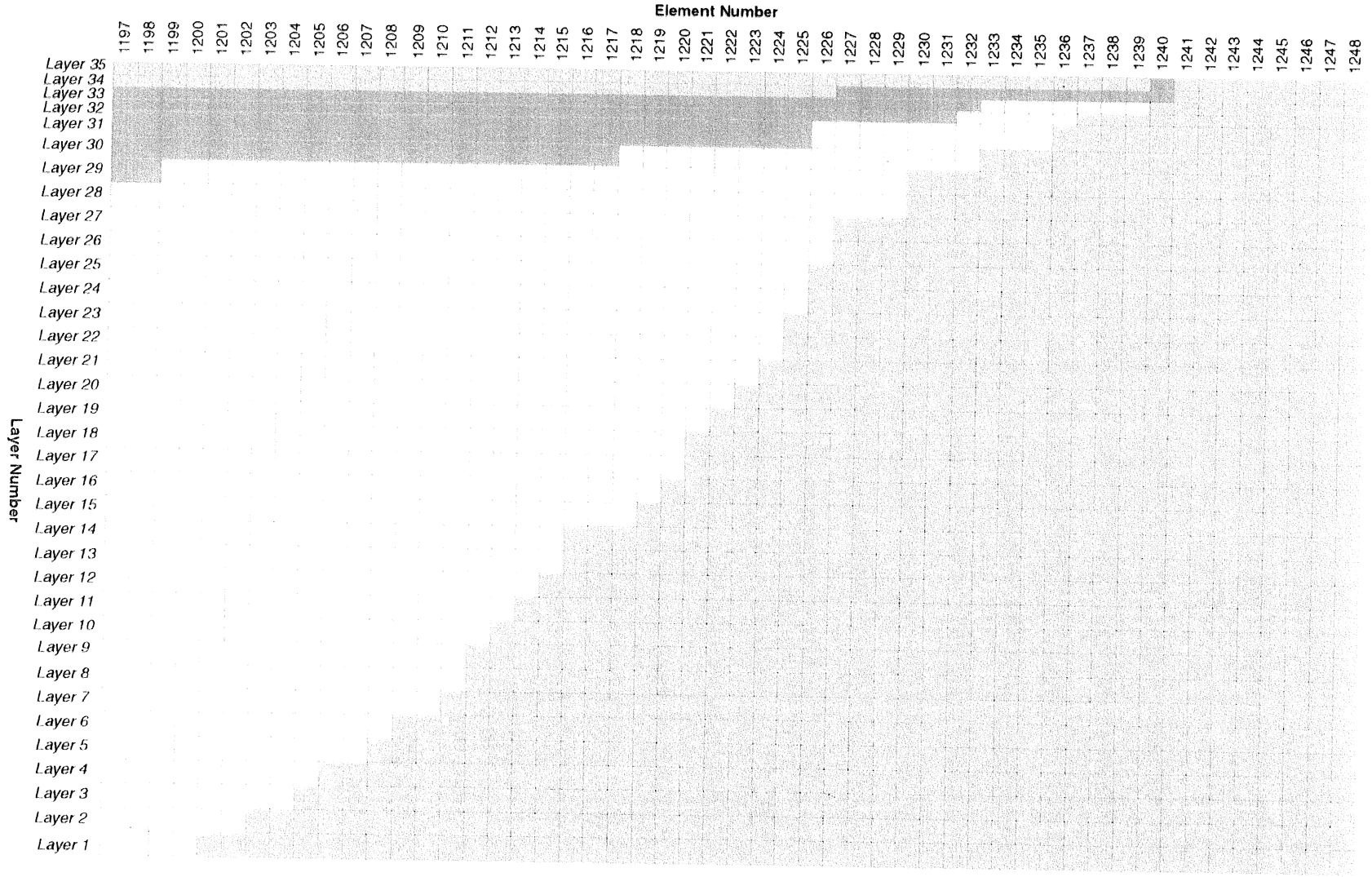

Figure 5. Simulated DBCP loading at the water table on the last day of 1980 (from Loague et al., 1996a). Only dissolved concentrations simulated above the detectable limit are shown.

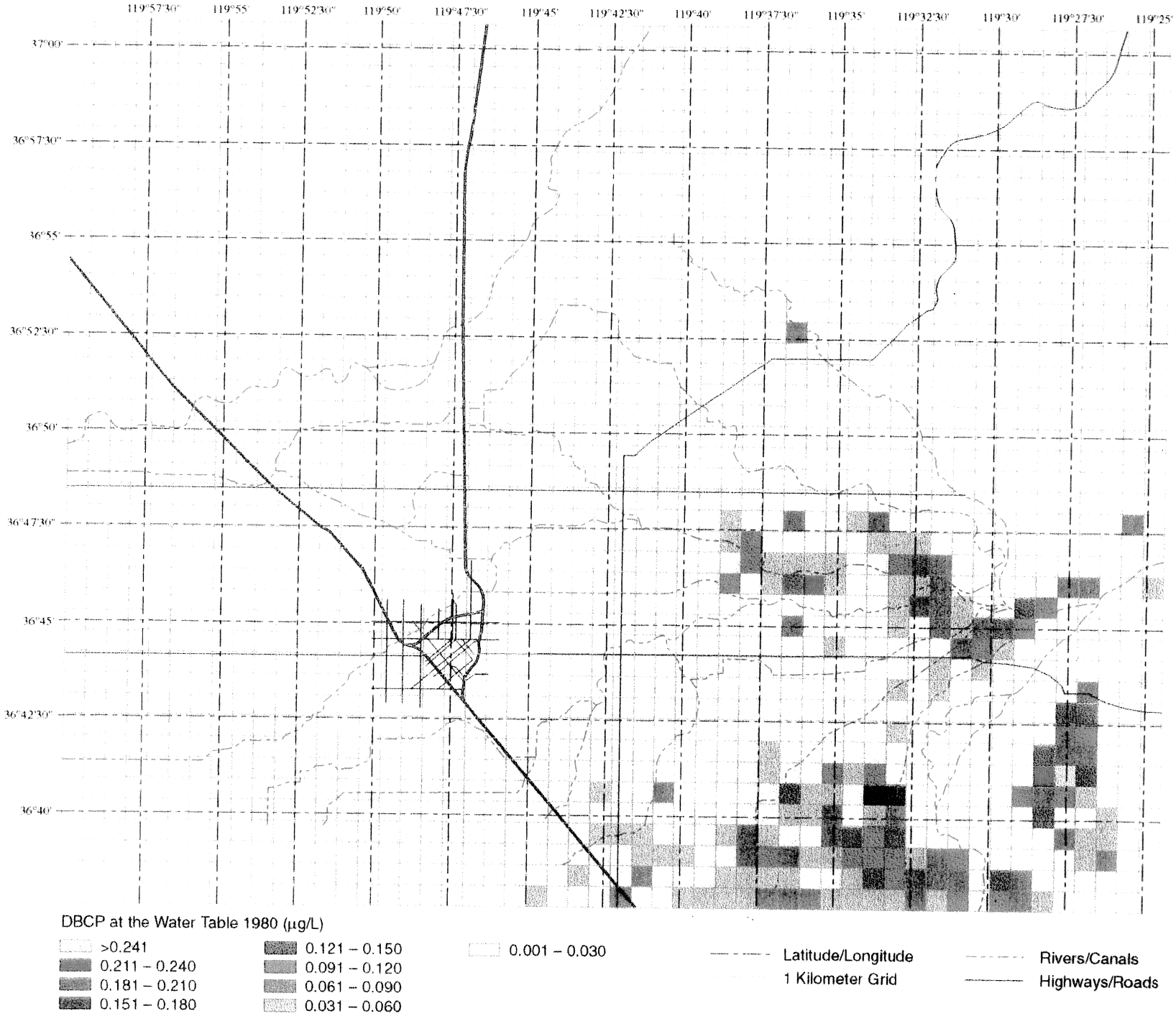
119°57'30"
119°55'
119°52'30"
119°50'
119°47'30"
119°45'
119°42'30"
119°40'
119°37'30"
119°35'
119°32'30"
119°30'
119°27'30"
119°25'
37°00'
36°57'30"
36°55'
36°52'30"
36°50'
36°47'30"
36°45'
36°42'30"
36°40'
DBCP at the Water Table 1980 (µg/L)
>0.241
0.211 – 0.240
0.181 – 0.210
0.151 – 0.180
0.121 – 0.150
0.091 – 0.120
0.061 – 0.090
0.031 – 0.060
0.001 – 0.030
Latitude/Longitude
1 Kilometer Grid
Rivers/Canals
Highways/Roads

Figure 6. Simulated DBCP concentrations in the younger sediments (from Loague et al., 1996b). Only dissolved concentrations simulated above the detectable limit are shown.

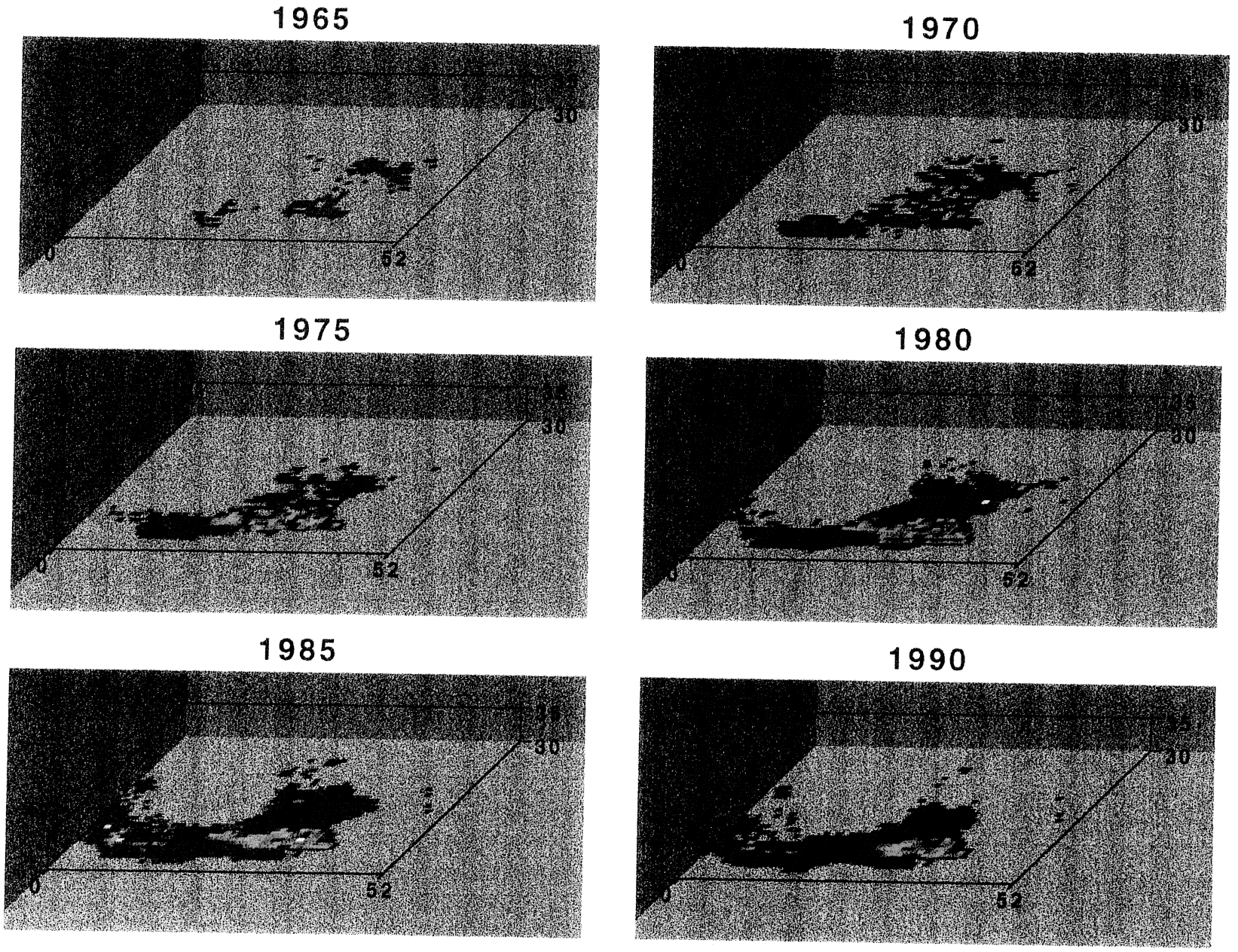
1965
1970
1975
1980
1985
1990
0
52
30
0.0
(μg/ kg)
0.060

Objective, Organization and Function of The University of California Kearney Foundation of Soil Science

Adopted August 4, 1969
Revised June 30, 1982

Objective

The Kearney Foundation of Soil Science shall focus its program and support research in definitive missions in the fields of soils, plant nutrition, and water science.

Organization

A. The Kearney Foundation of Soil Science is administratively responsible to the Vice President-Agricultural and University Services (A&US) through the Director of the Agricultural Experiment Station and the Associate Director of the Agricultural Experiment Station located on the campus on which the Director of the Foundation is resident.

B. The Kearney Foundation of Soil Science is administered for the Division of Agricultural Sciences by a Director with policy guidance by an Advisory Committee and assistance from a Technical Committee.

1. The Director is appointed by the Vice President-A&US, after approval by the Dean and Associate Director of the Agricultural Experiment Station and the Chancellor of the campus on which the Director is to be resident. The Advisory Committee will propose a slate of candidates for the position of Director to the Vice President-A&US for his consideration.

2. The Advisory Committee of the Kearney Foundation is appointed by the Vice-President-A&US and is responsible to him through the Director of the Agricultural Experiment Station for guidance of the Foundation. The Chairman of the Committee is the Associate Director of the Agricultural Experiment Station at the location where the Director of the Foundation resides. The remaining members are the chairmen, or designees, of the Departments of Land, Air and Water Resources at Davis, Plant and Soil Biology at Berkeley, Soil and Environmental Sciences at Riverside, and one representative from a crop production department, one representative from Agricultural Economics and one representative from Agricultural Extension.

3. The Technical Committee of the Kearney Foundation is appointed by the Vice President-A&US. The Technical Committee shall consist of the Foundation Director as Chairman and four to seven other individuals. Individuals will be selected for the Technical Committee on the basis of their expertise on the Kearney Foundation mission subject matter with consideration for appropriate campus, cooperative extension and possibly non-university representation.

4. The Foundation Director may employ necessary administrative, technical or clerical staff to accomplish the Kearney Foundation goals, but there shall be no permanent staff for the Foundation. The Foundation Director will submit an annual report as prescribed by the University for Multi-campus Research Units.

Functions

A. The function of the Kearney Foundation is to encourage and support research and information dissemination on a specific definitive mission approved by the Vice President-A&US upon the recommendation of the Advisory Committee for a period of five years. The mission shall be one of public concern on which useful contributions are likely to be made in a five-year period. Successive missions will be selected each five years with a new Director for each mission.

B. The Foundation Director shall (1) keep faculty and cooperative extension individuals on various campuses informed on the Foundation goals and objectives and on funding opportunity from the Foundation, (2) solicit research proposals from UC investigators and with help from the Technical Committee develop a proposal funding priority list for review by the Advisory Committee, (3) allocate funds, after review by the Advisory Committee, to accomplish the Foundation mission, (4) be responsible for administrative details including preparation of appropriate reports, (5) assist faculty members to seek funds from sources other than Kearney Foundation that will contribute to the Foundation mission, (6) encourage information dissemination on the mission subject matter to appropriate segments of society, and (7) prepare "wrap-up" document(s) which synthesize the information gained during the five year mission.

C. The Advisory Committee shall (2) advise the Foundation Director when needed, (2) recommend research policy, (3) evaluate progress on the mission research, (4) review recommended allocation of funds by Foundation Director, (5) encourage inter-campus coordination and cooperation to make optimum use of resources and facilities, (6) select a definitive five year research mission to succeed an existing mission, and (7) nominate qualified candidates for a succeeding Director of the Foundation.

D. The Technical Committee shall (2) assist the Director in defining research priorities, (2) evaluate and develop a priority rating on research proposals, and (3) provide advice as requested by the Foundation Director on matters related to technical subject matter.

General Operational Guidelines

A. Recommended missions and Foundation Director candidates are to be submitted to the Director of the Agricultural Experiment Station and the Vice President-A&US by July 1 preceding the final year of an existing research mission. The new mission and Director-designate are to be selected as soon thereafter as possible to enable the Director-designate to plan the program for activation the following July 1.

B. The Director will manage and authorize expenditures of all funds transferred to the Kearney Foundation as of July 1 of the last year of the mission. Any funds transferred into the Kearney Foundation after that time will be used to accomplish the goals of the succeeding mission.

C. The Director normally will use the year after the five year mission period to "wrap up" the mission by holding symposia, preparing publications, etc. Funds to accomplish this task must be reserved from the budget specifically assigned tot he mission during the preceding five years. The immediate past Kearney Foundation Director will report to the Vice President-A&US through the appropriate Dean and Advisory Committee on progress and budgetary expenditures in achieving wrap up of the mission. At the appropriate time, the mission will be considered complete, the Director formally released from responsibility and any unexpended funds will revert back to the Kearney Foundation for use in subsequent missions.

D. The Director and members of the Advisory and Technical Committees are eligible to submit proposals for funding. They must, however, be excluded from discussion or action related to the particular project.

E. Normally extramural contracts or grants supporting activities consistent with the Kearney Foundation mission will be assigned directly to the Department of the scientist serving as PI rather than to the Kearney Foundation. When an outside agency makes an offer or solicits a proposal from the Foundation Director, the Director will make that information known to the Advisory Committee.

F. Kearney Foundation resources are to supplement Agricultural Experiment Station budgets and provide incentives for research redirection. Because of the temporary nature of the funds, funding of non-career employees such as post-doctoral appointments, research assistantships and part time laboratory helpers is strongly encouraged and routinely approved. Justified funding for career employees with supplemental employee benefit costs must be approved by the Advisory Committee.

Kearney Foundation of Soil Science Advisory Committee

Kearney Foundation of Soil Science Technical Committee

Dr. Andrew C. Chang
Chair, Kearney Foundation of Soil Science Technical Committee
Director, Kearney Foundation of Soil Science
Professor of Agricultural Engineering and Agricultural Engineer
Department of Soil & Environmental Sciences
University of California
Riverside, CA 92521
(909) 787-5325

Dr. Arthur L. Craigmill
Cooperative Extension Toxicology Specialist
Department of Environmental Toxicology
University of California
Davis, CA 95616
(916) 752-2936

Dr. Dennis D. Focht
Professor of Soil Microbiology and Soil Microbiologist
Department of Soil & Environmental Sciences
University of California
Riverside, CA 92521
(909) 787-3446

Dr. Jan W. Hopmans
Associate Professor of Water Management and Assoc. Water Management Specialist
Director, Hydrologic Science Section, Department of Land, Air & Water Resources
University of Calfornia
Davis, CA 95616
(916) 752-3060 or (916) 752-0453

Dr. John G. McColl
Professor of Forest Soils
Department of Environmental Science, Policy and Management
University of California
Berkeley, CA 94720
(510) 642-1028 or (510) 643-6088

Dr. T. Ishwar Murarka
Senior Program Manager, Land and Water Quality Studies
Electrical Power Research Institute
P. O. Box 10412
Palo Alto, CA 94303
(415) 855-2150

Dr. Albert L. Page
Professor of Soil Science and Chemist
Department of Soil & Environmental Sciences
University of California
Riverside, CA 92521
(909) 787-3654

Dr. Martinus Th. Van Genuchten
Adjunct Professor of Soil Physics
Department of Soil & Environmental Sciences
United States Salinity Laboratory
University of California
Riverside, CA 92521
(909) 369-4847

Index of Principal Investigators

Sam Alvey
Graduate Student
Department of Soil & Environmental Sciences
University of California
Riverside, CA 92521
(909) 787-3785

Dr. Ronald G. Amundson
Profesor of Soil Science
Department of Environmental Science, Policy, and Management
University of California
Berkeley, CA 94720
(510) 643-7890

Dr. Michael A. Anderson
Assistant Professor of Soil Chemistry and Assistant Soil Chemist
Department of Soil & Environmental Sciences
University of California
Riverside, CA 92521
(909) 787-3757

Tim Arndt
Post Graduate Researcher
Department of Environmental Toxicology
University of California
Davis, CA 95616
(916) 752-5291

Dr. Paula Bosserman
Spectroscopist
Department of Soil & Environmental Sciences
University of California
Riverside, CA 92521
(909) 787-2970

Dr. Gordon E. Brown, Jr.
Professor of Earth Sciences and Professor of the Synchrotron Radiation Laboratory
Department of Geological and Environmental Sciences and
Synchrotron Radiation Laboratory
Stanford University
Stanford, CA 95305
(415) 752-9168

Dr. William H. Casey
Professor and Aqueous Geochemist
Department of Land, Air & Water Resources, Soil Science & Biogeochemistry Section
University of California
Davis, CA 95616
(916) 752-3211

Pete Clark
Staff Research Associate
Department of Soil & Environmental Sciences
University of California
Riverside, CA 92521
(909) 787-4653

Heike Clausnitzer
Postgraduate Researcher
Deptartment of Land, Air & Water Resources, Soils & Biogeochemistry Section
University of California
Davis, CA 95616
(916) 752-6081

Dr. Arthur L. Craigmill
Extension Specialist
Department of Environmental Toxicology
University of California
Davis, CA 95616
(916) 752-2936

Dr. David E. Crowley
Assistant Professor of Soil Science and Assistant Soil Chemist
Department of Soil & Environmental Sciences
University of California
Riverside, CA 92521
(909) 787-3785

Dr. Harvey E. Doner
Professor of Soil Chemistry
Department of Environmental Science, Policy, and Management
University of California
Berkeley, CA 94720
(510) 642-4148

Kristie A. Dunkin
Graduate Student Researcher
Department of Soil Science
University of Calfiornia
Berkeley, CA 94720
(510) 624-6847

Dr. Walter J. Farmer
Professor of Soil Science and Chemist
Department of Soil & Environmental Sciences
University of California
Riverside, CA 92521
(909) 787-3756

Dr. Mary K. Firestone
Chair, Department of Environmental Science, Policy and Management
Professor of Microbiology
University of California
Berkeley, CA 94720
(510) 642-3677

Dr. William T. Frankenberger, Jr.
Professor of Soil Microbiology
Department of Soil & Environmental Sciences
University of California
Riverside, CA 92521
(909) 787-3405

Carol Frate
Farm Advisor
University of California Cooperative Extension, Tulare County
Agricultural Building County Civic Center
Visalia, CA 93291
(209) 733-6483

Dr. Robert C. Graham
Associate Professor of Soil Mineralogy
Department of Soil & Environmental Sciences
University of California
Riverside, CA 92521
(909) 787-3751

Dr. David E. Hinton
Professor of Aquatic Toxicology
Department of Anatomy, Physiology, and Cell Biology
School of Veterinary Medicine
University of California
Davis, CA 95616
(916) 752-6413

Dr. Jan W. Hopmans
Associate Professor of Water Management and Assoc. Water Management Specialist
Department of Land, Air, & Water Resources, Hydrologic Science Section
University of California
Davis, CA 95616
(916) 752-3060 or (916) 752-0453

Dr. F. J. Leij
Assistant Research Soil Physicist
Department of Soil & Environmental Sciences
United States Salinity Laboratory
University of California
Riverside, CA 92521
(909) 369-4851

Dr. Roy B. Leipnik
Professor of Mathematics
Department of Mathematics
University of California
Santa Barbara, CA 93106
(805) 893-2738 or (805) 893-2171

Dr. John Letey
Associate Director, Centers for Water and Wildland Resources
Professor of Soil Physics and Soil Physicist
Department of Soil & Environmental Sciences
University of California
Riverside, CA 92521
(909) 787-5105 or (909) 787-4327

Dr. Keith Loague
Associate Professor of Geological & Environmental Sciences
Department of Geological & Environmental Sciences
School of Earth Sciences
Stanford University
Stanford, CA 94305
(415) 723-3090

Dr. Hugo A. Loaiciga
Professor of Geography/Hydrology
Department of Geography
University of California
Santa Barbara, CA 93106
(805) 893-8053 or (805) 893-3663

Dr. Miguel A. Marino
Professor of Water Science and Ground Water Hydrologist
Department of Land, Air & Water Resources, Hydrologic Science Section
University of California
Davis, CA 95616
(916) 752-0684 or (916) 752-0453

Dr. John G. McColl
Professor of Forest Soils
Department of Environmental Science, Policy and Management
University of California
Berkeley, CA 94720
(510) 642-1028 or (510) 643-6088

Dr. David R. Parker
Associate Professor of Soil Chemistry and Associate Soil Chemist
Department of Soil & Environmental Sciences
University of California
Riverside, CA 92521
(909) 787-5126

Dr. Carlos E. Puente
Associate Professor of Hydrologic Science and Associate Hydrologist
Department of Land, Air, and Water Resources
University of California
Davis, CA 95616
(916) 752-0689 or (916) 752-0453

Dr. Peter A. Rock
Professor of Chemistry
Department of Chemistry
University of California
Davis, CA 95616
(916) 752-0940

Marcia Salazar
Graduate Student
Department of Soil & Environmental Sciences
University of California
Riverside, CA 92521
(909) 787-3785

Dr. Kate M. Scow
Assistant Professor of Soil Science and Assistant Soil Microbial Ecologist
Department of Land, Air, & Water Resources, Soils & Biogeochemistry Section
University of California
Davis, CA 95616
(916) 752-4632 or (916) 752-1406

Dr. Peter J. Shouse
Soil Scientist
United States Salinity Laboratory
University of California
Riverside, CA 92521
(909) 369-4849

Dr. Michael J. Singer
Professor of Soil Science
Department of Land, Air, & Water Resources, Soils & Biogeochemistry Program
University of California
Davis, CA 95616
(916) 752-7499

Dr. Randal J. Southard
Associate Professor of Soil Genesis and Morphology, and
Director, Soils & Biogeochemistry Program
Department of Land, Air, & Water Resources
University of California
Davis, CA 95616
(916) 752-7041

Dr. Garrison Sposito
Professor of Soil Physical Chemistry
Department of Environmental Science, Policy and Management
University of California
Berkeley, CA 94720
(510) 643-8297 or (510) 643-9171

Dr. Michael W. Stimmann
Extension Pesticide Specialist and Statewide Pesticide Coordinator
Department of Environmental Toxicology
University of California
Davis, CA 95616
(916) 752-7011

Stephanie L. Thibault
Graduate Student
Department of Soil & Environmental Sciences
University of California
Riverside, CA 92521
(909) 787-3405

Dr. Martinus Th. Van Genuchten
Adjunct Professor of Soil Physics
Department of Soil & Environmental Sciences
United States Salinity Laboratory
University of California
Riverside, CA 92521
(909) 369-4847

Scott Wetzlichs
Staff Research Associate
Department of Environmental Toxicology
University of California
Davis, CA 95616
(916) 752-5291

Steven D. Wright
Farm Advisor
University of California Cooperative Extension, Tulare County
Agricultural Building County Civic Center
Visalia, CA 93291
(209) 733-6482

Dr. Marylynn V. Yates
Associate Professor of Environmental Microbiology and
Associate Cooperative Extension Agronomist -- Groundwater Quality
Department of Soil & Environmental Sciences
University of California
Riverside, CA 92521
(909) 787-5488

Mavrik Zavarin
Graduate Student
Department of Environmental Science, Policy, and Management
University of California
Berkeley, CA 94720
(510) 642-3794

OFFICE OF THE DIRECTOR
KEARNEY FOUNDATION OF SOIL SCIENCE
UNIVERSITY OF CALIFORNIA
RIVERSIDE, CA 92521
(909) 787-5325